LEABHARLANN CHOLÁISTE NA TRÍONÓIDE, BAILE ÁTHA CLIATH | TRINITY COLLEGE LIBRARY DUBLIN
Ollscoil Átha Cliath | The University of Dublin

Terms and Conditions of Use of Digitised Theses from Trinity College Library Dublin

Copyright statement

All material supplied by Trinity College Library is protected by copyright (under the Copyright and Related Rights Act, 2000 as amended) and other relevant Intellectual Property Rights. By accessing and using a Digitised Thesis from Trinity College Library you acknowledge that all Intellectual Property Rights in any Works supplied are the sole and exclusive property of the copyright and/or other IPR holder. Specific copyright holders may not be explicitly identified. Use of materials from other sources within a thesis should not be construed as a claim over them.

A non-exclusive, non-transferable licence is hereby granted to those using or reproducing, in whole or in part, the material for valid purposes, providing the copyright owners are acknowledged using the normal conventions. Where specific permission to use material is required, this is identified and such permission must be sought from the copyright holder or agency cited.

Liability statement

By using a Digitised Thesis, I accept that Trinity College Dublin bears no legal responsibility for the accuracy, legality or comprehensiveness of materials contained within the thesis, and that Trinity College Dublin accepts no liability for indirect, consequential, or incidental, damages or losses arising from use of the thesis for whatever reason. Information located in a thesis may be subject to specific use constraints, details of which may not be explicitly described. It is the responsibility of potential and actual users to be aware of such constraints and to abide by them. By making use of material from a digitised thesis, you accept these copyright and disclaimer provisions. Where it is brought to the attention of Trinity College Library that there may be a breach of copyright or other restraint, it is the policy to withdraw or take down access to a thesis while the issue is being resolved.

Access Agreement

By using a Digitised Thesis from Trinity College Library you are bound by the following Terms & Conditions. Please read them carefully.

I have read and I understand the following statement: All material supplied via a Digitised Thesis from Trinity College Library is protected by copyright and other intellectual property rights, and duplication or sale of all or part of any of a thesis is not permitted, except that material may be duplicated by you for your research use or for educational purposes in electronic or print form providing the copyright owners are acknowledged using the normal conventions. You must obtain permission for any other use. Electronic or print copies may not be offered, whether for sale or otherwise to anyone. This copy has been supplied on the understanding that it is copyright material and that no quotation from the thesis may be published without proper acknowledgement.

Neurophysiological Changes Associated with Olfactory Short-Term Habituation in *Drosophila melanogaster*

Isabell Twick

2016

A dissertation submitted to the University of Dublin
for the degree of Doctor of Philosophy



Trinity College Dublin
Coláiste na Tríonóide, Baile Átha Cliath
The University of Dublin

Trinity College Institute of Neuroscience
Department of Genetics

TRINITY LIBRARY
0 8 MAR 2017
DUBLIN

Declaration

I hereby declare this thesis to be my own work unless otherwise stated in the text, and that this work has not been submitted for any other degree or qualification. I agree the library may lend this upon request.

I agree to deposit this thesis in the Universitys open access institutional repository or allow the library to do so on my behalf, subject to Irish Copyright Legislation and Trinity College Library conditions of use and acknowledgement.

Summary

The term habituation describes a simple form of learning that is characterized by a behavioural response decrement following repeated or prolonged sensory stimulation (Christoffersen, 1997; Rankin et al., 2009; Thompson and Spencer, 1966; Thompson, 2009; Ramaswami, 2014). It constitutes a filtering mechanism for sensory stimuli that filters irrelevant sensory information and only allows salient and important stimuli, such as those that predict food sources or allude death, to be passed through to higher brain centres (Wilson and Linster, 2008; Rankin et al., 2009). Filtering of innocuous sensory information is thought to be a building block for higher cognitive tasks (Wilson and Linster, 2008).

In the fruit fly *Drosophila melanogaster*, a form of olfactory habituation has been extensively characterized behaviourally and some of the underlying neuronal mechanisms have been deciphered (Das et al., 2011b). Habituation of the olfactory avoidance response is based on a fly's innate repulsion to an aversive odourant which declines following continuous exposure to the odour (Das et al., 2011b). This form of olfactory habituation has been proposed to arise from enhanced inhibitory transmission from local interneurons onto odour-responsive projection neurons in the antennal lobe, the fly's primary processing centre for olfactory information (Das et al., 2011b). A short-term 30-minute odourant exposure gives rise to short-term habituation (STH) which is thought to rely on modifications of pre-existing proteins in inhibitory GABAergic local interneurons (Sadanandappa et al., 2013).

The present study aimed a) to test whether the neuronal circuit underlying olfactory avoidance habituation is universal to another form of olfactory habituation and b) to study neurophysiological changes associated with behavioural STH using functional Ca^{2+} imaging.

The experiments performed suggest that habituation of the odour-evoked locomotor startle response, which is based on a fly's sudden startle response upon presentation to a novel odour, is likely not mediated by the same neuronal circuit as olfactory avoidance habituation. Ca^{2+} imaging experiments utilizing a novel protocol and purpose-built odour delivery system revealed that the synapses between olfactory sensory neurons (OSNs) and projection neurons (PNs) exhibit reductions in odour-evoked Ca^{2+} influxes both pre- and postsynaptically following 15-minute odourant exposure. The changes occur in specific glomeruli, distinct neuropil regions of the antennal lobe, and largely coincide between OSN terminals and PN dendrites. The reduced odour-evoked activity in these neuronal types appears to be mediated by a combination of presynaptic inhibition onto OSNs and postsynaptic inhibition onto PNs as indicated by the requirement of $GABA_B$ and $GABA_A$ receptors in these cell

types for the exposure-induced changes, respectively.

Taking into account previous literature (Root et al., 2008; Olsen and Wilson, 2008b; Das et al., 2011b), a model is proposed where short-term odourant exposure causes increased pre- and postsynaptic inhibition that act in concert for both gain control and filtering of familiar odours. Presynaptic inhibition is believed to mediate gain control that ensures the transfer of the odour information to higher brain centres without saturating neuronal responses (Root et al., 2008; Olsen and Wilson, 2008b). Postsynaptic inhibition, on the other hand, is proposed to suppress neuronal responses with the effect of filtering out irrelevant and familiar odours as observed during behavioural habituation (Das et al., 2011b).

Acknowledgements

I would like to express my deepest gratitude to the people who have provided both scientific advice and emotional support over the past few years and in doing so have considerably contributed to this thesis. Special thanks are due to the following...

... my supervisor, Professor Mani Ramaswami, for sharing his scientific wisdom, for his guidance, patience and continuous support throughout the years.

... the past and present members of the Ramaswami lab (Adrian, Jens, Jörn, Eimear, Chris, Aoife, John and Sahar) for experimental assistance, constructive advice and for simply creating a friendly and sociable working environment.

... John Lee for sharing the excitements and struggles, for providing encouragement when needed and for many enjoyable scientific and non-scientific discussions.

... Professor Ronald Calabrese for his invaluable expertise and experimental support while on his sabbatical in the lab.

... David Kelly for sharing his valuable knowledge on linear regression models and R.

... my friends near and far for moral support, encouragement and for providing distractions from the sometimes stressful lab routine.

... and finally my parents and sister for their invaluable support from far away, for being understanding and encouraging and for their perpetual belief in me and my abilities.

I am truly grateful to have had such great support along the way of this doctoral journey.

Contents

1 Introduction **1**

1.1 Synaptic Plasticity Underlying Learning and Memory 1

1.2 Behavioural Habituation: "Filtering the Familiar" 3

1.2.1 Classical Theories of Habituation 5

1.2.2 The Synaptic Depression Model in Aplysia 5

1.3 The Model Organism *Drosophila melanogaster* 6

1.3.1 Binary Expression Systems 7

1.3.2 Genetically Encoded Calcium Indicators 8

1.4 Olfaction in *Drosophila melanogaster* 11

1.4.1 Architecture of the Olfactory System 12

1.4.2 Odour Information Processing 18

1.4.3 Encoding of Odour Valence 21

1.5 Olfactory Habituation in *Drosophila melanogaster* 22

1.5.1 Habituation of an Olfactory Avoidance Response 24

1.5.2 Neuronal Circuit Model for Olfactory Avoidance Habituation . . . 25

1.6 Aim of the Study 28

2 Materials and Methods **29**

2.1 Materials 29

2.1.1 Fly Stocks 29

2.1.2 Fly Food 31

2.1.3 Reagents and Consumables 31

2.1.4 Buffers and Solutions 32

2.1.5 Enzymes 32

2.1.6 Laboratory Equipment 33

2.2 Methods 35

2.2.1 Fly Husbandry 35

2.2.2 Testing Potential Recombinants 35

2.2.3 The Behaviour Assay 36

2.2.4 Calcium Imaging 39

3 Results **49**

3.1 Establishing a Novel Behaviour Assay for Studying Olfactory Habituation . 49

3.1.1 Continuous 30-minute EB Exposure 50

3.1.2 Pulsed Exposure to Different Odour Concentrations 52

3.1.3 Pulsed Exposure to Different Lengths of Interstimulus Intervals . . 54

3.1.4 Mutants Defective in Olfactory Short-Term Habituation 55

3.1.5 Discussion 58

3.2 Establishing a Calcium Imaging Protocol for Olfactory Short-Term Habituation 61

3.3 Characterisation of Odour-Evoked Synaptic Plasticity in Projection Neurons 71

3.3.1 Different Odour Concentrations 72

3.3.2 1-Hour Recovery 79

3.3.3 Mock-Exposure 83

3.3.4 Changes in Baseline 85

3.3.5 Discussion 88

3.4 The Requirement of Synaptic Proteins for Odour-Evoked Synaptic Plasticity 95

3.4.1 $GABA_A$ and NMDA Receptors in the PN Postsynapse 96

3.4.2 Synapsin in the GABAergic LN1 Presynapse 98

3.4.3 Discussion 99

3.5 Odour-Induced Cellular Adaptations in Other Cell Types 101

3.5.1 Olfactory Sensory Neurons 103

3.5.2 Local Interneurons 114

3.5.3 Discussion 117

3.6 Measuring Membrane Voltage and Synaptic Vesicle Release 125

3.6.1 Measuring Membrane Voltage Using ArcLight 126

3.6.2 Measuring Synaptic Vesicle Release Using SynaptopHluorin 131

3.6.3 Discussion 131

3.7 The Effect of Blocking Presynaptic Inhibition 135

3.7.1 $GABA_A$ and $GABA_B$ Receptors in OSN Terminals 136

3.7.2 Discussion 139

4 Discussion **143**

4.1 One Neuronal Circuit Underlying Different Forms of Olfactory Habituation? 143

4.2 Physiological Changes Associated with Olfactory Avoidance Habituation . 145

4.3 Peripheral or Central Adaptation? 146

4.4 Presynaptic vs. Postsynaptic Inhibition 148

4.5 Odour Image- or Glomerulus-Specific Inhibition? 150

4.6 A Modified Neuronal Circuit Model 152

4.7 Concluding Remarks 154

5 Appendices **157**

5.1 Appendix I: Fly Crosses 157

5.2 Appendix II: Statistical Tables 160

5.3 Appendix III: PID Measurements 218

List of Figures

1.1 Schematic of the Cameleon and GCaMP genetically encoded Ca^{2+} indicators 10
1.2 Anatomy of the *Drosophila* olfactory system 13
1.3 Neuronal map of the *Drosophila* olfactory system 16
1.4 Neuronal connectivity within the *Drosophila* olfactory system 17
1.5 Y-maze assay for measuring olfactory avoidance 24
1.6 Circuit model for olfactory avoidance habituation 26

2.1 The odour-evoked locomotor startle response assay 37
2.2 Fly holder 39
2.3 Fly preparation for functional imaging 40
2.4 Prototype odour delivery system 41
2.5 Final odour delivery system 43
2.6 Imaging protocols 44

3.1 Continuous 30-minute EB exposure to different concentrations 51
3.2 Pulsed EB exposure to different concentrations 53
3.3 Pulsed exposure to different lengths of interstimulus intervals 55
3.4 Odour-induced startle response habituation does not require *rutabaga* in GABAergic LNs and NMDA receptors in PNs 57
3.5 Dorsal view onto one of the antennal lobes 63
3.6 Representative images of the two planes imaged 64
3.7 Preliminary Ca^{2+} imaging protocol 66
3.8 Changes in odour-evoked Ca^{2+}-influxes in PNs after 15-minute odourant exposure to 10% EB 67
3.9 Final Ca^{2+} imaging protocol 69
3.10 GCaMP responses to a 10-second EB stimulus delivered by the final odour delivery system 70
3.11 Changes in odour-evoked Ca^{2+}-influxes in PNs after 15-minute odourant exposure to 3ppm EB 73
3.12 Comparison of odour- and KCl-evoked GCaMP6m fluorescence responses in PNs 74
3.13 Naïve odour-evoked Ca^{2+}-influxes in PNs to 3ppm and 20ppm EB 76

3.14 Quantified changes in odour-evoked Ca^{2+}-influxes in PNs after 15-minute odourant exposure to 3ppm and 20ppm EB 77
3.15 Changes and recovery in odour-evoked Ca^{2+}-influxes in PNs after 15-minute odourant exposure to 3ppm EB 80
3.16 Quantified changes and recovery in odour-evoked Ca^{2+}-influxes in PNs after 15-minute odourant exposure to 3ppm and 20ppm EB 82
3.17 Quantified comparisons of odour-evoked Ca^{2+}-influxes in PNs between a naïve, a 'mock' exposed, and a 1-hour delayed 3ppm EB presentation . . . 84
3.18 Baseline shifts in GCaMP signal in PNs after 15-minute odourant exposure to 3ppm EB 86
3.19 Quantified baseline fluorescence changes in PNs after 15-minute odourant exposure 87
3.20 The effect of $GABA_A$ and NMDA receptor knockdown in PNs on exposure-induced changes in PN GCaMP responses 97
3.21 The effect of synapsin knockdown in LN1 interneurons on exposure-induced changes in PN GCaMP responses 99
3.22 Schematic of the glomerular innervation pattern of different LN types . . . 102
3.23 Changes in odour-evoked Ca^{2+}-influxes in OSNs after 15-minute odourant exposure to 3ppm EB 104
3.24 Naïve odour-evoked Ca^{2+}-influxes in OSNs to 3ppm and 20ppm EB 106
3.25 Quantified changes in odour-evoked Ca^{2+}-influxes in OSNs after 15-minute odourant exposure to 3ppm and 20ppm EB 106
3.26 Quantified comparisons of odour-evoked Ca^{2+}-influxes in OSNs after 'mock' exposure 108
3.27 Quantified changes and recovery in odour-evoked Ca^{2+}-influxes in OSNs after 15-minute odourant exposure to 3ppm and 20ppm EB 110
3.28 Quantified baseline fluorescence changes in OSNs after 15-minute odourant and mock exposure 113
3.29 Changes in odour-evoked Ca^{2+}-influxes in GABAergic multiglomerular LN1 neurons after 15-minute odourant exposure 115
3.30 Changes in odour-evoked Ca^{2+}-influxes in GABAergic uni- and multiglomerular LN2 neurons after 15-minute odourant exposure 115
3.31 Changes in odour-evoked Ca^{2+}-influxes in glutamatergic OK371 neurons after 15-minute odourant exposure 116
3.32 Changes in odour-evoked depolarisation in PNs after 15-minute odourant exposure. 127
3.33 Quantified changes in odour-evoked depolarisation in PNs after 15-minute odourant exposure. 128
3.34 Changes in odour-evoked depolarisation in GH146-labelled PNs after 'mock' treatment. 129

3.35 ArcLight indicator range in antennal lobe neurons tested by EB odour or KCl bath application in representative neurons 130
3.36 $GABA_B$ receptor knockdown in OSNs alters exposure-induced changes in odour-evoked OSN GCaMP responses 137
3.37 $GABA_A$ receptor subunit knockdown in OSNs alters exposure-induced changes in odour-evoked OSN GCaMP responses 138

4.1 Increased pre- and postsynaptic inhibition following odourant exposure . . 155

List of Tables

1.1 Overview of the three sensilla types 14

2.1 Laser power for different genotypes 45

3.1 Statistics comparing odour- and KCl-evoked GCaMP6m responses in PNs . 74
3.2 PN GCaMP responses to 3ppm EB 78
3.3 PN GCaMP responses to 20ppm EB 78
3.4 Statistics: Recovery of PN GCaMP responses to 3ppm and 20ppm EB . . . 81
3.5 Statistics comparing GCaMP fluorescence baselines in PNs 88
3.6 Summary of exposure-induced changes in PN activity 90
3.7 OSN GCaMP responses to 3ppm EB 107
3.8 OSN GCaMP responses to 20ppm EB 107
3.9 Statistics: Recovery of OSN GCaMP responses to 3ppm EB 111
3.10 Statistics comparing GCaMP fluorescence baselines in OSNs 112
3.11 Summary of exposure-induced changes in glomerular GCaMP responses measured in OSNs or PNs 120
3.12 Comparison of exposure-induced changes in GCaMP and ArcLight responses in PNs 132

4.1 Summary of exposure-induced changes in OSN and PN activity 145

5.1 Likelihood ratio test models 161
5.2 Linear mixed effects analysis for GH146GCaMP6m 3ppm EB and KCl . . 162
5.3 Paired comparisons for GH146GCaMP6m 3ppm EB and KCl 163
5.4 Linear mixed effects analysis for GH146GCaMP6m 3ppm EB 164
5.5 Linear mixed effects analysis for GH146GCaMP6m 3ppm EB baseline . . 164
5.6 Paired comparisons for GH146GCaMP6m 3ppm EB 165
5.7 Linear mixed effects analysis for GH146GCaMP6m 20ppm EB 166
5.8 Linear mixed effects analysis for GH146GCaMP6m 20ppm EB baseline . . 166
5.9 Paired comparisons for GH146GCaMP6m 20ppm EB 167
5.10 Linear mixed effects analysis for GH146GCaMP6m comparing 3ppm and 20ppm EB 168
5.11 Linear mixed effects analysis for GH146GCaMP6m 3ppm EB recovery . . 169
5.12 Linear mixed effects analysis for GH146GCaMP6m 3ppm EB recovery DL1 170

5.13 Linear mixed effects analysis for GH146GCaMP6m 3ppm EB recovery DL5 170
5.14 Linear mixed effects analysis for GH146GCaMP6m 3ppm EB recovery DM1 171
5.15 Linear mixed effects analysis for GH146GCaMP6m 3ppm EB recovery DM2 171
5.16 Linear mixed effects analysis for GH146GCaMP6m 3ppm EB recovery DM3 172
5.17 Linear mixed effects analysis for GH146GCaMP6m 3ppm EB recovery DM5 172
5.18 Linear mixed effects analysis for GH146GCaMP6m 3ppm EB recovery DM6 173
5.19 Linear mixed effects analysis for GH146GCaMP6m 20ppm EB recovery . . 174
5.20 Linear mixed effects analysis for GH146GCaMP6m 20ppm EB recovery DL1 175
5.21 Linear mixed effects analysis for GH146GCaMP6m 20ppm EB recovery DL5 175
5.22 Linear mixed effects analysis for GH146GCaMP6m 20ppm EB recovery DM1 176
5.23 Linear mixed effects analysis for GH146GCaMP6m 20ppm EB recovery DM2 176
5.24 Linear mixed effects analysis for GH146GCaMP6m 20ppm EB recovery DM3 177
5.25 Linear mixed effects analysis for GH146GCaMP6m 20ppm EB recovery DM5 177
5.26 Linear mixed effects analysis for GH146GCaMP6m 20ppm EB recovery DM6 178
5.27 Linear mixed effects analysis for GH146GCaMP6m mock 179
5.28 Linear mixed effects analysis for GH146GCaMP6m mock baseline 179
5.29 Linear mixed effects analysis for GH146GCaMP6m mock DM5 179
5.30 Linear mixed effects analysis comparing naïve responses of flies expressing Rdl-RNAi in PNs and controls 180
5.31 Linear mixed effects analysis comparing naïve and exposed responses of flies expressing Rdl-RNAi in PNs and controls 180
5.32 Linear mixed effects analysis comparing naïve and exposed responses of flies expressing Rdl-RNAi in PNs and controls in DM5 181
5.33 Linear mixed effects analysis comparing naïve responses of flies expressing NR1-RNAi in PNs and controls 181
5.34 Linear mixed effects analysis comparing naïve and exposed responses of flies expressing NR1-RNAi in PNs and controls 182
5.35 Linear mixed effects analysis comparing naïve and exposed responses of flies expressing NR1-RNAi in PNs and controls in DM5 182
5.36 Linear mixed effects analysis comparing naïve responses of flies expressing Syn-RNAi in LN1s and controls 183
5.37 Linear mixed effects analysis comparing naïve and exposed responses of flies expressing Syn-RNAi in LN1s and controls 183
5.38 Linear mixed effects analysis for Or83bGCaMP6m 3ppm EB 184
5.39 Linear mixed effects analysis for Or83bGCaMP6m 3ppm EB baseline . . . 185
5.40 Paired comparisons for Or83bGCaMP6m 3ppm EB 186
5.41 Linear mixed effects analysis for Or83bGCaMP6m 20ppm EB 187
5.42 Linear mixed effects analysis for Or83bGCaMP6m 20ppm EB baseline . . 188
5.43 Paired comparisons for Or83bGCaMP6m 20ppm EB 189

5.44 Linear mixed effects analysis for Or83bGCaMP6m comparing 3ppm and 20ppm 190
5.45 Linear mixed effects analysis for Or83bGCaMP6m 3ppm EB recovery . . . 191
5.46 Linear mixed effects analysis for Or83bGCaMP6m 3ppm EB recovery DL1 192
5.47 Linear mixed effects analysis for Or83bGCaMP6m 3ppm EB recovery DL5 192
5.48 Linear mixed effects analysis for Or83bGCaMP6m 3ppm EB recovery DM1 193
5.49 Linear mixed effects analysis for Or83bGCaMP6m 3ppm EB recovery DM2 193
5.50 Linear mixed effects analysis for Or83bGCaMP6m 3ppm EB recovery DM3 194
5.51 Linear mixed effects analysis for Or83bGCaMP6m 3ppm EB recovery DM5 194
5.52 Linear mixed effects analysis for Or83bGCaMP6m 3ppm EB recovery DM6 195
5.53 Linear mixed effects analysis for Or83bGCaMP6m 20ppm EB recovery . . 196
5.54 Linear mixed effects analysis for Or83bGCaMP6m 20ppm EB recovery DL1 197
5.55 Linear mixed effects analysis for Or83bGCaMP6m 20ppm EB recovery DL5 197
5.56 Linear mixed effects analysis for Or83bGCaMP6m 20ppm EB recovery DM1 198
5.57 Linear mixed effects analysis for Or83bGCaMP6m 20ppm EB recovery DM2 198
5.58 Linear mixed effects analysis for Or83bGCaMP6m 20ppm EB recovery DM3 199
5.59 Linear mixed effects analysis for Or83bGCaMP6m 20ppm EB recovery DM5 199
5.60 Linear mixed effects analysis for Or83bGCaMP6m 20ppm EB recovery DM6 200
5.61 Linear mixed effects analysis for Or83bGCaMP6m mock 201
5.62 Linear mixed effects analysis for Or83bGCaMP6m mock baseline 201
5.63 Paired comparisons for Or83bGCaMP6m mock 202
5.64 Linear mixed effects analysis for LN1GCaMP6m 3ppm EB 203
5.65 Paired comparisons for LN1GCaMP6m 3ppm EB 203
5.66 Linear mixed effects analysis for LN2GCaMP6m 3ppm EB 203
5.67 Paired comparisons for LN2GCaMP6m 3ppm EB 204
5.68 Linear mixed effects analysis for OK371GCaMP6m 3ppm EB 204
5.69 Paired comparisons for OK371GCaMP6m 3ppm EB 204
5.70 Linear mixed effects analysis for GH146ArcLight 3ppm EB 205
5.71 Linear mixed effects analysis for GH146ArcLight 3ppm EB baseline 206
5.72 Paired comparisons for GH146ArcLight 3ppm EB 206
5.73 Linear mixed effects analysis for GH146ArcLight mock 207
5.74 Paired comparisons for GH146ArcLight mock 208
5.75 Linear mixed effects analysis for GH146ArcLight comparing naïve responses of mock and EB 208
5.76 Linear mixed effects analysis for GH146ArcLight comparing naïve and exposed responses of mock and EB 208
5.77 Linear mixed effects analysis comparing naïve responses of flies expressing GBi-RNAi in OSNs and controls 209
5.78 Linear mixed effects analysis comparing naïve and exposed responses of flies expressing GBi-RNAi in OSNs and controls 210

5.79 Linear mixed effects analysis comparing naïve and exposed responses of flies expressing GBi-RNAi in OSNs and controls in DM1 211
5.80 Linear mixed effects analysis comparing naïve and exposed responses of flies expressing GBi-RNAi in OSNs and controls in DM2 212
5.81 Linear mixed effects analysis comparing naïve and exposed responses of flies expressing GBi-RNAi in OSNs and controls in DM5 213
5.82 Linear mixed effects analysis comparing naïve responses of flies expressing Rdl-RNAi in OSNs and controls 214
5.83 Linear mixed effects analysis comparing naïve and exposed responses of flies expressing Rdl-RNAi in OSNs and controls 215
5.84 Linear mixed effects analysis comparing naïve and exposed responses of flies expressing Rdl-RNAi in OSNs and controls in DM1 216
5.85 Linear mixed effects analysis comparing naïve and exposed responses of flies expressing Rdl-RNAi in OSNs and controls in DM2 216
5.86 Linear mixed effects analysis comparing naïve and exposed responses of flies expressing Rdl-RNAi in OSNs and controls in DM5 217
5.87 PID measurements for GH146GCaMP6m 3ppm 218
5.88 PID measurements for GH146GCaMP6m 20ppm 218
5.89 PID measurements for GH146GCaMP6m KCl 218
5.90 PID measurements for Or83bCaMP6m 3ppm 219
5.91 PID measurements for Or83bCaMP6m 20ppm 219
5.92 PID measurements for Or83bCaMP6m mock 219
5.93 PID measurements for LN1CaMP6m 3ppm 220
5.94 PID measurements for LN2CaMP6m 3ppm 220
5.95 PID measurements for OK371CaMP6m 3ppm 220
5.96 PID measurements for GH146ArcD 3ppm 221
5.97 PID measurements for GH146ArcD mock 221

Abbreviations

AL	Antennal lobe
AMPAR	α-Amino-3-hydroxy-5-methyl-4-isoxazolepropionic acid receptor
Ca^{2+}	Calcium
CaM	calcium-binding protein calmodulin
cpGFP	circularly permuted green fluorescence protein
CO_2	Carbon dioxide
CS	CantonS
EB	ethyl butyrate
ECFP	enhanced cyan fluorescent protein
EYFP	enhanced yellow fluorescent protein
g	gram
GABA	Gamma-AminoButyric Acid
$GABA_ARs$	$GABA_A$ receptors
$GABA_BRs$	$GABA_B$ receptors
GAD1	Glutamate decarboxylase 1
GECI	Genetically Encoded Calcium Sensor
GEVI	Genetically Encoded Voltage Sensor
GFP	Green fluorescence protein
GPCRs	G protein-coupled receptors
GRs	Gustatory receptor
iGluRs	Ionotropic glutamate receptor
IP_3	Inositol 1,4,5-trisphosphate
IP_3R	Inositol 1,4,5-trisphosphate receptor
IRs	Ionotropic receptor
KCs	Kenyon Cells
L	litre
lexAop	LexA Operator (LexA binding domain)
LH	Lateral Horn
LHN	Lateral Horn Neurons
LNs	Local interneurons
LTH	Long-term habituation
LTD	Long-term depression

LTM	Long-term memory
LTP	Long-term potentiation
M13	CaM-interacting peptide
MBs	Mushroom Bodies
Mg^{2+}	Magnesium
mL	millilitre
mM	milliMolar
Na^{+}	Sodium
NMDA	N-methyl-D-aspartate
NMDARs	N-methyl-D-aspartate receptors
OSNs	Olfactory sensory neurons
ORs	Odorant receptors
PID	Photoionisation detector
PNs	Projection neurons
ppb	Parts per billion
ppm	Parts Per Million
PTFE	PolyTetraFluoroEthylene
QUAS	Upstream Activating Sequence
RyR	Ryanodine receptor
SSRs	Single-Sensillum Recordings
sr	Signed Rank
STH	Short-Term Habituation
STM	Short-Term memory
TRP	transient receptor potential
UAS	Upstream Activating Sequence
VGCCs	voltage-gated Ca^{2+} channels

1. Introduction

1.1 Synaptic Plasticity Underlying Learning and Memory

The complexity of neuronal wiring ranges from a few hundred neurons in nematodes to 100 billions in humans. While the overall structure of nervous systems is hard-wired, neuronal connections are constantly strengthened or weakened through experiences encountered by the organism. The process of experience-dependent changes in synaptic connectivity is called 'synaptic plasticity', a phenomenon that underlies varies forms of learning and memory (Kandel, 2001; Ho et al., 2011; Lamprecht and LeDoux, 2004).

Commonly, two fundamentally different forms of memory are being distinguished: *implicit* and *explicit* memory (Kandel et al., 2000). Implicit memory refers to learned performances of tasks such as reflexive motor or perceptual skills. Explicit memory relates to factual knowledge of previous experiences and information about people, places and things. Implicit memory arises through *associative* and *non-associative* forms of learning (Kandel et al., 2000). During associative learning either a stimulus is associated with a reinforcement such as a reward or punishment, as in the case of classical conditioning firstly described by Pavlov (Clark, 2004), or a behaviour is associated with a consequence of that behaviour, as in the case of operant conditioning studied by Skinner (Staddon and Cerutti, 2003). Non-associative learning occurs in response to a single stimulus, as in the case of *sensitisation*, leading to an increased behavioural response (Hawkins et al., 2006; Kandel, 2001), or *habituation*, resulting in a decreased behavioural output (Glanzman, 2009; Thompson, 2009; Christoffersen, 1997). Both, explicit and implicit forms of memory are initially stored as rather fragile short-term memory (STM) before they are transformed into a more permanent long-term memory (LTM; Kandel et al., 2000).

During learning, particular patterns of neuronal activity induce synaptic plasticity which lead to changes in synaptic efficacy and neural excitability that outlast the events that trigger them (Kandel, 2001; Ho et al., 2011; Lamprecht and LeDoux, 2004). Long-term potentiation (LTP) results in synaptic strengthening while long-term depression (LTD) yields synaptic weakening (Bear and Malenka, 1994; Malenka and Bear, 2004). Both, LTP and LTD occur at excitatory and inhibitory synapses (Malenka and Bear, 2004; Castillo et al., 2011; Kullmann and Lamsa, 2011). Different patterns of stimulation elicit changes in synaptic strength that persist over various durations, with short-lasting and long-lasting forms similar to the memory stages they underlie (Kandel, 2001). Short-term plasticity involves modifications of

pre-existing proteins that lead to the strengthening or weakening of pre-existing connections (Kandel, 2001) while long-term synaptic changes require protein synthesis and are accompanied by the growth of new synaptic connections (Yin and Tully, 1996; Silva et al., 1998). Short-term plasticity and long-term synaptic plasticity have pre- and postsynaptic components, although they are not necessarily both found at the same synapse (Malenka and Bear, 2004; Glanzman, 2010).

Presynaptic changes in synaptic strength alter the probability of neurotransmitter release upon neuronal stimulation (Castillo et al., 2011; Castillo, 2012; Ho et al., 2011; Malenka and Bear, 2004). By changing the number of synaptic vesicles available for release synapses are strengthened or weakened. A family of phosphoproteins called *synapsins* are involved in this process as these proteins promote the entry of synaptic vesicles into the readily releasable pool that is depleted upon neuronal stimulation (Ho et al., 2011; Bykhovskaia, 2011). Another form of presynaptic plasticity involves docking and priming of synaptic vesicles to the plasma membrane to allow rapid fusion following activity-dependent Ca^{2+} influx into the presynaptic terminal. This process is mediated by the RIM (Rab3-interacting molecule) family of proteins which cluster Ca^{2+} channels in the active zone and support efficient SNARE (soluble NSF-attachment protein receptor) complex formation required for bringing vesicle and membrane into close proximity (Castillo et al., 2011; Ho et al., 2011; Malenka and Bear, 2004). Several forms of presynaptic plasticity are triggered by retrograde messengers, molecules produced in the postsynaptic cell that travel back across the synapse to modulate presynaptic neurotransmitter release (Castillo et al., 2011; Castillo, 2012).

Synaptic strength at the postsynapse is predominantly altered by the number and sensitivity of neurotransmitter receptors present in dendritic spines (Ho et al., 2011; Malenka and Bear, 2004). One mechanisms of adjusting postsynaptic strength is the phosphorylation of postsynaptic proteins including neurotransmitter receptors which increases or decreases receptor channel function (Castillo et al., 2011; Ho et al., 2011; Malenka and Bear, 2004). Another form is activity-dependent insertion and removal of neurotransmitter receptors into or out of the plasma membrane (Ho et al., 2011). While the prevalence of α-Amino-3-hydroxy-5-methyl-4-isoxazolepropionic acid-type glutamate receptors (AMPARs) determines the strength of excitatory synapses that of inhibitory synapses is regulated by the frequency of Gamma-Amino Butyric Acid A-type receptors ($GABA_A$Rs; Castillo et al., 2011; Malenka and Bear, 2004). At many synapses, postsynaptic N-methyl-D-aspartate-type glutamate receptors (NMDARs), which are activated by the coincidence of presynaptic glutamate release and postsynaptic depolarisation, are required for the induction of plasticity changes (Ho et al., 2011; Malenka and Bear, 2004).

Longer-lasting forms of synaptic plasticity require both gene transcription and local mRNA translational of synaptic proteins that result in growth of synaptic connections (Ho et al., 2011; Kandel, 2001; Malenka and Bear, 2004). Activity-dependent regulation of gene transcription is achieved through kinases and transcriptional factors that translocate from the synapse to the nucleus. One example of a transcriptional regulator that mediates long-term

plasticity is the cAMP-responsive element binding protein (CREB) which binds the cAMP response element in gene regulatory sequences and thereby increases or decreases gene transcription (Kandel, 2001; Sakamoto et al., 2011). Synapse-specific plasticity is achieved by activity-dependent local translation of synaptic mRNAs, which are normally stored in a repressed state (Bramham and Wells, 2007; Costa-Mattioli et al., 2009; Martin and Zukin, 2006). This process is controlled by mRNA binding proteins (RBPs). Some RBPs directly bind specific sequences in the 3′ untranslated region of mRNAs to up- or down-regulate translation. Others interact with components of the microRNA pathway such as members of the RNA-induced silencing complex which either suppresses translation or facilitates degradation of their target mRNA.

1.2 Behavioural Habituation: "Filtering the Familiar"

The term habituation describes a behavioural response decrement that results from repeated or prolonged sensory stimulation and is not caused by sensory receptor adaptation or motor fatigue (Rankin et al., 2009; Thompson and Spencer, 1966; Thompson, 2009). Habituation is often referred to as the "the simplest form of learning" (Rankin et al., 2009; Wilson and Linster, 2008) and can occur at different time scales: habituation induced by a single training session is termed short-term habituation (STH), habituation resulting from extended or repeated training sessions is called long-term habituation (LTH; Rankin et al., 2009; Thompson and Spencer, 1966; Thompson, 2009). A number of habituation characteristics, originally described by Thompson and Spencer (1966) and more recently revised by Rankin et al. (2009), have been defined with the most important being: 1.) repeated or continuous presentation of a sensory stimulus results in a decreased behavioural response, 2.) presentation of a different stimulus results in an increase of the behavioural response decrement to the original stimulus (so called "dishabituation"), and 3.) within the same stimulus modality, less intense stimuli result in a more rapid and/or more pronounced decrease in the behavioural response than more intense stimuli (Rankin et al., 2009; Thompson and Spencer, 1966; Thompson, 2009).

Habituation provides an important filtering mechanisms for sensory information as it allows for filtering out irrelevant sensory stimuli to enable focussing on important ones such as novel and salient features of the environment (Rankin et al., 2009; Wilson and Linster, 2008). Filtering out innocuous sensory informations is a prerequisite for many cognitive tasks (Wilson and Linster, 2008). Psychological disorders such as schizophrenia and autism spectrum disorder have been hypothesised to be associated with defects in this filtering mechanism (Braff et al., 2001; Holt et al., 2005; Meincke et al., 2004; Akdag et al., 2003; Guiraud et al., 2011; Kleinhans et al., 2009; Lombardo et al., 2009). A common trait in individuals with these disorders is that they cannot effectively attend their environment as all sensory inputs compete, a feature which likely has negative effects on higher cognitive function such as different forms of learning and memory.

Habituation is considered to be the most basic form of non-associative implicit learning and belongs to the earliest studied forms of learning first described in the nineteenth century where Peckham and Peckham (1887) reported a spider's escape response caused by a vibrating tuning fork (Christoffersen, 1997). Here, a female spider displayed a diminished escape response to the sound of a vibrating fork after repeated presentations (Peckham and Peckham, 1887). Over a century of research has revealed that behavioural habituation can be ubiquitously found throughout the animal kingdom (Christoffersen, 1997). Examples for behaviours that exhibit habituation are the defensive withdrawal of the earthworm after tactile stimulation (Kuenzer, 1958), the escape swimming of the guppy when stimulated by a shadow (Russell, 1967), and the leg reflex in dogs (Sherrington, 1906).

Despite being studied for decades and the behaviour being well described, the neuronal and cellular mechanisms underlying habituation are only beginning to be understood. Classical theories explain habituation by either increased inhibition or opponent interactions between sensitisation and habituation (see section 1.2.1 for details). A prominent model which has been supported experimentally in some systems is the "synaptic depression model" where the decrement associated with habituation is explained by homosynaptic depression (Christoffersen, 1997; see section 1.2.2 for synaptic depression in *Aplysia*). However, more recent discoveries indicate that synaptic depression may only explain simple forms of habituation such as those associated with reflex arcs (Christoffersen, 1997; Ramaswami, 2014). It appears that a multitude of homo- and heterosynaptic mechanisms underlie habituation depending on the complexity of the system studied, the sensory modality, the level of sensory information processing, as well as the temporal stimulation pattern (Schmid et al., 2014; Ramaswami, 2014).

More complex forms of habituation are those where percepts that are encoded in a combinatorial neuronal code become familiar (Ramaswami, 2014), as for example during olfactory habituation. Here, an odour percept consists of the combined activity of individual sensory channels and each sensory channel contributes to several different odour percepts (Laurent, 1997). Filtering out inconsequential odour stimuli during habituation allows an organism to selectively focus on scents relevant for the organism's survival such as those that predict an approaching predator or a rich food source. In mammals, a transient form of olfactory habituation, lasting for a few minutes, is caused by synaptic depression within the mammalian piriform cortex, a higher brain centre involved in olfaction (McNamara et al., 2008; Wilson and Linster, 2008). A longer lasting form, persistent for at least 30 minutes, has been suggested to be due to changes in inhibitory transmission within the olfactory bulb, the mammalian primary olfactory processing centre (Chaudhury et al., 2010; McNamara et al., 2008; Wilson and Linster, 2008). However, advances in deciphering the underlying neuronal circuit and molecular changes of olfactory habituation in mammals have been complicated due to the complexity of the nervous system. In contrast, the olfactory system of the fruit fly *Drosophila melanogaster* is comparably simple but shares many architectural and functional similarities with mammalian olfactory systems (Su et al., 2009; Davis, 2004). These advan-

tages combined with its accessibility to functional studies and genetic manipulation make the fruit fly a valuable model organism for the investigation of olfactory habituation.

1.2.1 Classical Theories of Habituation

Over the years a number of theoretical frameworks have been proposed to explain the process of habituation with the most prominent ones being Evgeny Sokolov's Stimulus-Model Comparator Theory, Wagner-Konorski Gnostic Unit Theory, and Groves and Thompson Dual-Process Theory (Thompson, 2009).

Evgeny Sokolov's Stimulus-Model Comparator Theory is based on the idea that a sensory stimulus becomes encoded as a neural model after repeated presentations and as the neural model develops it exerts inhibition on the so called "amplifying system" which normally drives behavioural output (Sokolov, 1963). A naïve stimulus presentation exerts no or minimal inhibition on the amplifying system as the neural model has not been formed yet and the amplifying system therefore drives strong behavioural output. However, with repeated stimulus presentations the neural model becomes more similar to the sensory stimulus, thus driving strong inhibition onto the amplifying system and suppressing behavioural output. The Wagner-Konorski Gnostic Unit Theory is very similar to Sokolov's Stimulus-Model Comparator Theory with the only substantial difference that the neural model formed after repeated stimulus presentations is stored as a memory in the so called "gnostic assembly" (Wagner, 1979).

The Groves and Thompson Dual-Process Theory is based on the assumption that a sensory stimulus activates two independent opponent processes in the brain, a decremental (habituation) and an incremental (sensitization) which interact to yield a final behavioural outcome (Groves and Thompson, 1970). Within this model, habituation is opposed to behavioural sensitization, an independent mechanism that leads to an increased behavioural response. The dominant component of the two mechanisms thus determines the behavioural outcome.

1.2.2 The Synaptic Depression Model in Aplysia

Although habituation had been reported in a variety of invertebrate and vertebrate preparations before (Christoffersen, 1997), only when habituation was studied in the marine snail, *Aplysia californica*, some of the mechanisms underlying habituation were revealed (Glanzman, 2009; Gover and Abrams, 2009). Eric Kandel and colleagues were the first to investigate habituation of the defensive gill- and siphon-withdrawal reflex in response to weak tactile stimulation of the skin (Castellucci et al., 1970; Kupfermann et al., 1970). They identified sensory neurons in the abdominal ganglion that are activated by mechanical stimulation of the siphon skin (Castellucci et al., 1970) as well as their postsynaptic motor neurons which execute the withdrawal reflex (Kupfermann et al., 1970). Their findings defined the monosynaptic connection between sensory neurons and motor neurons as the critical locus for the

reflex and thus enabled the direct investigation of this form of habituation at a neuronal level.

Both, STH and LTH of the gill- and siphon-withdrawal reflex have been reported, lasting up to 30 minutes or 3 weeks respectively (Castellucci et al., 1970; Kupfermann et al., 1970; Carew et al., 1972). During both forms of learning the *Aplysia* sensorimotor synapses undergo rapid and profound homosynaptic depression (Castellucci and Kandel, 1974; Carew and Kandel, 1973). Short-term depression of these synapses appears to arise exclusively due to presynaptic changes in sensory neurons (Castellucci and Kandel, 1974). Depletion of the readily releasable pool of vesicles has historically been seen as the primary explanation for short-term depression (Gingrich and Byrne, 1985; Gover and Abrams, 2009). However, it is now thought that synaptic depression is predominantly mediated by an activity-dependent deactivation of vesicle release sites initiated by Ca^{2+} influx (Gover et al., 2002; Royer et al., 2000; Gover and Abrams, 2009). More persistent long-term depression that underlies LTH, however, cannot be explained by presynaptic changes solely but rather involves additional postsynaptic processes such as activation of AMPA and NMDA receptors as well as the activity of voltage-dependent Ca^{2+} channels (Esdin et al., 2010; Ezzeddine and Glanzman, 2003).

1.3 The Model Organism *Drosophila melanogaster*

Drosophila melanogaster was first implemented as a model organism by Thomas Hunt Morgan who performed mutant analysis and cross-breading experiments with the aim to study genetic heritability (Hales et al., 2015). Since his discovery of the first gene mutation in 1910, the sex-linked *white* gene responsible for the fly's eye colour (Morgan, 1910), mutant analysis are an essential aspect of *Drosophila* research. Since then numerous mutants have contributed considerably to the understanding of genetic heritability and have also proven extremely useful for the investigation of fly behaviour and its underlying mechanisms (Baker et al., 2001; Benzer, 1967, 1973; Vosshall, 2007).

Since Morgan's pioneering work a multitude of sophisticated genetic tools have been established that facilitate the analysis of gene function in the fly, making it the most genetically accessible model organism among higher eukaryotes (Venken et al., 2011; Beckingham et al., 2005). Examples for these genetic advances are balancer chromosomes which prevent uncontrolled recombination and thereby allow mutations to be maintained over generations (Muller, 1918), germline transformations which enable the stable implementation of transgenic material into the fly genome (Rubin and Spradling, 1982; Spradling and Rubin, 1982), binary expression systems which allow for spatio- and temporal-specific transgene expression (Brand and Perrimon, 1993; Lai and Lee, 2006; Potter et al., 2010; see section 1.3.1), as well as the sequencing of the whole *Drosophila* genome (Adams et al., 2000).

Besides its genetic advantages, *Drosophila melanogaster* is a popular model organism due to its short generation time, its simple and economic breeding and living conditions as well as its large numbered progeny (Beckingham et al., 2005; Greenspan, 1989; Hales

et al., 2015). For the study of neuronal circuits *Drosophila* is frequently selected due to its comparably simple nervous system. The fly brain consists of only ~10^5 neurons compared to an estimate of $10^8 - 10^{11}$ neurons in mammals (Venken et al., 2011). Nevertheless, the *Drosophila* and mammalian nervous systems share many commonalities ranging from neurotransmitters and synaptic proteins to cellular second messenger pathways (Venken et al., 2011; Yoshihara et al., 2001). Thus, discoveries in fruit flies have guided research efforts in vertebrates to a great extend (Bellen et al., 2010).

Importantly, despite their simplicity fruit flies demonstrate complex behaviours such as visual and olfactory associative learning and various forms of behavioural habituation (Waddell and Quinn, 2001; Vosshall, 2007; Engel and Wu, 2009; Simpson, 2009). While many fly behaviours have been characterised in much detail dating back to the beginnings of *Drosophila* research, monitoring the changes in neuronal activity associated with the behaviour has only become possible recently. Technical advances within the last two decades now allow electrophysiological patch clamp recordings, as a direct, and functional imaging methods (see section 1.3.2), as an indirect measure for neuronal activity (Simpson, 2009). Combining these techniques with genetic tools such as spatial- and temporal-restricted manipulations of neuronal activity or transgene expression enable the investigation of neuronal circuits and neuronal pathways underlying behaviour in *vivo* (White and Peabody, 2009; Venken et al., 2011; Simpson, 2009; Olsen and Wilson, 2008a).

1.3.1 Binary Expression Systems

Binary expression systems enable targeted gene expression of an effector construct in a cell- and time-specific manner (Duffy, 2002; Venken et al., 2011; del Valle Rodríguez et al., 2012). Examples for its application are labelling of distinct cell populations, spatial- and temporal-restricted gene expression, spatial- and temporal-restricted gene knockdown through the expression of transgenic RNAi constructs, manipulation of neuronal activity in distinct cell populations as well as spatio-restricted expression of genetically encoded fluorescence indicators (see section 1.3.2). The approach is based on the combination of two transgenic constructs in one animal. The first construct, termed the driver, determines the spatial expression of the second construct, termed the effector, which defines the transgene expressed (Duffy, 2002; Venken et al., 2011).

The Gal4/UAS binary expression system was the first developed and is also the one most frequently used (Fischer et al., 1988; Brand and Perrimon, 1993). Here, the driver carries the gene encoding for the yeast transcription factor GAL4 which is expressed under the control of either genomic or modified enhancer sequences. This enhancer sequence determines the spatial and temporal expression of the Gal4 protein (Fischer et al., 1988). The effector carries the gene of interest controlled by an Upstream Activating Sequence (UAS) which is specifically bound by the GAL4 (Brand and Perrimon, 1993). In flies carrying the Gal4 and the UAS elements, the GAL4 protein binds the UAS sequence and thus initiates the transcription of the gene of interest in a spatio-specific manner (Brand and Perrimon, 1993; Duffy, 2002;

Venken et al., 2011). To also allow for temporal control of transgene expression, a temperature sensitive version of the GAL4 repressor GAL80 is expressed along with the GAL4 and UAS constructs. $GAL80^{ts}$ prevents GAL4 expression at permissive temperatures but enables it upon shift to higher temperatures (McGuire et al., 2004b,a).

The LexA/LexAop and Q binary expression systems rely on the same principle. The LexA/LexAop system is based on a LexA transactivator that binds to the LexA binding domain from a bacterial transcription factor (the LexA operator or LexAop; Lai and Lee, 2006). In the Q system, which is based on a cluster of regulatory genes from *Neurospora crassa*, the transactivator QF binds to a QF Upstream Activating Sequence (QUAS) and thereby activates the transcription of the gene of interest (Potter et al., 2010). Combination of the different binary expression systems makes it possible to express a genetically encoded fluorescence indicator in one cell type (see section 1.3.2) while manipulating neuronal activity or expressing a protein in another.

1.3.2 Genetically Encoded Calcium Indicators

The investigation of how perturbing neuronal activity or gene expression levels in specific neuronal types alters a behavioural outcome is an important approach in order to discern whether a neuronal population or protein is required for the behaviour. To fully decipher the underlying neuronal circuitry it is, however, essential to also directly monitor the neuronal activity of neurons that are part of the circuitry. In *Drosophila*, physiological measurements have been proven difficult due to the fly's small neuron size which makes electrophysiological recordings of single cells challenging. Only recently, patch clamp recordings from central neurons of the *Drosophila* brain have been established (Wilson et al., 2004). However, these recordings can be mechanically invasive and are restricted to small numbers of neurons at a time whereas most sensory stimuli and motor outputs are encoded in neuronal ensembles. To enable simultaneous physiological recordings from tens to hundreds of neurons at a time, a large number of genetically encoded fluorescence indicators have been developed that target various aspects of neural physiology, from membrane depolarisation and ion flux to downstream signal transduction cascades (Barth, 2007; Looger and Griesbeck, 2012; Miyawaki, 2003). Many of these fluorescence indicators have been successfully used in *Drosophila*, such as sensors for cytosolic Ca^{2+} influx (reviewed in Riemensperger et al., 2012), membrane voltage (Cao et al., 2013), synaptic vesicle release (Ng et al., 2002), chloride influx (Haynes et al., 2015), and intracellular cAMP or protein kinase A concentration (Gervasi et al., 2010; Tomchik and Davis, 2009).

As with other model organisms (Grienberger and Konnerth, 2012), genetically encoded Ca^{2+} indicators (GECIs) which detect changes in Ca^{2+} concentration have been utilized to monitor neuronal activity in *Drosophila* (reviewed in Riemensperger et al., 2012). Ca^{2+} is a ubiquitous intracellular second-messenger molecule that enters the cell through receptor channels from the extracellular space or internal stores and controls numerous cellular processes (Clapham, 1995; Berridge et al., 2000; Bootman et al., 2001b,a). Neurons contain

voltage-gated Ca^{2+} channels (VGCCs) which open upon depolarisation of the cell allowing Ca^{2+} to rush into the cell. N- and P/Q-type VGCCs at synaptic endings trigger the release of neurotransmitters. The L-type voltage-gated VGCCs on the cell body, dendrites and spines provide Ca^{2+} signals that mediate transcriptional and translational control (Berridge et al., 2000). When Ca^{2+} enters the cell the majority is rapidly bound to various cytosolic buffers which control the amplitude and duration of the Ca^{2+} signal and limit the spatial spreading of Ca^{2+} signals, thus allowing for a local action of the signal (Berridge et al., 2000). After Ca^{2+} has carried out its signalling functions it is rapidly removed from the cytoplasm by various pumps and exchangers that transport it back into the extracellular space or internal stores (Berridge et al., 2000). As changes in intracellular Ca^{2+} concentrations are tightly coupled to membrane voltage (Berridge et al., 2000; Bootman et al., 2001a) GECIs provide an excellent tool for studying neuronal activity.

GECIs are composed of variants of the green fluorescent protein (GFP; Whitaker, 2010; Griesbeck, 2004). Since their development (Miyawaki et al., 1997; Romoser et al., 1997) a variety of probes have been described which differ in their principle mode of action, their dynamic range, Ca^{2+} affinities, selectivity, intrinsic baseline fluorescence and kinetic properties (Pérez Koldenkova and Nagai, 2013; Hires et al., 2008; Tian et al., 2012; Whitaker, 2010). Commonly two types of GECIs are being distinguished: FRET-based sensors and single chromophore sensors (Whitaker, 2010; Griesbeck, 2004). FRET-based sensors are dual-wavelength ratiometric fluorescence indicators (Whitaker, 2010). They consist of two GFP variants comprising a donor chromophore, often a cyan variant of GFP (e.g. enhanced cyan fluorescent protein, ECFP), and an acceptor chromophore, often a yellow variant of GFP (e.g. enhanced yellow fluorescent protein, EYFP). The two variants are linked by a Ca^{2+} binding sequence. In FRET-based GECIs that belong to the Cameleon family, the binding sequence consists of a Ca^{2+} binding domain of calmodulin (CaM) and the CaM binding peptide M13 (Miyawaki et al., 1997, see Figure 1.1 A). Ca^{2+} binding to the sensor leads to a conformational change which enhances the Föster resonance energy transfer (FRET) from donor to acceptor (Jares-Erijman and Jovin, 2003). In the case of ECFP/EYFP-based FRET sensors, an increase in the ligand concentration can be detected by a decrease in emission intensity from the donor chromophore ECFP (at ~485 nm) and an increase in emission intensity from the acceptor chromophore EYFP (at ~535 nm) when the donor chromophore ECFP was excited at ~440 nm (see Figure 1.1 A). Single chromophore sensors are single-wavelength nonratiometric sensors (Whitaker, 2010) and consist of a modified GFP variant coupled to a Ca^{2+} binding sequence. In many cases the GFP variant is a circularly permuted GFP variant (cpGFP) where new C- and N-termini have been introduced by fusing the former C- and N-termini. As for Cameleons, the Ca^{2+} binding sequence of nonratiometric sensors that belong to the GCaMP family consists of a CaM binding domain and M13 (Nakai et al., 2001, see Figure 1.1 B). Ca^{2+} binding to the binding sequence causes a conformational change of the entire molecule which results in an increase in fluorescence emission.

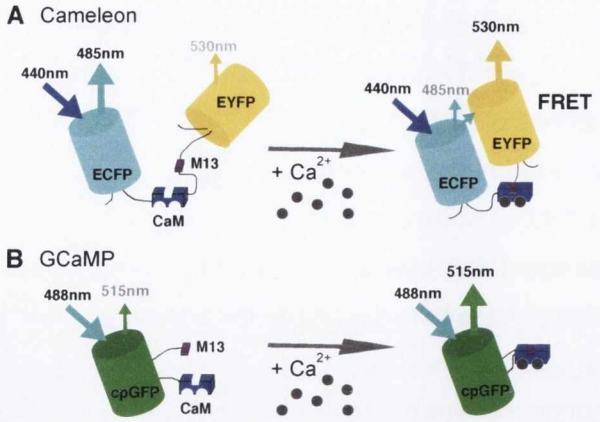


Figure 1.1: Schematic of the Cameleon and GCaMP genetically encoded Ca^{2+} indicators
Typically two types of genetically encoded Ca^{2+} indicators (GECIs) are distinguished: FRET-based sensors and single chromophore sensors. **(A)** FRET-based GECIs of the Cameleon family consist of two GFP variants: an enhanced cyan fluorescent protein (ECFP) as the donor chromophore and an enhanced yellow fluorescent protein (EYFP) as the acceptor chromophore. The two GFP variants are linked by the Ca^{2+} binding domain of calmodulin (CaM) and the CaM binding peptide M13 (Miyawaki et al., 1997). Ca^{2+} binding to the sensor leads to a conformational change which enhances the Föster resonance energy transfer (FRET) from donor to acceptor resulting in a decreased emission from ECFP and an increased emission from EYFP. **(B)** The single chromophore sensor GCaMP consists of a circularly permuted GFP variant (cpGFP) that is coupled to CaM and M13 (Nakai et al., 2001). Ca^{2+} binding to the sensor causes a conformational change which results in increase fluorescence emission. *Figure modified after Riemensperger et al., 2012*

In *Drosophila*, both ratiometric and nonratiometric GECIs have been used to study neuronal Ca^{2+} dynamics (Fiala and Spall, 2003; Riemensperger et al., 2012), with Cameleon and GCaMP variants being the most frequently availed (Fiala and Spall, 2003; Wang et al., 2003). FRET-based sensors have the advantage that changes in Ca^{2+} concentration are usually reported as the ratio between the intensity changes at the two wavelengths so that effects of confounding artefacts are minimized (Kao et al., 2010). However, single chromophore GCaMP sensors have been the favoured choice over the last few years as they provide a higher signal-to-noise ratio and require a less complicated optical imaging setup since simultaneous detection of two emission spectra is not required (Riemensperger et al., 2012).

The first GCaMP sensor available in flies was GCaMP1.3 (Nakai et al., 2001; Wang et al., 2003). Its effectiveness as a reporter of neuronal activity was studied by combining *in vivo* electrophysiological recordings from individual olfactory projection neurons and simultaneous Ca^{2+} imaging in response to odours (Jayaraman and Laurent, 2007). The sensor revealed limitations with respect to sensitivity and kinetics: GCaMP1.3 had a high detection threshold, often failed to capture spike response kinetics accurately and missed high instantaneous activity if that was not sustained. GCaMP1.3 signals were further only weakly correlated with the neurons mean firing rate even if the neuronal activity was well-above the detecting threshold of the sensor. GCaMP1.3 was followed by GCaMP1.6 (Ohkura et al., 2005). The two sensors were compared in an *in vivo* analysis with ten genetically encoded calcium indicators where Ca^{2+} imaging was performed in presynaptic boutons of the *Drosophila* larval neuromuscular junction (Reiff et al., 2005). GCaMP1.6 was among

the best sensor tested and showed substantial advancements in kinetics and sensitivity when compared to GCaMP1.3. GCaMP1.6 exhibited the largest and fastest fluorescence changes among the sensors tested but also suffered substantially from photo-bleaching. In contrast to GCaMP1.3 which only showed dim fluorescence at rest the baseline fluorescence of the GCaMP1.6 sensor was greatly increased. A considerable improvement was made with the development of the GCaMP3 variant (Tian et al., 2009). The sensor had a 3-fold higher baseline fluorescence, a greater protein stability, a 3-fold wider dynamic range and a 1.3-fold higher Ca^{2+}-affinity *in vitro* compared to its precursor GCaMP2 (Tallini et al., 2006). Since GCaMP2 did not express well in *Drosophila* (Hendel et al., 2008) the GCaMP3 indicator was compared to GCaMP1.6 in flies showing that GCaMP3 exhibited a better signal-to-noise ratio than GCaMP1.6 (Tian et al., 2009). Odour-evoked fluorescence responses in olfactory projection neurons were 4-6-fold increased with the GCaMP3 sensor. Subsequent optimizations of the GCaMP protein provided sensors with even higher signal-to-noise ratio, wider dynamic range and improved kinetics (Akerboom et al., 2012; Sun et al., 2013; Ohkura et al., 2012; Chen et al., 2013). The currently available GCaMP indicators, including fast GCaMPs and GCaMP6 variants, provide an excellent range of tools to investigate Ca^{2+}-dynamics in neuronal compartments and enable the choice between sensors that have particular fast kinetics or large signal-to noise ratio (Sun et al., 2013; Chen et al., 2013).

Ca^{2+} imaging In *Drosophila* has so far been particularly useful to investigate the mechanisms underlying sensory processing of olfactory, gustatory, visual, and auditory stimuli (reviewed in Riemensperger et al., 2005). Ca^{2+} imaging experiments determined the response spectra of particular sensory cells (Silbering et al., 2008), revealed how specific sensory stimuli are represented over a population of sensory neurons (Fiala et al., 2002; Wang et al., 2003), identified the specific projection patterns of sensory neurons that are activated by particular stimuli (Niewalda et al., 2011; Silbering et al., 2008) and discerned spatial organisation in the internal representation of sensory stimuli in higher brain centres (Strutz et al., 2014; Honegger et al., 2011). Ca^{2+} imaging has furthermore been used to study neuronal plasticity underlying associative and non-associative forms of learning and memory (Wang et al., 2008; Yu et al., 2006; Akalal et al., 2010; Sachse et al., 2007; Das et al., 2011b).

1.4 Olfaction in *Drosophila melanogaster*

Most animals have evolved olfactory systems to extract vital information from airborne, volatile chemical substances within their environment such as the presence of food or predators. Olfactory cues are not only essential for an animal's survival they also control social and sexual interactions between individuals of the same species. A good example are sex pheromones that stimulate mating behaviours (Dickson, 2008). To detect and distinguish between a huge diversity of odour identities complex olfactory systems have evolved which are widely conserved between species (Ache and Young, 2005; Hildebrand and Shepherd, 1997; Strausfeld and Hildebrand, 1999). The challenge of detecting a vast amount of odours

is met by a large repertoire of odour receptors, discrimination between them is achieved by a combinatorial coding strategy forming precise neural representations of individual odour stimuli within the brain (Su et al., 2009; Leinwand and Chalasani, 2011).

Most odours carry either positive or negative valence: Food odours are for instance innately attractive allowing for the localisation of food sources and thereby permitting survival while predator smells are aversive, alluding death (Knaden and Hansson, 2014). Olfactory associative learning where an odour stimulus is associated with reward or punishment can alter the innately encoded odour valence, thus enabling an animal to adjust its odour preferences to prior experiences (McGuire et al., 2005). Olfactory habituation allows an animal to focus only on vital odours, such as those which indicate an approaching predator or the location of a food source, while ignoring familiar ones in its environment (Wilson and Linster, 2008).

In the following, the architecture of the *Drosophila* olfactory system (section 1.4.1) and its way to process odour informations (section 1.4.2) will be described. The knowledge of how odour features are represented on a neuronal level is essential for the understanding of the neuronal changes occurring during olfactory habituation. The encoding of odour valence will further be overviewed (see section 1.4.3) as the mechanisms of olfactory habituation could either change the innately encoded valence of an odour, thus making the odour less aversive or attractive, or it could reduce the sensory perception of the odour entirely (Twick et al., 2014).

1.4.1 Architecture of the Olfactory System

Drosophila melanogaster detects odourants in its environment through olfactory sensory neurons (OSNs) that are located in two sensory organs: The antenna and the maxillary palp. OSNs project via the antennal nerve and the labial nerve to the antennal lobe (AL), a bilateral brain structure involved in primary processing of olfactory information. The main output from the AL are second-order projection neurons (PNs) that project to higher olfactory centres, primarily the mushroom bodies (MBs) and the lateral horn of the protocerebrum (LH). The MBs, among other things, are important for olfactory learning and memory whereas the LH is thought to be predominantly involved in innate olfactory behaviours (Figure 1.2) (reviewed in Vosshall and Stocker, 2007; Su et al., 2009).

Peripheral Odour Detection in the Antennae and Maxillary Palps

At the periphery odours are detected by odourant receptors expressed on the surface of olfactory sensory neurons (OSNs) which are housed in sensilla, hair-like structures covering the third antennal segments and the maxillary palps (Shanbhag et al., 1999). Three major sensilla types are distinguished with respect to their morphological structure and odour responsiveness (see Table 1.1). Basiconic sensilla are activated by food odours, coeloconic sensilla respond to odours contained in food as well as to small amines and humidity levels, and tricoid sensilla are highly sensitive to pheromones. Basiconic sensilla can be found on

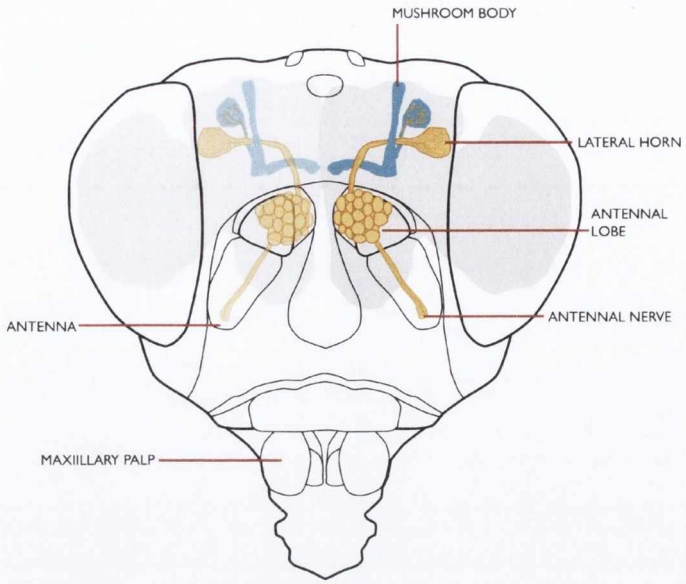


Figure 1.2: Anatomy of the *Drosophila* olfactory system
Odour molecules are detected at the dendrites of olfactory sensory neurons (OSNs) within the fly's antennae and maxillary palps. From here OSNs project via the antennal nerve and the labial nerve (omitted for clarity) to the antennal lobe (AL), the fly's primary olfactory processing centre. The principle output from the AL are second-order projection neurons (PNs) which project to higher olfactory centres, namely the mushroom bodies (MBs) and the lateral horn (LH). The MBs are important for olfactory associative learning and memory whereas the LH is thought to mediate innate olfactory behaviours. *Figure from Twick et al., 2014*

both the antenna and the maxillary palp, while trichoid and coeloconic sensilla are located exclusively on the antenna (Clyne et al., 1997; de Bruyne et al., 1999, 2001; Shanbhag et al., 1999; Stocker, 1994; Yao et al., 2005; Van Der Goes Van Naters and Carlson, 2007).

The odour response profile of a given sensilla type is dependent on the OSN types it houses. Each sensilla type contains a stereotyped set of OSN types, with one to four OSNs per sensillum (de Bruyne et al., 1999, 2001; Yao et al., 2005). Most OSNs express a unique odourant receptor which defines their odour response profile (Couto et al., 2005; Goldman et al., 2005; Hallem et al., 2004; Hallem and Carlson, 2006; Fishilevich and Vosshall, 2005; Silbering et al., 2011). Three classes of receptors have been described: odourant receptors (ORs), gustatory receptors (GRs), and ionotropic receptors (IRs) (reviewed in Nakagawa and Vosshall, 2009; Ronderos and Smith, 2009).

ORs are the fly's predominant class of odourant receptors. They form an insect-specific family of seven membrane-spanning protein domains with a cytoplasmic N-terminus and an extracellular C-terminus (Clyne et al., 1999; Vosshall et al., 1999; Gao and Chess, 1999; Lundin et al., 2007). Insect ORs act as part of a heteromeric complex composed of a variable odourant binding subunit, 1 of the 62 ORs (Vosshall et al., 2000; Fishilevich and Vosshall, 2005), and a universal co-receptor, the Or83b or Orco protein (Larsson et al., 2004; Neuhaus et al., 2005; Benton, 2006). ORs function primarily as ligand-gated ion channels however they have also been linked to an additional slower metabotropic pathway (Nakagawa and Vosshall, 2009; Sato et al., 2008; Smart et al., 2008; Wicher et al., 2008; Kain et al., 2008).

GRs are distantly related to ORs and predominantly expressed in taste neurons. However,

Sensilla Type	basiconic sensilla	coeloconic sensilla	trichoid sensilla
Location	antenna maxillary palps	antenna	antenna
Response Profile	food odours CO_2	pheromones	food odours small amines humidity levels
Receptors	1 of 62 ORs co-receptor Or83b (GR21a & GR63a)	1 of 64 IRs co-receptors IR8 & IR25a	1 of 62 ORs co-receptor Or83b

Table 1.1: Overview of the three sensilla types

two of these receptors, GR21a and GR63a, are co-expressed in one OSN type and are stimulated by carbon dioxide (CO_2) (Jones et al., 2007; Kwon et al., 2007). IRs are insect-specific members of the ionotropic glutamate receptor family (iGluRs). They have a distinct ligand-binding domain compared to other known iGluR classes but likewise form ion-channels that are directly activated by extracellular ligand-binding (Benton et al., 2009; Rytz et al., 2013). 66 IRs have been identified, two of which, IR8 and IR25a, appear to function as co-receptors (Benton et al., 2009). Similar to iGluRs, IRs form a heteromultimer complex that consists of up to three subunits: The individual odour-specific IR and one or two broadly expressed co-receptors (Abuin et al., 2011).

All basiconic and trichoid OSNs express OR genes, with the exception of the GR21a/GR63a CO_2-sensing neurons (Couto et al., 2005; Fishilevich and Vosshall, 2005; Jones et al., 2007; Kwon et al., 2007). The specific OR/Or83b subunit compositions within these OSNs determines whether the neuron responds to food odours or pheromones. Basiconic sensilla express ORs that are activated by food odours while trichoid ORs respond to pheromones (de Bruyne et al., 1999, 2001; Yao et al., 2005). Coeloconic sensilla house OSNs that express IRs and their respective co-receptors (Benton et al., 2009; Rytz et al., 2013).

OSN that extend their dendrites into the third antennal segment, bundle their axons in the antennal nerve. Those located in the maxillary palp join in the labile nerve. Both nerves, consisting of around 1200 OSNs per hemisphere, project to the antennal lobe (AL), a bilateral brain structure involved in primary olfactory processing (Stocker et al., 1990; Tanaka et al., 2012; Figure 1.3). Most axonal branches target both the ipsilateral and the contralateral side of the AL (Stocker et al., 1990). The AL is composed of around 56 distinct neuropils per hemisphere, called glomeruli (Laissue et al., 1999). Each glomerulus receives excitatory cholinergic input from a particular population of OSNs. With only few exceptions, all OSNs expressing the same odourant receptor converge upon a discrete glomerulus in the AL (Vosshall et al., 2000; Fishilevich and Vosshall, 2005; Couto et al., 2005; Goldman et al., 2005; Gao et al., 2000). Projections from different sensilla types tend to cluster in the AL:

Antennal basiconic neurons project to medial glomeruli, trichoid neurons to lateral ones, coeloconic to the ones ventral, and palp basiconic to anterior glomeruli (Couto et al., 2005; Grabe et al., 2015a).

Primary Olfactory Processing in the Antennal Lobe

Within a given glomerulus, OSNs form synapses with projection neurons (PNs), the AL output neurons, and local interneurons (LNs) whose arborisations are restricted to the AL (Stocker et al., 1990; Tanaka et al., 2012; Wang et al., 2014) (Figure 1.3). At the AL input a high convergence of information takes place (~25:1) as ~1,200 OSNs project onto ~50 glomeruli (Laissue et al., 1999; Stocker et al., 1990; Stocker, 2001). By contrast, a 1:4 divergence occurs at the AL output since more than ~200 PNs leave the ~50 glomeruli per hemisphere (Jefferis et al., 2001; Marin et al., 2002; Tanaka et al., 2012).

PN axons bundle together in one of four AL tracts which project to higher olfactory centres (Lai et al., 2008; Stocker et al., 1990; Tanaka et al., 2012). A major class of ~150 PNs are uniglomerular and cholinergic and therefore termed excitatory PNs (ePNs). This class receives synaptic input from OSNs and LNs and projects via the medial antennal lobe tract (mALT) to the MBs, the LH and other brain regions (Jefferis et al., 2001; Lai et al., 2008; Marin et al., 2002; Tanaka et al., 2004, 2012; Wong et al., 2002) (Figure 1.3). A second class with ~50 PNs, termed inhibitory PNs (iPNs), are multiglomerular and GABAergic (GABA = Gamma-AminoButyric Acid). Neurons of this class project via the medio-lateral antennal lobe tract (mlALT) and innervate the LH, bypassing the MB altogether (Lai et al., 2008; Marin et al., 2002; Okada et al., 2009; Tanaka et al., 2012; Wong et al., 2002) (Figure 1.3). The other two AL tracts, the lateral (lALT) and transverse (tALT), are more diverse in terms of their neuronal projections (Lai et al., 2008; Tanaka et al., 2012).

AL output is highly modulated by a dense network of around 200 local interneurons (LNs) that show a diversity of morphological structures and neurotransmitter types (Root et al., 2007; Chou et al., 2010; Seki et al., 2010; Tanaka et al., 2012). Around half of the LNs arborise unilaterally within one AL, while the other half arborise bilaterally between the lobes. The majority of LNs innervate several glomeruli, so called multiglomerular LNs, whereas only a minority are restricted to a small subset of glomeruli, the oliglomerular LNs (Chou et al., 2010; Lai et al., 2008; Okada et al., 2009; Seki et al., 2010; Tanaka et al., 2012). Within a given glomerulus LNs form chemical and/or electrical synapses with OSNs, PNs, and other LNs (Huang et al., 2010; Olsen and Wilson, 2008b; Tanaka et al., 2012; Yaksi and Wilson, 2010).

The two principle neurotransmitters secreted by LNs are GABA and glutamate, both of which are primarily inhibitory in the AL (Das et al., 2011a; Okada et al., 2009). Two major classes of GABA-releasing LNs are commonly distinguished: Type I and type II LNs (also termed LN1s and LN2s) (Chou et al., 2010; Okada et al., 2009; Seki et al., 2010; Tanaka et al., 2009). LN1s have extensive arborisations in most of the AL glomeruli with processes targeting the glomerular core (Okada et al., 2009; Tanaka et al., 2009, 2012). LN2s are

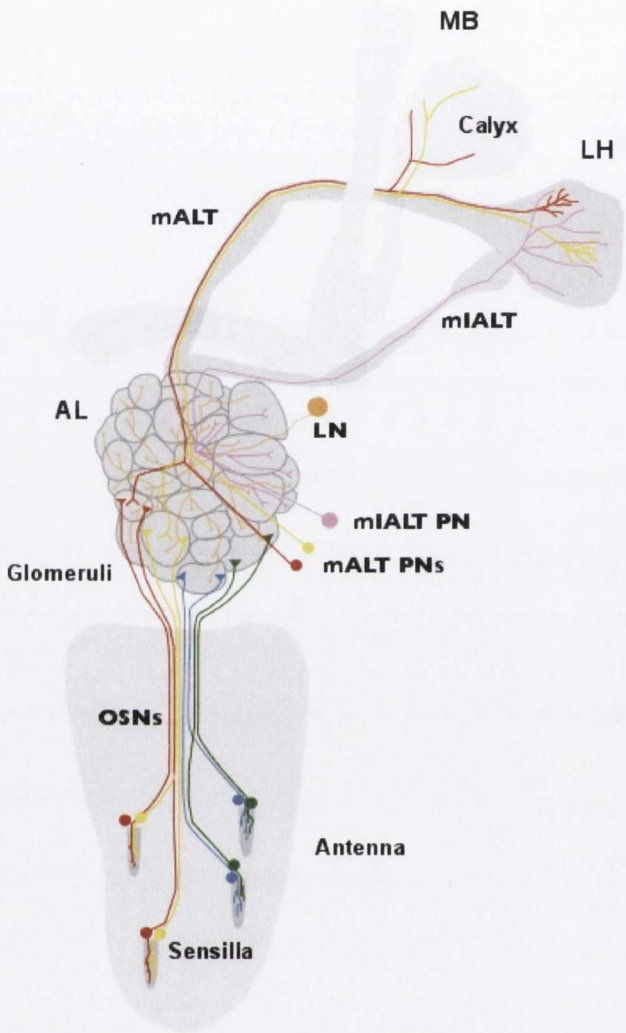


Figure 1.3: Neuronal map of the *Drosophila* olfactory system
Olfactory sensilla house one to four different olfactory sensory neuron (OSN) types in a stereotyped manner. Each OSN type expresses a unique odourant receptor and projects to a single glomerulus in the antennal lobe (AL) (represented by different colours). AL glomeruli form microcircuits composed of OSNs, projection neurons (PNs) and local interneurons (LNs). PNs, the AL output neurons, leave the AL in four tracts (only the medial (mALT) and medio-lateral (mLALT) antennal lobe tract are depicted). The majority of PNs runs through the mALT, including uniglomerular excitatory PNs (ePNs) (depicted in red and yellow), and project to the calyx of the mushroom bodies (MBs) and the lateral horn of the protocerebrum (LH). The mlALT contains multiglomerular inhibitory PNs (iPNs) (depicted in pink) and connects the AL to the LH, bypassing the MB calyx altogether. Within the AL olfactory information are substantially processed by LNs whose arborisations are restricted to the AL and innervate a subset or the majority of glomeruli (depicted in orange). Most LNs are inhibitory but excitatory and neuromodulatory LNs also exist. *Figure adapted from Twick et al., 2014*

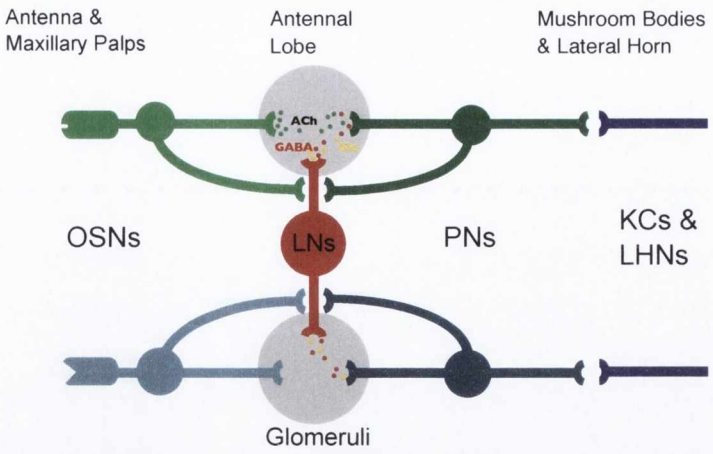


Figure 1.4: Neuronal connectivity within the *Drosophila* olfactory system
Each olfactory sensory neuron (OSN) type, characterized by expressing a unique odourant receptor, projects to a specific glomerulus in the antennal lobe (AL). In the AL, OSNs form synapses with projection neurons, the majority of which form synaptic connections with kenyon cells (KCs) and/or lateral horn neurons (LHNs) in the mushroom bodies and the lateral horn of the protocerebrum. Within the AL, odour-evoked neuronal responses are modulated by local interneurons (LNs) which are activated by OSNs and PNs. LNs are predominantly inhibitory and release the neurotransmitters GABA or glutamate. *Figure adapted from Twick et al., 2014*

more heterogeneous with some neurons arborising in most of the glomeruli and others with more restricted arborisation patterns of about two-third of the glomeruli (Okada et al., 2009; Tanaka et al., 2009, 2012). Unlike those of LN1s, LN2 terminals target both the core and the peripheral areas of a glomeruli (Okada et al., 2009; Tanaka et al., 2009). The different arborisation sites of the two classes within a glomerulus is of particular interest as OSN terminals reside in the glomerular rind whereas PN dendrites are situated in both the core and the rind of a glomerulus (Tanaka et al., 2009). The arborisation patterns therefore suggest that LN1s form synapses with PNs, while LN2s form synaptic connections with OSNs and PNs (Tanaka et al., 2009, 2011). In contrast to GABAergic LNs, glutamatergic LNs appear to have their neuronal processes primarily in the spaces between glomeruli (Das et al., 2011a).

Odour information processing within the AL is furthermore highly modulated by a diversity of intrinsic and extrinsic neuromodulatory neurons. Besides the inhibitory neurotransmitters, LNs also release acetylcholine (Huang et al., 2010; Seki et al., 2010; Shang et al., 2007), dopamine (Chou et al., 2010), and several neuropeptides (Carlsson et al., 2010; Ignell et al., 2009; Nässel and Homberg, 2006), some of which are believed to be co-released with other neurotransmitters (Carlsson et al., 2010; Ignell et al., 2009; Nässel and Homberg, 2006). Extrinsic neurons which link the AL neuropil to various other brain regions (Tanaka et al., 2012; Stocker et al., 1990) and thus allow for top-down modulation of olfactory processing release serotonin (Carlsson et al., 2010; Dacks et al., 2009; Roy et al., 2007; Tanaka et al., 2012), octopamine (Busch et al., 2009), and neuropeptides (Carlsson et al., 2010; Nässel, 2002).

Presentation of Odourant Information within Second-Order Olfactory Centres: The Mushroom Bodies and the Lateral Horn

The two major classes of PNs send projections to distinct higher brain areas, ePNs send their dendrites to the MBs and LH whereas iPNs only target the LH (Lai et al., 2008; Tanaka et al., 2012). The MB mediates olfactory memory formation (Heisenberg et al., 1985; Heisenberg, 2003; Davis, 2005), whereas the LH appears to be involved in innate olfactory behaviours (Heimbeck et al., 2001; Parnas et al., 2013; Strutz et al., 2014).

In the MB calyx (see Figure 1.3), the primary input region of the MBs, ePNs form synaptic connections with intrinsic MB neurons, called Kenyon cells (KCs) (Stocker et al., 1990). At the MB input a high divergence (1:17) of ~150 ePNs onto ~2500 KCs takes place. ePNs that receive input from a specific glomerular subset in the AL also target distinct zones within the MB calyx whereas each KC integrates PN inputs from a single to multiple of these target zones (Tanaka et al., 2004). Due to their high firing threshold and PN-input integration properties, KCs are thought to act as coincidence detectors that only fire when they receive excitatory input from all PNs they form synapses with, proposing a sparsening of odour coding within the MB neuropil (Heisenberg, 2003; Perez-Orive et al., 2002). In line with this, only very few KCs out of the large KC population respond to a given odour stimulus (Honegger et al., 2011; Luo et al., 2010; Turner et al., 2008). A sparse odour representation where each KC represents a specific odour percept is thought to not only enable the contextualisation of novel sensory experiences (Caron et al., 2013) but to also facilitate the association of the odour percept with a positive or negative valence, the foundation for associative forms of learning and memory (Heisenberg, 2003; Davis, 2005).

In the LH (see Figure 1.3), ePNs likewise map onto glomerular-dependent stereotypic zones, retaining the spatial representation established in the AL to a certain extend (Marin et al., 2002; Tanaka et al., 2004; Wong et al., 2002). The LH shows compartmentalization in terms of specific glomerular subgroups that ePNs innervate (Tanaka et al., 2004; Marin et al., 2002) and the ePN's responsiveness to fruity odours or pheromones (Jefferis et al., 2007). The arborisations of third-order LH neurons (LHN) are similarly restricted to the discrete target zones of ePN terminals (Tanaka et al., 2004). LHNs receive input from sparse and stereotyped combinations of glomeruli that are co-activated by odours (Fişek and Wilson, 2014), suggesting that only little integration between different odour channels takes place in the LH. This is consistent with its role for mediating innate behaviours to odours (Heimbeck et al., 2001; Tanaka et al., 2004).

1.4.2 Odour Information Processing

Olfactory systems are posed with the challenge of extracting physical features of an odour stimulus such as odour identity, odour concentration, and the rate of change in odour concentration. How do OSNs, as the first-order neurons of the *Drosophila* olfactory system, extract these features from the chemosensory space and how are they translated into neu-

ronal activity patterns using a spatio-temporal code? Furthermore, how is the encoding of these features altered in second-order neurons, the PNs, and how does the dense network of LNs reshape the neuronal representation of odour stimuli?

Olfactory Sensory Neurons

Odour identity at the OSN level is encoded by the pattern of active OSN types whereas each OSN type expresses a unique odourant receptor (Couto et al., 2005; Goldman et al., 2005; Fishilevich and Vosshall, 2005). Most OSN types are activated by multiple odourants and, conversely, most odourants trigger neuronal responses in multiple OSN types (de Bruyne et al., 1999, 2001; Hallem and Carlson, 2006; Silbering et al., 2011). Individual OSN types vary in levels of spontaneous activity and can be narrowly or broadly tuned in terms of their odourant specificity (de Bruyne et al., 1999, 2001; Hallem and Carlson, 2006). Notably, odours do not always have an excitatory effect on OSN spiking. Ligand binding to certain odourant receptors can suppress the spike rate below its spontaneous rate and thereby be inhibitory (de Bruyne et al., 1999, 2001; Hallem et al., 2004; Hallem and Carlson, 2006; Nagel and Wilson, 2011; Silbering et al., 2011).

At higher odour concentrations, OSNs become more broadly activated, their firing rates rise and additional OSN types are recruited (Hallem and Carlson, 2006). This recruitment is required as each OSN type is sensitive to a certain concentration range (Hallem and Carlson, 2006). OSN spike rates encode not only the odour concentration itself but also its rate of change (Nagel and Wilson, 2011). OSNs fire most strongly at odour onset, thereby increasing the speed at which the odour information is transmitted to higher brain regions (Nagel and Wilson, 2011). Within a certain concentration range the dynamics of OSN firing can be described by a linear-nonlinear model unique for each OR/odour pair (Nagel and Wilson, 2011; Martelli et al., 2013). Outside the concentration range, OSNs show tonic low-rate or prolonged high firing rate responses (Martelli et al., 2013).

Prolonged odourant exposure results in a time-dependent, reversible decay in OSN firing and also reduces the OSN's response to subsequent stimuli (de Bruyne et al., 1999; Nagel and Wilson, 2011). This phenomenon, termed sensory adaptation, allows OSNs to use their dynamic range more efficiently (Zufall and Leinders-Zufall, 2000): OSNs show a decreased sensitivity to weak stimuli but an increased sensitivity to strong stimuli.

Projection Neurons

Due to the high convergence of OSNs onto ePNs (~50:3), ePNs show less variable responses to the same odour stimulus than their presynaptic OSNs (Bhandawat et al., 2007; Kazama and Wilson, 2009). Sister PNs, those that innervate the same glomerulus, not only display similar spontaneous activity caused by spontaneous OSN spiking but also exhibit highly correlated odour-induced firing rates (Kazama and Wilson, 2009).

The temporal dynamics of odour-induced ePN activity are largely influenced by the characteristics of the OSN-PN synapse (Kazama and Wilson, 2008; Wilson, 2013). Due to the

synapse' high vesicular release probability and strong short-term depression ePN responses generally peak earlier and decay more quickly than their presynaptic OSNs (Bhandawat et al., 2010; Wilson et al., 2004). ePN responses are therefore more transient with the largest activity at odour onset, thus further increasing the speed of odour processing. The relationship between OSN and ePN activity is described as "compressive nonlinear", ePNs are sensitive to small changes in OSN input when presynaptic OSNs fire at a low rate whereas they show little sensitivity to small changes in presynaptic input when OSNs fire strongly (Bhandawat et al., 2010; Olsen et al., 2010; Wilson, 2013).

ePNs and iPNs are thought to process odour informations on dual pathways (Liang et al., 2013; Wang et al., 2014). Both populations are odour responsive to overlapping ligands, however, iPNs are broader tuned than ePNs (Wang et al., 2014). While ePNs encode odour identity (Wang et al., 2003; Silbering et al., 2008) iPNs enhance innate discrimination of closely related odours (Parnas et al., 2013) and suppress LH neurons response to food odours but not pheromones (Liang et al., 2013). iPNs are further divided into two morphological subgroups: one encoding for positive valence, the other encoding odour intensity (Strutz et al., 2014).

Lateral excitation and inhibition resulting from AL LNs furthermore shape odour-induced PN activity. Excitatory LNs broaden PN responses making them less odour selective than their presynaptic OSNs (Bhandawat et al., 2010; Olsen et al., 2007; Olsen and Wilson, 2008b; Wilson et al., 2004). Inhibitory interactions between glomerular processing channels recruited by additional activity in other PNs can furthermore suppress odour-induced activity in certain PNs (Olsen and Wilson, 2008b; Silbering and Galizia, 2007).

Local Interneurons

Lateral interactions are predominantly inhibitory (Olsen and Wilson, 2008b). The two main classes of iLNs are GABAergic (Chou et al., 2010; Okada et al., 2009; Tanaka et al., 2012) and glutamatergic (Liu and Wilson, 2013). They act on OSNs, PNs, and other LNs via $GABA_A$, $GABA_B$, or GluGlα receptors (Liu and Wilson, 2013; Olsen and Wilson, 2008b; Root et al., 2008; Wilson and Laurent, 2005).

GABAergic inhibition acts predominantly presynaptically on the OSN axon terminals allowing PNs to encode changes in concentration over a broader range of concentrations (Olsen and Wilson, 2008b; Oizumi et al., 2012; Root et al., 2008). However, PNs also receive postsynaptic inhibition, but it is less pronounced and on a slower time scale (Liu and Wilson, 2013; Wilson and Laurent, 2005; Yaksi and Wilson, 2010). Due to the slow and weak nature of the postsynaptic inhibitory events it has been questioned whether postsynaptic GABAergic inhibition is mediated through direct synaptic connections or rather through volume transmission in the form of long-distance diffusion (Wilson, 2013). LNs themselves are also targets of GABAergic inhibition (Wilson and Laurent, 2005; Huang et al., 2010; Yaksi and Wilson, 2010), however as for PNs their inhibitory connections are weak and slow (Wilson, 2013). Glutamatergic inhibition similarly acts on all major cell types within the AL:

OSNs, PNs, and other LNs and is primarily mediated through volume transmission from the interglomerular space (Liu and Wilson, 2013).

Lateral inhibition scales with total OSN activity: the higher the odour intensity, the larger the overall level of inhibition in the AL (Liu and Wilson, 2013; Olsen et al., 2010; Silbering and Galizia, 2007; Silbering et al., 2008). Scaling the amount of inhibition provides a mechanism for gain control within the AL (Olsen and Wilson, 2008b; Root et al., 2008). Adjusting PN firing to the level of total OSN activity enables odour discrimination in a concentration invariant manner (Olsen and Wilson, 2008b; Olsen et al., 2010; Wilson, 2013). Lateral inhibition also reduces a PNs sensitivity to presynaptic OSN activity as an increased OSN firing rate is necessary to drive PN firing to saturation which greatly extends the dynamic range of PNs (Olsen and Wilson, 2008b; Wilson, 2013). Inhibitory input also reshapes the temporal dynamics of odour-induced PN responses making them shorter (Olsen and Wilson, 2008b; Wilson and Laurent, 2005).

iLN activity in all glomeruli can be recruited by activating a single glomerulus (Hong and Wilson, 2015). The level of iLN activation is largely odour invariant (Hong and Wilson, 2015). However, not all glomeruli receive the same level of inhibition. Some glomeruli are more sensitive to inhibitory input than others (Hong and Wilson, 2015; Olsen et al., 2010; Root et al., 2008). Sensitivity to inhibition is an autonomous feature of a given glomerulus rather than the activity or innervation of iLNs in the specific glomerulus (Hong and Wilson, 2015) and may therefore be due to GABA and/or glutamate receptor expression at the OSN presynapses or PN postsynapse (Hong and Wilson, 2015; Root et al., 2008). Interestingly, a single odour often activates glomeruli with both high and low sensitivity of inhibition (Hong and Wilson, 2015). Glomeruli with low sensitivity for inhibition may be encoders for absolute odour concentration while those with a high sensitivity may be used for odour discrimination (Hong and Wilson, 2015).

Besides the large inhibitory population of LNs, a small cholinergic subset of LNs provides excitatory input onto PNs and other LNs (Olsen et al., 2007; Root et al., 2007; Shang et al., 2007). Driven by OSN and PN activity, eLNs depolarize PNs via gap junctions rather than chemical synapses (Yaksi and Wilson, 2010; Huang et al., 2010). Chemical and electrical connections with iLNs are thought to be required to recruit inhibition throughout the AL (Yaksi and Wilson, 2010; Huang et al., 2010). Thus, eLNs have opposing effects on PNs driving both excitation and recruiting inhibition (Yaksi and Wilson, 2010).

1.4.3 Encoding of Odour Valence

Odour valence, the assignment of a positive or negative value to an odourant, is innately encoded within the *Drosophila* olfactory system (Knaden and Hansson, 2014). Food odours are innately attractive while odours that predict predators or noxious environments are aversive (Knaden and Hansson, 2014). The innately encoded valence for certain odours is vital: flies would likely not get the chance to perform consecutive learning trials to associate an innately neutral odour with a predator or noxious environment (Knaden and Hansson, 2014).

Several lines of evidence suggest that olfactory valence for certain vital odours is mediated through dedicated receptor channels, the so called "labelled lines". Innate aversion to CO_2, for example, is mediated by a single OSN type projecting to the V glomerulus in the AL (Suh et al., 2004; Jones et al., 2007; Kwon et al., 2007) whereas aversion to acids is mediated by OSNs targeting the DC4 glomerulus (Ai et al., 2010). The microbial odourant geosmin which activates OSNs that project to the DA2 glomerulus has a negative valence, alerting flies to the presence of harmful microbes (Stensmyr et al., 2012). Innate attraction to ammonia and amines is mediated by the VM1 glomerulus (Min et al., 2013) and attraction to terpenes, which are present in citrus fruits, by activity in the DC1 glomerulus (Dweck et al., 2013). Dietary antioxidants which play an important role in preventing oxidative stress are detected by the VC2 glomerulus and are innately attractive (Dweck et al., 2015a; Fishilevich and Vosshall, 2005). Attraction behaviour elicited by pheromones is mediated by OSNs projecting to the VA1d glomerulus (Dweck et al., 2015b).

While some odours are vital for a fly's survival in that they enhance survival and reproductive success the majority of odours do not have this purpose but still have an inherently encoded valence. For these odours no designated labelled lines have been identified. Instead specific sets of OSNs/PNs seem to encode positive or negative odour valence for such odours (Semmelhack and Wang, 2009; Knaden et al., 2012). One study that investigated the innately encoded valence of the food odours apple cider vinegar and ethyl butyrate found that OSNs projecting to the DM1 and VA2 glomeruli mediate behavioural attraction at low odour concentrations (Semmelhack and Wang, 2009). At higher concentrations when the odours elicited repulsion an additional glomerulus, DM5, was recruited which was shown to mediate behavioural aversion (Semmelhack and Wang, 2009). Another study performed a behavioural screen where 110 odours were tested for their inherently encoded valence and found that the representation of odour valence is encoded at the level of PNs rather than OSNs (Knaden et al., 2012). The glomeruli DM2, DM4, and DM5 were found to mediate attraction while D, DL1, DL4, DL5, DA4, and DC3 mediate aversion (Knaden et al., 2012). Interestingly, 'appetitive' glomeruli were located at the medial part of the AL, whereas 'aversive' glomeruli were situated laterally (Knaden et al., 2012). While the studies disagree on the sets of glomeruli responsible for positive and negative valence as well as on the neuronal level where odour valence is encoded both suggest that the behavioural output of attraction or aversion is mediated by the balance between 'attractive' and 'aversive' glomeruli activated.

1.5 Olfactory Habituation in *Drosophila melanogaster*

The detailed knowledge of the anatomical structure of the *Drosophila* olfactory system and the way it encodes odour identity and intensity combined with its accessibility to genetic perturbations and neurophysiological recordings make it a particularly attractive system in which to study the cellular mechanisms and neuronal circuits underlying olfactory habituation. Indeed, olfactory habituation has been studied using a range of behavioural assays

which differ in how they measure the olfactory response, how habituation is induced and the odourants tested (Chandra and Singh, 2005; Cho et al., 2004; McKenna et al., 1989; Das et al., 2011b). The olfactory jump reflex assay and the odour-evoked locomotor startle assay have been used to study the underlying mechanisms of olfactory habituation in *Drosophila*. More recently, habituation of the olfactory avoidance response has been studied in more detail: a short-term and long-term form of this behaviour have been identified (section 1.5.1) and a likely neuronal circuit model underlying this form of habituation has been suggested (section 1.5.2).

The olfactory jump reflex takes advantage of the fly's innate jump reflex upon a brief presentation of an aversive odourant such as benzaldehyde (McKenna et al., 1989). With repeated exposure the odour-evoked jump response declines (Boynton and Tully, 1992; Tully and Koss, 1992). A four second odour puff delivered with interstimulus intervals of one minute induces habituation after only a few puffs (Asztalos et al., 2007a). Consistent with the characteristics of classically defined habituation (Rankin et al., 2009; Thompson and Spencer, 1966), habituation of the olfactory jump reflex recovers spontaneously, can be dishabituated, and is dependent on stimulus frequency and odour intensity such that higher frequencies and lower concentrations induce habituation more rapidly (Asztalos et al., 2007a). In an attempt to discern the molecular components required for habituation in this paradigm, flies carrying a mutation in the adenylate cyclase *rutabaga* or the cAMP phosphodiesterase *dunce* show defects in this form of behaviour (Asztalos et al., 2007a). Five potassium channel subunits have further been shown to be required (Joiner et al., 2007) while disruption of a *Drosophila* homologue of bruton tyrosine hydroxylase showed more rapid habituation (Asztalos et al., 2007b). A high-throughput assay has further identified another 36 genotypes defective in olfactory jump response habituation (Sharma et al., 2009).

The odour-evoked locomotor startle response assay is based on a fly's sudden increase in walking speed when presented to a novel odour (Wolf et al., 2002). Habituation is induced by repeated exposure to the specific odourant (Cho et al., 2004). After four 30 second pulses of ethanol vapour delivered every six minutes the startle response is significantly reduced (Cho et al., 2004). The behaviour likewise recovers spontaneously, can be dishabituated and occurs more rapidly at higher stimulus frequencies (Cho et al., 2004). Stimulus generalization was further observed between three different odours, two of which are known to be mediated by different OSN types, suggesting that this form of habituation occurs downstream of sensory adaptations in OSNs (Cho et al., 2004). Consistent with this, chemical ablation of the mushroom bodies reduces habituation without affecting the initial odour response (Cho et al., 2004). Several mutants show defects in this form of habituation, among them mutants disrupted in *rutabaga* or the GSK-3 ortholog *shaggy* (Cho et al., 2004; Eddison et al., 2012; Wolf et al., 2007).

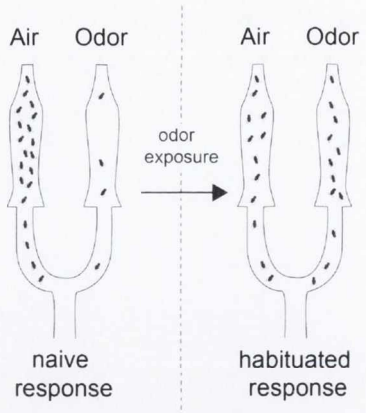


Figure 1.5: Y-maze assay for measuring olfactory avoidance
The upright positioned Y-maze apparatus consists of one arm containing an odourised air stream while the other contains pure air. Flies placed into an entry tube at the bottom of the maze move upwards due to their negative geotaxis. At the Y-junction of the two arms they have the choice of entering the odour arm or air arm. Since the odourant is aversive the majority of naïve flies choose to avoid the odour arm and instead enter the air arm. Flies that have been exposed to the specific odourant for an extended period of time show a diminished aversion of the odourant. *Figure from Twick et al. (2014)*

1.5.1 Habituation of an Olfactory Avoidance Response

Habituation of an olfactory avoidance response is measured using the 'Y-maze" assay (Rodrigues and Siddiqi, 1978) (see Figure 1.5) which is based on a fly's avoidance behaviour in response to an aversive odourant. The 'Y-maze" apparatus, a glass maze in form of a "Y", is positioned upright, one of its arms containing an odourised air stream, the other one pure air. Flies are placed into the entry tube on the bottom of the maze. Due to their innate negative geotaxis they instantly move upwards towards the air stream. When reaching the Y-junction of the two arms they have the choice to either enter the odourant arm or the air arm. The majority of naïve flies show an innate avoidance towards the aversive odourant and thus enter the air arm (Rodrigues and Siddiqi, 1978; Rodrigues, 1980). This behavioural avoidance response is calculated by an avoidance response index which represents the portion of flies choosing the air arm against the odour arm. If the flies are exposed to an odourant for an extended period of time and subsequently tested for odour preference to the same odourant, they show a diminished aversion to the aversive odour represented by a decreased avoidance response index (Das et al., 2011b).

Two different forms of olfactory avoidance habituation are distinguished according to the length of odourant exposure: Short-Term Habituation (STH) and Long-Term Habituation (LTH). STH is induced by a continuous 30-minute odourant exposure, recovers spontaneously, and can be dishabituated by either a mechanical stimulus or a puff of yeast odour (Das et al., 2011b; Sudhakaran et al., 2012). STH has been shown to occur to ethyl butyrate (EB), CO_2 and 3-octanol. Flies habituated to either of these odours do not show cross-habituation to any of the other odours (Das et al., 2011b; Sudhakaran et al., 2012). LTH, induced by four day odourant exposure to either EB, CO_2, benzaldehyde or isoamyl acetate, also recovers spontaneously, but over a longer time scale, and equally shows odourant se-

lectivity (Das et al., 2011b; Devaud et al., 2001). In contrast to STH, LTH is accompanied by morphological growth in odour-responsive glomeruli (Das et al., 2011b; McCann et al., 2011). LTH further shows a reduction in odour-evoked physiological activity in odourant-responsive glomeruli measured by GCaMP-based Ca^{2+}-imaging (Das et al., 2011b; Sachse et al., 2007). Whether STH is associated with similar changes in odour-evoked Ca^{2+} influxes into odour-responsive PNs is subject of this study.

Importantly, habituation of olfactory avoidance does not arise from peripheral adaptations of the sensory transduction machinery in OSNs. Artificial activation of genetically targeted subsets of OSNs, thus bypassing OR activation and subsequent signalling, using transgenetically expressed TRPA1 for 30 minutes to substitute for odourant exposure still elicits odour-selective STH (Das et al., 2011b). Similarly, LTH can be induced by an equally-designed 4-day artificial exposure (Das et al., 2011b). Odour-evoked neuronal activity of OSNs, measured by electroantennograms in the dendrites and by Ca^{2+}-imaging in the terminals, furthermore, remain unchanged after 4-day LTH odourant exposure (Devaud et al., 2001; Sachse et al., 2007). Taken together, these observations indicate that habituation of olfactory avoidance arises from central changes rather than sensory adaptations in OSN.

1.5.2 Neuronal Circuit Model for Olfactory Avoidance Habituation

Behavioural experiments that combined RNAi-mediated protein knockdowns or artificial activation or silencing of genetically targeted neuronal subpopulations point to a recurrent inhibitory circuit motif as the underlying source for the reduced olfactory avoidance response observed after prolonged odourant exposure (reviewed in Twick et al., 2014) (Figure 1.6). Feedback from odour-activated PNs onto LNs is thought to increase the release of the inhibitory neurotransmitter GABA back onto odour-responsive PNs, thereby decreasing odour-evoked responses and causing the animal to show a diminished avoidance to the respective odour (Das et al., 2011b; Larkin et al., 2010; Sudhakaran et al., 2012).

As for habituation of the olfactory jump reflex and the odour-evoked locomotor startle response, the rut^{2080} mutant, carrying a mutation in the Ca^{2+}/calmodulin adenylate cyclase *rutabaga*, displays defects in both STH and LTH, indicating a role of cAMP signalling in olfactory avoidance habituation (Das et al., 2011b). The requirement for a functioning *rutabaga* transgene was localized to the LN1 subset of mainly GABAergic, pan-glomerular LNs which arborise within the *Drosophila* AL. Using spatially and temporally controlled expression of a wildtype *rutabaga* transgene in LN1 neurons rescued both the STH and LTH defect of rut^{2080} mutants (Das et al., 2011b). Adult-specific RNAi-mediated knockdown of *rutabaga* in LN1 neurons further blocked STH and LTH in otherwise wildtype flies, supporting the necessity of *rutabaga* in the inhibitory LN1 cluster (Das et al., 2011b).

Following the identification of the LN1 population as an important neuronal location for olfactory avoidance habituation, inhibitory transmitter release from this population was shown to be necessary and the artificial activation of this population to be sufficient for the reduced avoidance response associated with olfactory habituation (Das et al., 2011b). Blocking

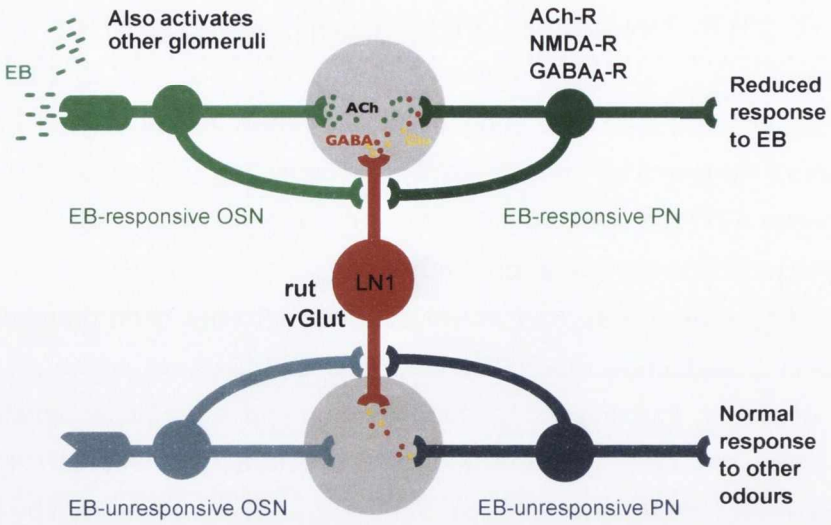


Figure 1.6: Circuit model for olfactory avoidance habituation
Olfactory avoidance habituation is thought to arise from increased GABAergic transmission from LN1 interneurons onto odour responsive PNs. An odour stimulus activates a specific set of OSNs and their respective PNs (depicted in green). PNs drive activity in LN1s, a sub-population of inhibitory local interneurons. During prolonged odour exposure NMDA receptors expressed in odour-responsive PNs are activated by the coincidence of odour-evoked depolarisation and glutamate release from LN1s. NMDA receptor activation triggers the potentiation of GABAergic transmission from LNs onto these specific PNs, possibly mediated through retrograde signalling. As NMDA receptors are only activated in odour-responsive PNs no potentiation of inhibition occurs in odour-unresponsive PNs (depicted in blue). This circuit model requires the Ca^{2+}/calmodulin adenylate cyclase *rutabaga* (rut) and the vesicular glutamate transporter vGlut in LN1 neurons as well as the NMDA and $GABA_A$ receptors in odour-responsive PNs. *Figure adapted from Twick et al. (2014)*

synaptic output from the predominantly GABAergic LN1 cluster during behavioural testing following odourant exposure using targeted expression of a *shibire^{ts}* transgene restored the olfactory avoidance response to naïve levels, for both STH and LTH (Das et al., 2011b). Artificial activation of LN1 neurons for 30 minutes using heat activated TRPA1, in contrast, was sufficient to substantially reduce the avoidance response of naïve flies. Consistent with the necessity of GABA release from LN1 neurons, LN1-restricted and adult-specific expression of an RNAi transgene targeted to degrade mRNA of the Glutamate decarboxylase 1 (GAD1), the enzyme that catalyses the production of GABA from L-glutamic acid, prevented STH and LTH (Das et al., 2011b). GABAergic transmission further has been shown to act on post-synaptic $GABA_A$ receptors in PNs. Adult-specific RNAi-mediated knockdown of $GABA_A$ receptors in PNs prevented both, STH and LTH (Das et al., 2011b).

Subsequent investigations showed that increased transmitter release from LN1 neurons is mediated through PNs rather than OSNs, suggesting that habituation of the olfactory avoidance response occurs through a recurrent motif where PN output drives LN activity (Sudhakaran et al., 2012). Artificial 30-minute activation of PNs using targeted expression of TRPA1 was sufficient to induce a reduced olfactory avoidance response that displayed similar characteristics as odour-induced STH and appears to be mediated through the same neuronal pathway (see Sudhakaran et al. (2012) for details). Consistently, odour-induced STH did not occur when synaptic output from PNs was blocked using targeted expression of

shibire^{ts} during odourant exposure (Sudhakaran et al., 2012). Further experiments showed that *shakB* mutants with disrupted gap junctions display deficits in STH suggesting that PN excitation of inhibitory LN1s occurs indirectly through the activation of eLNs (Sudhakaran et al., 2012).

Odour-selectivity within this recurrent inhibitory circuit is achieved by the activation of NMDA receptors in odour-responsive PNs (Das et al., 2011b). Targeted expression of an RNAi transgene against the NMDA receptor subunit NR1 in EB-responsive GH146 PNs prevented STH and LTH to EB but not to CO_2. Conversely, RNAi-mediated knockdown of the NMDA receptor subunit in CO_2-responsive V PNs prevented habituation to CO_2 but not to EB (Das et al., 2011b). As NMDA receptors are activated by the coincidence of neuronal depolarisation, here induced by the odour stimulus, and glutamate binding (Collingridge, 2003) the source of glutamate release was subsequently studied and could be located to the LN1 cluster of local interneurons (Das et al., 2011b). RNAi-mediated knockdown of DVGLUT, a vesicular glutamate transporter, in LN1s blocked STH and LTH (Das et al., 2011b).

In summary, the current model for olfactory avoidance habituation suggests that both STH and LTH arise from increased inhibitory transmission from LN1 interneurons onto odour-responsive PNs within the *Drosophila* AL (see Figure 1.6). Naïve odour presentation results in a strong behavioural avoidance as odour-responsive PNs are strongly activated due to the comparatively weak LN-PN synapse. During continuous odourant exposure PNs drive activity in LNs. The coincidence of odour-induced PN activation and glutamate release from LNs triggers NMDA receptors in odour-responsive PNs which cause an enhancement of GABAergic transmission from LNs onto these specific PNs, possibly mediated through retrograde signalling. Presentation of the same odour after odourant exposure thus activates odour-responsive PNs only weakly due to the strong GABAergic transmission from LNs resulting in a comparatively weak avoidance to the odourant.

While STH and LTH are both mediated through enhanced inhibitory transmission from LN1s onto odour-responsive PNs, they differ in the underlying neuronal mechanisms (reviewed in Twick et al. (2014)). STH, induced by 30 minute odourant exposure, requires phosphorylation of the synaptic vesicle associated protein synapsin in LN1 interneurons (Sadanandappa et al., 2013). Synapsin phosphorylation is thought to increase the pool of synaptic vesicles available for neurotransmitter release (Bykhovskaia, 2011) suggesting that STH is due to a transient increase in the active pool of synaptic vesicles (Sadanandappa et al., 2013). LTH, induced by 4 day odourant exposure, does not require synapsin phosphorylation but is, in contrast to STH, associated with increased volume of odour-responsive glomeruli (Sachse et al., 2007; Sadanandappa et al., 2013; Das et al., 2011b). Both, behavioural LTH and associated glomerular growth are dependent on transcriptional and translational factors. The transcriptional cAMP-responsive element binding protein (CREB) which binds the cAMP response element in gene regulatory sequences and thereby increases or decreases gene transcription is required in LN1 interneurons (Das et al., 2011b). Further, activity reg-

ulated local translation of synaptic mRNA that are normally stored in a repressed state also contributes to the synapse-specificity of LTH. Translational control of synaptic mRNAs at the LN1 presynapse as well as at the PN postsynapse is mediated by mRNA binding proteins such as dFMR1 and Ataxin2 which interact with components of the microRNA pathway (McCann et al., 2011; Sudhakaran et al., 2014).

1.6 Aim of the Study

Despite its first description in the late 19th century and its remarkably well characterized behaviour, habituation is still widely a black box in terms of its associated changes in neuronal activity and cellular signalling cascades. While good experimental evidence exists for homosynaptic depression to underlie simple forms of habituation such as habituation of reflex pathways, more complex forms such as habituation of perceptual experience cannot be explained by this synaptic phenomenon (Christoffersen, 1997; Ramaswami, 2014; see section 1.2). Recent advances in *Drosophila* suggest that habituation of odour percepts arises from potentiation of inhibitory transmission in the fly's primary olfactory processing centre, the antennal lobe (Das et al., 2011b; see section 1.5).

In the present study, two lines of research were pursued. Identifying the neuronal circuit underlying a specific form of olfactory habituation, namely habituation of the olfactory avoidance response (Das et al., 2011b), raised the question of the universality of the identified circuit for other forms of olfactory habituation. Thus, one aim of this study was to investigate whether a different form of olfactory habituation, specifically habituation of the locomotor startle response, is driven by the same neuronal circuit motif as the one previously shown.

Secondly, identification of the neuronal circuit underlying olfactory habituation largely relied on genetic perturbations combined with behavioural experiments without the direct measurement of physiological changes associated with the behaviour. Thus, another aim was to study neurophysiological changes associated with behavioural avoidance habituation using functional Ca^{2+} imaging. As the Ca^{2+} dynamics associated with long-term habituation had been investigated previously (Das et al., 2011b), the focus of the present study was to study the changes in Ca^{2+} influx that underlie short-term habituation.

2. Materials and Methods

2.1 Materials

2.1.1 Fly Stocks

Stock (chromosomal location)	**Reference**	**Provided by**
Wildtype:		
Canton S (CS)	Stern and Schaeffer, 1943	Laboratory Stock Collection
Mutants:		
rut^{2080} (X)	Levin et al., 1992	Martin Heisenberg (University of Wuerzburg, Germany)
$rut^{2080}; UAS-rut^{+}$ (X,II)	Zars et al., 2000b	Martin Heisenberg (University of Wuerzburg, Germany)
Gal4 Driver Lines:		
GH146-Gal4 (X)	Berdnik et al., 2008	Liquin Luo (Stanford University, USA)
GH146-Gal4 (II)	Stocker et al., 1997	Reinhard Stocker (University of Fribourg, Switzerland)
Gad1-Gal4 (II)	Ng et al., 2002	Gero Miesenboeck (Oxford University, UK)
LN1-Gal4 (NP1227) (II)	Okada et al., 2009	Kei Ito (University of Tokyo, Japan)
LN2-Gal4 (NP2426) (X)	Okada et al., 2009	Kei Ito (University of Tokyo, Japan)
OK371-Gal4 (vGlut) (II)	Mahr and Aberle, 2006	Bloomington *Drosophila* Stock Center (Indiana University, USA)
Or83b-Gal4 (III)	Ng et al., 2002	Leslie Vosshall (Rockefeller Institute, USA)
UAS Effector Lines:		
UAS-ArcD (III)	Cao et al., 2013	Aravinthan D.T. Samuel (Harvard University, USA)
UAS-GBi;UAS-GBi (X,III)	Root et al., 2008	Jing Wang (University of California, USA)
UAS-GCaMP3 (II)	Tian et al., 2009	Vivek Jayaraman (Janelia Farm Research Campus, USA)
20x UAS-IVS-GCaMP6M attp40 (II)	Chen et al., 2013	Bloomington *Drosophila* Stock Center (Indiana University, USA)
20x UAS-IVS-GCaMP6M VK00005 (III)	Chen et al., 2013	Bloomington Stock Center (Indiana University, USA)

UAS-dsNR1 RNAi (III)	Wu et al., 2007	Tim Tully (Cold Spring Harbor Laboratory, USA)
UAS-Rdl$^{8\text{-}10G}$ RNAi (III)	Liu et al., 2009	Ronald Davis (The Scripps Research Institute, USA)
UAS-rut RNAi 5569 (III)	Das et al., 2011b	Vienna *Drosophila* Resource Center (Vienna, Austria)
UAS-syn RNAi 46480/GD (III)	Sadanandappa et al., 2013	Vienna *Drosophila* Resource Center (Vienna, Austria)
UAS-n-syb-pHluorin (III)	Ng et al., 2002	Gero Miesenböck (University of Oxford, UK)
LexA/LexAop Lines:		
GH146-GAD::LexA (III)	Lai et al., 2008	Tzumin Lee (Janelia Farm Research Campus, USA)
5xLexAop2-GCaMP3 attp40 (II)		made by colleague Sahar Osman by subcloning GCaMP3 from pEGFP-N1GCaMP3 into pLOTGCaMPattB using bBglII (5-end) and NotI (3-end)
QF/QUAS Lines:		
GH146-QF,QUAS-mCD8-GFP (III)	Potter et al., 2010	Bloomington *Drosophila* Stock Center (Indiana University, USA)
Genomic Fusions:		
Or83b-RFP (III)	Li and Gong, 2015	John Carlson (Yale University, USA)

Expression pattern of the Gal4 drivers:

- *GH146-Gal4* expresses GAL4 in ~90 out of ~150 PNs antennal lobe projection neurons (Stocker et al., 1997; Jefferis et al., 2001). The anterodorsal lineage is composed of uni-glomerular PNs that project through the inner antennocerebral tract. The ventral lineage contains both, uni-glomerular and multi-glomerular PNs which project through the middle anntennocerebral tract. The lateral lineage includes multiple types of neurons including uniglomerular PNs, atypical PNs, local interneurons and neurons exterior to the AL (Lai et al., 2008; Tanaka et al., 2012).

- *Gad1-Gal4* expresses GAL4 in neurons expressing Glutamate decarboxylase 1 (Ng et al., 2002; Okada et al., 2009; Enell et al., 2007). Gad1-Gal4-positive cells are relatively few and form clusters in the rind of several neuropiles including the ALs, the supoesophageal ganglion, the ventrolateral protocerebrum, the optic lobes, the lateral cell body region, the superior and inferior posterior slope, the protocerebral bridge, the ellipsoid body and the mushroom body calyces (Okada et al., 2009; Enell et al., 2007).

- *LN1-Gal4* predominantly labels GABAergic multiglomerular LNs in the AL (Okada et al., 2009; Seki et al., 2010; Tanaka et al., 2009). It consists of ~18 neurons whose cell bodies are clustered in the dorsolateral area of the AL. 90-100% of the LN1 neurons are GABAergic and the majority has extensive arborisations in most of the AL glomeruli, predominantly targeting the glomerular core (Okada et al., 2009; Tanaka et al., 2009).

- *LN2-Gal4* mainly labels GABAergic uni- and multiglomerular LNs in the AL (Okada et al., 2009; Seki et al., 2010; Tanaka et al., 2009). It consists of ~37 neurons which are largely GABAergic (88-90%) and have their cell bodies dorsolateral and ventral to the AL. LN2-positive cells are heterogeneous with some arborising in most of the glomeruli and others arborising in about two-third of the glomeruli. LN2 terminals target both the core and the peripheral areas of a glomeruli (Okada et al., 2009; Tanaka et al., 2009). Beside the ALs, the LN2-Gal4 line also weakly expresses GAL4 in the optic lobes (Okada et al., 2009).

- *OK371-Gal4* expresses GAL4 in glutamatergic neurons that express the vesicular glutamate transporter VGlut (Mahr and Aberle, 2006). It labels motorneurons in the ventral nerve chord and a limited number of neuronal clusters in the brain which are situated in the optic lobes, the thoracic ganglion and the ALs (Mahr and Aberle, 2006; Liu and Wilson, 2013). OK371-positive cells represent roughly one third of the LNs in the AL (60-70 of ~200 total LNs) (Liu and Wilson, 2013). Their cell bodies are located ventrally to the ALs and their neuronal processes are primarily found in the spaces between glomeruli (Das et al., 2011a). OK371 neurons have diverse morphologies innervating all or a selective pattern of glomeruli or targeting a region posterior to the glomeruli (Liu and Wilson, 2013).

- *Or83b-Gal4* expresses the GAL4 protein in all OSNs that express the co-receptor Or83b (or Orco) (Larsson et al., 2004). It therefore labels all basiconic and trichoid OSNs with the exception of the CO_2-sensing neurons (Grabe et al., 2015b; Couto et al., 2005; Fishilevich and Vosshall, 2005; Jones et al., 2007; Kwon et al., 2007).

2.1.2 Fly Food

The cornmeal-agar medium consisted of 328g malt extract, 164g golden syrup, 308g polenta, 72g dry yeast and 34g agar made up in 4L of water with 18mL propionic acid and 40mL of 10% methyl 4-hydroxybenzoate (in ethanol) added.

2.1.3 Reagents and Consumables

Chemicals

Agarose	Sigma-Aldrich (St. Louis, MO, USA), CAS no: 9012-36-6
Ethyl butyrate	Sigma-Aldrich (St. Louis, MO, USA), CAS no: 105-54-4
Paraffin oil	Sigma-Aldrich (St. Louis, MO, USA), CAS no: 8012-95-1

Consumables

Aluminium foil	Thermo Fisher Scientific (Waltham, MA, US)
Eppendorf tubes	Sarstedt AG & Co (Nümbrecht, Germany)
Dumont #5SF Forceps	Fine Science Tools (Heidelberg, Germany)
Pipette tips	Thermo Fisher Scientific (Waltham, MA, US)
Paraffin wax	Sigma-Aldrich (St. Louis, MO, USA), CAS no: 8002-74-2

2.1.4 Buffers and Solutions

All components were ordered from Sigma-Aldrich (St. Louis, MO, USA).

Extracellular Saline

The saline used for functional imaging experiments was composed as follows: 103mM NaCl, 3mM KCl, 5mM TES, 10mM Trehalose-$2H_2O$, 10mM Glucose, 2mM Sucrose, 26mM $NaHCO_3$, 1mM NaH_2PO_4, and 1.5mM $CaCl_2$-$2H_2O$. Osmolarity and pH were adjusted to 280mOsm and 7.3, respectively.

KCl Solution

For KCl experiments a 106mM KCl solution was prepared by substituting NaCl by KCl in the extracellular saline described above. The KCl was then added to the bath covering the flies head resulting in a 70mM KCl solution.

Squishing Buffer

The saline used for single fly genomic DNA extractions was composed as follows: 10mM Tris-HCl (pH 8), 1mM EDTA, 25mM NaCl, 200g/mL proteinkinase K. Proteinkinase K was added freshly to the saline before the DNA extraction protocol was performed.

2.1.5 Enzymes

To check if recombinants carried the desired construct the following enzymes were used together with their respective buffers unless stated otherwise.

Protein kinase A	Qiagen (Hilden, Germany)
MyTaq^{TM} DNA polymerase	Bioline Reagents Ltd (London, UK)

2.1.6 Laboratory Equipment

General Equipment:

Barnstead™ Nanopure™	Thermo Fisher Scientific (Waltham, MA, US)
Block Heater SBH130DC	Mason Technology (Dublin, Ireland)
CyberScan pH 1500	Eutech Instruments (Landsmeer, The Netherlands)
Incubator MLR-351H	Sanyo Electric Co., Ltd. (Moriguchi, Japan)
Jenway 100 Hotplate and Stirrer	Bibby Scientific Limited (Staffordshire, UK)
LAS-3000 Imager	Fujifilm Holdings Corporation (Tokyo, Japan)
Mastercycler®gradient thermal cyclers	Eppendorf (Hamburg, Germany)
Microcentrifuge 5415D	Eppendorf (Hamburg, Germany)
Pipettes	Gilson Inc. (Middleton, WI, USA)
Scale mettler toledo B303	Mason Technology (Dublin, Ireland)
Submarine gel system classic CSSU	Thermo Fisher Scientific (Waltham, MA, US)
Stereo microscope Leica $MZ7_5$	Leica Microsystems (Wetzlar, Germany)
UV-transilluminator	Syngene (Cambridge, UK)
Vapro Pressure Osmometer 5520	Wescor Inc. (Logan, UT, USA)
Vortex-Genie®2	Scientific Industries, Inc. (New York, NY, USA)

Behavioural Setup:

Acrylic observation boxes	own design, mechanical engineering workshop TCD (Dublin, Ireland)
Light Panel LP-400	Universal Electronic Industries Ltd (Hong Kong, China)
316 stainless steel flux flow meter	Cole Parmer (Vernon Hills, IL, USA)
Flow tubes	Cole Parmer (Illinois, USA)
Schott Duran®glas bottles	Schott AG (Mainz, Germany)
Multiport GL45 bottle caps system	Schott AG (Mainz, Germany)
Multiport GL45 bottle caps system	Schott AG (Mainz, Germany)
Kinesis tubing connectors xp-301	Kinesis Ltd (Cambridgeshire, UK)
2-way solenoid valves open (993345)	NResearch Inc. (West Caldwell, NJ, USA)
2-way solenoid valves closed (993346)	NResearch Inc. (West Caldwell, NJ, USA)
Camera Basler A622f	Baseler AG (Ahrensburg, Germany)

Imaging Setup:

Confocal microscope LSM510 META	Carl Zeiss AG (Oberkochen, Germany)
Chameleon laser	Coherent Ltd. (Santa Clara, CA, USA)
Lense 63x/1.0VIS-IR	Carl Zeiss AG (Oberkochen, Germany)

Fly Preparation for Imaging Experiments:

Plastic fly holder	design from Vivek Jayaraman, mechanical engineering workshop TCD (Dublin, Ireland)
Metal holder	design from Vivek Jayaraman, mechanical engineering workshop TCD (Dublin, Ireland)
Peristaltic pump minipulse 3	Gilson, Inc. (Middleton, WI, USA)
Peristaltic pump tubing	Thermo Fisher Scientific (Waltham, MA, US)
Stereo microscope Leica MZ16 FA	Leica Microsystems (Wetzlar, Germany)
Waxlectric light II	Renfert GmbH (Hilzingen, Germany)

Odour Delivery System for Imaging Experiments:

Diaphragma pump N86KN.18	KNF Neuberger Inc. (Trenton, NJ, US)
Pressure regulator R07- 200-RNKG	Norgren (Birmingham, AL, US)
Flow controller (AS2000)	SMC Pneumatics (Noblesville, IN, US)
Carbon CapTM	Whatman (Maidstone, UK)
DC10-P5/U Heating Circulator Bath	Thermo Fisher Scientific (Waltham, MA, US)
Mass flow controllers FMA5402	Omega engineering (Stamford, CT, US)
316 stainless steel flux flow meter	Cole Parmer (Illinois, USA)
Flow tubes	Cole Parmer (Illinois, USA)
Schott Duran®glas bottles	Schott AG (Mainz, Germany)
Tygon tubing SE200	Saint-Gobain (Courbevoie, France)
PTFE tubing	Cole Parmer (Illinois, USA)
Luer fittings	Cole Parmer (Illinois, USA)
Three-way stopcock	Vaplock closed systems (California, USA)
Odour injection manifold	Vaplock closed systems (California, USA)
Programmable logic controller	Siemens (Munich, Germany)
2-way solenoid valves open (993345)	NResearch Inc. (West Caldwell, NJ, USA)
2-way solenoid valves closed (993346)	NResearch Inc. (West Caldwell, NJ, USA)
3-way solenoid valves (860469)	NResearch Inc. (West Caldwell, NJ, USA)
PID with integrated pump system pp-bRAe	Ribble Enviro Ltd (Clitheroe, UK)
Integraded PID sensor PID-AH	Alphasense Ltd (Essex, UK)
Arduino Mega 2560	Arduino
PID housing	own design, mechanical engineering workshop TCD (Dublin, Ireland)

2.2 Methods

2.2.1 Fly Husbandry

All fly strains were raised on standard *Drosophila* cornmeal-medium (see section 2.1.2) at 25°C, 60% humidity and a 12 hour light/dark cycle. *Drosophila* strains used are listed in section 2.1.1, the exact genotypes for each experiment are depicted in section 5.1.

2.2.2 Testing Potential Recombinants

The following recombinants were made after standard crossing schemes (chromosome location shown in brackets):

1. GH146-Gal4,UAS-GCaMP3 (II)
2. GH146-LexA,LexAop-GCaMP3 (II)
3. LN1-Gal4,LexAop-GCaMP3 (II)
4. GH146-Gal4,UAS-GCaMP6m (II)
5. Or83b-Gal4,UAS-GCaMP6m (III)
6. Or83b-Gal4,UAS-ArcD (III)
7. UAS-GCaMP6m, Or83b-RFP (III)
8. UAS-ArcD, Or83b-RFP (III)
9. UAS-SpH, Or83b-RFP (III)

Recombinants 1-6 were confirmed by checking for GCaMP3, GCaMP6m or ArcD transgene expression in the respective cell type with a GFP filter under fluorescent light in flies dissected as described in section 2.2.4. The presence of the UAS construct in recombinants 7-9 was tested by standard polymerase chain reaction (see below). The Or83b-RFP transgene in these recombinants was confirmed under fluorescent light with a RFP filter on a Stereo microscope Leica MZ16FA in flies dissected as described in section 2.2.4.

Single Fly DNA Extraction Protocol

To check for the UAS constructs in potential recombinants UAS-GCaMP6m,Or83b-RFP, UAS-ArcD,Or83b-RFP, and UAS-SpH,Or83b-RFP DNA was extracted using a single fly DNA extraction protocol: Proteinkinase K was added freshly to the squishing buffer (see section 2.1.4) before the DNA extraction protocol was performed. 1-2 flies were placed into a 0.5mL tube and mashed for 5-10 seconds with a yellow pipette tip containing ~30μL of squishing buffer. The tubes were incubated at 37°C for 30 minutes followed by incubation at 95°C for 3 minutes to inactivate the proteinkinase. The solid matter was spun down by brief centrifugation and the supernatant pipetted to a new tube.

Polymerase Chain Reaction (PCR)

The DNA fragments encoding the UAS constructs UAS-GCaMP6m, UAS-ArcD, and UAS-SpH were amplified by PCR. PCRs were set up in total volume of $25\mu L$. In case of the UAS-GCaMP6m construct, the PCR setup consisted of $0.25\mu L$ Taq polymerase, $1\mu L$ template, $1.25\mu L$ of each primer and a mastermix containing $17\mu L$ H_2O, $2.5\mu L$ $10xNH_4$ buffer, $1.5\mu L$ $MgCl_2$ solution, and $0.25\mu L$ dNTPs. In the case of UAS-ArcD and UAS-SpH, the PCR setups were composed of $0.25\mu L$ Taq polymerase, $1\mu L$ template, $1.25\mu L$ of each primer, $5\mu L$ 5x Taq reaction buffer and $16.25\mu L$ H_2O.

The primers used bound the UAS (forward primer) and the Hsp70 (reverse primer) regions of the pUAS transgenes. Using these primers, PCR products with a length of ~1500bp, ~2000bp, and ~1800bp were expected for the respective constructs UAS-GCaMP6m, UAS-ArcD, and UAS-SpH. Primer sequences were as follows:
forward: 5'- TAACCAGCAACCAAGTAAATCAA -3'
reverse: 5'- CCACAGAAGTAAGGTTCCTTC -3'

PCR was performed in the Mastercycler®gradient thermal cycler (Eppendorf, Hamburg, Germany). The following PCR protocol was used to amplify the three UAS constructs:

Cycle Step	Temperature	Time	Cycles
Initial denaturation	94°C	3min	1
Denaturation	94°C	30sec	
Annealing	60°C	20sec	33
Extension	72°	2min	
Final extension	72°	10min	1
Hold	4°C	∞	

Agarose Gel Electrophoresis

Agarose gel electrophoresis was used to inspect the length of the amplified PCR products. PCR products were run on 0.8% agarose gel which was composed of 0.4g agarose, 50mL of 0.5xTBE and $5\mu L$ Gel Red. 5x loading buffer was added to the DNA before loading it to the gel together with the Hyper Ladder 1 (Bioline).

2.2.3 The Behaviour Assay

The Locomotor Tracking System

The locomotor tracking experiments were performed with three transparent observation chambers that were filmed simultaneously from above. The acrylic boxes (3.4cm x 9.8cm x 0.5cm inner diameter), with one inlet for air/odour at one side and an outlet for exhaust at the

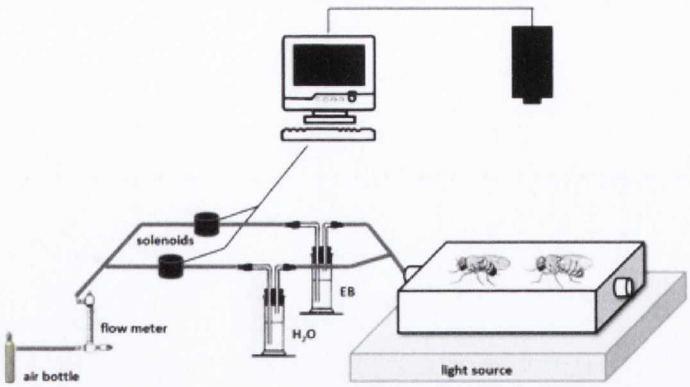


Figure 2.1: The odour-evoked locomotor startle response assay
The odour-evoked locomotor startle response assay used to study olfactory habituation is based on a fly's sudden increase in walking speed upon exposure to a novel odour. To perform habituation experiments flies were placed into one of three transparent observation chambers. Fly positions in the boxes were recorded simultaneously from above throughout the habituation protocol. Ethyl butyrate (EB) vapour or humidified air was delivered by bubbling an air stream through either EB dissolved in water or pure water. Airflow was directed into the water or EB bottle by opening or closing of solenoid valves controlled by a custom-written computer program.

other, were placed approximately 2cm above a light panel comprising LED lights to avoid heating of the boxes through the light source. EB vapour or humidified air was delivered by bubbling an air stream through either EB dissolved in water or pure water. Dilutions were exchanged daily. Air flows were calibrated with a 316 stainless steel flux flow meter and delivered simultaneously to the three boxes. Odour-evoked startle behaviour was indistinguishable between boxes (data not shown) indicating that odour delivery was equal to all boxes. Air flow rates and EB concentrations are described in section 3.1. Odour/air pulses were controlled by two-way solenoid valves triggered by a custom-written Valve Driver software (Nial Murphy). Fly positions in all three boxes were recorded simultaneously with a video camera (Basler A622f) connected to an Apple Mac Book Pro laptop. Movies were recorded with QuickTime Player 7.4 at 10 frames per second, a sufficient rate for capturing the full range of locomotor speeds.

The Habituation Protocol

Odour-evoked locomotor startle habituation experiments were performed at ~23°C, ~33% humidity and in constant darkness, except for the light source from the light box and the computer screen. 10-15 flies, males and females, were placed into each of the three habituation boxes without using anaesthesia. Flies could move freely within the boxes. Although the startle response has been shown to be independent of the flies' walking speed before the odour puff (Wolf et al., 2002), the flies were acclimatized to the habituation boxes for 10 minutes before the start of the experiment. After acclimatizing, the flies were exposed to EB according to various protocols, EB concentrations, and air flow rates, described in section 3.1. Air flow rates were kept the same for odour delivery and air interstimulus intervals to eliminate the possibility of inducing startle by flux changes.

Continuous 30-minute exposure: Flies received a 30-second EB puff before they were exposed to EB for 30 minutes which was followed by a 8-minute air interval and another 30-second EB puff (see Figure 3.1 A).

Pulsed exposure with various odour concentrations: Flies received ten 20-seconds long EB stimuli delivered with 3-minute inter pulse intervals (see Figure 3.2 A).

Pulsed exposure with different lengths of interstimulus intervals: Flies received six 30-seconds long EB stimuli delivered with a 6- or 9-minute inter stimulus interval (see Figure 3.3 A).

Final protocol for testing the underlying neuronal circuit: Flies received six 30-seconds long EB stimuli delivered with a 9-minute inter stimulus interval (see Figure 3.4 A).

Data Analysis

Movies were processed in ImageJ (Mtrack2) (Schneider et al., 2012) and a custom-written Matlab (MathWorks) program (Jörn Hülsmeier). ImageJ analysis identified individual flies as dark objects on a light background and traced the paths of individual flies between frames. Incomplete traces of paths taken for individual flies occurred when one or more flies came within close proximity of one another resulting in a smaller number of identified flies than flies present in the chamber. Whenever this occurred new paths were started.

The preprocessed ImageJ data was fed into a custom-written matlab program which calculated the mean movement of flies over time as well as the total movement during an odour presentation. The mean movement over time was calculated by computing the distance travelled by a fly from one frame to the next and averaging over the number of paths that contained information for both frames. The total movement during each odour presentation was calculated as the integrated mean movement over time per box. The percent of naïve fly movement was calculated by dividing the total movement travelled at a certain pulse by the total movement travelled during the first pulse and multiplying the resulting value by 100.

Significance was established by two-tailed students t-test assuming unequal variance or by single factor ANOVA with posthoc comparisons using Tukey's test. Error bars in all experiments represent $\pm$ SEM. In all figures, n corresponds to the number of experiments performed on individual groups comprising 10-15 flies.

2.2.4 Calcium Imaging

Fly Preparation

All experiments were carried out on adult female flies 3-4 days after eclosion. Flies were anaesthetized in a glass vial placed on ice just until movement stopped. A female was selected and gently positioned in a custom cut hole in a piece of aluminium foil that was glued to a teflon holder (custom-designed by Vivek Jayaraman, Figure 2.2). The fly position in the hole was adjusted until the head and thorax were horizontally aligned with the head lying flat against the thorax and the ridge between the second and third antennal segments resting on the edge of the aluminium foil (see Figure 2.3 A/A'). Small drops of low melting point wax (55°C) around the eyes and thorax at the dorsal side of the foil were used to seal the fly in the hole (see Figure 2.3 B). On the ventral side, application of wax around the eyes further stabilized the fly in the hole leaving the legs unrestricted. The proboscis was gently extended and attached to a piece of hair which was waxed to the holder to prevent movements of the oesophagus and thereby movements of the brain (see Figure 2.3 B'). The dorsal side of the foil was bathed in saline (see composition in section 2.1.4) while the ventral side including the antennae and maxillary palps remained dry and accessible to odours. A window was then cut using fine forceps in the dorsal head cuticule between the eyes, extending from the ocelli to the first antennal segment (see Figure 2.3 C'). Underlying fat tissue and air sacs were removed to expose the lobes (see Figure 2.3 C''). Removal of muscle 16 which runs close to the medial area of the lobes furthermore prevented pulsating movements of the brain. To gain a better view onto the lobes the 'ridge' connecting the first antennal segments was likewise removed and the second antennal segments were occasionally eased under the aluminium foil. Each fly was checked during the dissection procedure and also after the experiment for controlled and coordinated leg movements to verify the viability of the animal.

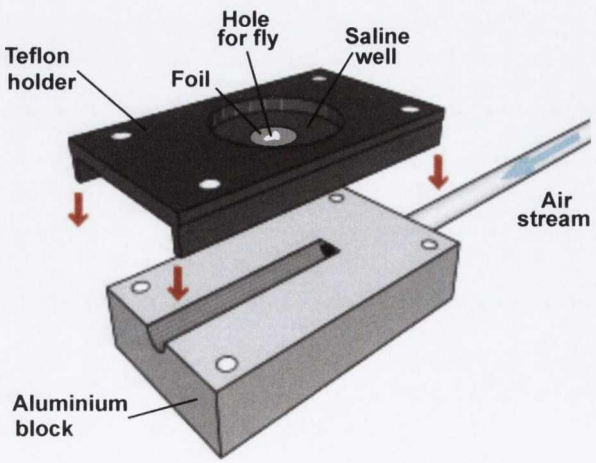


Figure 2.2: Fly holder
An immobilised fly was positioned in a hole cut in a piece of aluminium foil that was glued to a custom-designed teflon holder. For the experiments, the fly holder was mounted on an aluminium block that contained a channel for air/odour delivery to the fly. *Figure adapted from Lee (2015)*

When the dissection was completed the teflon holder was mounted on an aluminium block (see Figure 2.2) that contained a channel for air/odour delivery and immersed the ventral side including the antennae in the air/odour stream. A peristaltic pump perfused the well with a saline solution (see section 2.1.4) at approximately 1 mL/min throughout the experimental protocol. A 95% O_2 / 5% CO_2 mixture was continuously bubbled through the solution to maintain the viability of the brain.

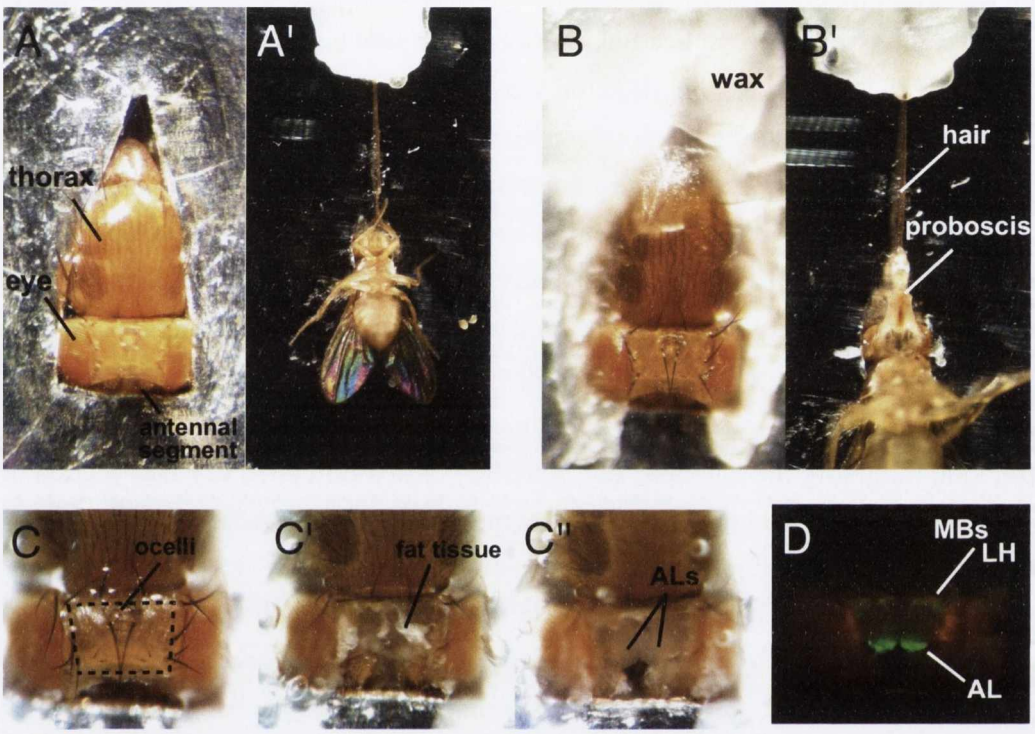


Figure 2.3: Fly preparation for functional imaging
The immobilized fly was positioned in a hole cut into aluminium foil seen dorsally in (A) and ventrally in (A'). Application of wax around the eyes and thorax stabilized the position of the fly (B/B'). The proboscis was extended and waxed to a piece of hair to prevent its movement (B'). The dorsal side of the foil was bathed in saline leaving the ventral side including the antennae and maxillary palps dry (C). The dorsal head cuticle between the eyes was removed (C'), as well as fat tissue and air sacs covering the brain (C''). Muscle 16 was removed to prevent pulsating movements of the brain. (D) shows the fly preparation depicted in A-C''' under transmitted light. The fly expresses the green fluorescence protein (GFP) in a large subset of olfactory PNs (labelled by the enhancer trap line GH146). PN projections from the antennal lobes (ALs) to the mushroom bodies (MBs) and lateral horn (LH) are visible.

Odour Delivery Systems

Prototype Odour Delivery System:

A pressure regulator on a compressed air cylinder maintained an inlet pressure of 0.5 bar above atmosphere. The air was humidified by directing it through a water bottle. Humidified air was split into three separate channels: The main, subsidiary, and priming air stream. Flow controllers consisting of rotameters/flow tubes with integrated needle valves monitored and controlled the flow rates in all three lines. The total air flow was set to 500mL min^{-1}, the

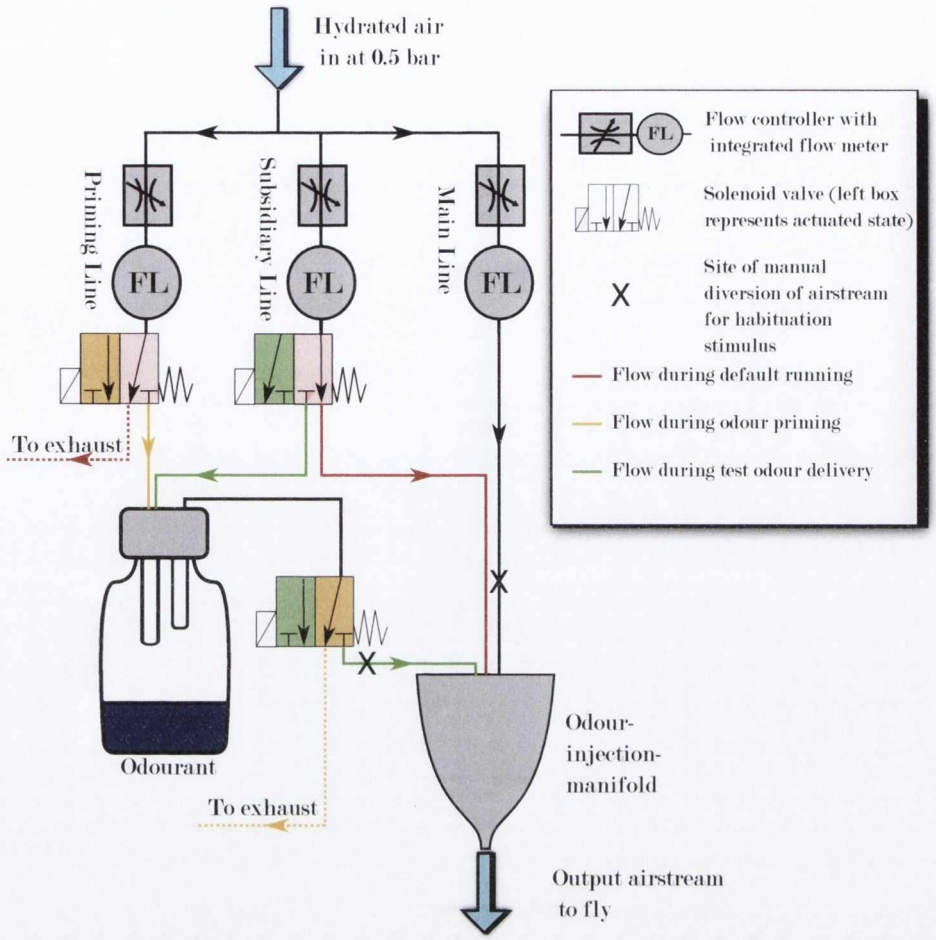


Figure 2.4: Prototype odour delivery system
A constant supply of humidified air was split into three separate lines: The main, subsidiary, and priming line. During times where the fly was not exposed to the odourant, the main and subsidiary (red solid line) lines were directed to the fly. The priming air stream was normally directed to the exhaust (red dotted line). Before an odour presentation to the fly, the odour channel was flushed to remove accumulated odour residues within the odour bottle and attached tubing aiming to establish a dynamic equilibrium. Five minutes before the odour presentation to the fly, the priming line was directed through the odour bottle (yellow solid line) into the exhaust (yellow dotted line). For odour presentations to the fly, the priming line was switched back into the exhaust (red dotted line) and the subsidiary line was directed through the odour bottle to an odour injection manifold (green solid line) where the odour stream was mixed with the main air and directed to the fly. Odourant exposure was carried out by manually switching the airflow through the odour bottle to the fly using separate tubing and odour injection manifold to reduce odour contamination of the system (see X for the position within the setup). *Figure adapted with permission from Lee (2015).*

main and subsidiary/priming streams were split 90:10 resulting in the main air stream being set at ~450mL min^{-1} and both the subsidiary and priming air stream set at 50mL min^{-1}. During times where the fly was not exposed to the odourant, the main and subsidiary (Figure 2.4, red solid line) air stream were directed to the fly. The priming air stream was normally directed to the exhaust (Figure 2.4, red dotted line). Before each odour presentation to the fly, the odour channel was flushed to remove accumulated odour residues within the odour bottle and attached tubing. Five minutes before the odour presentation to the fly, the priming air stream was directed through the odour bottle (Figure 2.4, yellow solid line) and from there into the exhaust (Figure 2.4, yellow dotted line). The odour bottle contained an EB

dilution of 10% in liquid paraffin oil with a total volume of 10mL. By priming the odour line, a dynamic odour equilibrium in the head space of the odourant bottle was established to ensure a stable odour concentrations given to the fly. To direct an odour presentation to the fly, the priming stream was switched back into the exhaust (Figure 2.4, red dotted line) and the subsidiary line was directed through the odour bottle to an odour injection manifold (Figure 2.4, green solid line) where the odour stream was mixed with the main air and then directed to the fly. The resulting air speed at the fly was ~1.04ms^{-1}. A programmable logic controller actuated 3-way solenoid valves to switch the airflow to different lines. To reduce odour contamination of the system, odourant exposure was carried out by manually diverting the main air and odour stream using a luer 3-way stopcock (Figure 2.4, *X*) through separate tubing and an alternative odour injection manifold. By daily cleaning of the odour manifold and weekly cleaning of all tubing within the system using detergent (Cabiclean ultra; Manepa Lim., Dublin, Ireland) and ethanol odour contaminations were further prevented. This odour delivery system depicted here was only used for some experiments described in section 3.2.

Final Odour Delivery System:

A diaphragma pump supplied air to the system. An inlet pressure of 1.5 bar above atmosphere was maintained by an in-line pressure regulator. The air was split into two streams, one of which was humidified by passing it through a water bottle while the other unhumidified stream was directed to an 'odour bottle' which contained pure odourant with a total volume of 10mL (Figure 2.5). A carbon filter was placed downstream of the humidification bottle to filter odour originating from the bottle. A mass flow controller which operated at a range of 0-10mL min^{-1} (at standard temperature and pressure) controlled the air flow into the 'odour bottle' by injecting small amounts of air. To control for the effects of temperature changes on the equilibrium vapour pressure of the odourant, both the hydration bottle and the 'odour bottle' were placed in a water bath. The humidified air stream was split into a main, subsidiary, and mixing line (Figure 2.5). Flow controllers consisting of rotameters/flow tubes with integrated needle valves monitored and controlled the flow rates in all three lines. The total air flow at the fly was set to 200mL min^{-1} resulting in an air speed of 0.42ms^{-1}, the main and subsidiary/priming streams were split 1:1. The main and subsidiary air streams were both directed to the fly when the fly was not presented with an odour (Figure 2.5, solid orange line). The mixing line was directed into another bottle, the 'mixing bottle', where the air was mixed with the odour concentrated air coming from the 'odour bottle'. The odour line leaving the 'mixing bottle' was normally directed into the exhaust to establish an odour concentration equilibrium (Figure 2.5, dashed orange line). When the fly was presented with an odour the odour line was switched to the fly where it was mixed with the main air (Figure 2.5, dashed green line). The subsidiary air stream was then directed to the exhaust (Figure 2.5, solid green line). A programmable logic controller actuated 3-way solenoid valves to switch the airflow to different lines. To maintain a constant flow-rate independent of whether the odour stream was directed to the exhaust or the main air stream, these streams were balanced by matching them to an equivalent 100mL

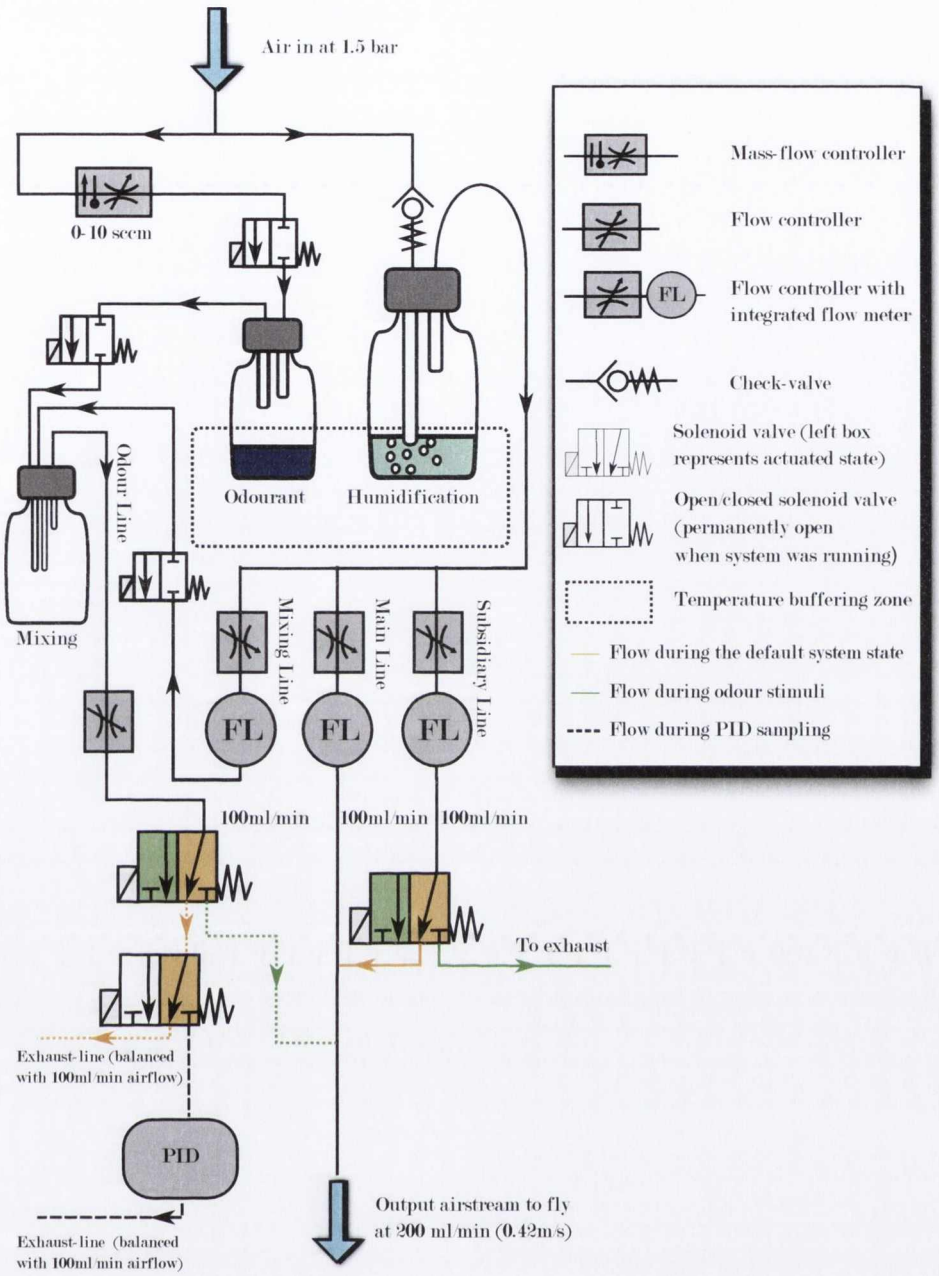


Figure 2.5: Final odour delivery system
Air at a pressure of 1.5 bar was initially split into two streams. A humidified air stream which was split into a main, subsidiary, and mixing line and an unhumidified stream that was directed to a mass flow controller which injected small amounts of air into a bottle, the odour bottle, containing pure odourant. The main and subsidiary (solid orange line) air streams were both directed to the fly when the fly was not presented with an odour. The mixing line was directed into another bottle, the mixing bottle, where the air was mixed with the odour concentrated air coming from the odour bottle. The odour line leaving the mixing bottle was normally directed into the exhaust to establish an odour concentration equilibrium (dashed orange line). When the fly was presented with an odour, the odour line was switched to the fly where it was mixed with the main air (dashed green line). The subsidiary air stream was then directed to the exhaust (solid green line). To monitor the odour concentration given to the fly the odour stream was directed to a PID shortly after each odour presentation (dashed black line). *Figure adapted with permission from Lee (2015).*

min^{-1}. A flow-controller placed in-line after the odour mixing bottle further ensured that the pressure of the odour-mixing bottle was held at around 1 bar above atmosphere and

that a constant odour flow of 100mL min^{-1} was delivered regardless of small deviations in pressure existing downstream in the system. To monitor the odour concentration given to the fly, the odour stream was directed to a photoionisation detector (PID) shortly after each odour presentation (Figure 2.5, black dashed line; also see Appendix 5.3).

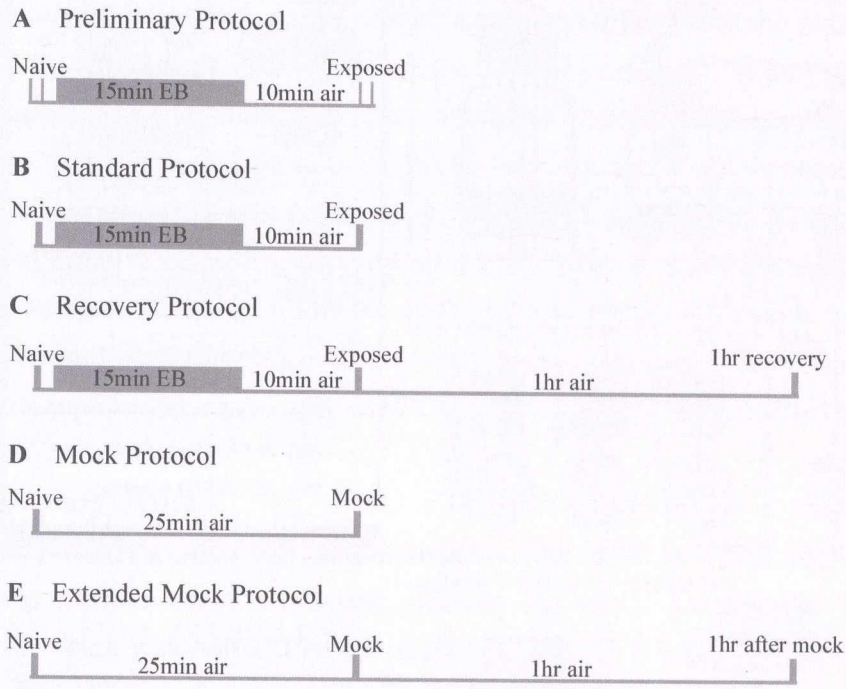


Figure 2.6: Imaging protocols
Depicted are the five different imaging protocols utilized in the present study: the preliminary imaging protocol (A), the standard imaging protocol (B), the recovery protocol (C), the mock protocol (D), and the extended mock protocol (E). See text for details.

Ca^{2+} Imaging Protocols

Preliminary Protocol: Two 1-second odour stimuli to ethyl butyrate (EB) were presented to the fly with a 2-minute air interval in between. Two odour pulses were delivered to allow for imaging from both identified focal planes (see Figure 3.6). Following the two odour presentations the flies were exposed to EB for 15 minutes continuously. A 10-minute air interval after odourant exposure allowed for the recovery from sensory adaptation that was expected to occur in OSNs (Störtkuhl et al., 1999). Another two 1-second odour stimuli with a 2-minute air interval in between were delivered after the air interval (see Figure 2.6 A).

Standard Protocol: A 10-second EB stimulus was presented before a 15-minute EB exposure followed by a 10-minute air interval and a 10-second EB stimulus (see Figure 2.6 B).

Recovery Protocol: To test for recovery from the changes induced by 15-minute EB exposure, another 10-second EB stimulus was presented 1 hour after the standard imaging protocol (see Figure 2.6 C).

Mock Protocol: For the 'mock' treatment, a 10-second EB stimulus was presented before a 25-minute air interval and another 10-second EB stimulus. The 25-minute air interval was composed of a 15-minute 'mock' exposure and the 10-minute air interval normally following the exposure (see Figure 2.6 D).

Extended Mock Protocol: To test for the well-being of the fly for a minimum of at least one and a half hours, another 10-second EB stimulus was presented 1 hour after the 'mock' imaging protocol (see Figure 2.6 E).

Image Acquisition

Two-photon imaging was performed using a LSM 510 meta confocal microscope from Zeiss coupled to a Chameleon ultra-fast laser (Coherent) with excitation wavelength set at 930nm and emission collected between 500 and 550nm. Images were collected at 4 frames/second (250 ms/frame), with a resolution of 512x512 pixels. Laser powers were adjusted for different genotypes as some exhibited larger baseline GCaMP fluorescence than others (see Table 2.1). Setting the laser power to 20% of full output at most prevented thermal or excitotoxic damage.

Genotype	Laser power
GH146 x GCaMP	20%
Or83b x GCaMP	10%
LN1 x GCaMP	20%
LN2 x GCaMP	20%
OK371 x GCaMP	20%
GH146 x ArcLight	15%
Or83b x ArcLight	10%
LN1 x ArcLight	20%
LN2 x ArcLight	20%

Table 2.1: Laser power for different genotypes

Definition of Regions of Interest

Glomeruli were initially identified using the published glomerular atlas by Laissue et al. (1999). Glomeruli identifications were confirmed by coincident expression of RFP in single OSN populations, to mark a specific glomerulus, and GFP in GH146 marked PNs, for the EB-responsive glomeruli studied, by combining the Q and Gal4/UAS binary expression systems.

Data Analysis

Reasoning behind the data analysis:

To determine the relation between a Ca^{2+} indicators fluorescence emission to its binding of free Ca^{2+} the sensor has to be calibrated. For nonratiometric Ca^{2+} indicators like GCaMP

the free Ca^{2+} concentration $[Ca^{2+}]$ is given by $[Ca^{2+}] = K_d((F - F_{min})/(F_{max} - F)$ whereas F_{min} is the indicator fluorescence intensity at zero Ca^{2+}, F_{max} the indicator fluorescence at saturating high Ca^{2+}, F the measured fluorescence intensity for which the corresponding value of Ca^{2+} needs to be determined and K_d the dissociation constant which is predetermined in *vitro* (Kao et al., 2010). Thus, to calibrate the Ca^{2+} indicator the cell expressing the sensor needs to be depleted of all Ca^{2+} and saturated with Ca^{2+} to obtain F_{min} and F_{max}, respectively. However, calibration of Ca^{2+} sensors proves difficult, especially *in vivo*. Thus, changes in indicator fluorescence are usually reported in form of the fluorescence intensity relative to baseline intensity (F/F_0) or the change in fluorescence intensity relative to baseline intensity $(\Delta F/F_0 = (F - F_0)/F_0)$.

Fluorescence changes are typically reported in relation to baseline fluorescence to provide a reference in the form of a percentage increase with respect to the baseline Ca^{2+} binding. While this is a useful measure when for instance describing how strongly an odour stimulus activates a given PN type compared to another, it proved impractical for reporting changes in odour-evoked Ca^{2+} levels following prolonged exposure. The reason for this are baseline shifts that occur after odourant exposure (see sections 3.3.4 and 3.5.1). If changes in fluorescence intensity relative to baseline intensity were reported for the GCaMP measurement preceding and succeeding odourant exposure the reported values would be confounded by the shifts in baseline. 'Naïve' and 'exposed' GCaMP responses that exhibit a similar absolute increase in fluorescence intensity would show up as different when normalized to different baselines. To allow for the quantitative comparison of 'naïve' and 'exposed' GCaMP responses absolute changes in fluorescence intensity independently of the respective baselines are reported in this study (*pers. comm. with Ronald Calabrese*).

Quantification:

Data collection and analysis was performed blinded. Using a custom written Matlab program (John Lee), each glomerulus was separately highlighted as a region of interest (ROI). Within each ROI, the mean pixel intensity at time t, F(t), was calculated over the length of the recording. To correct for background levels, the mean intensity of a user-defined region outside the AL was subtracted from F(t). F(t) was aligned to the odour stimulus with the time point t = 0 seconds coinciding with solenoid opening. For the experiments performed in section 3.3 and 3.5.1, a TTL trigger sent from the logic controller started image acquisition with the ZEN program to enable alignment. For the other experiments, recording and odour stimulus were retrospectively aligned by determining the time point where F(t) rose four standard deviations above baseline and taking into account the delay from solenoid opening to the odour stimulus reaching the fly.

Following background subtraction and alignment, the change in fluorescence intensity over time was calculated for the individual recordings:

$$\Delta F(t) = F(t) - F_0$$

where:

- F(t) is the fluorescence within the region of interest at time t
- F_0 is the baseline fluorescence computed by averaging F(t) for the two seconds preceding the odour response

The difference between two odour responses was calculated as the paired difference of the two $\Delta F(t)$ traces over time, as for example when comparing 'naïve' and 'exposed' indicator responses:

$$\text{Change in } \Delta F(t) = \Delta F_{\mathrm{E}}(t) - \Delta F_{\mathrm{N}}(t)$$

where:

- $\Delta F_{\mathrm{N}}(t)$ and $\Delta F_{\mathrm{E}}(t)$ are the change in fluorescence intensity of the 'naïve' and 'exposed' indicator responses

For statistical comparisons of the 'naïve' odour-evoked responses, the integral under the curve of the 'naïve' indicator response over the 10-second odour stimulus was calculated. The integral was divided by the 10-second odour stimulus interval to obtain the area under the curve within one second:

$$\int_0^{10} \Delta F(t)\,\mathrm{d}t = \int_0^{10} \Delta F_{\mathrm{N}}(t)\,\mathrm{d}t/10$$

where:

- $\Delta F_{\mathrm{N}}(t)$ is the change in fluorescence intensity of the 'naïve' indicator (e.g. GCaMP or ArcLight) responses

For statistical comparisons of the differences in fluorescence responses to the 'naïve' and 'exposed' EB stimulus, the integral under the curve for the paired difference of the 'naïve' and 'exposed' responses over the 10-second odour stimulus was calculated and likewise divided by the 10-second odour stimulus:

$$\text{Change in } \int_0^{10} \Delta F(t)\,\mathrm{d}t = \int_0^{10} \Delta F_{\mathrm{E}}(t) - \Delta F_{\mathrm{N}}(t)\,\mathrm{d}t/10$$

where:

- $\Delta F_{\mathrm{N}}(t)$ and $\Delta F_{\mathrm{E}}(t)$ are the change in fluorescence intensity of the 'naïve' and 'exposed' indicator responses

Both change in $\Delta F(t)$ and change in $\int_0^{10} \Delta F(t)\,\mathrm{d}t$ were accordingly calculated when comparing 'recovery' and 'exposed' as well as 'recovery' and 'naïve' indicator responses.

To determine changes in baseline fluorescence levels, the change in baseline was calculated by subtracting the baseline of the 'exposed' from the 'naïve' indicator responses:

$$\text{Change in Baseline} = F_{\mathrm{E}\,0} - F_{\mathrm{N}\,0}$$

where:

- F_{N0} and F_{E0} are the baseline fluorescence of the 'naïve' and 'exposed' indicator responses computed by averaging F(t) values for the two seconds preceding the odour response

As a measure of how much odourant exposure altered naïve odour-evoked indicator responses and to facilitate comparisons between glomeruli or neuron types, the percent change with respect to the naïve odour-evoked response was calculated:

$$\int_0^{10} \Delta F_E(t) - \Delta F_N(t)\,dt / \int_0^{10} \Delta F_N(t)\,dt * 100$$

where:

- $\Delta F_E(t) - \Delta F_N(t)$ is the paired difference between the 'exposed' and 'naïve' indicator responses
- $\Delta F_N(t)$ is the 'naïve' indicator response

Statistics:

Statistical comparisons were made using R (R 3.2.2 GUI 1.66) and Matlab (R2014a). The R package *lm4* (Bates, Maechler & Bolker, 2012) was used to perform *linear mixed effects analyses fit by maximum likelihood* where appropriate due to repeated measurements designs (Winter, 2014; see Table 5.1 for full lists of comparisons). Linear mixed-effects models were fitted with fixed effects such as *run* ('naïve', 'exposed', and 'recovery'), *glomerulus* (DL1, DL5, DM1, DM2, DM3, DM5, DM6) and *concentration* (3ppm, 20ppm) and their respective interaction terms (e.g. *run * glomerulus*, see Table 5.1 for all fixed effects, interaction terms and the fitted models). A random intercept model was fitted with *fly* as the random effect due to the repeated measures design where two or more measures were taken from the same fly. Visual inspection of residual plots revealed small deviations from homoscedasticity in models where all seven glomeruli where included in the same model. No obvious deviations from homoscedasticity were observed in models where only one glomerulus was fitted. Further, visual inspection did not reveal any obvious deviations from normality in any of the models (see 5.3 for residual and normality plots). Estimated values for the differences of the effect in question was determined by the linear mixed-effects model fit by maximum likelihood. P-values were obtained by likelihood ratio tests of the full model with the effect in question against the model without the effect in question (see Table 5.1 for the experimental model (full model) and the null model (full model without the effect in question)).

Paired comparisons were performed in Matlab and R. For comparing 'naïve'/'exposed', 'naïve'/'recovery' and 'exposed'/'recovery' indicator responses for both EB exposures and mock treatments, *Paired Student T-Tests* ($\alpha = 0.05$) with adjusted standard deviations were conducted using R. All other paired comparisons were performed in Matlab using *Paired Student T-Tests* ($\alpha = 0.05$) or *Wilcoxon Signed Rank Tests* ($\alpha = 0.05$) depending on whether the data was normally distributed according to an *Anderson-Darling Normality Test* ($\alpha = 0.05$, see tables in section 5.3). No corrections for multiple comparisons were made. *Two-Sample Student T-Tests* ($\alpha = 0.05$) were performed in Matlab to compare 'naïve' odour-evoked indicator responses of different genotypes in a specific glomerulus.

3. Results

3.1 Establishing a Novel Behaviour Assay for Studying Olfactory Habituation in *Drosophila*

The Y-maze assay established by our collaborators at the National Centre for Biological Sciences in Bangalore displays an elegant behaviour paradigm in which to study habituation of the olfactory avoidance response in *Drosophila* (see section 1.5.1). Experiments performed using this paradigm improved the understanding of olfactory habituation substantially. Several mutants defective in this simple form of learning have been discovered and their necessity and sufficiency in distinct neuronal types of the *Drosophila* AL has been shown (Das et al., 2011b; McCann et al., 2011; Sadanandappa et al., 2013; Sudhakaran et al., 2012, 2014). The findings enabled the mapping of a previously unknown inhibitory circuit where potentiation of inhibitory transmission from local interneurons (LNs) onto odour-responsive projection neurons (PNs) mediates the reduced behavioural output characteristic of habituation (see section 1.5.2).

The initial incentive of this study was to test whether this inhibitory circuit mechanism also underlies other forms of olfactory habituation. For this reason, a behaviour assay was implemented and optimized to study habituation of the odour-evoked locomotor startle response. The odour-evoked locomotor startle response assay first described by Ulrike Heberleins group (Bainton et al., 2000; Wolf et al., 2002) had previously been successfully used to study olfactory habituation to pulsed odour presentations (Cho et al., 2004). The assay is based on a fly's immediate and transient increase in walking speed upon exposure to a novel odour (Cho et al., 2004; Wolf et al., 2002, see section 1.5). With repeated exposures to the specific odourant this startle response diminishes. Attenuation of the startle response displays characteristics typical of classically defined habituation (Thompson and Spencer, 1966; Rankin et al., 2009) such as spontaneous recovery after 30 minutes, dishabituation by mechanical stimulation, and generalization to similar stimuli (Cho et al., 2004). To induce habituation, Cho et al. (2004) exposed flies to eight 30 second pulses of ethanol vapour delivered every six minutes. With each pulse, the flies' maximal velocity as well as their total movement during ethanol exposure decreased while the onset of each startle peak was progressively delayed. A nearly maximal state of attenuation was achieved after four or five ethanol pulses (Cho et al., 2004).

The aim of the research performed in this chapter was (a) to implement the odour-evoked

locomotor startle response assay in the laboratory, (b) to show that wildtype flies show habituation of the odour-evoked startle response while mutants disrupted in the adenylate cyclase *rutabaga* do not, as reported in Cho et al. (2004), and (c) to test whether the neuronal circuit that mediates habituation of the olfactory avoidance response also underlies habituation of the odour-evoked startle response.

3.1.1 Continuous 30-minute EB Exposure

The locomotor tracking assay implemented in the laboratory was built based on a previously published design (Cho et al. (2004); Wolf et al. (2002), see Figure 2.1 and section 2.2.3 for details on the assay). To perform the assay, 10-15 flies were placed into each of three transparent observation chambers that contained an inlet and an outlet through which the air/odour stream was delivered. The flies' movement in response to odour presentations was tracked with a video camera from above (see Figure 2.1 and section 2.2.3 for details).

Initially, the experimental protocol was kept as closely as possible to the experiments conducted with the Y-maze, the aim being to mimic the induction of olfactory avoidance habituation. To induce short-term habituation (STH) in the Y-maze paradigm, flies are exposed to ethyl butyrate (EB) for half an hour continuously (Das et al., 2011b). Thus, the first approach was to expose flies to EB for 30 minutes. The protocol was composed as follows (Figure 3.1A). Flies were acclimatized to the habituation boxes for 10 minutes before they received a 30-second EB puff to measure their naïve startle response to a novel odour. After a continuous 30 minute EB exposure and a subsequent air interval of 8 minutes, the flies received another 30-second EB puff to measure their habituated startle response to the odour. The 8 minute air interval served to avoid potential effects of adaptation that occur in sensory neurons and last for up to several minutes (Störtkuhl et al., 1999; Zufall and Leinders-Zufall, 2000; de Bruyne et al., 1999). The flies' movement in response to the 'naïve' and 'exposed' odour presentation was tracked over a 60-second period starting 30 seconds before the 30-second EB pulse (as in Cho et al., 2004).

To further match the experimental conditions of the two assays, the air flow during testing and exposure was adjusted. In the Y-maze paradigm, the flies are tested in an air stream while the odourant exposure takes place in static air (Das et al., 2011b). The design of the habituation boxes did not allow odourant exposure via odour diffusion in static air, instead the flies were exposed to a lower air flow (380mL/min) than tested (1,202mL/min). The odour concentrations used were determined through preliminary tests showing that 0.3% was the lowest EB concentration that induced a startle response (data not shown). The concentration for the EB testing puffs was therefore kept at 0.3%. For EB exposure, different EB concentrations ranging from 0.1% to 0.5% were tested to determine the value that gave best results for the attenuation of the startle response.

To establish the best conditions for habituation of the startle response, the habituation behaviour of two fly strains was studied. A positive control that was expected to show pronounced habituation was compared to a negative control which was thought to exhibit defects

in the behaviour. *CantonS* (CS) wildtype flies served as positive controls as they show strong olfactory habituation in the locomotor startle response assay to repeated odour stimuli (Cho et al., 2004) as well as in the Y-maze assay to continuous 30 minute odourant exposure (Das et al., 2011b). The learning mutant *rutabaga* (*rut*), in contrast, (Levin et al., 1992; Han et al., 1992) which displays olfactory habituation defects in both assays (Cho et al., 2004; Das et al., 2011b) served as the negative control. *Rutabaga* mutants which have been extensively studied for their role in learning (Livingstone et al., 1984; Zars et al., 2000a; McGuire et al., 2003) are defective in the *rutabaga* gene which encodes a Ca^{2+}/calmodulin adenylate cyclase (Livingstone et al., 1984; Livingstone, 1985; Levin et al., 1992). Flies carrying rut^{2080};*UAS-rut*$^{+}$ were used instead of rut^{2080} as these flies showed increased movement at rest compared to CS wildtype flies (data not shown).

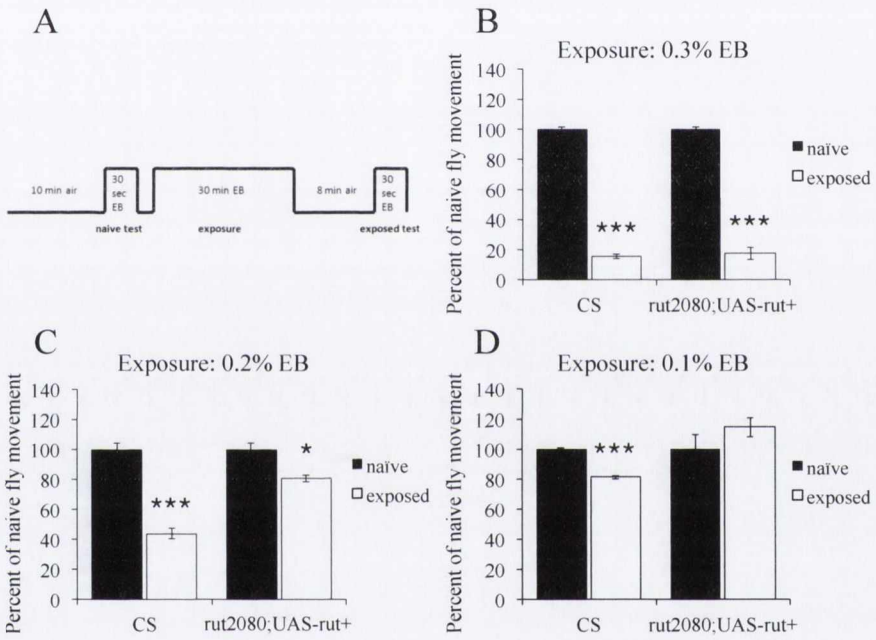


Figure 3.1: Continuous 30-minute EB exposure to different concentrations
Black bars represent startle response during a 30-second EB puff before exposure; white bars represent startle responses to a 30-second EB puff 8 minutes after 30-minute EB exposure. Testing was performed at a concentration of 0.3% EB, exposure was conducted at various concentrations. **(A)** Schematic of the experimental protocol. **(B/C)** Exposure to 0.3% (A) and 0.2% EB (B). CS and rut^{2080};*UAS-rut*$^{+}$ flies show a reduced startle response after exposure to both concentrations (*Student t-test, CS:* $t_{(4)}=36.98$, $P<0.001$ *(B) and* $t_{(4)}=9.574$, $P<0.001$ *(C),* rut^{2080};*UAS-rut*$^{+}$*:* $t_{(4)}=18.73$, $P<0.001$ *(B) and* $t_{(4)}=3.924$, $P=0.017$ *(C), n=3/bar*). **(D)** Exposure to 0.1% EB. CS flies show a significant reduction of the startle response in contrast to rut^{2080};*UAS-rut*$^{+}$ flies (*Student t-test,* $t_{(4)}=12.75$, $P<0.001$ *and* $t_{(4)}=1.273$, $P=0.272$, *n=3/bar*). $*$ $p<0.05$; $**$ $p<0.01$; $***$ $p<0.001$; error bars indicate mean $\pm$ SEM

Initially, a higher EB concentration was chosen for exposure than testing, similar as to the habituation experiments performed with the Y-maze. However, after 30 minutes of exposure to 0.5% EB some flies were immobile and lay on their sides or backs (data not shown). A similar observation was made by Wolf et al. (2002) after a 25-minute ethanol vapour exposure. When exposed to 0.3% EB for 30 minutes flies did not show any signs of incapacitation. CS wildtype and rut^{2080};*UAS-rut*$^{+}$ mutants, both displayed strong habituation of the olfac-

tory startle response after 0.3% EB exposure (*t-test*, $t_{(4)}=36.98$, $P<0.001$ *and* $t_{(4)}=18.73$, $P<0.001$; Figure 3.1B). Controls and mutants both decreased their startle response by approximately 80%. Exposure to 0.2% EB resulted in a strong attenuation of the startle response in CS flies (*t-test*, $t_{(4)}=9.574$, $P<0.001$; Figure 3.1C). They reduced their movement in response to the odour by approximately 60%. Rut^{2080};*UAS-rut*$^{+}$ flies also showed olfactory habituation but to a lower degree (*t-test*, $t_{(4)}=3.924$, $P=0.017$; Figure 3.1C). Their startle response decreased by approximately 20%. Finally, flies were exposed to 0.1% EB. CS flies showed a low but still highly significant degree of habituation of approximately 20% (t-test, $t_{(4)}=12.75$, $P<0.001$; Figure 3.1D). In contrast, rut^{2080};*UAS-rut*$^{+}$ mutants did not habituate to this concentration but showed a slightly increased startle response after exposure (*t-test*, $t_{(4)}=1.273$, $P=0.272$; Figure 3.1D).

Taken together, exposure to 0.1% EB appeared to induce habituation in CS flies but not in rut^{2080};*UAS-rut*$^{+}$ mutants. However, the quantitative difference between the positive and negative control was remarkably small, especially when compared to results obtained with the Y-maze assay. In the Y maze paradigm, CS flies show a decreased avoidance of 40-60% following 30 minute exposure while the avoidance behaviour of rut^{2080};*UAS-rut*$^{+}$ remains unchanged (Das et al., 2011b). A further concern was that odour residues may have lingered in the habituation boxes after the 30-minute odour exposure since exposure and testing was performed in the same boxes. The odourant exposure was performed inside the habituation chambers as taking the flies out of the boxes to expose them separately would have required anaesthesia. Anaesthesia was avoided due to its potential 'dishabituating' effect besides its well known detrimental consequences on fly behaviour (Barron, 2000). To diminish the problem of odour residues lingering around and to obtain a more substantial difference between the positive and negative control, flies were subsequently habituated to pulsed EB stimuli.

3.1.2 Pulsed Exposure to Different Odour Concentrations

Pulsed exposure offered the advantage that flies could be exposed to higher EB concentrations without suffering paralysis. It further allowed the rate of habituation to be directly monitored as each odour puff was recorded. The pulsed exposure performed initially consisted of ten 20-seconds lasting EB stimuli delivered with a 3-minute inter pulse interval (Figure 3.2A). In comparison to the previous experiments, the length of the odour stimuli was shortened to 20-seconds to reduce the time for movie analysis. A 20-second odour stimulus allowed video tracking over a 40 second period, capturing the flies movement 20-seconds before and 20-seconds during the odour presentation. Preliminary data showed that a 20-second EB puff was sufficient to induce a startle response (data not shown). The length of the inter pulse intervals was adapted from Cho et al. (2004) who reported similar degrees of habituation for three and six minute inter pulse intervals. Although Cho et al. (2004) performed most of their experiments with inter pulse intervals of six minutes three minute intervals were chosen to accelerate data collection. The air flow was set to 2,355mL/min.

Four different concentrations were tested to determine if there is a concentration at which there is a difference in startle response habituation between CS flies and *rutabaga* mutants.

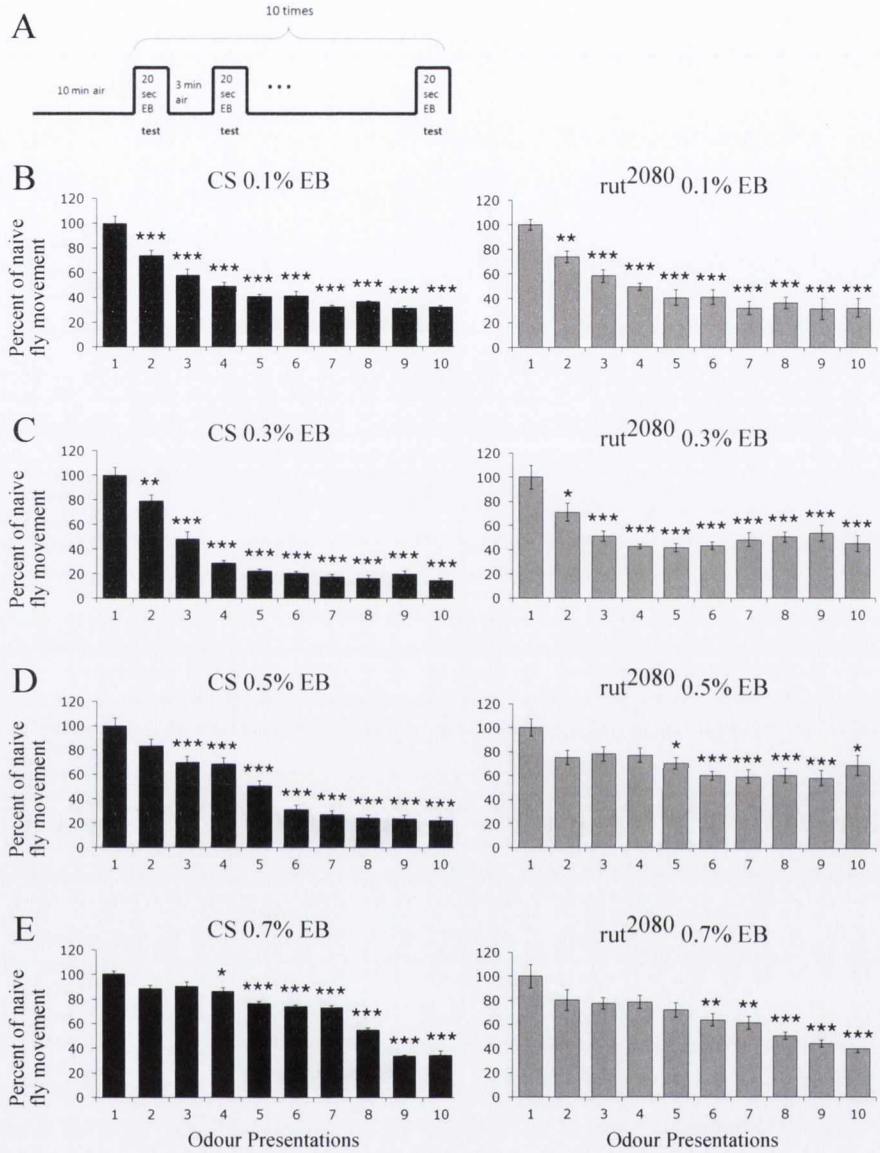


Figure 3.2: Pulsed EB exposure to different concentrations
Flies were exposed to ten 20-second EB pulses delivered every three minutes. Black (CS) and grey (*rut*^{2080}) bars indicate percent of naïve fly movement in response to the EB pulse delivery. EB concentrations varied between experiments. **(A)** Schematic of the experimental protocol. **(B/C)** Pulsed exposure to 0.1% and 0.3% EB. CS and *rut*^{2080} mutant show a decreased startle response from the second pulse onwards at both concentrations (*ANOVA, CS:* $F_{(9,20)}= 61.77$, $P<0.001$, *Tukey,* $P \leq 0.05$ *(B) and* $F_{(9,50)}= 75.79$, $P<0.001$, *Tukey,* $P \leq 0.05$ *(C), rut*^{2080}*:* $F_{(9,50)}=14.64$, $P<0.001$, *Tukey,* $P \leq 0.05$ *(B) and* $F_{(9,50)}=9.482$, $P<0.001$, *Tukey,* $P \leq 0.05$ *(C), n=6/bar*). **(D)** Pulsed exposure to 0.5% EB. CS flies show a decreased startle response from the third pulse onwards, *rut*^{2080} from the fifth pulse onwards (*ANOVA,* $F_{(9,110)}= 46.15$, $P<0.001$, *Tukey,* $P \leq 0.05$ *and* $F_{(9,110)}=4.436$, $P<0.001$, *Tukey,* $P \leq 0.05$, *n=12/bar*). **(E)** Pulsed exposure to 0.7% EB. CS flies display a reduced startle response from the fourth pulse onwards, *rut*^{2080} mutants from the sixth pulse onwards (*ANOVA,* $F_{(9,20)}= 95.38$, $P<0.001$, *Tukey,* $P \leq 0.05$ *and* $F_{(9,20)}=10.06$, $P<0.001$, *Tukey,* $P \leq 0.05$, *n=3/bar*). $*$ $p<0.05$; $**$ $p<0.01$; $***$ $p<0.001$. Error bars indicate mean $\pm$ SEM.

At the lowest exposure concentration, at 0.1% EB, both strains showed strong habituation of the olfactory startle response. CS controls and *rut*^{2080} mutants showed a decreased

response to the naïve first pulse from the second pulse onwards (*ANOVA, $F_{(9,20)}$= 61.77, P<0.001, Tukey, P* $\leq$ 0.05 *and $F_{(9,50)}$=14.64, P<0.001, Tukey, P* $\leq$ 0.05, Figure 3.2B). When exposed to 0.3% EB the startle response of both, CS and rut^{2080} flies, was reduced from the second pulse onwards (*ANOVA, $F_{(9,50)}$= 75.79, P<0.001, Tukey, P* $\leq$ 0.05 *and $F_{(9,50)}$=9.482, P<0.001, Tukey, P* $\leq$ 0.05, Figure 3.2C). Pulsed exposure to 0.5% EB resulted in a decreased startle response in CS flies from the third pulse onwards, in rut^{2080} from the fifth pulse onwards (*ANOVA, $F_{(9,110)}$= 46.15, P<0.001, Tukey, P* $\leq$ 0.05 *and $F_{(9,110)}$=4.436, P<0.001, Tukey, P* $\leq$ 0.05, Figure 3.2D). At the highest concentration of 0.7% EB, CS flies showed a reduced startle response from the fourth pulse onwards, rut^{2080} mutants from the sixth pulse onwards (*ANOVA, $F_{(9,20)}$= 95.38, P<0.001, Tukey, P* $\leq$ 0.05 *and $F_{(9,20)}$=10.06, P<0.001, Tukey, P* $\leq$ 0.05, Figure 3.2E).

Taken together, CS flies displayed strong habituation to all concentrations tested. rut^{2080} mutants, that have shown defects in odour induced startle response habituation previously (Cho et al., 2004), also habituated to all concentrations tested even if to a smaller degree than CS flies. As *rut* flies appeared to exhibit the least pronounced habituation to an EB concentration of 0.5%, this concentration was chosen for the following experiments.

3.1.3 Pulsed Exposure to Different Lengths of Interstimulus Intervals

To possibly obtain a more distinctive difference between CS and *rut* flies, the behavioural protocol was further improved by changing the air intervals in between EB presentations. Two separate experiments were performed with 6-minute and 9-minute interstimulus intervals. To rule out the possibility that the length of the EB pulses had an effect on the rate of habituation, odour pulse length was increased to 30 seconds, as in most of the experiments performed by Cho et al. (2004). Accordingly, video tracking was conducted over a 60 second period, starting 30 seconds before the EB pulse. The number of odour pulses delivered was limited to six to reduce the amount of video analysis conducted. In this way, the duration of the experiment performed was also kept comparable to those conducted with the Y-maze paradigm. To further eliminate the possibility that the air pressure delivered into the habituating chambers was too high the air flow rate was reduced to 1,202mL/min.

Pulsed exposure to 0.5% EB with an interstimulus interval of 6 minutes resulted in a reduced startle response in CS flies from the second pulse onwards (*ANOVA, $F_{(5,30)}$= 13.12, P<0.001, Tukey, P* $\leq$ 0.05, Figure 3.3B). The odour-induced startle response of rut^{2080}*;UAS-*rut^{+} *mutants*, in contrast, was indistinguishable in between pulses delivered every six minutes (*ANOVA, $F_{(5,30)}$= 0.8344, P=0.536*, Figure 3.3B). Pulsed exposure with an interstimulus interval of 9 minutes yielded similar results. CS flies showed a decrement in odour-induced startle response from the second pulse onwards, the startle response of rut^{2080}*;UAS-*rut^{+} mutants, however, was indistinguishable in between pulses (*ANOVA, $F_{(5,66)}$= 56.13, P<0.001, Tukey, P* $\leq$ 0.05 *and $F_{(5,66)}$= 0.04351, P=0.999*, Figure 3.3C).

Taken together, increasing the interstimulus interval to 6 or 9 minutes yielded in pronounced differences in habituation behaviour between CS flies and *rut* mutants. The dif-

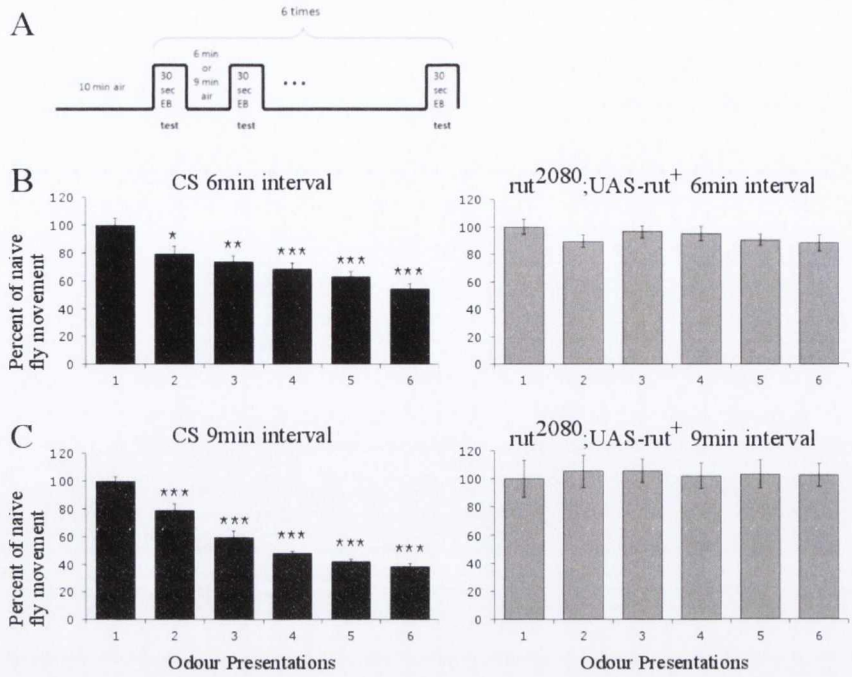


Figure 3.3: Pulsed exposure to different lengths of interstimulus intervals
Flies were exposed to six 30-second EB pulses at a concentration of 0.5%. Black (CS) and grey (*rut*^{2080}) bars indicate percent of naïve fly movement in response to the EB pulse delivery. Interstimulus intervals were 6 (B) or 9 (C) minutes. **(A)** Schematic of the experimental protocol. **(B/C)** Pulsed exposure with an interstimulus interval of 6 (B) or 9 (C) minutes. At both interstimulus intervals, CS flies showed a reduced startle response from the second pulse onwards while the odour-induced startle response of *rut*^{2080} mutants was indistinguishable in between pulses (*ANOVA, CS:* $F_{(5,30)}$*= 13.12, P<0.001, Tukey,* $P \leq 0.05$ *(B) and* $F_{(5,66)}$*= 56.13, P<0.001, Tukey,* $P \leq 0.05$ *(C),* *rut*^{2080}*;UAS-rut*$^{+}$*:* $F_{(5,30)}$*= 0.8344, P=0.536 (B) and* $F_{(5,66)}$*= 0.04351, P=0.999 (C), n=9/bar (B) and 12/bar (C)).* $*$ $p<0.05$; $**$ $p<0.01$; $***$ $p<0.001$. Error bars indicate mean $\pm$ SEM.

ferences in their ability to habituate were comparable to those observed with the Y-maze paradigm. In the experiments conducted with an interstimulus interval of 9 minutes, the odour-evoked startle response was reduced by approximately 60% in CS flies in response to the sixth odour presentation while the startle response of *rut* mutants remained unchanged.

3.1.4 Mutants Defective in Olfactory Short-Term Habituation

After establishing a protocol that allowed the study of mutants for their ability to show habituation of the odour-evoked startle response, it was aimed to test whether olfactory avoidance habituation and habituation of the odour-evoked startle response relied on an universal neuronal circuit situated in the *Drosophila* AL. A circuit underlying olfactory avoidance habituation has been proposed previously (Das et al., 2011b). Potentiation of inhibitory transmission from inhibitory local interneurons (LNs) onto odour-responsive projection neurons (PNs) is believed to drive this form of habituation (Das et al., 2011b, see section 1.5.2). Among others, the Ca^{2+}/calmodulin adenylate cyclase *rutabaga* is required in the LN1 class of inhibitory LNs for the formation of olfactory avoidance habituation as well as NMDA receptors (NMDARs) in odour-responsive PNs (Das et al., 2011b). To test whether habituation

of the locomotor startle response likewise requires *rutabaga* and NMDARs in the respective cell types, RNAi-mediated protein knockdowns targeted to the specific neuronal types were used as well as spatially-restricted expression of a functional protein construct in a mutant background.

Firstly, to show that *rutabaga* is necessary in inhibitory local interneurons its function was blocked through expression of a transgenic RNAi construct in all GABAergic GAD1 expressing neurons (*GAD1-Gal4>UAS-rutRNAi*) as well as in LNs of the inhibitory LN1 population (*LN1-Gal4>UAS-rutRNAi*). If habituation of the odour-evoked startle response was mediated through the same circuit in the antennal lobe one would expect that *rutabaga* RNAi knockdown in GABAergic and LN1 neurons prevents the decline in odour-evoked startle responses observed in wildtype flies. The established protocol was used composing six 30 seconds lasting EB pulses at a concentration of 0.5% and 9-minute air intervals (Figure 3.4A). CS controls showed a reduced startle response to the odour delivery from the fourth pulse onwards (*ANOVA*, $F_{(5,30)}= 15.64$, $P<0.001$, *Tukey*, $P \leq 0.05$, Figure 3.4B). *Rutabaga* knockdown in GABAergic neurons (*GAD1-Gal4>UAS-rutRNAi*) or inhibitory AL local interneurons (*LN1-Gal4>UAS-rutRNAi*) did not impair habituation. *GAD1-Gal4>UAS-rutRNAi* flies decreased their startle response from the fifth pulse onwards, *LN1-Gal4>UAS-rutRNAi* from the fourth pulse onwards (*ANOVA*, $F_{(5,30)}= 19.76$, $P<0.001$, *Tukey*, $P \leq 0.05$ *and* $F_{(5,30)}= 5.249$, $P=0.001$, *Tukey*, $P \leq 0.05$, Figure 3.4C,D).

To confirm these results, spatially controlled expression of a wildtype *rutabaga* transgene in the respective cell types in a mutant background was performed to check whether the mutant phenotype could be rescued. Thus, wildtype *rutabaga* was expressed in GABAergic neurons (*GAD1-Gal4>*rut^{2080}*;UAS-rut*$^{+}$) and inhibitory local interneurons in the AL (*LN1-Gal4>*rut^{2080}*;UAS-rut*$^{+}$) in a mutant rut^{2080} background (the entire genotype is listed in section 5.1). If olfactory habituation in the startle response assay arose from potentiation of GABAergic transmission in the AL one would expect that transgenic expression of functional *rutabaga* rescued the habituation deficit observed in rut^{2080}*,UAS-rut*$^{+}$ *flies*. As shown before, rut^{2080}*,UAS-rut*$^{+}$ flies did not show habituation of odour-induced startle responses. Their startle responses were indistinguishable in between odour pulse deliveries (*ANOVA*, $F_{(5,30)}= 0.4089$, $P=0.839$, Figure 3.1.4F). Rescue of functional *rutabaga* in GABAergic neurons (*GAD1-Gal4>*rut^{2080}*;UAS-rut*$^{+}$) or in AL local interneurons (*LN1-Gal4>*rut^{2080}*;UAS-rut*$^{+}$) did not rescue startle response habituation. Both fly strains displayed indistinguishable startle responses to the EB pulses delivered (*ANOVA*, $F_{(5,30)}= 0.1457$, $P=0.980$, *and* $F_{(5,30)}= 0.5593$, $P=0.730$, Figure 3.4G,H). Taken together, the results neither show a habituation defect in flies with a RNAi based *rutabaga* knockdown in GABAergic neurons or LN1 local interneurons nor a rescue of the habituation phenotype in flies that express a functional *rutabaga* transgene in GABAergic or LN1 neurons in a *rutabaga* mutant background. Thus, *rutabaga* appears to be neither necessary nor sufficient in inhibitory local interneurons in the AL for olfactory startle response habituation.

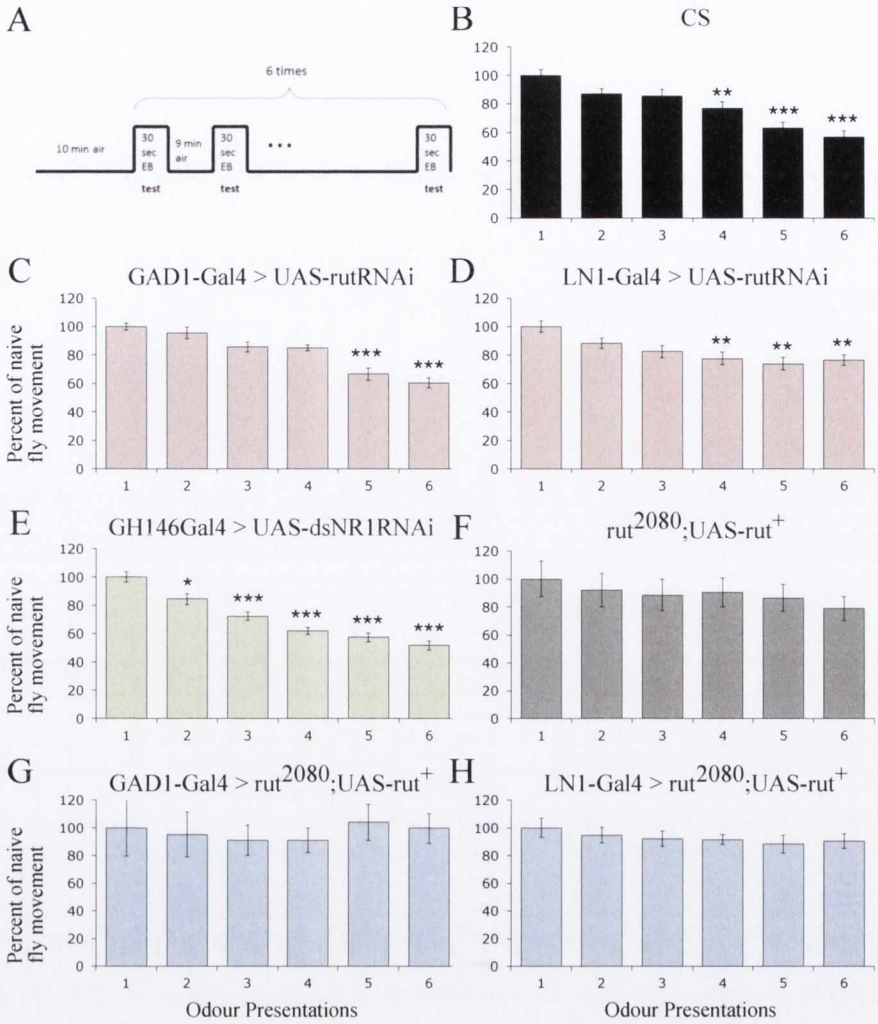


Figure 3.4: Odour-induced startle response habituation does not require *rutabaga* in GABAergic LNs and NMDA receptors in PNs

Flies were exposed to six 30-second lasting EB pulses at a concentration of 0.5%. EB pulses were delivered with an interstimulus interval of 9 minutes. Bars indicate percent of naïve fly movement in response to the EB pulse delivery. **(A)** Schematic of the experimental protocol. **(B)** CS controls show a reduced startle response from the fourth pulse onwards (*ANOVA, $F_{(5,30)}$= 15.64, P<0.001, Tukey, P ≤ 0.05, n=6/bar*). **(C/D)** RNAi based *rutabaga* knockdown in GABAergic neurons (*GAD1-Gal4>UAS-rutRNAi*) or LN1 local interneurons (*LN1-Gal4>UAS-rutRNAi*) does not impair habituation. *GAD1-Gal4>UAS-rutRNAi* flies reduce their startle response from the fifth pulse onwards, *LN1-Gal4>UAS-rutRNAi* from the fourth pulse onwards (*ANOVA, $F_{(5,30)}$= 19.76, P<0.001, Tukey, P ≤ 0.05 and $F_{(5,30)}$= 5.249, P=0.001, Tukey, P ≤ 0.05, n=6/bar*). **(E)** Transgenic RNAi knockdown against NR1, a subunit of NMDA receptors, (*GH146-Gal4>UAS-dsNR1*) does not affect habituation. Flies reduce their startle response from the second pulse onwards (*ANOVA, $F_{(5,30)}$= 30.76, P<0.001, Tukey, P ≤ 0.05, n=6/bar*). **(F)** *Rut^{2080},UAS-rut^{+}* flies do not show habituation of odour-induced startle responses. Their startle response is indistinguishable in between odour pulse deliveries (*ANOVA, $F_{(5,30)}$= 0.4089, P=0.839, n=6/bar*). **(G/H)** Rescue of functional *rutabaga* in GABAergic neurons (*GAD1-Gal4>rut^{2080};UAS-rut^{+}*) or LN1 local interneurons (*LN1-Gal4>rut^{2080};UAS-rut^{+}*) does not rescue startle response habituation. Flies display indistinguishable startle responses to the EB pulses delivered (*ANOVA, $F_{(5,30)}$= 0.1457, P=0.980, and $F_{(5,30)}$= 0.5593, P=0.730, n=6/bar*). * p<0.05; ** p<0.01; *** p<0.001. Error bars indicate mean ± SEM

As a second approach, it was studied whether NMDARs are necessary in EB-responsive PNs for odour-induced startle response habituation. Thus, NMDAR function was blocked

through the expression of a transgenic RNAi construct against the NMDAR subunit NR1 in PNs using the GH146 Gal4 line (*GH146-Gal4>UAS-dsNR1RNAi*). GH146 expresses the Gal4 protein in ~90 out of the ~150 PNs in total including those that are activated by EB. NMDA receptor knockdown in PNs also did not affect habituation behaviour in the startle response assay. *GH146-Gal4>UAS-dsNR1RNAi* flies showed a decreased startle response from the second pulse onwards (*ANOVA*, $F_{(5,30)}= 30.76$, $P<0.001$, *Tukey*, $P \leq 0.05$, Figure 3.4E). Thus, NMDARs in odour-responsive PNs likewise do not appear necessary for odour-induced startle response habituation.

3.1.5 Discussion

Implementing the Odour-Evoked Startle Response Assay to Study Habituation

The initial aim was to implement the odour-evoked locomotor startle response assay in the laboratory and to show that wildtype flies exhibit strong olfactory habituation in this assay while mutants disrupted in the Ca^{2+}/calmodulin adenylate cyclase *rutabaga* do not, as shown by Cho et al. (2004). The odour-evoked locomotor startle response assay was built based on previously published designs (Cho et al., 2004; Wolf et al., 2002, see 2.2.3 for details). A number of protocols for inducing habituation of the locomotor startle response were tested. Odourant exposures differed with respect to continuous or pulsed stimulation (see sections 3.1.1 and 3.1.2), odour concentration (see sections 3.1.1 and 3.1.2), and interstimulus length in the case of pulsed odour exposure (see section 3.1.3). Best results were obtained with a protocol that consisted of six 30-second EB pulses with a concentration of 0.5% and an interstimulus interval of 9 minutes. This protocol resulted in an approximately 60% reduction in startle response in CS flies whereas the startle response of *rutabaga* mutants remained unchanged (Figure 3.2C).

While implementing the protocol typical characteristics of habituation were observed, some of which had been shown previously (Cho et al., 2004). Typically, the degree of the behavioural decrement associated with habituation is dependent on the interstimulus length when the odour stimulation is pulsed. More frequent stimulation results in more rapid and/or more pronounced habituation (Rankin et al., 2009; Thompson and Spencer, 1966). In line with this, smaller interstimulus intervals between the odour pulses increased habituation of the odour-evoked startle response in the present study (Figure 3.3). This effect was observed in CS flies as well as *rutabaga* mutants. Notably, although titled a 'learning mutant' *rutabaga* mutants show habituation (Cho et al., 2004; Asztalos et al., 2007a) and learning (McGuire et al., 2003) albeit to lower degrees than wildtype flies. Another characteristic of behavioural habituation is its dependence on stimulus intensity. Typically, less intense stimuli result in more rapid and/or more pronounced habituation (Rankin et al., 2009; Thompson and Spencer, 1966). Consistently, pulsed odourant exposure to lower concentrations resulted in more rapid habituation of the startle response compared to higher concentration (see Figure 3.2). This was again observed in CS flies and *rutabaga* mutants.

Interestingly, opposite findings were made for 30-minute continuous exposure. Here, both wildtype and mutant flies showed more pronounced habituation following exposure to a higher odour concentration compared to lower concentrations (Figure 3.1). A potential explanation for this observation are the odour concentrations used for testing and exposure. 0.3% was the lowest EB concentration that exhibited a startle response whereas 30-minute exposure as high as 0.5% resulted in incapacitation of single flies. It was thus only possible to expose the flies to the same or a lower concentration than the 0.3% used for the test pulses. In comparison, for short-term habituation of the olfactory avoidance response measured using the Y-maze the odourant exposure is performed at a higher concentration than testing. The findings obtained in the present study may suggest that flies not only 'habituate' to an odour but also to its concentration. As seen in Figure 3.1B, flies reduce their startle response when they are tested and exposed at the same concentration of 0.3% EB. However, when exposed to a lower concentration (0.1% EB) than tested (0.3% EB) the startle response is less substantially reduced, as seen in Figure 3.1D. Further noteworthy is that the observations made after 30-minute continuous exposure are possibly confounded by sensory adaptation occurring in olfactory sensory neurons (OSNs). Adaptation of odourant receptor transduction reduces odour-evoked OSN responses which likewise results in a reduced behavioural outcome and lasts for several minutes (Nagel et al., 2015; Störtkuhl et al., 1999). To avoid potential effects of sensory adaptation an 8 minute air interval was given following the 30-minute exposure and preceding the subsequent odour presentation. However, since the odourant exposure was performed in the same habituation chambers as the subsequent testing for the flies' odour-evoked startle response, the odour may have not cleared out of the boxes rapidly enough to allow for recovery from adaptation.

An Identical Neuronal Circuitry Underlying Different Form of Olfactory Habituation?

Following the implementation of the odour-evoked startle response assay for the study of habituation, the assay was used to test the hypothesis of whether different forms of olfactory habituation utilize a universal neuronal circuit. Since habituation of the olfactory avoidance response has been studied extensively and a neuronal circuit has been proposed (Das et al., 2011b), genetically modified flies that showed defects in the Y-maze paradigm were tested for their ability to show habituation of the odour-evoked startle response. However, knockdown of specific gene function in particular neurons such as performed in *LN1-Gal4>UAS-rutRNAi*, *GAD1-Gal4>UAS-rutRNAi*, and *GH146-Gal4>UAS-dsNR1RNAi* flies did not cause habituation defects in the olfactory startle response assay. Moreover, rescuing *rutabaga* function by genetically expression of a wildtype *rutabaga* construct in subsets of neurons which rescued the behavioural phenotype in the Y-maze paradigm did not rescue rut^{2080} flies' habituation defect in the olfactory startle response assay. A potential reason for failing to block habituation of the odour-evoked startle response using RNAi could theoretically be that the RNAi constructs against *rutabaga* and *dsNR1* did not sufficiently knock down the target protein. Failure of rescuing the habituation phenotype by expressing wild-

type *rutabaga* in specific neuronal subsets could further be due to insufficient expression of the protein to rescue its function. However, these explanations are unlikely as the same genotypes have shown effects in the Y-maze assay. All in all, the findings thus suggest that habituation of the odour-evoked startle response is likely not mediated through the inhibitory circuit in the antennal lobe as it has been shown for habituation of the olfactory avoidance response.

Potential reasons for the different underlying neuronal mechanisms could be the nature of the odourant exposure (continuous vs. pulsed) or the behaviour that is measured (startle response vs. odour choice). As of yet, the inhibitory neuronal circuit in the fly antennal lobe has exclusively been implicated in mediating habituation to aversive odourants in adult *Drosophila* and appetitive odours in larvae (Das et al., 2011b; Larkin et al., 2010). Both forms, are induced by continuous odourant exposure, consisting of 5-minute exposure to ethyl acetate in larvae and 30-minute exposure to EB in adults, and were tested in choice assays. Habituation of the odour-evoked startle assay, on the other hand, is induced by repeated odour presentations and measured in the form of odour-evoked increases in walking speed. It is thus not too surprising that the two forms of olfactory habituation may utilize different neuronal mechanisms. In line with the finding that habituation of the odour-evoked startle response may not be mediated by potentiation of inhibition within the fly antennal lobe, the mushroom bodies (MBs) have been implicated in driving this form of habituation. Both, chemical ablation of the MBs and their inactivation by tetanus toxin disrupted habituation of the startle response to pulsed ethanol stimulation (Cho et al., 2004).

3.2 Establishing a Novel Calcium Imaging Protocol for Olfactory Short-Term Habituation in *Drosophila*

Olfactory short-term and long-term habituation (STH and LTH) have been extensively studied behaviourally, using the Y-maze paradigm, and genetically, by means of mutant analyses and cell-directed RNAi-mediated knockdowns. This led to the identification of a range of synaptic proteins that are required for these simple forms of learning (Das et al., 2011b; McCann et al., 2011; Sadanandappa et al., 2013; Sudhakaran et al., 2012, 2014). The findings point to an inhibitory recurrent circuit motif that drives olfactory avoidance habituation (Ramaswami, 2014; Twick et al., 2014). Increased GABAergic transmission from LN1 interneurons is predicted to suppress PN activity which in turn is thought to reduce behavioural aversion. However, behavioural analysis of genetically modified animals is limited in that they cannot directly show physiological changes associated with the behaviour. Recent advances using functional Ca^{2+} imaging have shown that LTH is accompanied by reductions in PN activity as predicted by the behavioural data (Das et al., 2011b; Sachse et al., 2007; Sudhakaran et al., 2014). To similarly investigate the physiological underpinnings of olfactory STH, it was aimed to likewise measure changes in Ca^{2+} transients following a STH protocol.

Ca^{2+} imaging in olfactory PNs provides an excellent tool for measuring the synaptic plasticity that occurs during STH. Ca^{2+} transients are a good indicator for neuronal activity as changes in intracellular Ca^{2+} influx are tightly coupled with changes in membrane voltage (Berridge et al., 2000; Bootman et al., 2001b). However, to study whether STH is accompanied by similar changes in odour-evoked Ca^{2+} levels as LTH, a number of adjustments had to be made to the already existing LTH Ca^{2+} imaging protocol: A STH protocol with a shorter odourant exposure needed to be implemented, a novel fly preparation adapted, and the odour-delivery system modified.

For the LTH experiments only the testing of EB-evoked PN response was performed under the microscope, the four day exposure was done separately in an odour-filled bottle. This could not be directly adapted for STH imaging, the reason being that STH memory is labile and has a half-life time of around 30 minutes. By the time the odour-exposed fly would be dissected and positioned under the microscope to be tested, STH would have already recovered significantly. Handling of the fly could furthermore cause dishabituation. Therefore, a protocol needed to be established that allowed the whole experiment to be performed under the microscope, including a 'naïve' test, the exposure itself, and an 'exposed' test. This approach furthermore offered the advantage that odour-evoked Ca^{2+} responses preceding and succeeding odourant exposure could be measured and compared within the same fly without the need for any intervention or physical manipulation.

Implementation of such a protocol required the adaptation of a fly preparation that remained alive for the whole duration of the protocol. The LTH Ca^{2+} imaging experiments performed previously made use of an isolated brain preparation which exhibited only a limited life time (Das et al., 2011b). For STH imaging a fly preparation was required that

remained alive for hours rather than tens of minutes without showing any signs of neuronal deterioration. This was necessary since the aim was to not only expose the fly preparation to an odourant but to also investigate whether changes observed recovered spontaneously.

Finally, the odour delivery system needed to be modified to continuously deliver a stable odour concentration allowing the exposure of the fly under the microscope. The odour delivery system used for the LTH experiments consisted of a main air stream that was continuously directed to the fly and a second air stream that was normally also pointed to the fly but diverted through an odour bottle during odour presentation (based on the design from Wang et al., 2003). The odour bottle contained the diluted odourant on a piece of filter paper. While this system was adequate for testing the odour responses of LTH exposed flies, since the air stream was only briefly run through the odour bottle, prolonged air flow, as would have been required for STH exposure, would have likely rapidly dried out the filter paper and therefore changed the odour concentration substantially. The odour concentration would have presumably not only dropped from one fly to the next but also from the 'naïve' to the 'exposed' test making a quantitative comparison of odour-evoked GCaMP responses before and after odourant exposure fraught with error. Thus, a new odour delivery system was required that not only delivered stable concentrations for each odour presentation but that was also able to hold the concentration during prolonged odourant exposure.

Multiple changes to the odour delivery system and STH Ca^{2+} imaging protocol were required as described subsequently. Implementing the STH protocol, adopting the fly preparation and particularly building a modified odour delivery system was done in collaboration with colleague John Lee (for a detailed description on the technical specifications of the odour delivery system see section 2.2.4 and Lee, 2015).

Ca^{2+} Imaging Preparation

To ensure the viability of the fly throughout the entire protocol, an *in vivo* fly preparation that showed good health for more than three hours was adapted. The preparation acquired, which is based on cutting a window into the head cuticule of a restrained fly (see 2.2.4 for details), has been widely used for patch clamp recordings and functional Ca^{2+} imaging experiments in the *Drosophila* antennal lobes (AL) (Wilson et al., 2004; Wilson and Laurent, 2005; Jayaraman and Laurent, 2007). It reveals a dorsal view onto the lobes (see Figure 3.5).

To perform Ca^{2+} imaging from PNs, the Ca^{2+} indicators GCaMP3 or GCaMP6m were expressed in a wide range of PNs using the Gal4 driver line GH146 (see section 3.3.1 for details on the expression pattern of GH146). At the beginning of the work performed for this study the genetically encoded Ca^{2+} indicator (GECI) GCaMP3 was the furthest developed sensor with greater baseline fluorescence (3-fold), protein stability, dynamic range (3-fold) and Ca^{2+}-affinity (1.3-fold) than its precursor protein (Tian et al., 2009), thus providing an ideal tool for assessing the changes in odour-evoked Ca^{2+} influxes in PNs. Later the more advanced GECI GCaMP6 was available which offered higher Ca^{2+} sensitivity than GCaMP3.

Two photon microscopy was availed to record Ca^{2+} dynamics in restricted glomerular

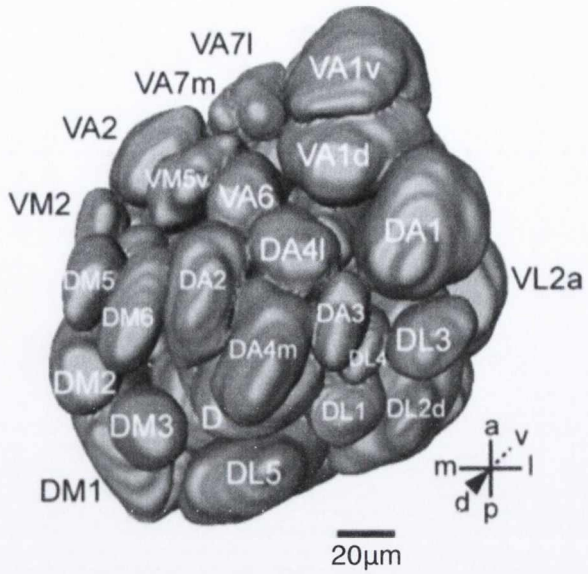


Figure 3.5: Dorsal view onto one of the antennal lobes
Depicted is are the different glomeruli seen from a dorsal view onto one of the antennal lobes. Among others, the glomeruli imaged in the present study are shown. DM5, DM2 and DM1 as well as DM6 and DM3 re situated medially while DL5 and DL1 can be seen posteriorly (Figure from Grabe et al., 2015a)

compartments in the AL. It offers the advantage that neurons can be imaged from deep brain regions while it provides good spatial resolution and reduced tissue damage and fluorophore photobleaching compared to other imaging techniques (Oheim et al., 2006). In the majority of the preparations studied, the two most dorsal glomerular layers could be reliably imaged using two photon microscopy. In the deeper glomerular layers the detection of individual glomerular was only possible in few preparations due to low fluorescence.

The dorsal view onto the AL revealed by the live preparation enabled a straightforward identification of DM2 and DM5, the two glomeruli for which reductions in EB-evoked GCaMP responses after 4-day EB exposure had been shown previously (Das et al., 2011b). Whether odour-evoked GCaMP responses in these glomeruli were also reduced following an STH exposure protocol was subject of this study. To investigate whether decreases in odour-evoked GCaMP responses was a general phenomenon following short-term odourant exposure, the number of glomeruli studied was extended beyond the two studied following long-term exposure. An additional set of five glomeruli could be determined reliably from the two most dorsal glomerular layers. In the most dorsal plane the glomeruli DM6, DM3, DL5, and DL1 were identified. In a ~10μm more ventral focal plane the glomeruli DM5, DM2, and DM1 were easily recognizable (see Figure 3.6 for representative images). The glomerular identity was initially identified using the glomerular atlas of Laissue et al. (1999) and confirmed by coincident expression of RFP in single OSN populations to mark a specific glomerulus and GFP in GH146 marked PNs by combining the Q and Gal4/UAS binary expression systems (data not shown).

All of the glomeruli identified apart from the DL5 exhibited an increase in the GCaMP signal upon ethyl butyrate (EB) stimulation (see Figure 3.11 blue traces). Notably, EB does

not exclusively activate these glomeruli. Olfactory sensory neurons that project to the dorsal DC1 glomerulus, which was only infrequently identified in the present study, and those innervating more ventral glomeruli such as VC3, VM2, VM3, VM5d, VM5v VC3, and VC4, which were too far ventral to be studied here, were also reported to respond to EB stimulation (Hallem and Carlson, 2006).

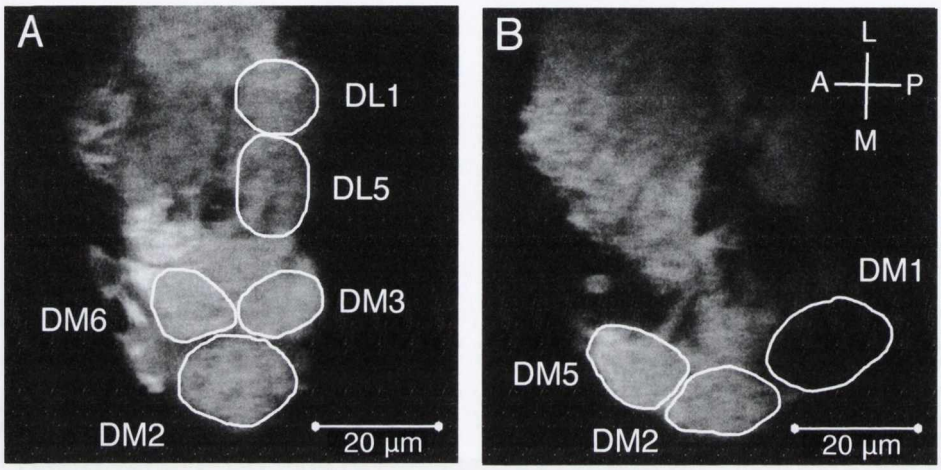


Figure 3.6: Representative images of the two planes imaged
Odour-evoked Ca^{2+} responses were recorded within two planes of the *Drosophila* antennal lobe. Depicted are the location of the seven glomeruli studied in flies expressing GFP in GH146-labelled PNs (*GH146-QF x QUAS-GFP*). **(A)** In the most-dorsal plane the medial-located glomeruli DM6 and DM3 were reliably recognized as well as the posterior-located DL5 and DL1. **(B)** In a ~10μm more ventral plane the medial glomeruli DM5, DM2, and DM1 were reliably identified.

Preliminary Odour Delivery System

The objective of performing short-term odourant exposure under the microscope necessitated the delivery of a stable odour concentration throughout the exposure but also for the 'naïve' and 'exposed' odour stimuli to allow for quantitative comparisons of the odour-evoked GCaMP signals. To minimize odour depletion and to match the odour supply with that of the behavioural testing apparatus, an odour delivery system was implemented that was based on an odourant dilution in paraffin oil. However, even when the odour was diluted in paraffin oil a more slowly but steady odour depletion was expected to occur over time. To further prevent this effect air was not run continuously through the odour bottle but instead was 'primed' before each odour presentation by directing an air line through the bottle and then into the exhaust before switching the line to the fly. In this way, the odour channel was flushed and accumulated odour residues within the bottle and attached tubing was removed. By priming the odour line in this way, a dynamic odour equilibrium in the head space of the odourant bottle was aimed to be established to ensure a stable odour concentration of the subsequently given odour stimulus to the fly (see section 2.2.4 for details on the established odour delivery system).

Preliminary Ca^{2+} Imaging Protocol

For the implementation of an experimental protocol for studying neurophysiological changes associated with STH using Ca^{2+} imaging, the aim was to match it to the behavioural protocol as much as possible to ensure that the same neuronal mechanisms were studied for behaviour and imaging. The standardized behaviour protocol for STH is carried out as follows (Das et al., 2011b): Flies are pretested in the Y-maze assay at a concentration of 10^{-3} EB diluted in paraffin oil to measure their naïve odour avoidance. Subsequently the flies are exposed to 5% EB for 30 minutes. For exposure the flies are transferred into a 100mL bottle that contains a suspended Eppendorf with a 1mL odour/paraffin dilution. The Eppendorf is covered by a plastic foil with perforated holes to allow for odour diffusion in the bottle. Odour exposure is followed by another test in the Y-maze assay to determine their 'habituated' avoidance response (see Figure 1.5 and section 1.5.1 for details about the Y-maze assay).

Despite attempting to establish a Ca^{2+} imaging protocol as similar as possible to the behaviour a few discrepancies could not be overcome. Namely the two protocols differed in terms of the length and nature of the odourant exposure and the exact odour concentration delivered. For the standard behavioural protocol, flies are exposed to the odour for 30 minutes however 15 minute exposure elicits a similar reduction in behavioural aversion as 30 minutes, even though with a shorter recovery time (pers. comm. with collaborators in NCBS, Bangalore, India). To enhance the data collection this shorter exposure time was adopted for the Ca^{2+} imaging experiments. As the flies were supposed to be exposed under the microscope and only one fly at a time could run through the protocol a 30-minute exposure would have taken too long. To induce behavioural STH the flies are further exposed in static air with the odour slowly diffusing in the bottle. However, for the imaging such an exposure could not be implemented. To expose flies under the microscope they were subjected to a constant odour stream throughout the exposure. Moreover it was not possible to exactly match the odour concentrations used for the behaviour and the Ca^{2+} imaging as the odour delivery differed between the two and the actual concentration reaching the fly could not be determined.

The established Ca^{2+} imaging protocol was carried out as outlined in Figure 3.7. It consisted of two 1-second odour stimuli delivered before a 15-minute odourant exposure which was followed by a 10-minute air interval and another set of 1-second odour stimuli. Two odour pulses were delivered preceding and succeeding odourant exposure to allow for imaging from both identified focal planes (see Figure 3.6). A 2-minute air interval separated the two odour stimuli to prevent potential confounding effects due to sensory adaptation that occur in olfactory sensory neurons (Störtkuhl et al., 1999; Zufall and Leinders-Zufall, 2000; de Bruyne et al., 1999). Preliminary data showed that a 2-minute inter pulse interval was sufficient as odour-evoked Ca^{2+} were indistinguishable between two consecutive odour presentations spaced two minutes apart (data not shown). The 10-minute air interval following 15-minute odourant exposure allowed for the recovery of sensory adaptations in OSNs which were assumed to occur (Störtkuhl et al., 1999; Zufall and Leinders-Zufall, 2000; de Bruyne

et al., 1999). Although the neuronal circuit underlying habituation of the olfactory avoidance response appears to be independent of changes in OSNs (Das et al., 2011b), sensory adaptations could confound the results obtained by Ca^{2+} imaging. As adaptation in sensory neurons last for several minutes (Störtkuhl et al., 1999; Zufall and Leinders-Zufall, 2000; de Bruyne et al., 1999), a 10-minute air interval was determined to be sufficient for these changes to recover.



Figure 3.7: Preliminary Ca^{2+} imaging protocol
The preliminary Ca^{2+} imaging protocol consisted of two 1-second odour presentations spaced 2 minutes apart followed by a 15-minute odour exposure, a 10-minute air interval and another two 1-second odour presentations. Two odour pulses were delivered before and after odourant exposure to enable Ca^{2+} imaging from both identified glomerular planes in each fly. The 10-minute air interval allowed for the effects of sensory adaptation to decay before the 'exposed' odour-evoked Ca^{2+} response was assessed.

An EB dilution of 10% in paraffin was chosen as this concentration elicited GCaMP response in most of the identified glomeruli, except for the DL5 glomerulus, but still only activated a restricted glomerular subset of all glomeruli. If widespread GCaMP responses were seen in the entire lobe this would be indicative for an odour concentration that possibly saturated neuronal responses, as higher odour concentrations recruit additional glomeruli (Hallem and Carlson, 2006). Since the odour concentration that reaches the fly is highly dependent on details of the odour delivery system (Vetter et al., 2006), it was difficult to compare the concentration delivered to that of other studies.

Preliminary Data Collection

With the described fly preparation, odour delivery system and experimental protocol, the effects of 15-minute odour exposure on odour-evoked GCaMP responses in PNs targeting seven glomeruli in the two identified glomerular planes in the *Drosophila* AL were studied. EB-evoked GCaMP3 responses to the first odour pulses were recorded from the second glomerular layer, including PNs projecting to the DM5, DM2, and DM1 glomerulus. GCaMP3 responses to the second pulse were recorded from two glomeruli situated in the first layer, namely DM6 and DM3.

Upon the onset of the odour stimulus, PNs projecting to all glomeruli showed a rapid increase in the GCaMP fluorescence (see 3.8 A-C blue traces for GCaMP responses in the glomeruli DM5, DM2, and DM1). The sudden increase in GCaMP levels reflects Ca^{2+} rushing into the neurons from the extracellular space, through neurotransmitter receptors and voltage-gated Ca^{2+} channels, as well as from intracellular Ca^{2+} stores, through inositol-1,4,5-trisphosphate and ryanodine receptors (Berridge et al., 2000). Once the odour stimulus diminishes, the GCaMP signal slowly decreases reflecting the removal of Ca^{2+} from the cytoplasm by various pumps and exchangers, such as Ca^{2+}-ATPase pumps and Na^{+}/Ca^{2+} exchangers which transport Ca^{2+} back into the extracellular space (Berridge et al., 2000).

PNs projecting to all five glomeruli studied here showed this typical odour-evoked GCaMP response with a rapid increase in GCaMP fluorescence upon odour onset and a slow decay at the odour offset. However, naïve EB-evoked GCaMP fluorescence responses substantially differed with respect to their amplitudes, as exemplified on the glomeruli DM1, DM2, and DM5 in Figure 3.8 A-C (blue traces). The change in GCaMP fluorescence responses between the 'naïve' and 'exposed' odour presentation also varied among different glomeruli, as seen in the curves of the paired differences of the 'exposed' and 'naïve' GCaMP traces in Figure 3.8 A'-C'.

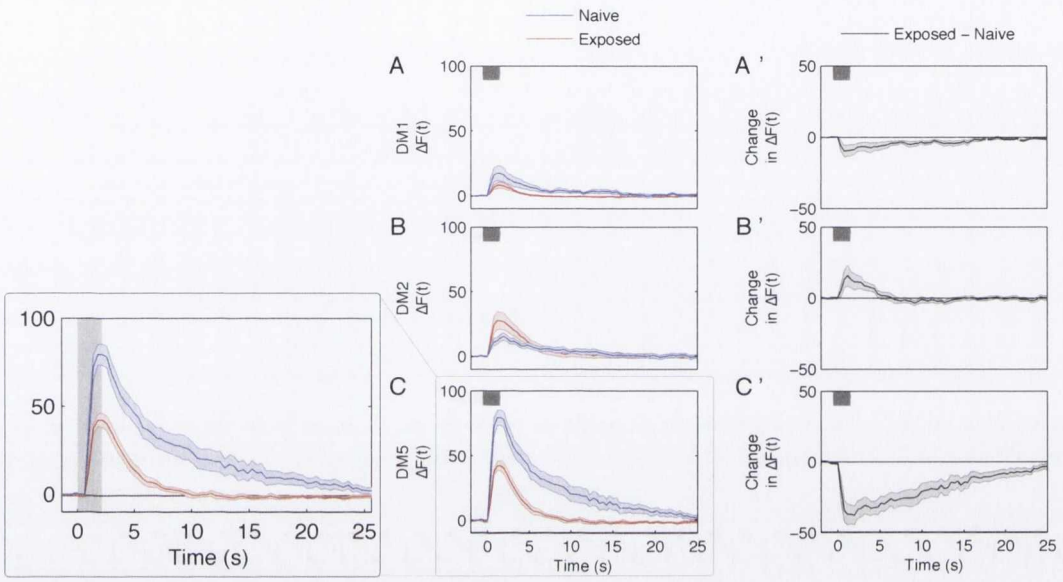


Figure 3.8: Changes in odour-evoked Ca^{2+}-influxes in PNs after 15-minute odourant exposure to 10% EB.
Two-photon Ca^{2+}-imaging was performed during a naïve and an exposed 1-second odour presentation to ethyl butyrate (EB) using GCaMP3 expressed in GH146-labelled projection neurons (PNs). Ca^{2+} dynamics were recorded from PNs projecting to the DM1, DM2, and DM5 glomerulus. The EB stimulus was delivered by the preliminary odour delivery system (see section 2.2.4 for details on the odour delivery system) **(A-C)** EB-evoked increases in GCaMP3 fluorescence to the naïve (blue) and exposed (red) EB presentation shown as changes in fluorescence over time. **(A'-C')** Paired differences of the odour-evoked GCaMP3 increases in A-C) shown as the difference of the changes in fluorescence over time. A negative deviation indicates a decrease in the odour-evoked Ca^{2+}-influxes in PNs after odourant exposure. Graphs represent mean (dark line) ± SEM (shaded region) of ΔF. The grey bars indicate the time window of odour presentation.

While this preliminary data looked promising a few obvious drawbacks in the acquired data became apparent quickly. Firstly, repetitions of the experiment revealed that the data was quite variable from experiment to experiment (data not shown). Secondly, odour-evoked PN GCaMP responses to a 1-second odour stimulus lasted for tens of seconds, as for instance seen in PNs projecting to DM5 (see magnification Figure 3.8). Thus, to get a better idea of the odour concentrations delivered during a 1-second odour pulse and potential odour depletion from experiment to experiment, a commercially available photo ionisation detector (PID) was rented to measure the odour delivered directly to the fly.

The PID measurements revealed that the odour was only slowly cleared out of the system after the 1-second test pulse which appeared to be the reason for the slow decay in PN

GCaMP responses (Figure 3.8). Instead of experiencing an approximately square-shaped 1-second odour pulse, the flies received a steadily-increasing several seconds-lasting odour stimulus that only decayed slowly (data not shown). PID recordings also revealed that the odour concentration did not reach its peak within the 1-second odour stimulus. Thus, the odour concentration of the testing pulses given to the fly were significantly lower than the concentration of the exposure. While the test pulses were recorded around 20ppm, the odour exposure reached up to 200ppm. Furthermore, the odour concentration delivered steadily decreased over the experimental day (data not shown). Flies tested in the morning therefore received a higher concentrated odour pulse than those tested in the afternoon. Since repeated administration of a stable odour concentration to the fly was crucial for the quantification of the Ca^{2+} imaging experiments, the odour delivery system required further modifications to enhance the accuracy and reliability of odour pulse delivery.

Final Adjustments to the Odour Delivery System

The modified odour delivery system, which was utilized for the experiments presented in this study, gave sufficiently stable odour concentration with only small variations. Its major improvement over the previous odour delivery system was its ability to deliver stable odour concentrations as well as its faster odour clearance. The installation of a PID to record the odour concentration given to each fly furthermore proved useful as deviations in odour concentration delivered could be detected immediately (see section 2.2.4 for a detailed description of the system).

The decrease in odour concentration throughout the day observed in the old system was solved by the use of pure odourant to prevent odour depletion that occurs more quickly in an odour/paraffin dilution. The use of pure odourant necessitated the introduction of a mass flow controller which injected a small but stable amount of odour into the air stream. The odour concentration was maintained stable by use of a continuous flow of air through the odour bottle which facilitated the formation of an odour concentration equilibrium within the system.

Stabilisation of odour concentrations for testing and exposure were facilitated by implementing a pressurized system which enabled the odour concentration to reach its peak within seconds (data not shown). The extension of the testing odour stimuli to 10 seconds ensured that the concentration peak was reached during the odour pulse. Pressure differences between different compartments which would cause increased air flow from one compartment to the other were reduced in two ways. Firstly, air streams were balanced such that the air flow within the different compartment was the same. Secondly, the introduction of a flow-controller ensured the delivery of a constant odour flow regardless of small pressure deviations. The implementation of the pressurized system had the additional advantage of increasing the temporal dynamics of the odour stimulus which resulted in a faster clearance of the odour out of the system.

Final Adjustment to the Ca^{2+} Imaging Protocol

The extension of the testing odour stimuli to 10 seconds to ensure the concentration peak was reached during the odour pulse made it more likely that the first odour pulse affected the odour-evoked responses to the second pulse due to sensory adaptation occurring in OSNs (Störtkuhl et al., 1999; Zufall and Leinders-Zufall, 2000; de Bruyne et al., 1999). To prevent this confounding factor, only a single odour stimulus was presented before and after the exposure in a given fly after introducing the final odour delivery system. The standardized imaging protocol utilized for most of the experiments in this study therefore consisted of a 10-second odour presentation before the 15-minute odour exposure followed by a 10-minute air interval and another 10-second odour presentations (see Figure 3.9). A disadvantage of giving a single odour pulse preceding and succeeding odourant exposure was that only one glomerular layer could be imaged per fly. Thus, to obtain Ca^{2+} imaging data from all seven glomeruli identified, twice as many flies were required which reduced the speed of data collection.



Figure 3.9: Final Ca^{2+} imaging protocol
The final Ca^{2+} imaging protocol consisted of a 10-second odour stimulus preceding the 15-minute odour exposure followed by a 10-minute air interval and another 10-second odour stimulus. The 10-minute air interval allowed for the effects of sensory adaptation to decay before the 'exposed' odour-evoked Ca^{2+} response was assessed.

Data Collected with the Final Odour Delivery System

Utilizing the improved odour delivery system and the adjusted experimental protocol, the previously performed Ca^{2+} imaging experiment to study the effect of 15-minute odourant exposure on odour-evoked GCaMP responses in PNs was repeated (see section 3.3.1 for results). As the GCaMP6 Ca^{2+} indicator became available, this improved version was used to study Ca^{2+} influxes in GH146-labelled PNs (see section 3.3 for details on the expression pattern of GH146 and the GCaMP6 Ca^{2+} indicator).

The odour delivery system was set to deliver a concentration of ~3ppm. This constitutes an EB concentration well within the receptive range of the sensory neurons (Andersson et al., 2012; Pelz et al., 2006). OSNs that target the DM2 glomerulus, as one of the most sensitive to EB (Hallem and Carlson, 2006), begin to respond to EB at a concentration of 2ppb and still fire at ~18ppm EB (Andersson et al., 2012). However, these neurons are likely to be activated by even higher concentrations of EB as shown by another study that investigated the sensitivity of these neurons to different odours and concentrations (Pelz et al., 2006). The concentrations that elicited half maximal responses ranged from 100ppb to 21ppm in OSNs innervating DM2. While the receptive concentration range of other EB-responsive OSNs have also been studied (Hallem and Carlson, 2006), the concentrations reported are not easily comparable to the concentrations used in the present study. As the build of the odour delivery

system largely affects the concentration that reaches the fly (Vetter et al., 2006), the reported volume dilutions cannot be easily converted into ppm values experienced by the fly. Notably, 3ppm constitutes a lower concentration than the one delivered with the preliminary odour delivery system. PID measurements revealed that the previously used EB/paraffin dilution of 10% corresponds to a concentration of approximately 20ppm. A concentration of 20ppm was utilized later in this study to compare the effects of two different odour concentrations (3ppm and 20ppm, see section 3.3.1).

In terms of GCaMP responses, the 3ppm EB stimulus delivered with the final odour delivery system evoked responses with faster kinetics than those described for the preliminary odour delivery system (compare Figure 3.8 and Figure 3.10). As exemplified by GCaMP responses in PNs targeting the DM5 glomerulus in Figure 3.10, GCaMP responses exhibited a rapid increase upon odour onset reflecting Ca^{2+} rushing into the neuron (Berridge et al., 2000). During the 10-second odour pulse the GCaMP signal slowly decayed following an initial peak. This phenomenon has been ascribed to sensory adaptation in OSN terminals (Nagel and Wilson, 2011). Upon odour offset, the GCaMP response decreases reflecting Ca^{2+} clearance from the cytoplasm.

The improvements of the odour delivery system with respect to delivering odour stimuli of stable concentration and faster kinetics appeared to have solved the problems of high variability between experiments and GCaMP responses lasting for tens of seconds following the odour stimulus. The final Ca^{2+} imaging protocol and odour delivery system were therefore considered to be suitable to study changes in odour-evoked Ca^{2+} influxes in PNs induced by short-term exposure.

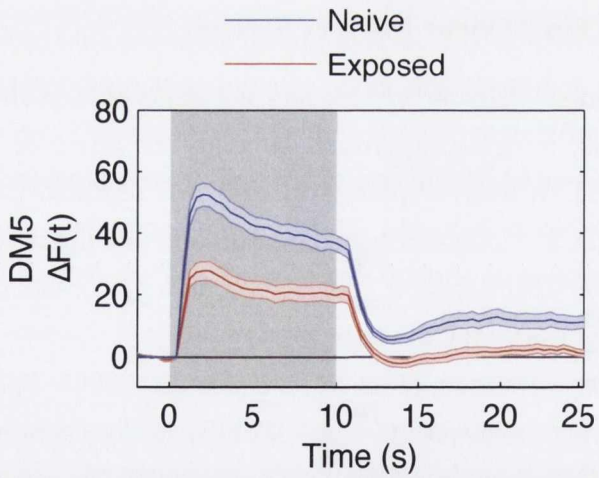


Figure 3.10: GCaMP responses to a 10-second EB stimulus delivered by the final odour delivery system

Odour-evoked GCaMP responses were recorded in flies expressing GCaMP6m in GH146-labelled PNs. Depicted are the GCaMP signals of PNs projecting to the DM5 glomerulus in response to a 10-second EB stimulus delivered by the final odour delivery system (see section 2.2.4 for details on the odour delivery system). Graphs represent mean (dark line) ± SEM (shaded region) of ΔF. The grey bars indicate the time window of odour presentation.

3.3 Characterisation of Odour-Evoked Synaptic Plasticity in the *Drosophila* Antennal Lobe

After establishing a Ca^{2+} imaging protocol for olfactory short-term habituation, the first aim was to investigate whether odour-responsive PNs show a reduction in odour-evoked neuronal activity after prolonged STH odour exposure as predicted by the behaviour experiments performed with the Y-maze assay (Das et al., 2011b). The 'negative image model' proposed following the behavioural findings suggests that during olfactory habituation neuronal excitation in PNs is scaled by inhibitory input according to the strength of excitation within a specific PN (Ramaswami, 2014). It predicts that strongly activated PNs are targets of greater inhibition than those that are only weakly activated. To support the 'negative image model', neuronal activity in all odour-responsive PNs should show a decrease following odourant exposure. The degree of the reduction would be dependent on the naïve odour-evoked response in the specific PN subset. To test the hypothesis of whether PN activity is inhibited according to its naïve odour-evoked responses, Ca^{2+} influxes, as a measure of neuronal activity, were recorded using the Ca^{2+} indicator GCaMP6 expressed in a large subset of PNs in the *Drosophila* olfactory system.

The GCaMP6 Ca^{2+} sensors have only recently been published and they provided the most advanced GECI available at the time of the experiments (Chen et al., 2013). Briefly, the GCaMP family consists of a circularly permuted green fluorescence protein (cpGFP), the calcium-binding protein calmodulin (CaM) and the CaM-interacting M13 peptide (Nakai et al., 2001). The GCaMP6 protein was engineered by induced mutagenesis in the CaM and the M13-CaM interface resulting in a substantially improved Ca^{2+} sensitivity of GCaMP6 sensors compared to their precursors GCaMP5 and GCaMP3. GCaMP6 sensors exhibit up to 10-fold larger signals and up to 10-fold improved signal-to-noise ratio in cultured neurons compared to GCaMP3. GCaMP6 comes in three variants GCaMP6s, GCaMP6m, and GCaMP6f according to their slow, medium, and fast kinetics with GCaMP6s having the slowest kinetics but being the most sensitive. GCaMP6f shows increased kinetics with an approximate twofold faster rise time and a 1.7-fold faster decay time compared to GCaMP3 measured in cultured neurons whereas GCaMP6m and GCaMP6s both show slower kinetics in rise and decay times. Two-photon imaging of AL PNs expressing the three different GCaMP6 variants largely supported the characteristics of the sensor with respect to Ca^{2+} sensitivity and kinetics (Chen et al., 2013). Ca^{2+} imaging of PNs projecting to the DC1 glomerulus in response to a 3-octanol stimulus revealed that the three variants show similar Ca^{2+} sensitivities and signal-to-noise ratios with GCaMP6f exhibiting faster kinetics in rise time than the other two variants. In this study, the GCaMP6m variant was used as it offers intermediate sensitivity and kinetics with respect to the GCaMPs and GCaMPf variants.

To measure odour-evoked neuronal activity preceding and succeeding short-term exposure, the binary expression system Gal4/UAS was used to drive expression of GCaMP6m in PNs using the Gal4 driver line GH146. This enhancer trap line expresses Gal4 in ~90

out of ~150 PNs in total (~60%) and shows projections in 37 glomeruli in the AL including those responsive to EB (Stocker et al., 1997; Semmelhack and Wang, 2009; Strutz et al., 2014; Lai et al., 2008; Jefferis et al., 2001; Grabe et al., 2015a). It predominantly targets uni-glomerular ePNs, however some iPNs are also labelled (Tanaka et al., 2012).

The aim of the research performed in this chapter was (a) to demonstrate changes in neuronal activity that occur after continuous 15-minute exposure to EB, (b) to investigate whether the changes associated with short-term odourant exposure are scaled by naïve odour-evoked excitation as predicted by the 'negative image model', and (c) to test whether the changes exhibit similar characteristics as behavioural habituation such as spontaneous recovery and its dependence on stimulus intensity with lower intensities resulting in more pronounced habituation.

3.3.1 Different Odour Concentrations

Firstly, 3-4 day old female flies expressing GCaMP6m in GH146-labelled PNs were exposed to 3ppm EB. According to the experimental protocol detailed earlier, the flies were tested for their naïve EB-evoked GCaMP response before the 15-minute EB exposure followed by a 10-minute air interval and another test to EB (see Figure 3.9). Both testing and exposure was carried out at an EB concentration of 3ppm (see Table 5.87 for PID measurements). This constitutes an EB concentration well within the receptive range of the sensory neurons (Andersson et al., 2012). 3ppm EB activated a restricted glomerular subset of the for Ca^{2+} imaging accessible glomeruli, indicating that the concentration did not saturate the olfactory sensory channels (for details on the choice of the concentration, see section 3.2). Ca^{2+} dynamics were recorded from PNs projecting to seven distinct glomeruli within the antennal lobe, the DL1, DL5, DM1, DM2, DM3, DM5, and DM6 glomerulus.

Naïve EB-evoked GCaMP response traces are shown in Figure 3.11 A-G (blue traces). All apart from one glomerulus, namely DL5, showed an increase in GCaMP6m fluorescence in response to the EB stimulus (see Figure 3.13 A and Table 3.2). The DL1, DM5, and DM6 glomeruli showed stronger increases in the GCaMP6 signal than the other three. The DM5 glomerulus exhibited the strongest response, followed by DM6 and DL1. Odour-evoked GCaMP6 signals in PNs projecting to DM1, DM2, and DM3 were smaller.

Importantly, stimulation with 3ppm EB did not saturate the GCaMP6 Ca^{2+} indicator in the PNs that were activated the strongest, as shown by bath application of KCl (Figure 3.12, see Table 5.89 for PID measurements). KCl depolarisation induced a large entry of Ca^{2+} into the neuron which is bound by free GCaMP proteins, thus increasing GCaMP emission. Figure 3.12 shows the GCaMP peak intensities of both, KCl- and EB-evoked fluorescence changes. Peak responses are depicted instead of the area under the curve as KCl-evoked depolarisation showed slower dynamics due to its manual application to the bath covering the brain.

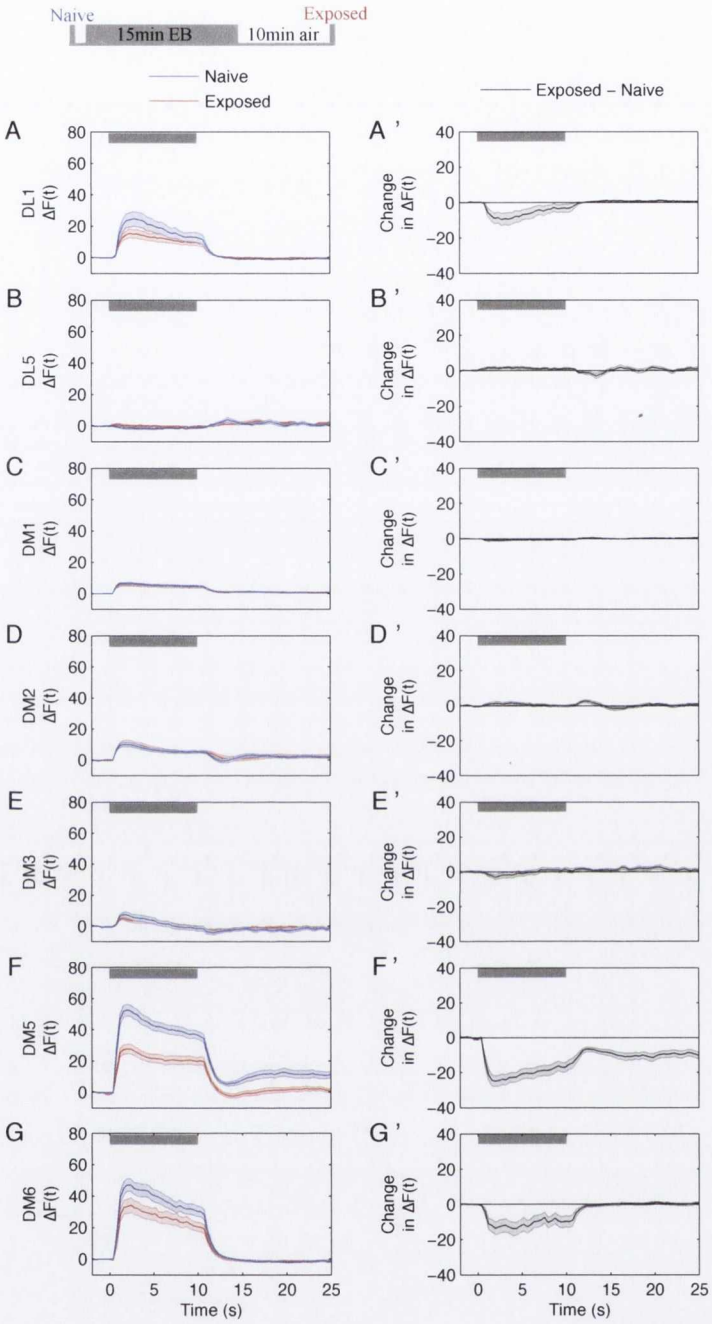


Figure 3.11: Changes in odour-evoked Ca^{2+}-influxes in PNs after 15-minute odourant exposure to 3ppm EB.

Two-photon Ca^{2+}-imaging was performed during a naïve and an exposed 10-second odour presentation to ethyl butyrate (EB) at a concentration of 3ppm. The Ca^{2+} indicator GCaMP6m was expressed in GH146-labelled projection neurons (PNs). Ca^{2+} dynamics were recorded from PNs projecting to seven distinct glomeruli within the antennal lobe (DL1, DL5, DM1, DM2, DM3, DM5, DM6). **(A-G)** Mean of EB-evoked increases in GCaMP6m fluorescence to the naïve (blue) and exposed (red) EB presentation shown as changes in fluorescence (ΔF) over time. **(A'-G')** Paired differences of the odour-evoked GCaMP6m increases in A-G) shown as the difference of the changes in fluorescence over time (Change in ΔF). A negative deviation indicates a decrease in the odour-evoked Ca^{2+}-influxes in PNs after odourant exposure. Graphs represent mean (dark line) ± SEM (shaded region), n=15-34/glomerulus (see Table 5.6). The grey bars indicate the time window of odour presentation.

The type of stimulation, EB or KCl, had a significant effect on the peak GCaMP response (*Likelihood ratio test, $\chi(7)=16.072$, $p=0.025$*). GCaMP6m fluorescence signals were significantly higher in DL1, DL5, DM2, DM5, and DM6 when the neurons were depolarised by a 70mM KCl solution rather than 3ppm EB (see Table 3.1). KCl-evoked GCaMP6 responses of PNs projecting to the glomeruli DM1 and DM3 were indistinguishable from those evoked by 3ppm EB. However, this result does not necessarily mean that the GCaMP sensor is saturated in these glomeruli. Due to the large number of inhibitory local interneurons in the AL which are also activated by the KCl solution neuronal activation of PNs could be overridden by inhibitory input from LNs. It is thus not unambiguously verifiable whether the sensor is saturated in these PNs. For the majority of the PNs studied, however, the neuronal activation evoked by a 3ppm EB stimulus seems to be well within the sensitivity range of the sensor.

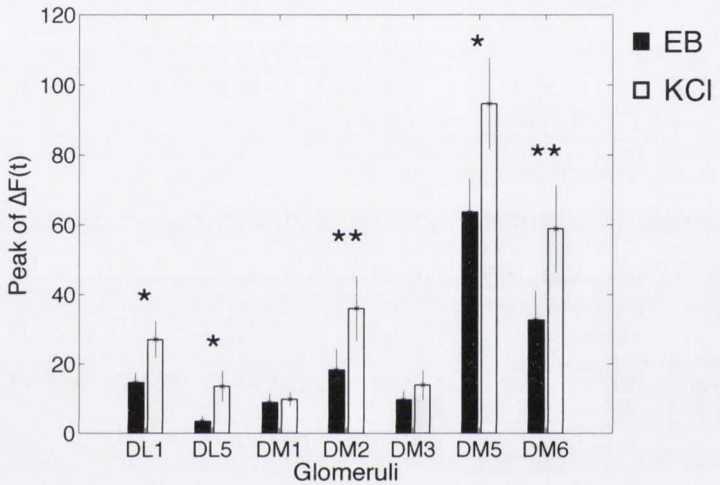


Figure 3.12: Comparison of odour- and KCl-evoked GCaMP6m fluorescence responses in PNs Two-photon Ca^{2+}-imaging was performed in PNs during a 10-second odour presentation to 3ppm EB and 3 minute later application of 70mM KCl. Ca^{2+} dynamics were recorded from seven glomeruli. Depicted are the peak GCaMP6 fluorescence responses in PNs evoked by the 3ppm EB and 70mM KCL stimulation. The type of stimulation, EB or KCl, had a significant effect on the peak GCaMP response (*Likelihood ratio test, $\chi(7)=16.072$, $p=0.025$*, see Table 3.1 for paired statistical comparisons of each glomulus, n=6-10/glomerulus (see Table 5.3)). GCaMP6 fluorescence responses evoked by 70mM KCl in PNs projecting to the DL1, DL5, DM2, DM5, and DM6 glomeruli were significantly larger than those evoked by 3ppm EB (see Table 3.1). * $p<0.05$; ** $p<0.01$; *** $p<0.001$; bars indicate mean ± SEM.

DL1	DL5	DM1	DM2	DM3	DM5	DM6
t-test	t-test	t-test	wilcoxon	t-test	t-test	t-test
p=0.040	p=0.026	p=0.694	p=0.004	p=0.096	p=0.022	p=0.007
t=2.604	t=3.135	t=0.407	sr =54	t=2.049	t=2.771	t=3.973
df=6	df=5	df=9	n=10	df=5	df=9	df=6
*	*	n.s.	**	n.s.	*	**

Table 3.1: Statistics comparing odour- and KCl-evoked GCaMP6m responses in PNs

15-minute exposure to 3ppm EB had a significant effect on odour-evoked GCaMP6 responses in PNs (*Likelihood ratio test,* $\chi(7)=89.717$, $p<0.001$), lowering the response by -5.611 $\pm$ 2.793 arb. units (value determined by a linear mixed-effects model fit by maximum likelihood). Mean GCaMP6m traces in response to a 3ppm EB stimulus after EB exposure in relation to the naïve EB-evoked response are shown in Figure 3.11 A-G, the paired differences of the naïve and exposed odour presentation are depicted in Figure 3.11 A'-G' whereas a negative deviation indicates a decrease in the odour-evoked Ca^{2+}-influxes in the specific PN subset. Reductions in odour-evoked GCaMP6m responses were observed in the DL1, DM5, and DM6 glomerulus (Figure 3.14 A and Table 3.2) suggesting that PNs innervating these glomeruli show reduced EB-evoked neuronal activity following odourant exposure. The largest absolute reduction in Ca^{2+}-influxes occurred in PNs projecting to DM5 followed by those innervating DM6 and DL1. Odour-evoked GCaMP6m fluorescence increased in the DL5 glomerulus and remained unchanged in DM1, DM2, and DM3 (Figure 3.14 A and Table 3.2).

To obtain a measure of how much short-term odourant exposure altered naïve odour-evoked GCaMP6 responses the percent of the response change of a given PN type with respect to its naïve EB-evoked GCaMP response was calculated ($\int_0^{10} \Delta F_E(t) - \Delta F_N(t)\,dt / \int_0^{10} \Delta F_N(t)\,dt * 100$ with $\Delta F_E(t) - \Delta F_N(t)$ being the trace for the paired difference between the 'exposed' and 'naïve' GCaMP responses and $\Delta F_N(t)$ that of the 'naïve' GCaMP response). While this approach is a somewhat crude measure as it does not take into account error bars, it serves to compare different PN types with respect to their naïve EB-evoked GCaMP6 responses and is useful when comparing PN responses with those of other neuronal types in the following chapters (see section 3.5). PNs projecting to DM5 show the largest percent decrease with -48%, those targeting DL1 the second largest with -34% followed by those innervating DM6 with -29%. The DL5 glomerulus increased its odour-evoked GCaMP6 responses by 109%. The respective percent changes of the three glomeruli that did not show a significant change after odourant exposure to 3ppm are -12% for DM1, 9% for DM2, and -25% for DM3. Notably, the glomeruli that were activated the strongest by the odour stimulus, namely DM5, DM6, and DL1, also showed the largest reduction after short-term odourant exposure.

One of the characteristics of behavioural habituation is its dependency on stimulus intensities. Higher intensities result in less pronounced behavioural decrements than lower intensities (Thompson and Spencer, 1966; Rankin et al., 2009). To test whether the observed changes in Ca^{2+} influxes in PNs are also less pronounced after exposure to a higher odourant concentration the same experimental protocol was performed (see Figure 3.9) at a testing and exposure concentration of 20ppm (see Table 5.88 for PID measurements). A higher concentration was chosen since it was not possible to deliver concentrations lower than 3ppm reliably with the odour delivery system used. 20ppm was selected as it was still within the receptive range of the sensory neurons (Andersson et al., 2012; Pelz et al., 2006) and only ac-

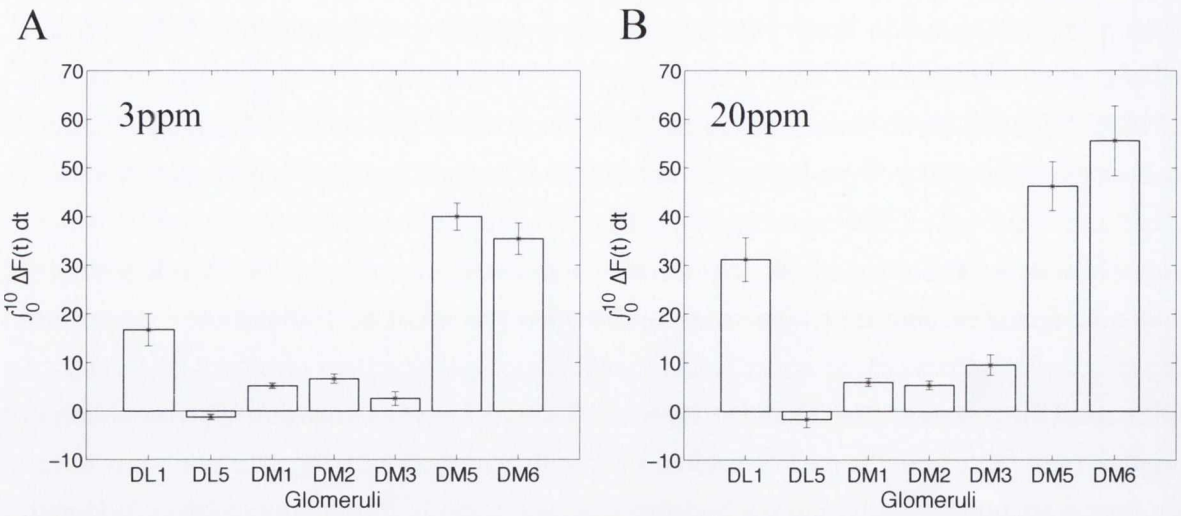


Figure 3.13: Naïve odour-evoked Ca^{2+}-influxes in PNs to 3ppm and 20ppm EB
Two-photon Ca^{2+}-imaging was performed in GH146-labelled PNs during a naïve 10-second odour presentation to 3ppm (A) and 20ppm (B) EB. Ca^{2+} dynamics were recorded from PNs projecting to DL1, DL5, DM1, DM2, DM3, DM5, and DM6. Depicted are naïve EB-evoked GCaMP6m fluorescence responses shown as the area under the curve of the GCaMP trace over a 10 seconds period ($\int_0^{10} \Delta F\, dx$). n=15-34/glomerulus (A) and n=15-22/glomerulus (B) (see Tables 5.6 and 5.9).

tivated a restricted set of glomeruli (for details on the choice of the concentration, see section 3.2). As before, the GCaMP6 Ca^{2+} indicator was expressed in GH146 PNs. PNs projecting to DL1, DM5, and DM6 showed the strongest naïve GCaMP6 responses to odour stimulation (Figure 3.13 B and Table 3.3), similar to what had been observed for 3ppm. The 20ppm EB stimulus evoked the strongest GCaMP6 signal in PNs projecting to DM6, followed by those innervating DM5 and DL1. PNs projecting to DM1, DM2, and DM3 again exhibited only small GCaMP6 responses.

As for 3ppm, 15-minute exposure to 20ppm EB likewise had a significant effect on odour-evoked GCaMP6 responses in PNs (*Likelihood ratio test,* $\chi(7)=93.432$, $p<0.001$), lowering the response by -12.257 ± 3.629 arb. units (value determined by a linear mixed-effects model fit by maximum likelihood). Reductions in odour-evoked GCaMP6m responses were observed in PNs projecting to the DL1, DM1, DM5, and DM6 glomerulus (Figure 3.14 B and Table 3.3). The most substantial reduction in odour-evoked GCaMP responses with respect to absolute values occurred in DM5, followed by those innervating DM6, DL1, and DM1. Odour-evoked GCaMP6m fluorescence remained unchanged in DL5, DM2, and DM3 (Figure 3.14 B and Table 3.3). With respect to their naïve odour-evoked GCaMP response, PNs that were activated the strongest again showed the largest reduction, with the exception of PNs projecting to DM1 which were comparatively weakly activated but showed a large change. The three glomeruli that exhibited large naïve GCaMP fluorescence responses were reduced by -66% in case of DM5, by -39% in case of DL1, and by -34% in that of DM6. PNs targeting DM1 reduced their GCaMP responses by -46%. The respective percent changes of the three glomeruli that did not show a significant change after 20ppm EB exposure were 14% for DL5, 18% for DM2, and -18% for DM3.

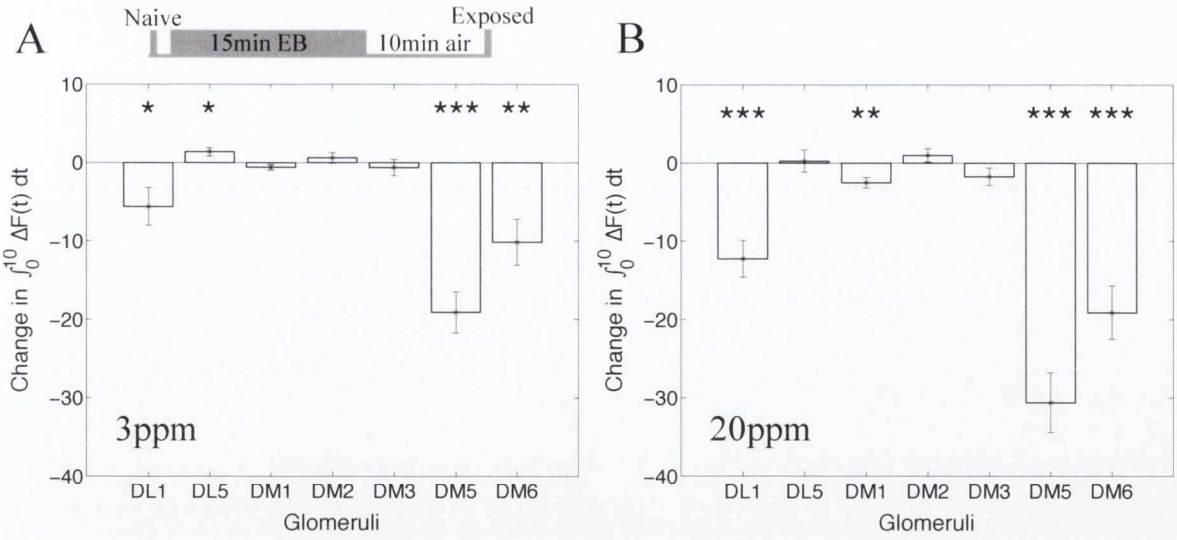


Figure 3.14: Quantified changes in odour-evoked Ca^{2+}-influxes in PNs after 15-minute odourant exposure to 3ppm and 20ppm EB

Two-photon Ca^{2+}-imaging was performed in GH146-labelled PNs during a naïve and an exposed 10-second odour presentation to 3ppm (A) and 20ppm (B) EB. Ca^{2+} dynamics were recorded from seven distinct glomeruli. Depicted are the changes in odour-evoked GCaMP6m fluorescence in PNs induced by 15-minute odourant exposure shown as the area under the curve of the paired differences between the exposed and naïve GCaMP6m responses over a 10 seconds period ($\int_0^{10} \Delta F \, dx$, whereas ΔF reflects the paired differences over time). **(A)** 15-minute exposure to 3ppm EB had a significant effect on the overall odour-evoked GCaMP6 responses in PNs (*Likelihood ratio test, $\chi(7)=89.717$, $p<0.001$, $n=15\text{-}34$/glomerulus* (see Table 5.6)). Significant changes in odour-evoked GCaMP6m responses were observed in the DL1, DL5, DM5, and DM6 glomerulus (see Table 3.2). **(B)** 15-minute exposure to 20ppm EB had a significant effect on odour-evoked GCaMP6 responses in PNs (*Likelihood ratio test, $\chi(7)=93.432$, $p<0.001$, $n=15\text{-}22$/glomerulus* (see Table 5.9)). Significant reductions in odour-evoked GCaMP6m responses were observed in the DL1, DM1, DM5, and DM6 glomerulus (see Table 3.2). * $p<0.05$; ** $p<0.01$; *** $p<0.001$; bars indicate mean ± SEM.

The choice of EB concentration had a significant effect on overall GCaMP fluorescence levels (*Likelihood ratio test, $\chi(8)=58.742$, $p<0.001$*), with 20ppm increasing the responses by 15.699 ± 2.944 arb. units compared to 3ppm. Further, there is also an interaction effect between the concentration and the odour exposure (*Likelihood ratio test, $\chi(1)=7.810$, $p=0.005$*) with a negative estimate of -4.492 of the linear mixed-effects model fit by maximum likelihood indicating that the reduction in odour-evoked GCaMP6m responses is greater after 20ppm odourant exposure than after 3ppm exposure (see Figure 3.14). Exposure to a more intense odour stimulus, therefore, resulted in larger reductions in odour-evoked PN activity.

	DL1	**DL5**	**DM1**	**DM2**	**DM3**	**DM5**	**DM6**
naïve (arb. units)	16.685 ± 3.305	-1.250 ± 0.557	5.162 ± 0.573	6.603 ± 0.953	2.555 ± 1.419	39.936 ± 2.808	35.387 ± 3.256
change (arb. units)	-5.611 ± 2.406	1.357 ± 0.536	-0.615 ± 0.373	0.593 ± 0.683	-0.630 ± 1.016	-19.091 ± 2.618	-10.156 ± 2.931
statistics change	wilcoxon p=0.030 z=-2.165 n=20 *	t-test p=0.024 t=2.530 df=14 *	t-test p=0.108 t=-1.650 df=32 n.s.	t-test p=0.392 t=0.869 df=32 n.s.	wilcoxon p=0.951 z=-0.061 n=23 n.s.	t-test p<0.001 t=-7.293 df=33 ***	t-test p=0.002 t=-3.465 df=23 **
change (%)	**-34%**	**109%**	**-12%**	**9%**	**-25%**	**-48%**	**-29%**

Table 3.2: PN GCaMP responses to 3ppm EB

	DL1	**DL5**	**DM1**	**DM2**	**DM3**	**DM5**	**DM6**
naïve (arb. units)	31.154 ± 4.506	-1.630 ± 1.684	5.961 ± 0.826	5.362 ± 0.860	9.491 ± 2.114	46.210 ± 4.999	55.534 ± 7.163
change (arb. units)	-12.257 ± 2.342	0.230 ± 1.423	-2.531 ± 0.658	0.972 ± 0.839	-1.747 ± 1.109	-30.599 ± 3.813	-19.120 ± 3.388
statistics change	t-test p<0.001 t=-5.233 df=19 ***	wilcoxon p=0.215 z=1.241 n=18 n.s.	t-test p=0.001 t=-3.844 df=20 **	t-test p=0.259 t=1.160 df=21 n.s.	t-test p=0.137 t=-1.576 df=14 n.s.	t-test p<0.001 t=-8.024 df=20 ***	t-test p<0.001 t=-5.643 df=15 ***
change (%)	**-39%**	**14%**	**-46%**	**18%**	**-18%**	**-66%**	**-34%**

Table 3.3: PN GCaMP responses to 20ppm EB

3.3.2 1-Hour Recovery

Another characteristic of behavioural habituation is its spontaneous recovery when the habituating stimulus is removed (Rankin et al., 2009; Thompson and Spencer, 1966). STH of the olfactory avoidance response recovers with a half life of 30 minutes (Das et al., 2011b). To test whether the observed changes in PN activity recover within the same time frame, odour-evoked PN activity was measured 1-hour after performing the standardized habituation protocol (see Figure 3.9). Thus, odour-evoked GCaMP responses were measured in response to the EB stimulus preceding and succeeding EB exposure as well as to a 1-hour delayed odour presentation. Testing and exposure was carried out at an EB concentration of 3ppm and Ca^{2+} dynamics were recorded from the same PN subset as before. Mean GCamP6m traces in response to the three EB stimuli are shown in Figure 3.15 A-G. The paired differences of the 'naïve' and 'exposed' odour presentations are depicted in Figure 3.15 A'-G' whereas a negative deviation indicates a decrease in the odour-evoked Ca^{2+} -influxes in the specific PN subset. Figure 3.15 A"-G" shows the paired differences of the 'exposed' and 'recovered' odour presentations. A positive deviation here indicates recovery from the decrease in odour-evoked Ca^{2+}-influxes in PNs after 15-minute odourant exposure. Figure 3.15 A"'-G"' shows the paired differences of the 'recovered' and 'exposed' odour presentations whereas a negative deviation indicates that the decrease in odour-evoked Ca^{2+}-influxes in PNs after short-term exposure have not completely recovered after an 1 hour air interval.

A significant difference in the overall odour-evoked GCaMP6m responses in PNs was observed between the three EB presentations delivered (*Likelihood ratio test,* $\chi(14)=64.587$, $p<0.001$), while the response from the 'naïve' to the 'exposed' odour presentations was lowered by -7.924 $\pm$ 4.188 arb. units and that from the 'exposed' to the '1-hour delay' EB stimulus was increased by 8.303 $\pm$ 4.188 arb. units (values determined by a linear mixed-effects model fit by maximum likelihood). A likelihood ratio test restricted to a single PN type revealed significant differences in odour-evoked GCaMP responses between the three odour presentations in the glomeruli DL5, DM1, and DM5 at an EB concentration of 3ppm (see Table 3.4). Subsequently performed paired t-tests with common standard deviations for all groups of the certain glomerulus only showed significant changes in GCaMP responses in the DL5 and DM5 glomerulus (see Table 3.4). No significant differences were detected in PNs projecting to DL1, DM2, DM3, and DM6. Thus, while there seems to be a trend of recovery from the changes in odour-evoked GCaMP responses after short-term odourant exposure to 3ppm no statistical significant recovery was detected when performing paired t-tests with adjusted standard deviations for the measurements of a given PN type. Take note, that this experiment is less powered as the one shown in section 3.3.1 as it was performed with less flies 3.3.1. Adjusting the standard deviations is further, while appropriate, more conservative than taking the standard deviation of only two groups as in section 3.3.1. These are potential reasons why the PNs projecting to DL1 and DM6 do not show significant decreases in their odour-evoked GCaMP responses after short-term exposure in the given data set (see Figure 3.16 A).

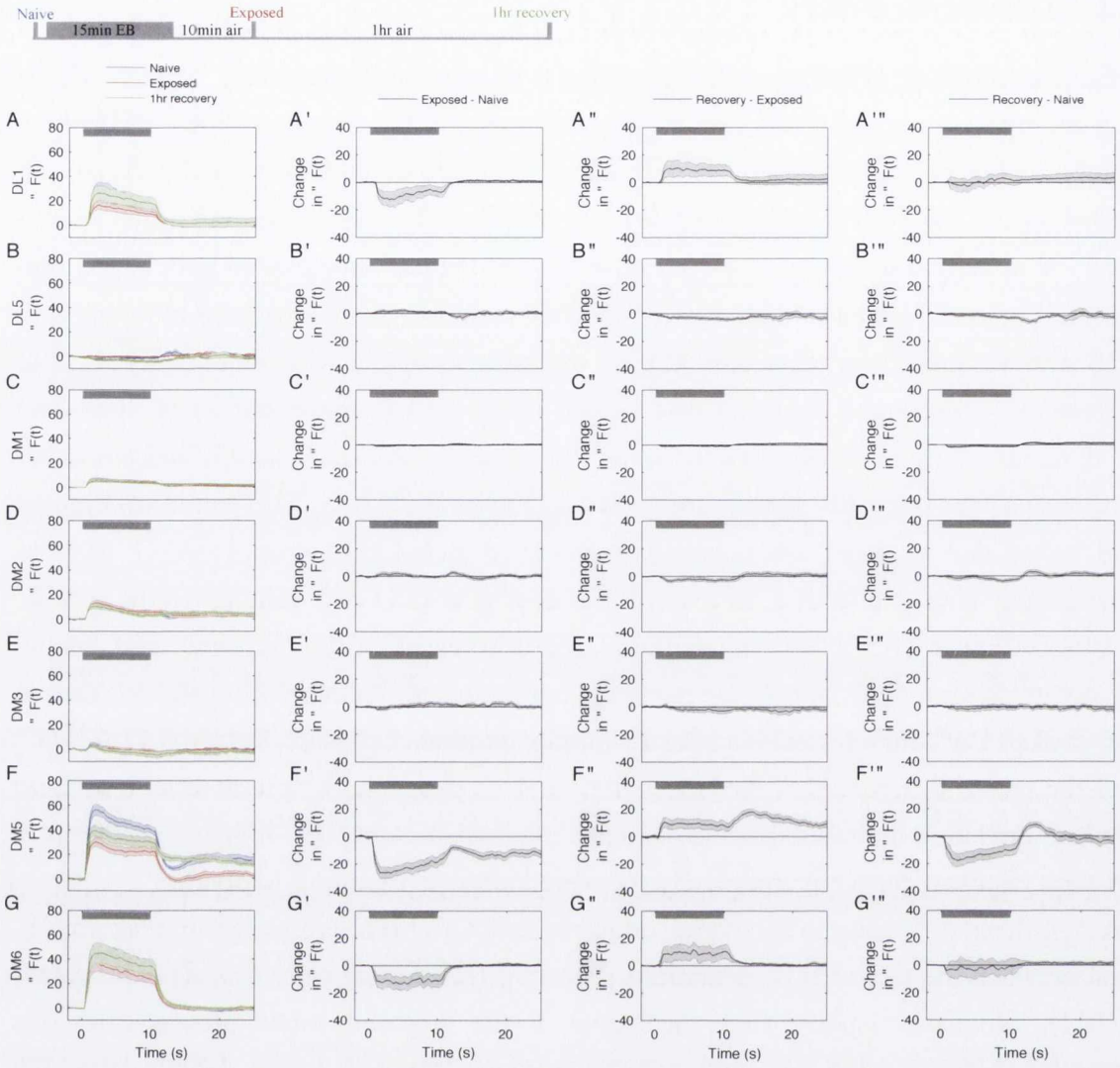


Figure 3.15: Changes and recovery in odour-evoked Ca^{2+}-influxes in PNs after 15-minute odourant exposure to 3ppm EB

Two-photon Ca^{2+}-imaging was performed in GH146-labelled PNs during a naïve, an exposed, and a 1-hour delayed 10-second odour presentation to 3ppm EB. Ca^{2+} dynamics were recorded from PNs projecting to seven distinct glomeruli within the antennal lobe. **(A-G)** Mean of EB-evoked increases in GCaMP6m fluorescence to the naïve (blue), exposed (red), and 1hr recovery (green) EB presentation shown as changes in fluorescence (ΔF) over time. **(A'-G')** Paired differences of the odour-evoked GCaMP6m increases of the naïve and exposed EB puff in A-G) shown as the difference of the changes in fluorescence (Change in ΔF) over time. A negative deviation indicates a decrease in the odour-evoked Ca^{2+}-influxes in PNs after odourant exposure. **(A"-G")** Paired differences of the odour-evoked GCaMP6m responses of the exposed and 1hr recovery EB puff in A-G) shown as the difference of the changes in fluorescence (Change in ΔF) over time. A positive deviation indicates recovery from the decrease in odour-evoked Ca^{2+}-influxes in PNs after odourant exposure. **(A'"-G'")** Paired differences of the odour-evoked GCaMP6m responses of the naïve and 1hr recovery EB puff in A-G) shown as the difference of the changes in fluorescence (Change in ΔF) over time. In this panel, a negative deviation indicates that the decrease in odour-evoked Ca^{2+}-influxes in PNs after odourant exposure have not completely recovered after 1 hour. Graphs represent mean (dark line) $\pm$ SEM of the given paired comparison (shaded region) of ΔF. n=9-22/glomerulus (see Table 3.4). The grey bars indicate the time window of odour presentation.

In order to further investigate a potential recovery of the changes in odour-evoked PN activity the same experiment was performed with an EB concentration of 20ppm. As for 3ppm, the overall odour-evoked GCaMP6m responses showed a significant difference between the three EB presentations at a concentration of 20ppm (*Likelihood ratio test,* $\chi(14)=90.813$, $p<0.001$), while the response from the 'naïve' to the 'exposed' odour presentations was lowered by -12.768 ± 4.285 arb. units and that from the 'exposed' to the '1-hour delay' EB stimulus by -6.260 ± 4.285 arb. units. A likelihood ratio test restricted to a single PN type revealed significant differences in odour-evoked GCaMP responses between the three odour presentations in the glomeruli DL1, DL5, DM1, DM5 and DM6 (see Table 3.4). Paired t-tests with common standard deviations for all groups showed significant changes in GCaMP responses for the comparisons 'exposed - naïve' and 'recovery - naïve' in the glomeruli DL1, DL5, DM5 and DM6 (see Table 3.4). No significant differences were detected in PNs projecting to DM2 and DM3. In contrast to the 3ppm recovery experiment, there was no trend of recovery in the given data set. The full linear mixed-effects model fit by maximum likelihood suggests that the odour-evoked PN responses decrease after exposure to 20ppm and decline further after a 1-hour recovery period. Paired comparisons with common standard deviations do not show any further significant decreases in odour-evoked GCaMP levels after the 1-hour recovery period, when comparing the 'exposed' and 'recovered' GCaMP responses (Figure 3.16 B'). However, the exposure-induced changes are more pronounced in the DL1 and DM6 glomerulus after the 1 hour recovery than directly after odourant exposure (Figure 3.16 A'/C').

		DL1	**DL5**	**DM1**	**DM2**	**DM3**	**DM5**	**DM6**
3ppm	likelihood ratio test $\chi(2)$	5.457 p=0.065 n.s.	10.777 p=0.005 **	7.751 p=0.020 *	5.329 p<0.001 n.s.	1.678 p=0.432 n.s.	26.675 p<0.001 ***	5.153 p=0.076 n.s.
	t-test							
	exposed - naïve		p=0.145	p=0.680			p<0.001	
	recovery - exposed		p=0.004	p=0.480			p=0.088	
	recovery - naïve		p=0.115	p=0.270			p=0.009	
	numbers	11	9	22	22	13	22	14
20ppm	likelihood ratio test $\chi(2)$	15.005 p<0.001 ***	6.015 p=0.049 *	8.258 p=0.016 *	0.339 p=0.844 n.s.	3.511 p=0.173 n.s.	20.980 p<0.001 ***	11.673 p=0.003 **
	t-test							
	exposed - naïve	p=0.047	p=0.095	p=0.082			p<0.001	p=087
	recovery - exposed	p=0.311	p=0.589	p=0.913			p=0.113	p=0.199
	recovery - naïve	p=0.005	p=0.034	p=0.067			p=0.001	p=0.006
	numbers	7	6	6	6	6	6	7

Table 3.4: Statistics: Recovery of PN GCaMP responses to 3ppm and 20ppm EB

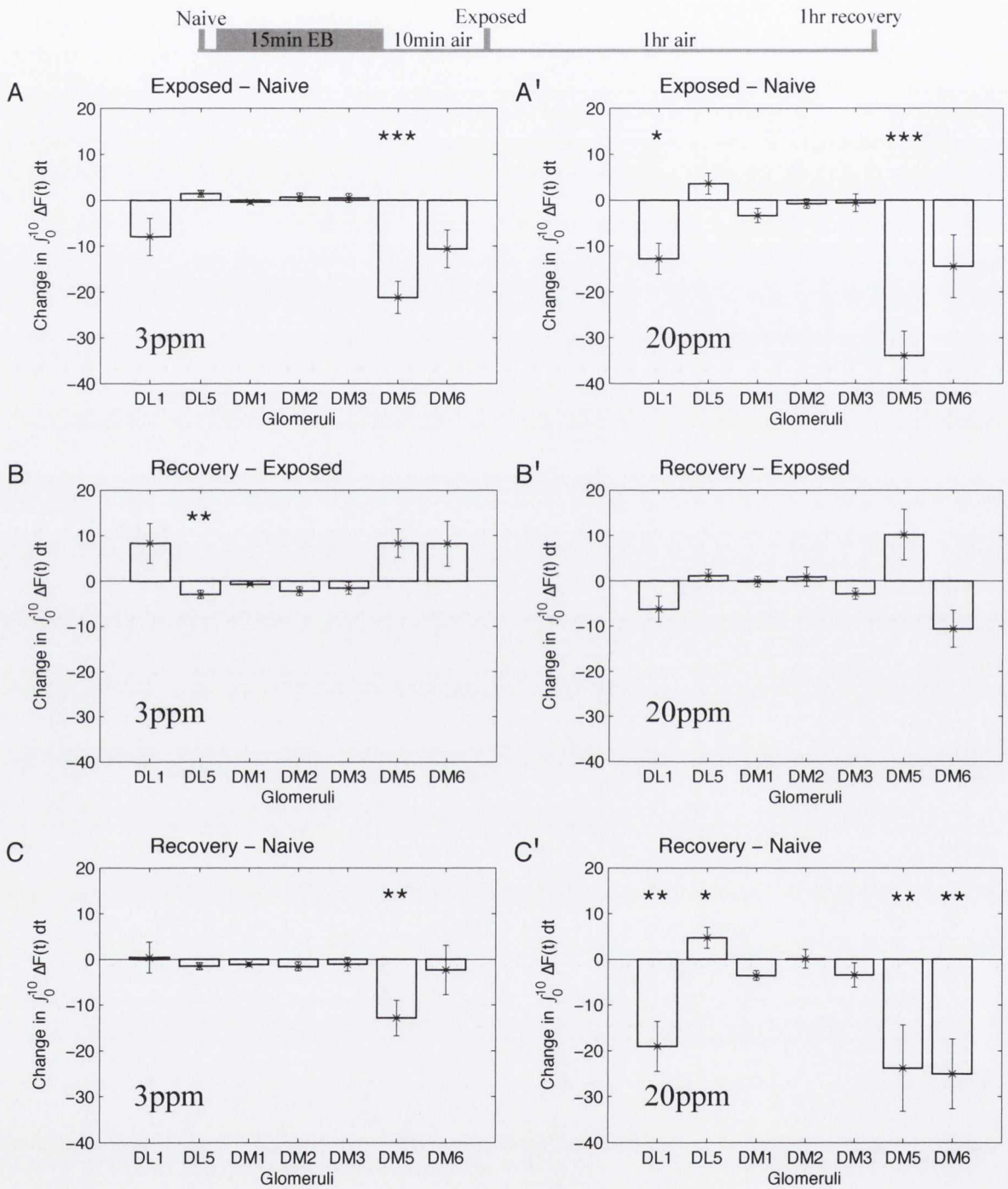


Figure 3.16: Quantified changes and recovery in odour-evoked Ca^{2+}-influxes in PNs after 15-minute odourant exposure to 3ppm and 20ppm EB *Figure legend on following page.*

Figure 3.16: Quantified changes and recovery in odour-evoked Ca^{2+}-influxes in PNs after 15-minute odourant exposure to 3ppm and 20ppm EB
Two-photon Ca^{2+}-imaging data from a naïve, an exposed, and a 1-hour delayed 10-second odour stimulus to 3ppm and 20ppm EB shown as the area under the curve of the paired differences between the compared GCaMP6m responses over a 10 seconds period ($\int_0^{10} \Delta F \, dx$, whereas ΔF reflects the paired differences over time). **(A/A')** Changes in odour-evoked GCaMP6m fluorescence in PNs induced by short-term odourant exposure to 3ppm (A) and 20ppm (A'). A negative deviation indicates a decrease in the odour-evoked Ca^{2+}-influxes in PNs after odourant exposure. **(B/B')** Changes in odour-evoked GCaMP6m fluorescence occurring during a 1 hour 'recovery' period following short-term odourant exposure to 3ppm (B) and 20ppm (B'). A positive deviation indicates recovery from the decrease in odour-evoked Ca^{2+}-influxes in PNs after odourant exposure. **(C/C')** Comparison of odour-evoked GCaMP6m fluorescence responses to the naïve and the 1 hour recovery EB puff. A negative deviation indicates that the decrease in odour-evoked Ca^{2+}-influxes in PNs after odourant exposure have not completely recovered after 1 hour. A significant difference in the overall odour-evoked GCaMP6 responses in PNs was observed between the three EB presentations delivered at both concentrations (*Likelihood ratio test, $\chi(14)=64.587$, $p<0.001$, n=9-22/glomerulus (A-C) and $\chi(14)=90.813$, $p<0.001$, n=6-7/glomerulus (A'-C')*, see Table 3.4 for detailed statistics). $*$ $p<0.05$; $**$ $p<0.01$; $***$ $p<0.001$; bars indicate mean $\pm$ SEM of the given paired comparison.

3.3.3 Mock-Exposure

In order to confirm that the observed changes in odour-evoked PN responses indeed result from the odourant exposure rather than a slowly deteriorating fly due to its freely exposed brain the following control experiment was performed. Instead of a 15-minute odourant exposure the flies were subjected to a 'mock' treatment consisting of an initial odour presentation followed by a 15-minute 'mock' air exposure, a 10-minute air resting period (thus, resulting in an in total 25-minute air interval), and subsequent 10-second odour presentation. This experimental approach allowed us to check whether changes in odour-evoked PN responses also occurred in the absence of short-term odourant exposure. If they did this would suggest that the changes observed after 15-minute odourant exposure were not due to the exposure itself but rather resulted from the experimental approach. To further confirm the well-being of the fly for a minimum of at least one and a half hours, which was required for the recovery experiments described earlier (section 3.3.2), odour-evoked GCaMP responses were further measured 1 hour after the 'mock' treatment. Odour concentration of all three EB stimuli delivered were 3ppm and Ca^{2+} dynamics were again recorded from the seven selected glomeruli. No significant difference in the overall odour-evoked GCaMP6m responses in PNs was observed between the three EB presentations delivered (*Likelihood ratio test, $\chi(14)=9.328$, $p=0.810$*, see Figure 3.17) indicating that the fly preparation stays alive for at least 1.5 hours without affecting odour-evoked GCaMP responses in PNs. As seen in Figure 3.17A odour-evoked GCaMP responses of PNs projecting to DM5 appear to slightly decrease following the 'mock' treatment. Thus, a likelihood ratio test restricted to PNs innervating DM5 was performed. However, no significant difference in odour-evoked GCaMP responses was detected between the three odour presentations ($\chi(2)=4.180$, $p=0.124$).

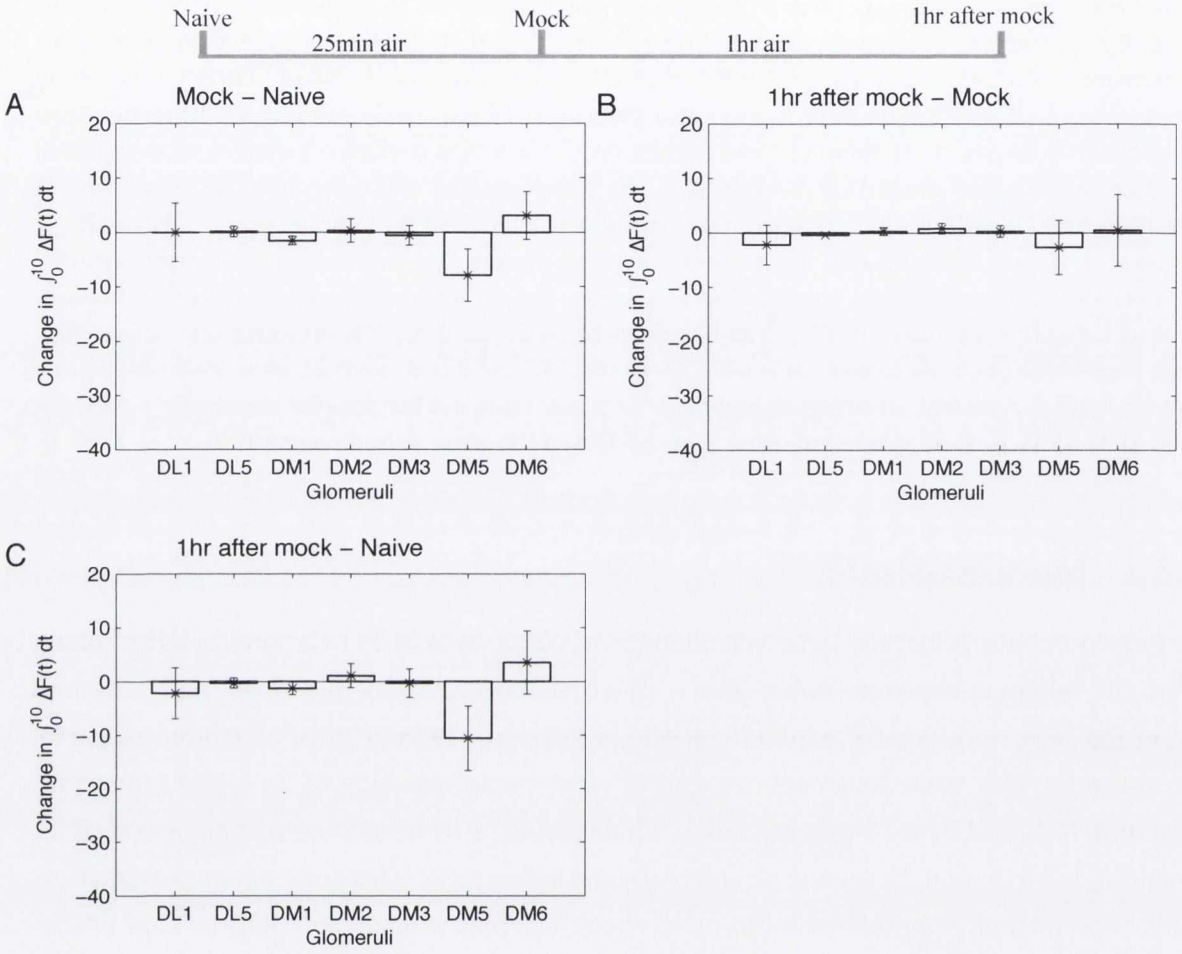


Figure 3.17: Quantified comparisons of odour-evoked Ca^{2+}-influxes in PNs between a naïve, a 'mock' exposed, and a 1-hour delayed 3ppm EB presentation

Two-photon Ca^{2+}-imaging was performed in GH146-labelled PNs during a naïve, a 'mock' air exposed, and a 1-hour delayed 10-second odour presentation to 3ppm EB. Shown are the areas under the curve of the paired differences between the compared GCaMP6m responses over a 10 seconds period ($\int_0^{10} \Delta F \, dx$, whereas ΔF reflects the paired differences over time). **(A)** Comparison of odour-evoked GCaMP6m fluorescence responses to the naïve and the 'mock' air exposed EB puff. A negative deviation indicates a decrease in the odour-evoked Ca^{2+}-influxes in PNs after 'mock' exposure. **(B)** Comparison of odour-evoked GCaMP6m fluorescence responses to the EB stimulus following 'mock' exposure and a 1-hour delayed EB presentation. **(C)** Comparison of odour-evoked GCaMP6m fluorescence responses to the naïve and the 1 hour delayed EB puff. A negative deviation indicates that the decrease in odour-evoked Ca^{2+}-influxes in PNs after 'mock' exposure have not completely recovered after 1 hour. No significant difference in the overall odour-evoked GCaMP6m responses in PNs was observed between the three EB presentations delivered (*Likelihood ratio test,* $\chi(14)=9.328$, $p=0.810$, *n=4-13/glomerulus*). Bars indicate mean ± SEM of the given paired comparison.

3.3.4 Changes in Baseline

As briefly mentioned in section 2.2.4, the changes in odour-evoked PN responses following short-term odourant exposure were accompanied by changes in the baseline levels of the GCaMP6m sensor. Figure 3.18 shows raw (A-G) and mean (A'-G') GCaMP6m traces from the experiment presented in section 3.3.1, where flies were exposed and tested to 3ppm EB. Raw and mean GCaMP traces are shown as raw pixel values. As noticeable in the GCaMP6 levels preceding an odour presentation, especially PNs projecting to DM2 and DM3 show downward shifts in baseline GCaMP fluorescence (see magnification Figure 3.18) . Figure 3.19 shows the quantification of these baseline shifts for both experiments presented in section 3.3.1 where testing and exposure was performed at an EB concentration of 3ppm or 20ppm.

A significant difference in the baseline GCaMP fluorescence levels in PNs was observed for the two recordings taken at 3ppm (*Likelihood ratio test,* $\chi(7)=61.98$, $p=<0.001$). 15-minute exposure to 3ppm EB resulted in baseline fluorescence shifts in five out of the seven glomeruli (Figure 3.19 A). Paired differences of the GCaMP6m fluorescence baseline levels adjacent to the 'exposed' and naïve' odour pulse showed significant downward shifts for the glomeruli DL1, DM1, DM2, DM3, and DM6 (Table 3.5). The reductions were most substantial in the glomeruli DM2 and DM3 (see Figure 3.19 A and Table 3.5). GCaMP6m baseline fluorescence remained unchanged in DL5 and DM5 (Table 3.5). 20ppm odourant exposure likewise had a significant effect on baseline GCaMP fluorescence levels in PNs (*Likelihood ratio test,* $\chi(7)=45.053$, $p=<0.001$). For 20ppm, reductions in baseline GCaMP levels were observed in the DL1, DL5, DM1, DM2, DM3, and DM6 glomerulus (see Figure 3.19 B and Table 3.5). Reductions were most pronounced in the glomeruli DM2, DM3, and DM6 (see Figure 3.19 and Table 3.5). GCaMP6m baseline fluorescence remained unchanged in DM5. Importantly, fluorescence baseline shifts were not observed after 'mock' treatment. 'Mock' air exposure did not have an effect on baseline fluorescence levels (*Likelihood ratio test,* $\chi(7)=4.709$, $p=<0.695$; see Figure 3.19 C) suggesting that the downwards shifts in GCaMP fluorescence baselines were caused by the odourant exposure.

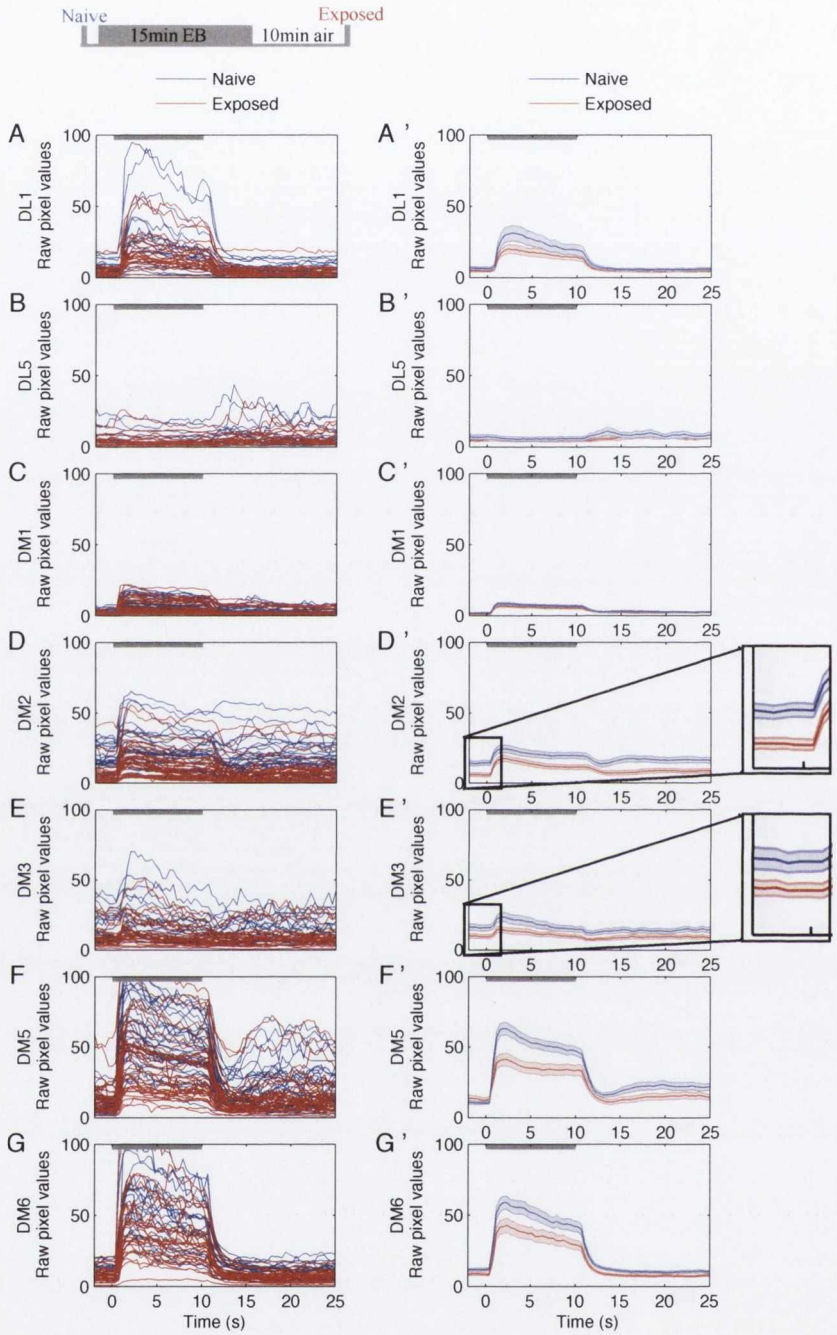


Figure 3.18: Baseline shifts in GCaMP signal in PNs after 15-minute odourant exposure to 3ppm EB

Two-photon Ca^{2+}-imaging was performed in GH146-labelled PNs during a naïve and an exposed 10-second odour presentation to 3ppm EB. Take note of the shifts in baseline GCaMP6m fluorescence of some of the glomeruli after odourant exposure. **(A-G)** Raw EB-evoked GCaMP6m fluorescence traces to the naïve (blue) and exposed (red) EB presentation shown as raw pixel values over time. **(A'-G')** Mean of the EB-evoked increases in GCaMP6m fluorescence to naïve (blue) and exposed (red) EB presentation shown as raw pixel values over time. Graphs represent mean (dark line) ± SEM (shaded region). n=15-34/glomerulus (see Table 5.6). The grey bars indicate the time window of odour presentation. See Figure 3.19 and Table 5.6 for statistical comparisons of these baseline shifts.

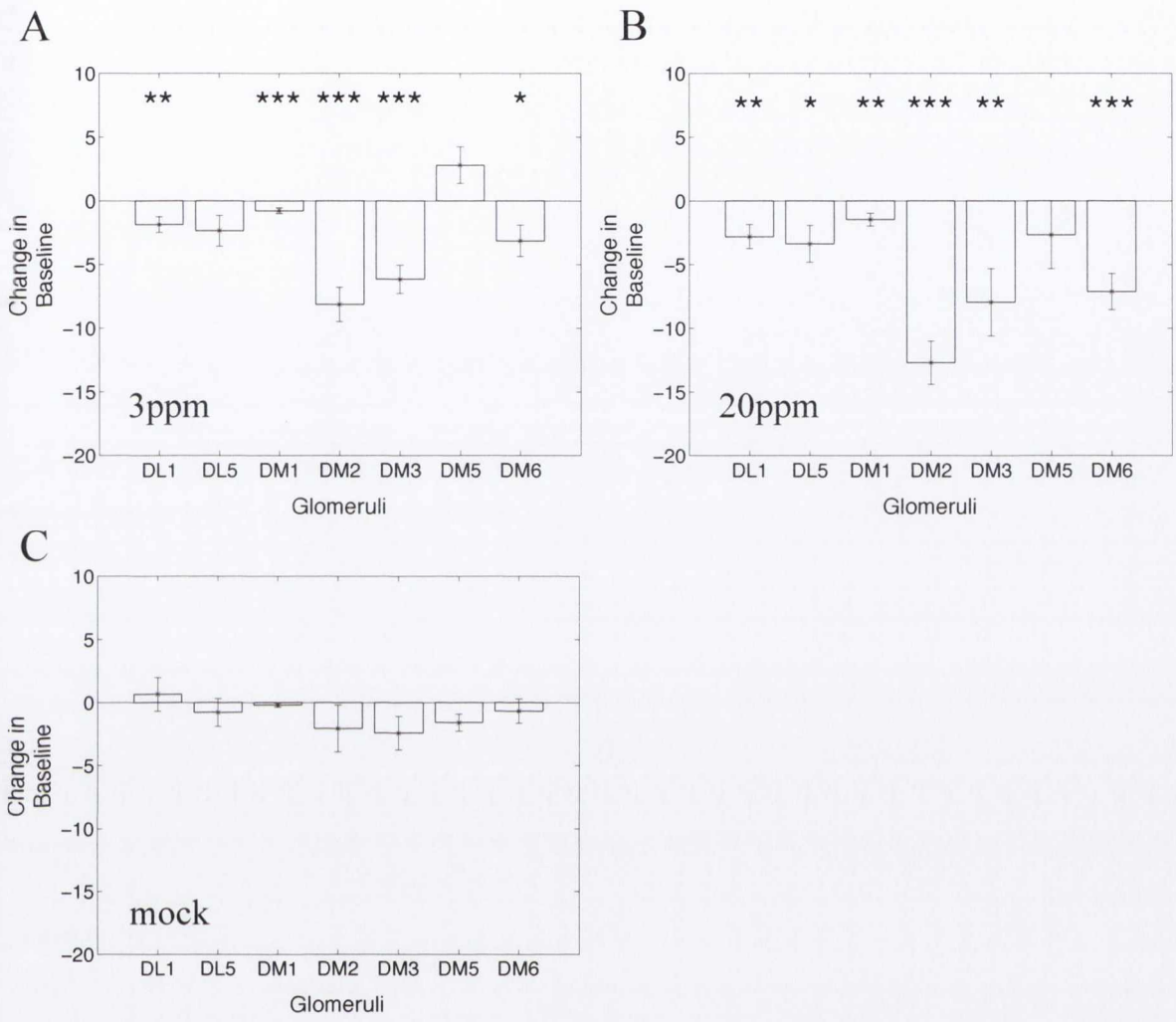


Figure 3.19: Quantified baseline fluorescence changes in PNs after 15-minute odourant exposure

Two-photon Ca^{2+}-imaging was performed preceding a naïve and an exposed or mock exposed 10-second odour presentation to compare GCaMP baseline levels. Depicted are the changes in odour-evoked GCaMP6m baseline fluorescence shown as the paired differences of the GCaMP fluorescence baselines adjacent to the 'exposed'/'mock' and 'naïve' odour pulse (Change in Baseline). **(A)** 15-minute exposure to 3ppm EB had a significant effect on GCaMP baseline fluorescence in PNs (*Likelihood ratio test, $\chi(7)=61.098$, $p<0.001$, n=15-34/glomerulus* (see Table 5.6)). Significant reductions in baselines were observed in the DL1, DM1, DM2, DM3, and DM6 glomerulus (see Table 3.5). **(B)** 15-minute exposure to 20ppm EB had a significant effect on GCaMP baseline fluorescence in PNs (*Likelihood ratio test, $\chi(7)=45.53$, $p<0.001$, n=15-22/glomerulus* (see Table 5.9)). Significant reductions in baselines were observed in the DL1, DL5, DM1, DM2, DM3, and DM6 glomerulus (see Table 3.5). **(C)** Baseline fluorescence was not affected by 'mock' treatment (*Likelihood ratio test, $\chi(7)=4.709$, $p=<0.695$, n=4-13/glomerulus*). $*$ $p<0.05$; $**$ $p<0.01$; $***$ $p<0.001$; bars indicate mean $\pm$ SEM.

		DL1	DL5	DM1	DM2	DM3	DM5	DM6
3ppm	change (arb. units)	-1.865 ± 0.624	-2.352 ± 1.201	-0.769 ± 0.223	-8.116 ± 1.349	-6.155 ± 1.099	2.800 ± 1.433	-3.137 ± 1.228
	statistics	t-test p=0.008 t=-2.989 df=19 **	wilcoxon p=0.073 sr=28 n=15 *	wilcoxon p<0.001 z=-3.690 n=33 **	t-test p=<0.001 t=-6.017 df=32 ***	t-test p=<0.001 t=-5.598 df=22 **	t-test p=0.059 t=1.954 df=33 n.s.	t-test p=0.018 t=-2.556 df=23 ***
20ppm	change (arb. units)	-2.806 ± 0.942	-3.381 ± 1.447	-1.470 ± 0.503	-12.704 ± 1.695	-7.962 ± 2.629	-2.662 ±2.6608	-7.119 ± 1.422
	statistics	t-test p=0.008 t=-2.977 df=19 ***	t-test p=0.032 t=-2.336 df=17 n.s.	wilcoxon p=0.006 z=-2.763 n=21 **	t-test p<0.001 t=-7.493 df=21 n.s.	wilcoxon p=0.002 sr=9 n=15 n.s.	t-test p=0.329 t=-1.001 df=20 ***	t-test p<0.001 t=-5.006 df=15 ***

Table 3.5: Statistics comparing GCaMP fluorescence baselines in PNs

3.3.5 Discussion

The experiments performed in this chapter aimed to investigate changes in odour-evoked neuronal activity in olfactory PNs following short-term odourant exposure. Since Ca^{2+}-dynamics are tightly correlated with neuronal activity (Berridge et al., 2000; Bootman et al., 2001b) Ca^{2+}-imaging was performed to quantify odour-evoked PN activity before and after 15-minute continuous odourant exposure. The Ca^{2+} indicator GCaMP6m was expressed in GH146-labelled PNs and Ca^{2+}-influxes were recorded from PNs projecting to seven distinct glomeruli within the antennal lobe. Testing and exposure was performed at two different odour concentration, 3ppm and 20ppm.

Naïve EB-Evoked GCaMP Responses

The 10-second EB stimulus elicited a rise in GCaMP levels in PNs projecting to six out of the seven glomeruli. Both, 3ppm and 20ppm odour stimuli evoked largest GCaMP signals in DM5, DM6, and DL1 (see Figure 3.13). PNs projecting to DM1, DM2, and DM3 were only weakly activated, those innervating DL5 showed a reduction in the GCaMP signal. The EB concentration delivered affected the overall GCaMP6m responses with 20ppm increasing GCaMP signals significantly. The naïve odour-evoked GCaMP responses reported here are largely consistent with previously published data (Hallem et al., 2004; Hallem and Carlson, 2006; de Bruyne et al., 2001; Semmelhack and Wang, 2009).

Ca^{2+} imaging has been widely used to study PN-response-profiles to a range of different odours (Wang et al., 2003; Barth et al., 2014; Silbering and Galizia, 2007; Silbering et al., 2008; Schubert et al., 2014). Wang et al. (2003), for instance, investigated odour-

evoked Ca^{2+} influxes in PNs projecting to 23 different glomeruli in response to 16 different odourants. Their results not only show that different odours activate different combinations of glomeruli they also demonstrate that higher odour concentrations increase odour-evoked GCaMP responses and activate more glomeruli. In line with this, a 20ppm EB stimulus in the present study caused a significantly larger odour-evoked GCaMP response than a 3ppm EB stimulus (see section 3.3.1). Despite the numerous studies on PN/odour-response-profiles PN responses elicited by EB have only been described in one study and only in four glomeruli located in a single AL layer (Semmelhack and Wang, 2009). Semmelhack and Wang (2009) report EB-evoked GCaMP responses in the DM1, DM2, VM7, and DM5 glomerulus and find strongest GCaMP responses in PNs targeting DM5 and VM2 followed by those innervating DM2 and DM1. These results mirror what has been found in the present study.

A more extensive investigation of the EB-response profile has been performed at the OSN level in form of single-sensillum recordings (SSRs) (Hallem et al., 2004; Hallem and Carlson, 2006; de Bruyne et al., 2001). SSRs are extracellular recordings from the sensillum lymph which bathes the sensory dendrites of OSNs (Pellegrino et al., 2010). de Bruyne et al. (1999) described strong responses to EB in OSNs projecting to DM1 and DM2, smaller responses in those targeting DM5 and only weak responses in DL1, DL5, and DM3 associated OSNs (de Bruyne et al., 1999). EB-evoked responses in OSNs innervating DM6 were not reported. Another two studies largely supported these observations (Hallem et al., 2004; Hallem and Carlson, 2006). Hallem et al. (2004) and Hallem and Carlson (2006) reported strongest EB-elicited responses in OSNs projecting to DM2 and DM6, followed by those projecting to DM5 and DM3, while OSNs targeting DL1 and DL5 only showed small responses in their study. OSNs projecting to DM1 were not investigated. Discrepancies between the results obtained from these three studies which exploited SSRs and the Ca^{2+} imaging data presented here predominantly lie in EB-elicited response in the glomeruli DM1, DM2, and DL1. While the SSRs show strong responses in DM1 and DM2 associated OSNs and weak responses in OSNs targeting DL1, the contrary was observed with Ca^{2+} imaging in their respective PNs.

Potential reasons for these discrepancies are numerous. Firstly, two different techniques were used to measure EB-evoked neuronal activity. While SSRs enable the detection of action potentials in a single neuron, Ca^{2+}-imaging detects Ca^{2+} changes in a population of neurons. Thus, the discrepancies could arise due to recordings from a single neuron versus a neuronal population or due to the differences in spiking and Ca^{2+}-dynamics. Generally, neuronal activity in single neurons is more variable than in a neuronal population. Neuronal spiking and Ca^{2+} influxes into neurons are highly correlated, however, differences exist especially in terms of temporal dynamics as changes in Ca^{2+} can be significantly slower than changes in membrane voltage (Berridge, 1998). Secondly, the two studies measured neuronal activity in two different neuronal types. SSRs monitor EB-evoked responses in OSNs whereas Ca^{2+} imaging was performed in PNs. While both spiking and Ca^{2+} dynamics are similar in OSNs and PNs (Wang et al., 2003; Root et al., 2007; Silbering et al., 2008; Bhandawat et al., 2007),

they are not identical. PNs are generally more broadly tuned than their presynaptic OSNs (Bhandawat et al., 2007) and are subjected to inhibitory, excitatory, and neuromodulatory inputs that further shape their responses (Silbering and Galizia, 2007; Olsen and Wilson, 2008b; Olsen et al., 2010). Neuronal activity of OSNs is further more variable than that of PNs as PNs integrate the activity of a number of OSNs (Bhandawat et al., 2007; Kazama and Wilson, 2009). Thirdly, an important difference between the studies, besides the techniques used and the neuronal type recorded from, are the odour concentrations delivered. For the SSR the odours were expelled from a syringe or pasteur pipette over filter paper containing 10^{-8} to 10^{-2} diluted odourant (Hallem et al., 2004; Hallem and Carlson, 2006; de Bruyne et al., 2001). The odourant concentration reaching the flies was not determined and could have therefore been substantially different from the ones delivered in the present study.

Exposure-Induced Changes in EB-Evoked GCaMP Responses

15-minute exposure to EB significantly reduced EB-evoked GCaMP responses in selected glomeruli. Ca^{2+} influx in PNs projecting to DL1, DM5, and DM6 showed a significant decrease after short-term odourant exposure at both concentrations (see Figure 3.14). Additionally, odour-evoked GCaMP responses of PNs targeting DL5 were significantly increased after 3ppm EB exposure and those targeting DM1 were significantly decreased after 20ppm EB exposure. 15-minute 'mock' exposure to air did not cause any changes in odour-evoked Ca^{2+}-influx in PNs (Figure 3.17). A summary of the percent changes with respect to the naïve odour-evoked GCaMP responses is shown in table 3.6.

		DL1	DL5	DM1	DM2	DM3	DM5	DM6
GH146	**3ppm**	-34%	109%	-12% (n.s.)	9% (n.s.)	-25% (n.s.)	-48%	-29%
	20ppm	-39%	14% (n.s.)	-42%	18% (n.s.)	-18% (n.s.)	-66%	-34%

Table 3.6: Summary of exposure-induced changes in PN activity
Percent response change of a given PN type at the two different concentrations with respect to its naïve EB-evoked GCaMP response as a measure of how much short-term odourant exposure altered naïve odour-evoked GCaMP6 responses. (n.s.) indicates a non-significant change.

Odour-induced changes in neuronal activity in the *Drosophila* AL have been reported following various protocols: Repeated 5-second odour presentations reduce odour-evoked Ca^{2+}-influxes in OSN axon terminals (Murmu et al., 2011), 4-day continuous odourant exposure decreases GCaMP responses in odourant-selective PNs (Das et al., 2011b), and olfactory classical conditioning alters the representation of odours within AL PNs (Yu et al., 2004). Thus, the occurrence of changes in neuronal activity within the *Drosophila* AL is a well known phenomenon. To our knowledge, this study provides the first demonstration of

changes in neuronal activity in the *Drosophila* AL after 15-minute continuous odourant exposure. However in the olfactory bulb of the rat, the effect of 20-minute odourant exposure on neuronal activity of mitral/tufted cells, the mammalian counterparts to invertebrate PNs, have been investigated (Buonviso et al., 1998). Naïve rats were exposed to isoamyl acetate for 20 minutes and tested 24 hours after the exposure using single cell recordings (Buonviso et al., 1998). The proportion of mitral/tufted cells responding to the odourant was substantially decreased compared to those in a non-exposed control group, similar to what has been shown in the present study.

Interestingly, comparable to what has been observed in rats (Buonviso et al., 1998) not all PN types showed a decrease in odour-evoked neuronal activity after 15-minute odourant exposure. EB-evoked GCaMP responses were mainly reduced in PNs projecting to the DL1, DM5, and DM6 glomerulus raising the question whether there is something unique about these glomeruli. Not much is known about specific glomeruli apart from those that solely respond to a single vital odour, the so called 'labelled lines' (see section 1.4.3 for details). Neither DL1, nor DM5 or DM6 belong to this class of glomeruli. However, DM5 has been implicated in mediating aversion (Semmelhack and Wang, 2009). Using Ca^{2+} imaging in PNs, Semmelhack and Wang (2009) showed that PNs projecting to DM5 are recruited at higher concentrations of apple cider vinegar, in a range that turn an appetitive odour to an aversive one. When Or85a OSNs that project to the DM5 glomerulus were silenced the flies showed attraction to a normally aversive concentration of apple vinegar. Specific activation of Or85a (by restoring Or83b expression in Or85a neurons in an Or83b mutant background) elicited repulsion behaviour to a normally attractive apple vinegar concentration. While this study suggests that DM5 independently mediates aversion, another study came to a different conclusion reporting that a number of glomeruli mediate aversion while DM5 is not one of them (Strutz et al., 2014). Their results indicate that medially located glomeruli including DM5 mediate attraction while lateral glomeruli including DL1 and DL5 mediate aversion.

If DM5 (or DL1) was indeed the glomerulus that predominantly mediates aversion the reduced activation of the DM5 (or DL1) glomerulus following short-term odourant exposure would suggest that repulsion to the aversive odourant is reduced. This is in line with the behavioural experiments performed in the Y maze where the flies are less repulsed by an aversive odour following odourant exposure (Das et al., 2011b). However, DM5 (or DL1) was not the only glomerulus that showed reduced responses after odourant exposure in this study. EB-evoked responses in DM1 and DM6 were also decreased. While it has yet to be studied whether these glomeruli serve a specific function they could also simply encode odour identity together with other glomeruli. Reducing odour-evoked activity in these glomeruli could simply serve to filter odour information that reach higher brain regions. However, if this was the case why is neuronal activity not equally suppressed in all glomeruli? Among the glomeruli studied, DM2 and DM3 remained unchanged following odourant exposure suggesting that neuronal activity is not equally diminished across all glomeruli. Instead the odour-specific combinatorial code is changed following odour exposure.

Changes in EB-Evoked GCaMP Signals with Respect to Their Naïve Responses

The PN types strongest activated by EB, namely DL1, DM5, and DM6, also showed a significant decrease in odour-evoked GCaMP responses after 15-minute odourant exposure at both concentrations, with the exceptions of PNs projecting to DM1. The PNs innervating this glomerulus showed a significant change after 20ppm exposure while only being weakly activated at that concentration (see Figure 3.14). The question whether neuronal activity is only decreased in PNs that show a strong naïve response is of interest as that is suggested by the so called negative image model (Ramaswami, 2014).

The negative image model was proposed following the behavioural findings which suggest that habituation of the olfactory avoidance response results from increased inhibition onto odour-responsive PNs within the *Drosophila* AL (Das et al., 2011b). The model proposes that unreinforced repeated or continuous excitatory stimuli create an inhibitory (or negative) image of itself which then acts as a selective filter for the familiar stimulus pattern, meaning familiar stimuli which form the same excitatory pattern are suppressed by the inhibitory image (Ramaswami, 2014). Thus, during olfactory habituation neuronal excitation in PNs is supposed to be scaled by inhibitory input according to the strength of naïve excitation within a specific PN. Strongly activated PNs are thought to be target of greater inhibition than those that are only weakly activated.

The data presented in this section supports the negative image model to some extent. An 'ideal' negative image would decrease all responses in odour-responsive PNs whereas the degree of reduction would depend on the naïve odour-evoked response in the specific PN type. In the presented data sets (see Figure 3.13 and 3.14), significant reductions in odour-evoked PN responses were only observed in those glomeruli that are most strongly activated by the odour (with the exception of DM1 as mentioned previously). PNs that were only weakly activated remained unchanged. It is possible that reductions in these PNs were not detected due to a too low power of the experiments (the numbers were 15-34 for each glomerulus). However, assuming the power of the performed experiments was sufficient to detect changes, these results suggest that there are two types of PNs, those that adjust their activity to prolonged activation and those that do not. The two PN types may encode for different properties of the odour stimulus, such as identity and valence (Strutz et al., 2014; Hong and Wilson, 2015), and only PNs that are prone to modifying their activity may follow the 'negative image model'. Alternatively, weak but detectable levels of activity in PNs may not be sufficient to trigger exposure-induced synaptic plasticity. Thus, inhibitory potentation may only occur in strongly activated PNs. Further experiments with controlled PN-specific activation are required to resolve this issue.

Characteristics of Behavioural Habituation

Behavioural habituation shows a range of characteristics including spontaneous recovery, dishabituation and dependence on stimulus intensity with lower intensities resulting in quicker and/or more pronounced habituation (Thompson and Spencer, 1966; Rankin et al.,

2009). STH of the olfactory avoidance response shows spontaneous recovery with a half life of 30 minutes and can also be dishabituated by either a mechanical stimulus or a puff of yeast odour (Das et al., 2011b; Sudhakaran et al., 2012). The effect of different stimulus intensities has not yet been studied for this behaviour. To test whether the changes in odour-evoked Ca^{2+}-influxes in PNs exhibit similar characteristics as behavioural habituation, the effect of two different odour concentrations was investigated as well as whether spontaneous recovery occurred with a similar time scale as STH of the olfactory avoidance response. Dishabituation could not be studied without substantial modification of the experimental setup.

Comparing the changes in odour-evoked GCaMP6m responses following 3 and 20ppm EB exposure revealed that the reductions in odour-evoked GCaMP6m responses were greater after exposure to 20ppm than to 3ppm (see section 3.3.1, especially Figure 3.14). These results are not obviously congruent with the defined characteristics of behavioural habituation (Rankin et al., 2009; Thompson and Spencer, 1966) as the less intense 3ppm stimulus does not cause more pronounced changes in odour-evoked PN activity than the 20ppm stimulus. Assuming the established Ca^{2+} imaging protocol induces olfactory habituation that follows the typical characteristics, the obtained result suggest that a low intense odour stimulus causes stronger behavioural habituation but weaker changes in PN activity than a high intense stimulus, a notion that cannot be easily rationalized. Further experiments, ideally those that measure action potential firing in PNs and the behaviour coincidently, will be needed to address this apparent contradiction.

To test whether changes in PN activity recover spontaneously, another EB stimulus was given an hour after the standardized habituation protocol was performed. A 1-hour delay was considered to be sufficient to observe some form of recovery as the behaviour already showed some recovery after only 30 minutes. No significant recovery from the changes induced by odourant exposure to either 3ppm or 20ppm was observed (see section 3.3.2, especially Figure 3.16). Comparisons of naïve and 1.5 hour delayed odour-evoked PN responses in flies that did not undergo odour exposure were unchanged suggesting that the fly preparation stayed alive for at least 1.5 hours without affecting odour-evoked GCaMP responses (see section 3.3.3, especially Figure 3.17). Again these results do not agree with the defined characteristics of behavioural habituation. A potential reason why no recovery occurred could be the time point at which the recovery was tested. It seems reasonable to check for recovery after an hour as the behaviour recovers within this time frame. However, during the behavioural experiments the flies are transferred from the 'exposure' bottle to the Y-maze paradigm which possibly causes some sort of 'dishabituation'. Thus, 'habituation' induced using the experimental approach here may be more pronounced than behavioural habituation and may therefore take longer to recover. Further experiments will have to address the question whether odour-evoked changes in PN activity indeed recover spontaneously.

Shifts in Baseline

Changes in odour-evoked Ca^{2+}-influxes in PNs were accompanied by changes in baseline GCaMP6m fluorescence. At both concentrations, 3ppm and 20ppm, a downward shift in GCaMP baseline levels was observed (see Figure 3.19). After 'mock' air exposure no significant changes were detected (see Figure 3.19) suggesting that the baseline changes are due to the odourant exposure rather than being an artefact of the imaging itself. The changes in baseline differ between the different PN types. PNs targeting DM2 and DM3 exhibit more pronounced changes for both EB concentration than those innervating the other glomeruli.

Downward shifts in baseline GCaMP levels indicate decreased Ca^{2+} binding to the GCaMP sensor. Potential reasons for decreased Ca^{2+} binding are reduced spontaneous neuronal activity and increased clearance of Ca^{2+} from the cytoplasm. Spontaneous activity in PNs is largely due to spontaneous excitatory input from cognate OSNs (Kazama and Wilson, 2009). Spontaneous activity in OSNs, in turn, results from spontaneous opening of odourant receptors (ORs) (Dobritsa et al., 2003; Wilson, 2013). Thus, sensory adaptation in ORs could result in reduced spontaneous OSN activity which would in turn cause decreased spontaneous PN activity leading to a downward shift in GCaMP baseline levels in PNs. The differences in the baseline shifts between the different glomeruli could be explained by varying degrees of OR adaptations. Spontaneous activity in OSNs, and thus PNs, could further be reduced by increased tonic inhibition onto presynaptic OSN terminals. While tonic inhibition has not been explicitly described in the *Drosophila* antennal lobe, GABA-mediated inhibition in the absence of an odourant is a well-known phenomenon in the mammalian olfactory bulb (Pírez and Wachowiak, 2008; McGann, 2013). The presence of odour-evoked presynaptic inhibition onto presynaptic OSN terminals in the fly antennal lobe (Root et al., 2008; Olsen and Wilson, 2008b) indicate that tonic inhibition could likewise occur.

Alternatively, increased clearance of Ca^{2+} from the cytoplasm could account for the observed reductions in GCaMP baseline fluorescence. During the short-term odour exposure a likely vast amount of Ca^{2+} rushes into odour-responsive PNs. To avoid cell death due to prolonged high Ca^{2+} levels (Clapham, 1995; Berridge et al., 2000, 1998) the intracellular Ca^{2+} concentration may be controlled and reduced by cellular mechanisms such as Ca^{2+} buffering and Ca^{2+} transport out of the intracellular space (Berridge et al., 2000). 'Overshooting' of this Ca^{2+} clearance or preventive action for another prolonged odour stimulus could result in an overall lower intracellular Ca^{2+} concentration leading to reduced GCaMP baseline levels.

3.4 The Requirement of Synaptic Proteins for Odour-Evoked Synaptic Plasticity

Following the establishment of a Ca^{2+} imaging protocol to study the neurophysiological changes associated with behavioural habituation it was aimed to determine whether the neuronal correlate of the behaviour was based on the same neuronal circuit. As detailed earlier (see section 1.5.2) habituation of the olfactory avoidance response relies on increased GABAergic release from LN1 local interneurons onto odour-responsive PNs for both, long and short term protocols (Das et al., 2011b). Blocking $GABA_A$ receptors ($GABA_A$Rs) or NMDA receptors (NMDARs) in odour-responsive PNs through the expression of transgenic RNAi constructs prevents behavioural STH and LTH (Das et al., 2011b). Behavioural STH further requires the synapse-associated protein synapsin in LN1 local interneurons as blocking its function in the LN1 subtype using RNAi-mediated knockdown impaired STH but not LTH (Sadanandappa et al., 2013). The aim of the experiments presented in this chapter was to test whether the changes in odour-evoked Ca^{2+} influxes in PNs are similarly blocked by RNAi-directed knockdowns of $GABA_A$Rs and NMDARs in PNs as well as synapsin in LN1s as shown for behavioural STH.

$GABA_A$Rs are ionotropic chloride channels that open upon GABA binding and mediate postsynaptic inhibition through direct hyperpolarisation (Buckingham et al., 2005; Hosie et al., 1997; Knipple and Soderlund, 2010). They are pentameric and exist as homomers or heteromers (Hosie et al., 1997). Three $GABA_A$R subunits have been discovered so far, the most common is *Resistance to Dieldrin* (Rdl; Ffrench-Constant and Mortlock, 1991). Rdl is widely distributed throughout the *Drosophila* nervous system and is required for olfactory habituation and inhibition of olfactory learning (Aronstein et al., 1996; Das et al., 2011b; Liu et al., 2007, 2009).

NMDARs are cation-selective ionotropic receptors that mediate excitation upon simultaneous glutamate/glycine binding and postsynaptic membrane depolarization (McBain and Mayer, 1994). As their activation is voltage-dependent requiring the removal of a Mg^{2+} capping ion they are believed to act as 'Hebbian coincidence detectors' integrating presynaptic synaptic transmission and postsynaptic membrane depolarization (Tsien, 2000). NMDARs are required for synaptic plasticity that underlies various types of learning and memory (Malenka and Nicoll, 1993). *Drosophila* NMDARs are heteromers composed of the NR1 and NR2 subunits which are both weakly expressed throughout the brain (Xia et al., 2005). The NR1 subunit has been shown to be required for olfactory associative learning as well as olfactory habituation (Xia et al., 2005).

Synapsins are synaptic vesicle associated proteins that when phosphorylated by kinases allow synaptic vesicles to detach from the reserve pool and to enter an active pool (Bykhovskaia, 2011). By making synaptic vesicles available for transmitter release synapsins induce pre-synaptic facilitation (Bykhovskaia, 2011). The *Drosophila* genome only encodes a single synapsin gene which is required for olfactory associative learning as

well as olfactory habituation (Klagges et al., 1996; Das et al., 2011b; Michels et al., 2005, 2011).

For behavioural STH of the olfactory avoidance response $GABA_A$Rs and NMDARs are required in odour-responsive PNs while functional synapsin and its phosphorylation is required in the GABAergic LN1 type of local interneurons (Das et al., 2011b; Sadanandappa et al., 2013). The proposed model for olfactory STH suggests that phosphorylation of synapsin in LN1s mediates facilitation of GABA release at the LN1-PN synapse. GABA binding onto $GABA_A$Rs leads to inhibition of odour-evoked PN activation and thus a reduced behavioural avoidance. Importantly, potentiation of GABAergic inhibition is selective to odour-responsive PNs which is mediated by the activation of NMDARs via co-release of glutamate from the LN1 population. The coincidence of odour-evoked PN activation and glutamate release from LNs activates NMDA receptors in odour-responsive PNs which is believed to cause an enhancement of GABAergic transmission from LNs onto these specific PNs, through an as of yet unidentified retrograde messenger.

The aim of the experiments performed in this chapter was to determine whether odour exposure induced changes in Ca^{2+} influxes in PNs are prevented by targeted RNAi transgene expression against the $GABA_A$R subunit Rdl and the NMDAR subunit NR1 in PNs as well as against synapsin in LNs. If the changes in PN Ca^{2+} influxes were prevented due to RNAi expression this would be an indication that behavioural STH and the physiological changes presented here underlie the same neuronal circuitry.

3.4.1 $GABA_A$ and NMDA Receptors in the PN Postsynapse

To test whether $GABA_A$Rs and NMDARs are required in PNs for changes in odour-evoked Ca^{2+} influxes in PNs induced by the short-term odourant exposure protocol, transgenic RNAi constructs against the $GABA_A$R subunit Rdl or the NMDAR subunit NR1 were expressed in GH146-labelled PNs together with the GECI GCAMP6m under GAl4/UAS control. Flies that expressed the Ca^{2+} indicator but not the RNAi construct served as controls. UAS-Rdl-RNAi made by Liu et al. (2009) was previously used to knock down Rdl-containing $GABA_A$R expression in PNs and mushroom body kenyon cells (Liu et al., 2009; Das et al., 2011b). UAS-dsNR1-RNAi was generated by Wu et al. (2007) and is known to suppress NR1 expression required for long-term memory consolidation and, when expressed in PNs, for olfactory STH (Das et al., 2011b).

When comparing the naïve EB-evoked GCaMP responses between controls (*GH146-Gal4,UAS-GCaMP6m*) and Rdl-RNAi-expressing flies (*GH146-Gal4,UAS-GCaMP6m;UAS-RdlRNAi*) they did not differ, as the genotype had no significant effect on odour-evoked GCaMP6 responses in PNs (*Likelihood ratio test, $\chi(3)=5.241$, $p=0.155$, $n=13$-16 per genotype and glomerulus*, see Figure 3.20 A). Likewise no interaction effect between genotype and odour presentation (naïve vs. exposed) could be detected (*Likelihood ratio test, $\chi(1)=2.339$, $p=0.126$*, see Figure 3.20 B) suggesting that the overall exposure-induced changes were indistinguishable between Rdl-RNAi-expressing flies and

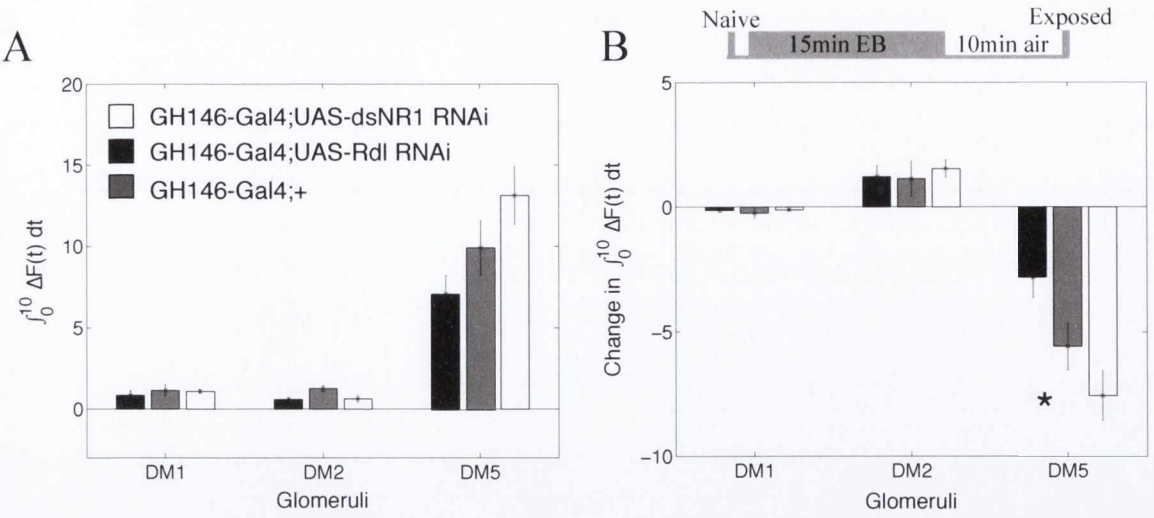


Figure 3.20: The effect of $GABA_A$ and NMDA receptor knockdown in PNs on exposure-induced changes in PN GCaMP responses
Two-photon Ca^{2+}-imaging was performed in GH146-labelled PNs during a naïve and an exposed 10-second odour presentation to 3ppm EB. Ca^{2+} dynamics were recorded from PNs projecting to the DM1, DM2, and DM5 glomerulus. Comparisons were made between the experimental groups that expressed an RNAi construct against either the $GABA_A$ receptor subunit Rdl (*GH146-Gal4,UAS-GCaMP6m;UAS-RdlRNAi*, black bars) or the NMDA receptor subunit NR1 (*GH146-Gal4,UAS-GCaMP6m;UAS-dsNR1RNAi*, white bars) and controls (*GH146-Gal4,UAS-GCaMP6m*, grey bars). (**A**) Naïve odour-evoked Ca^{2+}-influxes in PNs shown as the area under the curve of the GCaMP trace over a 10 seconds period. (**B**) Changes in odour-evoked GCaMP6m fluorescence induced by short-term odourant exposure shown as the area under the curve of the paired differences between the exposed and naïve GCaMP6m responses over a 10 seconds period. A significantly smaller change in the DM5 glomerulus was detected in Rdl-RNAi-expressing flies compared to controls (*Likelihood ratio test, $\chi(1)=3.853$, $p=0.0497$, n=13-16 per genotype and glomerulus.*)

controls. However, Rdl-RNAi-expressing flies appeared to exhibit smaller reductions in odour-evoked PN GCaMP responses in the DM5 glomerulus compared to controls. Seemingly, the likelihood ratio test on the overall exposure-induced changes in PN GCaMP responses was not able to discern this subtle difference between the two genotypes. Thus, a likelihood ratio test restricted to the DM5 glomerulus was performed which detected a small but significant interaction effect between genotype and odour presentation (naïve vs. exposed; *Likelihood ratio test, $\chi(1)=3.853$, $p=0.0497$*, see Figure 3.20 B). Importantly, naïve EB-evoked GCaMP responses in the DM5 glomerulus were not statistical different between the Rdl-RNAi expressing flies and controls (*DM5: T-Test, $p=0.160$, $t=1.444$, $df=27$, n=16 for experimental and 13 for control*). These results indicate that Rdl and thus $GABA_AR$ expression in PNs may be necessary for the reduction in GCaMP responses in the DM5 glomerulus.

The results obtained when comparing dsNR1-RNAi-expressing flies (*GH146-Gal4,UAS-GCaMP6m;UAS-dsNR1RNAi*) and controls (*GH146-Gal4,UAS-GCaMP6m*) were similar: The genotype had no significant effect on the overall naïve EB-evoked GCaMP responses in PNs (*Likelihood ratio test, $\chi(3)=6.082$, $p=0.108$, n=13-14 per genotype and glomerulus*, see Figure 3.20 A) and no interaction effect between genotype and odour presentation

(naïve vs. exposed) could be detected (*Likelihood ratio test, $\chi(1)=0.348$, $p=0.555$*, see Figure 3.20 B). Notably, RNAi transgene expression against NR1 seemed to increase the naïve EB-evoked PN GCaMP responses specifically in the DM5 glomerulus and enhance the exposure-induced changes in the same glomerulus. However, neither of these was statistically significant even if the DM5 glomerulus was analysed separately (naïve: *T-Test, $p=0.196$, $t=-1.329$, $df=25$, $n=14$ for experimental and 13 for control*, change: *Likelihood ratio test, $\chi(1)=1.520$, $p=0.218$*). These results indicate that RNAi-mediated knockdown of NR1 in PNs may not prevent exposure-induced changes in in odour-evoked Ca^{2+} influxes in PNs.

3.4.2 Synapsin in the GABAergic LN1 Presynapse

To check for the requirement of synapsin for the changes in Ca^{2+} influxes in PNs, both the Gal4 and the LexAop binary expression systems were used. While an RNAi construct against synapsin was expressed in LN1 local interneurons under Gal4/UAS control, GCaMP3 was driven by GH146-LexA in PNs. GCaMP3, although exhibiting smaller signals and lower signal-to noise ratio (Chen et al., 2013), was used instead of GCaMP6m since the LexAop-GCaMP6m sensor was not available at the time of the experiments. The LexAopGCaMP3 transgene was made in the laboratory by colleague Sahar Osman. The UAS-syn-RNAi was obtained from VDRC and expression of this transgene in LN1 interneurons had been previously shown to impair olfactory STH (Sadanandappa et al., 2013).

Naïve EB-evoked GCaMP responses did not differ between syn-RNAi-expressing flies (*GH146LexA,LexAopGCaMP3/LN1Gal4;UASsynRNAi*) and controls (*GH146LexA, LexAopGCaMP3/LN1Gal4*) as the genotype had no significant effect on odour-evoked GCaMP6 responses in PNs (*Likelihood ratio test, $\chi(3)=0.851$, $p=0.837$, $n=13$-15 per genotype and glomerulus*, see Figure 3.21 A). Likewise no interaction effect between genotype and odour presentation (naïve vs. exposed) could be detected (*Likelihood ratio test, $\chi(1)=0.464$, $p=0.496$*, see Figure 3.21 B) indicating that RNAi-mediated synapsin knockdown in LN1 interneurons does not affect exposure-induced changes in PNs.

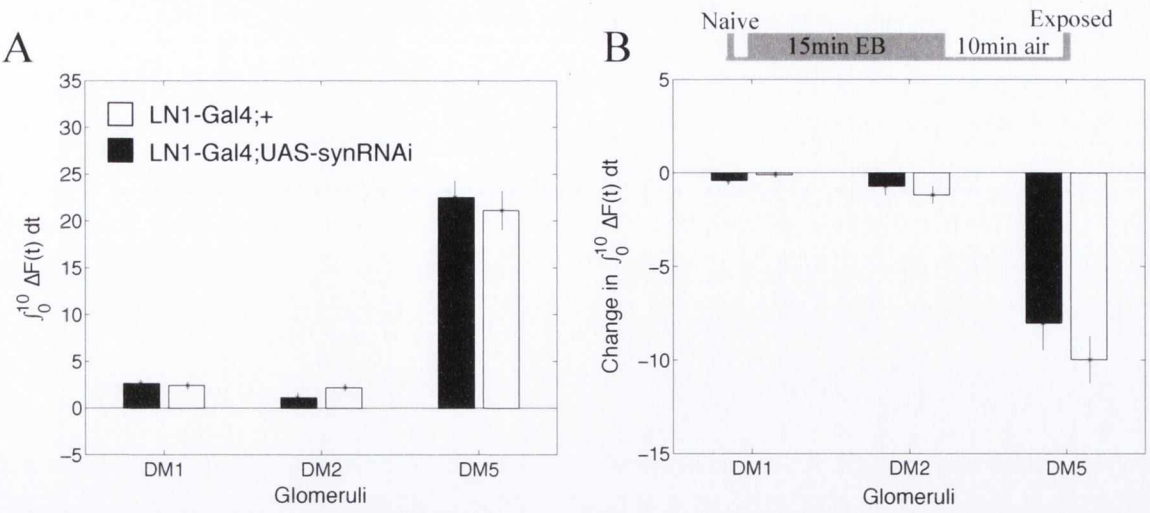


Figure 3.21: The effect of synapsin knockdown in LN1 interneurons on exposure-induced changes in PN GCaMP responses
Two-photon Ca^{2+}-imaging was performed in GH146-labelled PNs during a naïve and an exposed 10-second odour presentation to 3ppm EB. Ca^{2+} dynamics were recorded from PNs projecting to the DM1, DM2, and DM5 glomerulus. Comparisons were made between the experimental group that expressed an RNAi construct against synapsin in LN1 interneurons (*GH146LexA,LexAopGCaMP3/LN1-Gal4;UAS-synRNAi*, black bars) and controls (*GH146LexA,LexAopGCaMP3/LN1Gal4*, white bars). (**A**) Naïve odour-evoked Ca^{2+}-influxes in PNs shown as the area under the curve of the GCaMP trace over a 10 seconds period. (**B**) Changes in odour-evoked GCaMP3 fluorescence induced by short-term odourant exposure shown as the area under the curve of the paired differences between the exposed and naïve GCaMP6m responses over a 10 seconds period. n=13-15 per genotype and glomerulus.

3.4.3 Discussion

The experiments performed in this chapter aimed to investigate whether behavioural STH and the neurophysiological changes in PNs induced by similar exposure protocols rely on the same neuronal circuit in the *Drosophila* AL. Thus, it was tested whether targeted RNAi transgene expression against the $GABA_AR$ subunit Rdl and the NMDAR subunit NR1 in PNs as well as synapsin in LN1 local interneurons prevents the changes in PN Ca^{2+} influxes observed. RNAi knockdown of these synaptic proteins in the respective neuronal types had previously been shown to impair behavioural STH.

Neither RNAi-mediated knockdown of Rdl or NR1 in PNs (see Figure 3.20) nor knockdown of synapsin in LN1s (see Figure 3.21) had an effect on the overall naïve EB-evoked GCaMP responses or the overall exposure-induced changes in PN GCaMP responses. However, when the analysis was restricted to the DM5 glomerulus, Rdl knockdown in PNs reduced the exposure-induced changes in PN Ca^{2+} influxes without affecting naïve PN responses. Notably, while the naïve EB-evoked PN GCaMP responses of Rdl-RNAi-expressing flies did not statistically differ from control flies they appeared to be smaller than those of the controls (see Figure 3.20). The reduced changes after short-term odourant exposure could therefore simply result from smaller naïve GCaMP responses. To get an idea of whether this could be the case the percent change relative to the naïve GCaMP response

was calculated for each genotype separately. While this is a rather crude measure as it does not take into account the error bars it nonetheless gives an indication of the different amplitudes of the changes observed. The percent change in PN GCaMP responses in the DM5 glomerulus of Rdl-RNAi-expressing flies was -40% while that of the controls -54% showing that the changes relative to the naïve GCaMP response also differed between the two genotypes, thus strengthening the observation that Rdl expression is required for the full extend of the reduction in Ca^{2+} influxes observed in PNs projecting to DM5.

While RNAi-mediated knockdown of the $GABA_AR$ subunit Rdl reduces the changes observed in PNs projecting to the DM5 glomerulus they do not completely block them. Moreover, RNAi transgene expression against NR1 in PNs and synapsin in LN1s had no effect on the exposure-induced changes. These results can be interpreted in several ways: RNAi transgene expression could have knocked down the mRNA of the target protein only partially and the residual protein could have been sufficient to induce the physiological changes observed. In contrast, for the behaviour experiments, RNAi-mediated suppression may have been more effective. Assuming the protein levels were knocked down appropriately, the small reductions in the physiological changes observed in PNs projecting to DM5 could have also been sufficient to prevent behavioural habituation. As DM5 is thought to mediate aversion (Semmelhack and Wang, 2009), preventing the decrements in odour-evoked neuronal activity in DM5, even if only slightly, may be enough to suppress habituation to the aversive odourant. Alternatively, the neurophysiological changes induced here may not reflect the processes that underlie STH, especially since synapsin and NMDARs do not appear to be required. Further studies will have to address these possibilities.

In some cases RNAi transgene expression of a single RNAi construct is not sufficient to knockdown the targeted protein completely (see Root et al., 2008). However, targeted expression of a single RNAi copy of the respective RNAi has been shown to impair STH behaviour (Das et al., 2011b; Sadanandappa et al., 2013) suggesting that one copy is sufficient to knockdown the mRNA of the respective proteins. Notably however, in the case of Rdl and NR1 knockdown in PNs the UAS-RNAi constructs were driven by two Gal4 copies which additionally also drove the expression of the GCaMP protein. The GAL4 protein levels thus may have not been sufficient to drive the UAS-RNAi constructs adequately resulting in an incomplete knockdown of the protein. In the case of synapsin LN1-Gal4 drove the UAS-synRNAi transgene in the same way as for the behavioural STH experiments (Sadanandappa et al., 2013). Since synapsin RNAi expression did not block the neurophysiological changes this might indicate that the behaviour and the physiology may indeed not rely on the same circuitry although they both require $GABA_AR$ expression in PNs. This idea is supported by the fact that the characteristics which underlie STH do not completely match those of the neurophysiological changes as discussed previously (see section 3.3). However, as mentioned in section 3.2, the experimental protocols for behavioural STH and Ca^{2+} imaging differ with respect to odour concentration, the length of the odourant exposure and air flows which could potentially result in the discrepancies observed.

3.5 Odour-Induced Cellular Adaptations in Other Cell Types within the Antennal Lobe

As shown in the previous section (section 3.4) neither synapsin in LN1 local interneurons nor NMDAR in PNs appear to be required for exposure-induced changes in odour-evoked GCaMP responses. RNAi-mediated knockdown of the $GABA_A$Rs further did not completely block the changes in Ca^{2+} influxes in PNs suggesting that the cellular adaptations observed are not solely mediated by $GABA_A$Rs in PNs. To further investigate the effect of odourant exposure on the odour responsiveness in the *Drosophila* AL, odour-evoked GCaMP responses in other prevalent cell types in the AL were studied. Finding similar or opposing changes in other cell types would give an indication of where the cellular mechanisms arise and what their underlying mechanism are. As OSNs and PNs are tightly coupled (Wilson et al., 2004; Bhandawat et al., 2007), it was sought to study whether cellular changes may also arise presynaptically, in OSN terminals. Furthermore, since both OSNs and PNs receive inhibitory input from a range of local interneuron classes (Liu and Wilson, 2013; Olsen and Wilson, 2008b), potentially responsible for the odour exposure-induced changes in Ca^{2+} influx, Ca^{2+} dynamics were also studied in three types of inhibitory LNs.

Ca^{2+}-imaging is a useful tool for measuring neuronal activity at both the pre- and postsynapse. Postsynaptically, a rise in intracellular Ca^{2+} concentration is essential for activity-dependent synaptic plasticity (Zucker, 1999). Presynaptically, Ca^{2+} influx is tightly coupled with neurotransmitter release (Heidelberger et al., 1994; Neher and Sakaba, 2008) and Ca^{2+} levels are decreased following both presynaptic adaptation (Catterall and Few, 2008; Zucker, 1999) and inhibition (Neher and Sakaba, 2008; Wu and Saggau, 1997). Ca^{2+} imaging from OSN terminals and LN arborisations in the AL is, thus, a suitable method to further assess changes in odour-evoked activity in the AL. Decreased odour-evoked Ca^{2+} levels in OSN terminals would provide evidence of potential presynaptic adaptation or inhibition that may contribute to the habituated state. Increased odour-evoked Ca^{2+} levels in LNs, on the other hand, would be an indication for elevated neuronal activity and a greater degree of vesicle release from these cells.

To measure odour-evoked neuronal activity preceding and succeeding continuous short-term exposure GCaMP6m was expressed under the control of the Or83b- (or Orco-) Gal4 driver line in the case of OSNs and the LN1- (NP1227), LN2- (NP2426), and OK371-Gal4 drivers in case of LNs. These LN drivers were chosen as they represent the major inhibitory local interneuron classes in the AL with LN1 and LN2 being predominantly GABAergic while OK371 neurons are glutamatergic (see section 1.4.1).

The Or83b enhancer trap line labels all OSNs that express the co-receptor Or83b (or Orco) (Larsson et al., 2004), including all basiconic and trichoid OSNs, with the exception of the CO_2-sensing neurons (Grabe et al., 2015a; Couto et al., 2005; Fishilevich and Vosshall, 2005; Jones et al., 2007; Kwon et al., 2007). It therefore expresses the GAL4 protein in all OSNs that respond to food odours or pheromones (de Bruyne et al., 2001, 1999; Yao et al.,

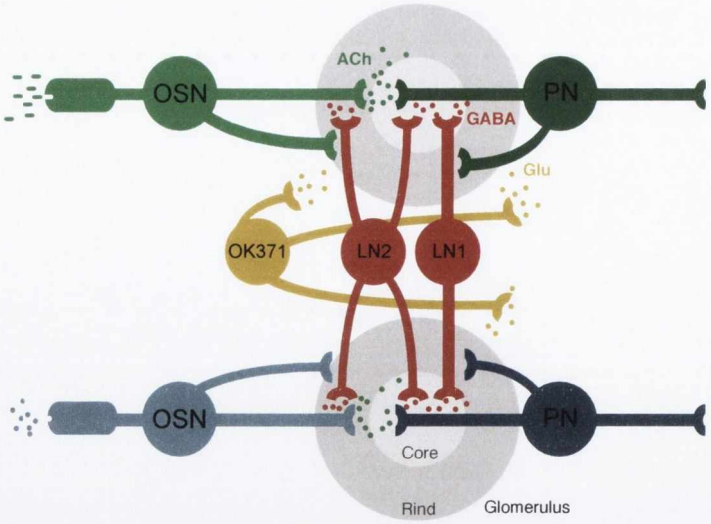


Figure 3.22: Schematic of the glomerular innervation pattern of different LN types
The LN1 and LN2 classes of GABAergic local interneurons directly innervate the glomeruli (Tanaka et al., 2009). LN1 neurons target the glomerular core while LN2s send projections to the core and the rind of a glomerulus. These innervation patterns coincide with neuronal processes of OSNs and PNs. OSN terminals reside in the glomerular rind whereas PN dendrites are situated in both the core and the rind (Tanaka et al., 2009, *projections to the rind omitted here*). In contrast to LN1 and LN2 neurons, the neuronal processes of glutamatergic OK371 neurons reside predominantly in the spaces between the glomeruli. (*OSN-LN and PN-LN synapses mostly omitted for clarity.*)

2005). Coeloconic sensilla which express IRs and respond to odours contained in food, small amines and humidity levels are not labelled (Grabe et al., 2015a; Benton et al., 2009; Rytz et al., 2013). Or83b-Gal4 labels a total of 39 out of 54 glomeruli (Grabe et al., 2015a). GH146-Gal4, used in the previous chapter, likewise labels 39 glomeruli, however, only 32 overlap with the Or83b line (Grabe et al., 2015a). Importantly, the glomeruli studied in the present study, namely DL1, DL5, DM1, DM2, DM3, DM5, and DM6, are labelled by both the Or83b and GH146 line (Grabe et al., 2015a).

The LN1 (or NP1227) enhancer trap line predominantly labels GABAergic multiglomerular LNs (Okada et al., 2009; Seki et al., 2010; Tanaka et al., 2009). It consists of ~18 neurons, 90-100% of which are GABAergic (Okada et al., 2009; Tanaka et al., 2009). The driver labels neurons with extensive arborisations in most of the AL glomeruli predominantly targeting the glomerular core (Okada et al., 2009; Tanaka et al., 2009, 2012, see Figure 3.22). The LN2 (or NP2426) enhancer trap line labels mainly GABAergic uni- and multiglomerular LNs (Okada et al., 2009; Seki et al., 2010; Tanaka et al., 2009). The Gal4 line consist of ~37 neurons which are largely GABAergic (88-90%) (Okada et al., 2009; Tanaka et al., 2009). It labels neurons that are more heterogeneous than those labelled by LN1-Gal4. Some LN2 neurons arborise in most of the glomeruli, others are more restricted and arborise in about two-third of the glomeruli (Okada et al., 2009; Tanaka et al., 2009, 2012). Unlike those of LN1s, LN2 terminals target both the core and the peripheral areas of a glomeruli (Okada et al., 2009; Tanaka et al., 2009, see Figure 3.22). The OK371 enhancer trap line labels glutamatergic neurons that express the vesicular glutamate transporter (Mahr and Aberle, 2006; Liu and Wilson, 2013). Roughly one third of the LNs in the AL (60-70 of

~200 total LNs) are labelled by this line (Mahr and Aberle, 2006; Liu and Wilson, 2013). In contrast to GABAergic LNs, glutamatergic LNs have their neuronal processes primarily in the spaces between glomeruli (Das et al., 2011a, see Figure 3.22).

The aim of the research performed in this chapter was (a) to determine whether the odour exposure induced changes in PN activity arise in presynaptic OSNs, (b) if changes in OSNs were observed, to test whether these show similar characteristics as those seen in PNs, and (c) to test whether 15-minute odour exposure also induces neuronal activity changes in three different LN types in the AL.

3.5.1 Olfactory Sensory Neurons

Different Odour Concentrations and Mock

To investigate changes in odour-evoked Ca^{2+} influxes in OSNs GCaMP6m was expressed under the control of the Gal4 driver Or83b. 3-4 day old female flies were tested and exposed to an EB concentration of 3ppm according to the standard imaging protocol (see Figure 3.9 and Table 5.90 for PID measurements). Ca^{2+} dynamics were recorded from OSNs that send their dendrites to the same set of seven glomeruli, DL1, DL5, DM1, DM2, DM3, DM5, and DM6, that were studied for odour-evoked changes in PN Ca^{2+} influxes.

Naïve EB-evoked GCaMP response traces are shown in Figure 3.23 A-G (blue traces). All the seven OSN types showed an increase in GCaMP6m fluorescence in response to the first EB stimulus (Figure 3.24 A). OSNs sending their dendrites to DM5 exhibiting the largest increase in the GCaMP6 response followed by DM6 and DM2 (see Table 3.7). Odour-evoked GCaMP6 signals in OSNs projecting to DL1, DL5, DM1, and DM3 were small.

15-minute exposure to 3ppm EB had a significant effect on odour-evoked GCaMP6 responses in OSNs (*Likelihood ratio test,* $\chi(7)=54.165$, $p<0.001$), lowering the response by -1.716 $\pm$ 5.161 arb. units (value determined by a linear mixed-effects model fit by maximum likelihood). Mean GCaMP6m traces in response to a 3ppm EB stimulus after EB exposure in relation to the naïve EB-evoked response are shown in Figure 3.23 A-G, the paired differences of the naïve and exposed odour presentation are depicted in Figure 3.23 A'-G'. A negative deviation indicates a decrease in the odour-evoked Ca^{2+}-influxes in the specific OSN type. Reductions in odour-evoked GCaMP6m responses were observed in the DM1, DM2, and DM5 glomerulus (see Table 3.7 and Figure 3.25 A). Largest absolute decreases were found in PNs projecting to DM5, followed by those innervating DM2 and DM1 (see Table 3.7). Odour-evoked GCaMP6m fluorescence remained unchanged in the DL1, DL5, DM3, and DM6 glomerulus. As for PNs the percent change was calculated with respect to the naïve EB-evoked GCaMP response in the respective OSN types. The largest reduction in odour-evoked GCaMP responses was observed in OSNs that send their dendrites to DM5 with a -50% decrease, followed by those targeting DM2 and DM1 with decreases of -42% and -38%, respectively. The respective percent changes of the glomeruli that did not show a significant change in odour-evoked GCaMP responses were -19% for OSNs targeting DL1,

-174% for OSNs projecting to DL5, -42% for OSNs that send dendrites to DM3, and -35% for DM6 OSNs.

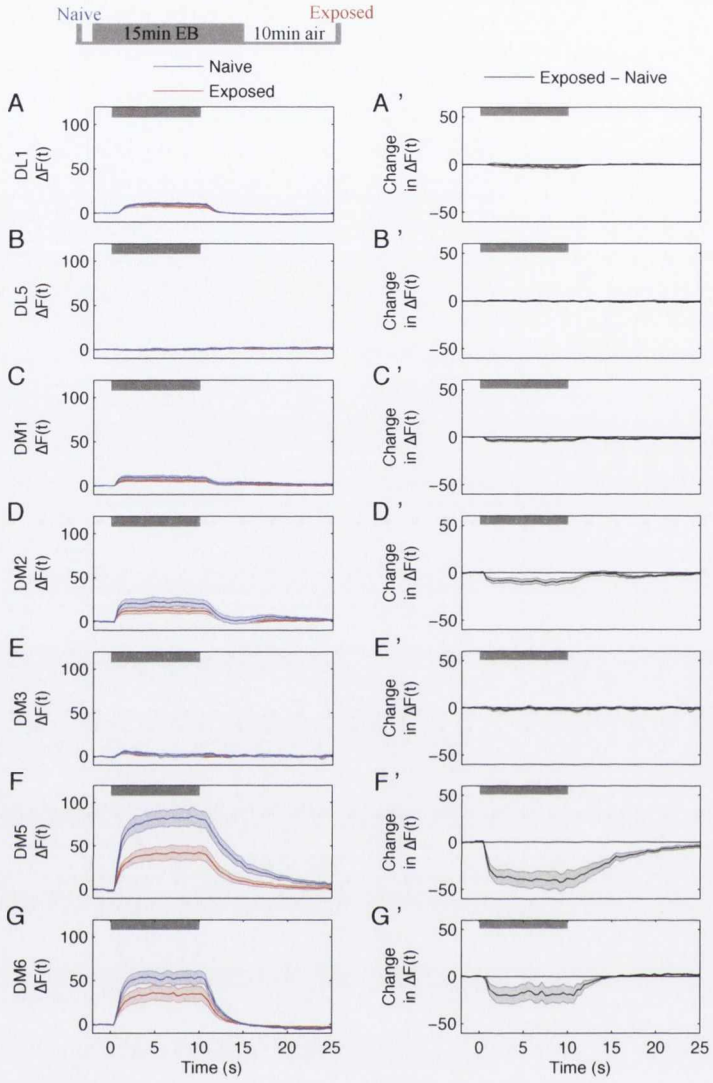


Figure 3.23: Changes in odour-evoked Ca^{2+}-influxes in OSNs after 15-minute odourant exposure to 3ppm EB.

Two-photon Ca^{2+}-imaging was performed in Or83b-labelled OSNs during a naïve and an exposed 10-second odour presentation to EB. Ca^{2+} dynamics were recorded from OSNs projecting to seven distinct glomeruli within the antennal lobe (DL1, DL5, DM1, DM2, DM3, DM5, DM6). **(A-G)** Mean of EB-evoked increases in GCaMP6m fluorescence to the naïve (blue) and exposed (red) EB presentation shown as changes in fluorescence (ΔF) over time. **(A'-G')** Paired differences of the odour-evoked GCaMP6m increases in A-G) shown as the difference of the changes in fluorescence (Change in ΔF) over time. A negative deviation indicates a decrease in the odour-evoked Ca^{2+}-influxes in OSNs after odourant exposure. Graphs represent mean (dark line) ± SEM (shaded region) of ΔF. n=13-15/glomerulus (see Table 5.40). The grey bars indicate the time window of odour presentation.

As odour-evoked changes in GCaMP responses following short-term exposure to 3ppm EB were unexpectedly found in the OSN terminals, these were characterized further in order to investigate whether the presynaptic OSN changes align with those found in postsynaptic PN dendrites. Thus, to study whether similar changes in odour-evoked Ca^{2+} influxes could be observed at a higher intensity odour stimulus, flies expressing GCaMP6m in OSNs labelled by the Or83b driver were then tested and exposed to an EB concentration of 20ppm (see Table 5.91 for PID measurments). As with PN responses, all OSN types, with the exception of DL5, showed larger naïve odour-evoked GCaMP responses to the 20ppm EB stimulus compared to their naïve responses to 3ppm (Figure 3.24 B). As for 3ppm, OSNs sending their dendrites to DM5 and DM6 showed the strongest GCaMP responses. OSNs projecting to DM2, DM3, and DL1 exhibited smaller responses and OSNs targeting DM1 were activated the weakest. Similar to the odour-evoked GCaMP responses in PN dendrites, OSNs projecting to DL5 showed decreases in GCaMP levels in response to the 20ppm EB stimulus.

As for 3ppm, 15-minute exposure to 20ppm EB had a significant effect on odour-evoked GCaMP6 responses in OSNs (*Likelihood ratio test,* $\chi(7)=81.940$, $p<0.001$), lowering the response by -10.688 $\pm$ 4.779 arb. units. Reductions in odour-evoked GCaMP6m responses were observed in OSNs projecting to all studied glomeruli apart from those innervating DL5 which showed a significant increase in odour-evoked GCaMP levels (see Table 3.8 and Figure 3.25 B). OSNs innervating DM5 and and DM6 showed the largest decreases with respect to absolute values. The absolute changes depicted in Figure 3.25 B correspond to the following percent changes in relation to naïve odour-evoked GCaMP responses: The DM5 glomerulus which displayed the largest naïve response also showed the largest percent change of -45%. The other glomeruli, with the exception of DL5, exhibited slightly lower reductions of -36% in the case of DL1 and -34% in that of DM6, DM2 decreased by -31%, DM1 by -30%, and DM3 by -28%. OSNs targeting DL5 which showed a reduction in the GCaMP signal in response to the naïve odour stimulus increased their responses by 81%.

The choice of EB concentration had a significant effect on overall GCaMP fluorescence levels (*Likelihood ratio test,* $\chi(8)=46.289$, $p<0.001$), with 20ppm increasing the responses by 16.200 $\pm$ 5.144 arb. units compared to 3ppm as determined by a linear mixed-effects model fit by maximum likelihood. However, 15-minute odourant exposure to 20ppm EB did not induce more substantial changes in odour-evoked Ca^{2+} influxes in OSNs than exposure to 3ppm EB (see Figure 3.25). No interaction effect was detectable between concentration and odour presentation (naïve) or exposed; *Likelihood ratio test,* $\chi(1)=1.746$, $p=0.18$). The reduction in odour-evoked OSN activity was therefore similar at the two different odour concentrations.

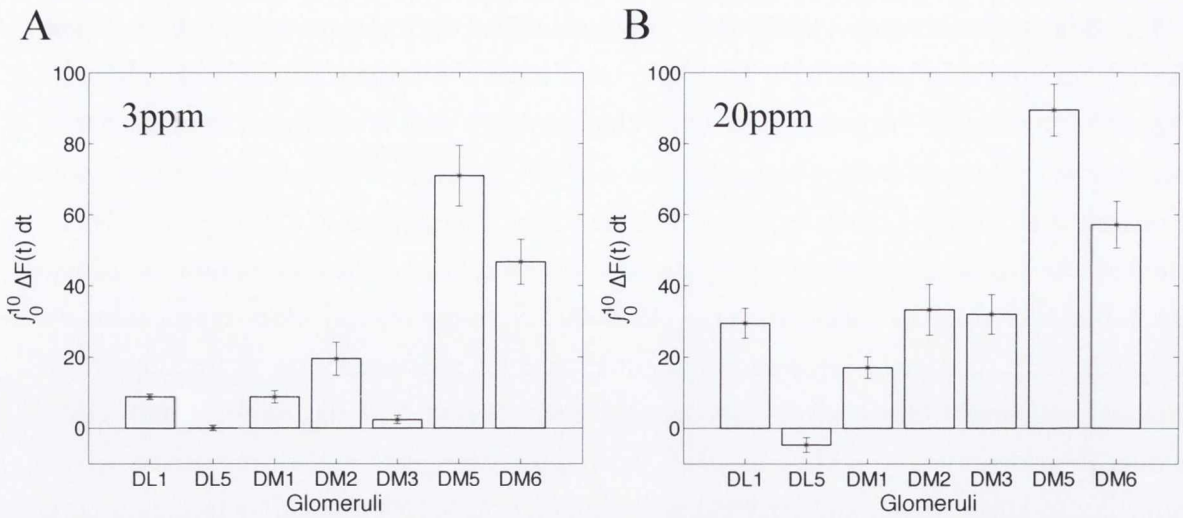


Figure 3.24: Naïve odour-evoked Ca^{2+}-influxes in OSNs to 3ppm and 20ppm EB
Two-photon Ca^{2+}-imaging was performed in Or83b-labelled OSNs during a naïve 10-second odour presentation. Ca^{2+} dynamics were recorded from OSNs projecting to seven distinct glomeruli within the antennal lobe. Depicted are the naïve odour-evoked GCaMP6m fluorescence responses to 3ppm (A) and 20ppm (B) EB shown as the area under the curve of the GCaMP trace over a 10 seconds period ($\int_0^{10} \Delta F\, dx$). n=13-15/glomerulus (A) and n=11-18/glomerulus (B) (see Tables 5.40 and 5.43).

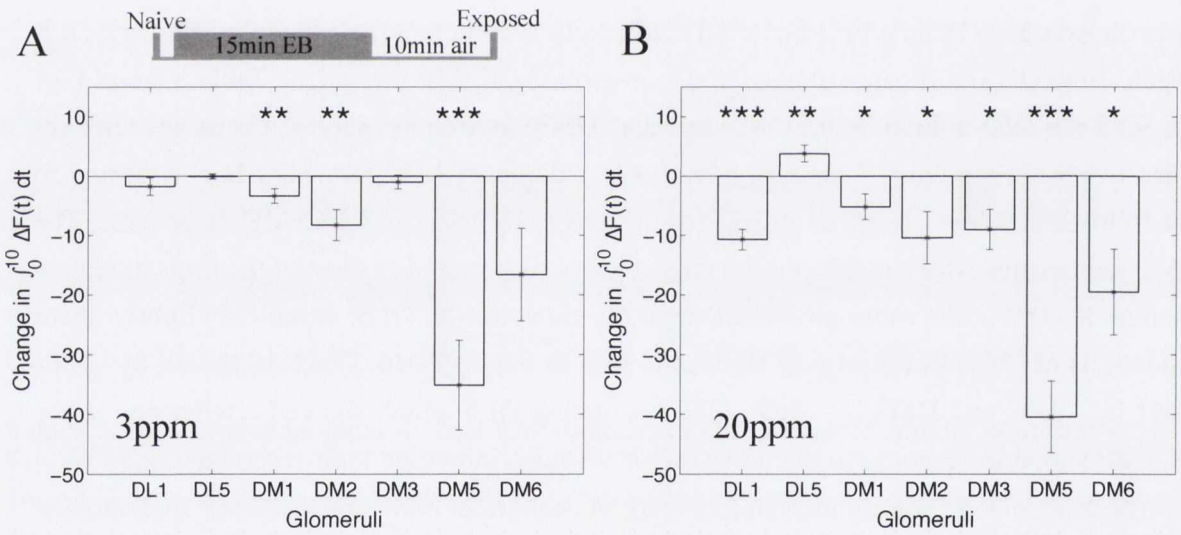


Figure 3.25: Quantified changes in odour-evoked Ca^{2+}-influxes in OSNs after 15-minute odourant exposure to 3ppm and 20ppm EB
Two-photon Ca^{2+}-imaging was performed in Or83b-labelled OSNs during a naïve and an exposed 10-second odour presentation to 3ppm or 20ppm EB. Ca^{2+} dynamics were recorded from OSNs projecting to seven distinct glomeruli within the antennal lobe. Depicted are the changes in odour-evoked GCaMP6m fluorescence induced by short-term odourant exposure shown as the area under the curve of the paired differences between the exposed and naïve GCaMP6m responses over a 10 seconds period ($\int_0^{10} \Delta F\, dx$, whereas ΔF reflects the paired differences over time). **(A)** 15-minute exposure to 3ppm EB had a significant effect on odour-evoked GCaMP6 responses in OSNs (*Likelihood ratio test, $\chi(7)=54.165$, $p<0.001$ n=13-15/glomerulus* (see Table 5.40)). Significant reductions in odour-evoked GCaMP6m responses were observed in the DM1, DM2, and DM5 glomerulus (see Table 3.7). **(B)** 15-minute exposure to 20ppm EB had a significant effect on odour-evoked GCaMP6 responses in OSNs (*Likelihood ratio test, $\chi(7)=81.940$, $p<0.001$, n=11-18/glomerulus* (see Table 5.43)). Significant reductions in odour-evoked GCaMP6m responses were observed in DL1, DM1, DM2, DM3, DM5, and DM6 (see Table 3.8). * $p<0.05$; ** $p<0.01$; *** $p<0.001$; bars indicate mean ± SEM.

	DL1	DL5	DM1	DM2	DM3	DM5	DM6
naïve (arb. units)	8.866 ± 0.809	0.039 ± 0.808	8.764 ± 1.699	19.500 ± 4.621	2.388 ± 1.170	70.941 ± 8.516	46.749 ± 6.343
change (arb. units)	-1.716 ± 1.479	-0.068 ± 0.430	-3.351 ± 1.234	-8.262 ± 2.615	-1.004 ± 1.145	-35.118 ± 7.489	-16.577 ± 7.767
statistics change	t-test p=0.269 t=-1.160 df=12 n.s.	t-test p=0.877 t=-0.158 df=14 n.s.	wilcoxon p=0.008 sr=9 n=13 **	t-test p=0.008 t=-3.160 df=12 **	t-test p=0.398 t=-0.877 df=12 n.s.	wilcoxon p<0.001 sr=0 n=13 ***	t-test p=0.054 t=-2.134 df=12 n.s.
change (%)	**-19%**	**-174%**	**-38%**	**-42%**	**-42%**	**-50%**	**-35%**

Table 3.7: OSN GCaMP responses to 3ppm EB

	DL1	DL5	DM1	DM2	DM3	DM5	DM6
naïve (arb. units)	29.502 ± 4.182	-4.677 ± 2.084	17.023 ± 3.017	33.268 ± 7.161	31.976 ± 5.569	89.436 ± 7.340	57.162 ± 6.523
change (arb. units)	-10.689 ± 1.716	3.781 ± 1.393	-5.177 ± 2.156	-10.392 ± 4.389	-8.999 ± 3.367	-40.438 ± 6.004	-19.528 ± 7.206
statistics change	t-test p<0.001 t=-6.229 df=17 ***	wilcoxon p=0.004 z=2.864 n=17 **	t-test p=0.030 t=-2.401 df=15 *	t-test p=0.031 t=-2.368 df=16 *	t-test p=0.019 t=-2.673 df=13 *	t-test p<0.001 t=-6.736 df=17 ***	t-test p=0.022 t=-2.710 df=10 *
change (%)	**-36%**	**+81%**	**-30%**	**-31%**	**-28%**	**-45%**	**-34%**

Table 3.8: OSN GCaMP responses to 20ppm EB

As for Ca^{2+} imaging in PNs, flies carrying the Or83b-Gal4 and UAS-GCaMP6m constructs were also subjected to a 'mock' treatment consisting of an initial odour presentation followed by a 15-minute 'mock' air exposure, a 10-minute air resting period (thus, resulting in an in total 25-minute air interval), and another odour presentation. This experimental setup allowed us to check whether changes in odour-evoked OSN responses also occurred in the absence of odourant exposure. EB stimuli were delivered at a concentration of 3ppm (see Table 5.92 for PID measurements) and Ca^{2+} dynamics were again recorded from the seven selected glomeruli. No significant difference in the overall odour-evoked GCaMP6m responses in PNs was observed between the EB presentations delivered (*Likelihood ratio test,* $\chi(7)=5.273$, *0.627*, Figure 3.26) indicating that 'mock' treatment does not affect odour-evoked GCaMP responses in OSNs. However, as seen in Figure 3.26 odour-evoked GCaMP responses of OSNs projecting to DM5 appeared to be decreased following mock treatment, an effect that was not picked up by the likelihood ratio test. A paired t-test comparing naïve and 'mock' exposed responses revealed a significant reduction in the GCaMP signals in the DM5 glomerulus (*t-test, p=0.008; t=-3.082; df=15, n=16*) suggesting that 'mock' treatment lowered odour-evoked Ca^{2+} influxes in the DM5 glomerulus. Importantly, the reductions observed after 3ppm and 20ppm odourant exposure were substantially larger than those after 'mock' exposure with percent decreases of -50% and -45% compared to -16%.

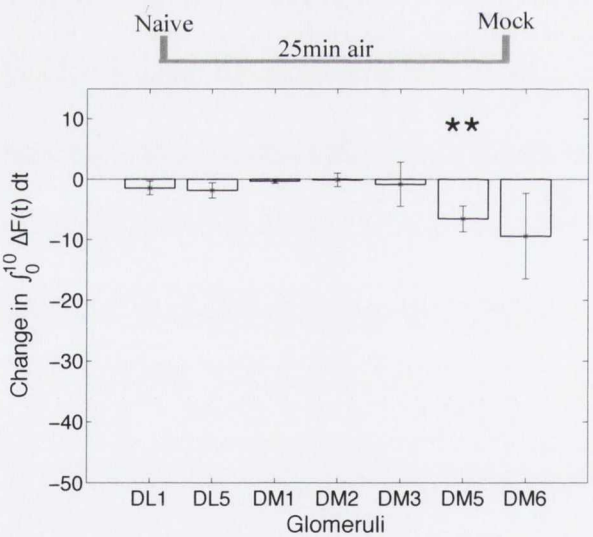


Figure 3.26: Quantified comparisons of odour-evoked Ca^{2+}-influxes in OSNs after 'mock' exposure

Two-photon Ca^{2+}-imaging was performed in Or83b-labelled during a naïve and a 'mock' air exposed 10-second odour presentation to 3ppm EB. Ca^{2+} dynamics were recorded from OSNs projecting to seven distinct glomeruli within the antennal lobe. Depicted are the changes in odour-evoked GCaMP6m fluorescence before and after a 15-minute 'mock' air exposure shown as the area under the curve of the paired differences between the 'mock' and naïve GCaMP6m responses over a 10 seconds period. A significant difference in the odour-evoked GCaMP6m responses was detected in the DM5 glomerulus (*t-test, p=0.008; t=-3.082; df=15, n=16*). Bars indicate mean ± SEM. n=6-16/glomerulus (see Table 5.63).

1-Hour Recovery

To test whether the changes in OSN activity recover within an hour following exposure, OSN activity was measured 1-hour after performing the standardized habituation protocol (see Figure 3.9). Odour-evoked GCaMP responses were, therefore, measured in response to a 3ppm EB stimulus before, 10 minutes after and an 1-hour delayed odour presentation.

A significant difference in the overall odour-evoked GCaMP6 responses in OSNs was observed between the three EB presentations delivered (*Likelihood ratio test,* $\chi(14)=56.393$, $p<0.001$), while the response from the 'naïve' to the 'exposed' odour presentations was lowered by -2.516 ± 6.577 arb. units and that from the 'exposed' to the '1-hour recovery' EB stimulus by -2.039 ± 6.577 arb. units. A likelihood ratio test restricted to a single OSN type revealed significant differences in odour-evoked GCaMP responses between the three odour presentations in the glomeruli DL1, DM1, DM2, DM5, and DM6 at an EB concentration of 3ppm (see Table 3.9 and Figure 3.27 A-C). Subsequently performed paired t-tests with common standard deviations for all groups of a given glomerulus only showed significant changes in GCaMP responses for the 'exposed - naïve' and 'recovery - naïve' comparisons in the DM5 and DM6 glomerulus (see Table 3.9). No significant differences were detected in PNs projecting to DL5 and DM3 (see Table 3.9). Thus, changes in odour-evoked GCaMP responses in OSNs induced by short-term exposure to 3ppm EB were not recovered after 1 hour.

Similar results were obtained when the experiment was performed with an EB concentration of 20ppm. Again, a significant difference in the overall odour-evoked GCaMP6m responses in OSNs was observed between the three EB presentations delivered (*Likelihood ratio test,* $\chi(14)=75.101$, $p<0.001$), while the response from the 'naïve' to the 'exposed' odour presentations was lowered by -10.294 ± 5.393 arb. units and that from the 'exposed' to the '1-hour delay' EB stimulus by -1.033 ± 5.393 arb. units. A likelihood ratio test restricted to a single OSN type revealed significant differences in odour-evoked GCaMP responses between the three odour presentations in the glomeruli DL1, DL5, DM3, DM5, and DM6 at an EB concentration of 20ppm (see Table 3.9 and Figure 3.27 A'-C'). Subsequently performed paired t-tests with common standard deviations for all groups of a glomerulus only showed significant changes in GCaMP responses for the 'exposed - naïve' and 'recovery - naïve' comparisons in the DL5, DM5, and DM6 glomerulus (see Table 3.9). No significant differences were detected in PNs projecting to DM1 and DM2 (see Table 3.9). Thus, also at a concentration of 20ppm no recovery of the changes in odour-evoked GCaMP responses in OSNs was detected after 1 hour.

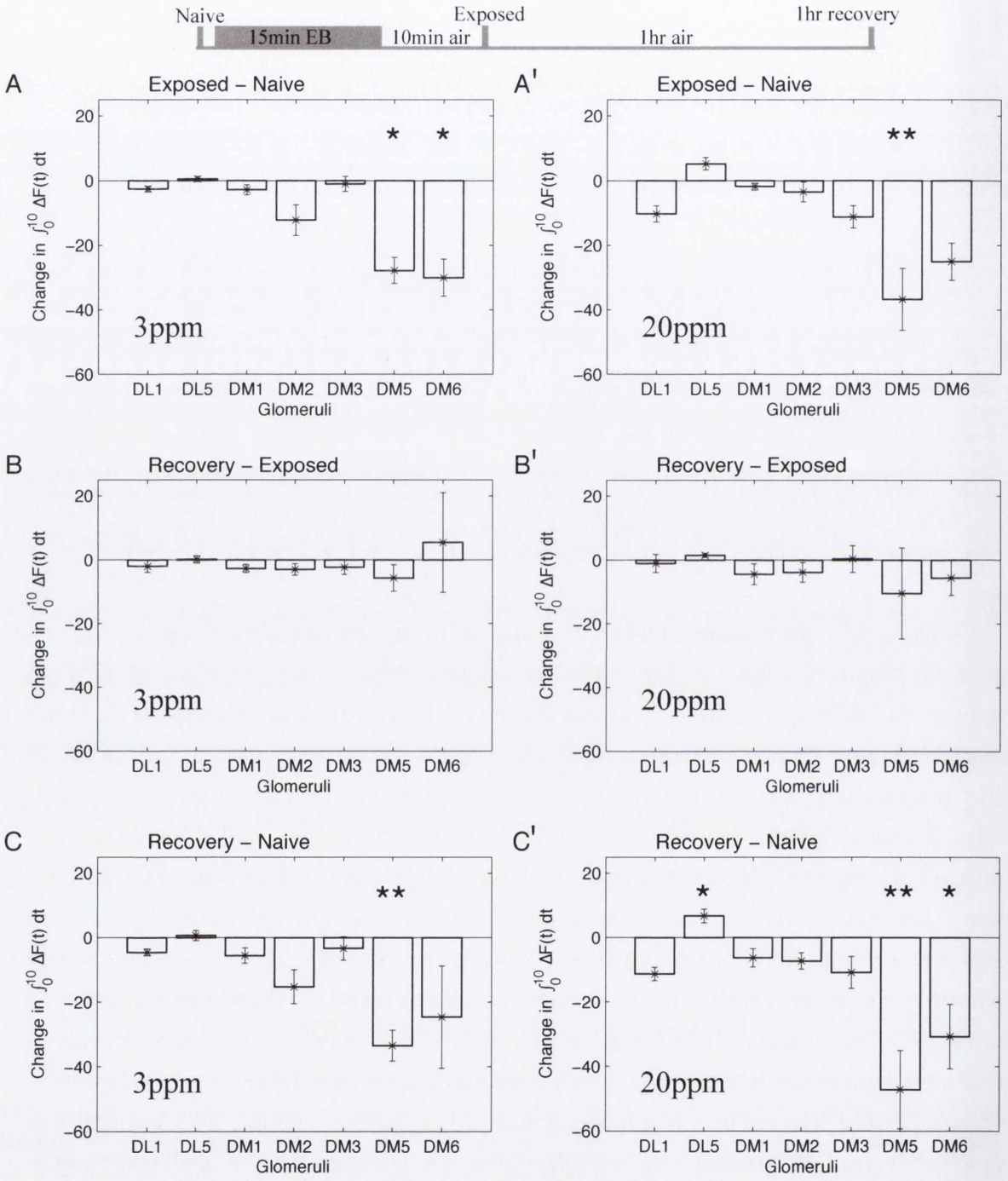


Figure 3.27: Quantified changes and recovery in odour-evoked Ca^{2+}-influxes in OSNs after 15-minute odourant exposure to 3ppm and 20ppm EB *Figure legend on following page.*

Figure 3.27: Quantified changes and recovery in odour-evoked Ca^{2+}-influxes in OSNs after 15-minute odourant exposure to 3ppm and 20ppm EB
Two-photon Ca^{2+}-imaging was performed in Or83b-labelled OSNs during a naïve, an exposed, and a 1-hour delayed 10-second odour presentation to 3ppm and 20ppm EB, shown as the area under the curve of the paired differences between the compared GCaMP6m responses over a 10 seconds period ($\int_0^{10} \Delta F \, dx$, ΔF reflects the paired differences over time). **(A/A')** Changes in odour-evoked GCaMP6m fluorescence induced by odourant exposure to 3ppm (A) and 20ppm (A'). A negative deviation indicates a decrease in the odour-evoked Ca^{2+}-influxes in PNs after odourant exposure. **(B/B')** Changes in odour-evoked GCaMP6m fluorescence occurring during a 1 hour 'recovery' period following odourant exposure to 3ppm (B) and 20ppm (B'). A positive deviation indicates recovery from the decrease in odour-evoked Ca^{2+}-influxes in OSNs after odourant exposure. **(C/C')** Comparison of odour-evoked GCaMP6m fluorescence responses to the naïve and the 1 hour recovery EB puff. A negative deviation indicates that the decrease in odour-evoked Ca^{2+}-influxes in OSNs after odourant exposure have not completely recovered after 1 hour. A significant difference in the overall odour-evoked GCaMP6 responses in OSNs was observed between the three EB presentations delivered at both concentrations (*Likelihood ratio test, $\chi(14)=56.393$, $p<0.001$, n=6/glomerulus (A-C) and $\chi(14)=75.101$, $p<0.001$, n=5-8/glomerulus (A'-C')*, see Table 3.9 for detailed statistics). $*$ $p<0.05$; $**$ $p<0.01$; $***$ $p<0.001$; bars indicate mean $\pm$ SEM.

		DL1	DL5	DM1	DM2	DM3	DM5	DM6
3ppm	likelihood ratio test $\chi(2)$	9.190 p=0.010 *	0.347 p=0.841 n.s.	8.173 p=0.017 *	10.827 p=0.005 **	1.661 p=0.436 n.s.	24.742 p<0.001 ***	6.958 p=0.031 *
	t-test							
	exposed - naïve	p=0.289		p=0.380	p=0.134		p=0.025	p=0.025
	recovery - exposed	p=0.387		p=0.410	p=0.703		p=0.619	p=0.659
	recovery - naïve	p=0.065		p=0.100	p=0.067		p=0.009	p=0.059
	numbers	6	6	6	6	6	6	6
20ppm	likelihood ratio test $\chi(2)$	16.576 p<0.001 ***	12.509 p=0.002 **	5.876 p=0.053 n.s.	5.816 p=0.055 n.s.	7.763 p=0.021 *	13.556 p=0.001 **	12.415 p=0.002 **
	t-test							
	exposed - naïve	p=0.140	p=0.118			p=0.280	p=0.009	p=0.066
	recovery - exposed	p=0.880	p=0.638			p=0.970	p=0.395	p=0.659
	recovery - naïve	p=0.110	p=0.048			p=0.290	p=0.002	p=0.029
	numbers	8	7	5	5	6	5	5

Table 3.9: Statistics: Recovery of OSN GCaMP responses to 3ppm and 20ppm EB

Changes in Baseline

As observed in PNs, OSNs similarly showed changes in GCaMP baseline levels after 15-minute odourant exposure. Figure 3.28 shows the quantification of these baseline shifts for both experiments presented in Figure 3.25 where testing and exposure was performed at an EB concentration of either 3ppm or 20ppm.

A significant difference in the baseline GCaMP fluorescence levels in OSNs was observed for the two recordings taken at 3ppm (*Likelihood ratio test,* $\chi(7)=43.701$, $p<0.001$). All seven glomeruli showed reductions in GCaMP baselines after odourant exposure (see Table 3.10 and Figure 3.28 A). The largest shifts in GCaMP baseline levels were observed in OSNs projecting to DM2, DM3, DM5, and DM6 (see Table 3.10 and Figure 3.28 A).

20ppm odourant exposure likewise had a significant effect on baseline GCaMP fluorescence levels in OSNs (*Likelihood ratio test,* $\chi(7)=85.015$, $p<0.001$). Again, all seven glomeruli showed reductions in GCaMP baselines after odourant exposure (see Table 3.10 and Figure 3.28 B). At 20ppm, changes in baseline GCaMP levels were most pronounced in OSNs projecting to the DM2 glomerulus, followed by those innervating DM3 (see Table 3.10 and Figure 3.28 B).

As for Ca^{2+} imaging in PNs, fluorescence baseline shifts in OSNs were not observed after 'mock' treatment. 'Mock' air exposure did not have an effect on baseline fluorescence levels (*Likelihood ratio test,* $\chi(7)=5.644$, $p=0.582$) suggesting that the downwards shifts in GCaMP fluorescence baselines were caused by short-term odourant exposure.

		DL1	DL5	DM1	DM2	DM3	DM5	DM6
3ppm	change (arb. units)	-1.995 ± 0.987	-5.384 ± 1.762	-5.454 ± 1.710	-13.014 ± 3.673	-14.944 ± 4.834	-15.647 ± 5.982	-12.918 ± 3.756
	statistics	wilcoxon p=0.021 sr=13 n=13 *	t-test p=0.009 t=-3.056 df=14 **	wilcoxon p<0.001 sr=0 n=13 ***	wilcoxon p<0.001 sr=0 n=13 ***	t-test p=0.009 t=-3.092 df=12 **	wilcoxon p<0.001 sr=0 n=13 ***	t-test p=0.005 t=-3.439 df=12 **
20ppm	change (arb. units)	-3.999 ± 0.726	-10.648 ± 3.172	-10.464 ± 3.199	-33.404 ± 6.306	-19.603 ± 3.706	-11.270 ± 4.467	-11.336 ± 2.947
	statistics	wilcoxon p<0.001 z=-3.724 n=18 ***	wilcoxon p<0.001 z=-3.479 n=17 ***	wilcoxon p=0.002 z=-3.154 n=16 **	t-test p<0.001 t=-5.297 df=16 ***	wilcoxon p<0.001 sr=0 n=14 ***	t-test p=0.022 t=-2.523 df=17 *	wilcoxon p<0.001 sr=0 n=11 ***

Table 3.10: Statistics comparing GCaMP fluorescence baselines in OSNs

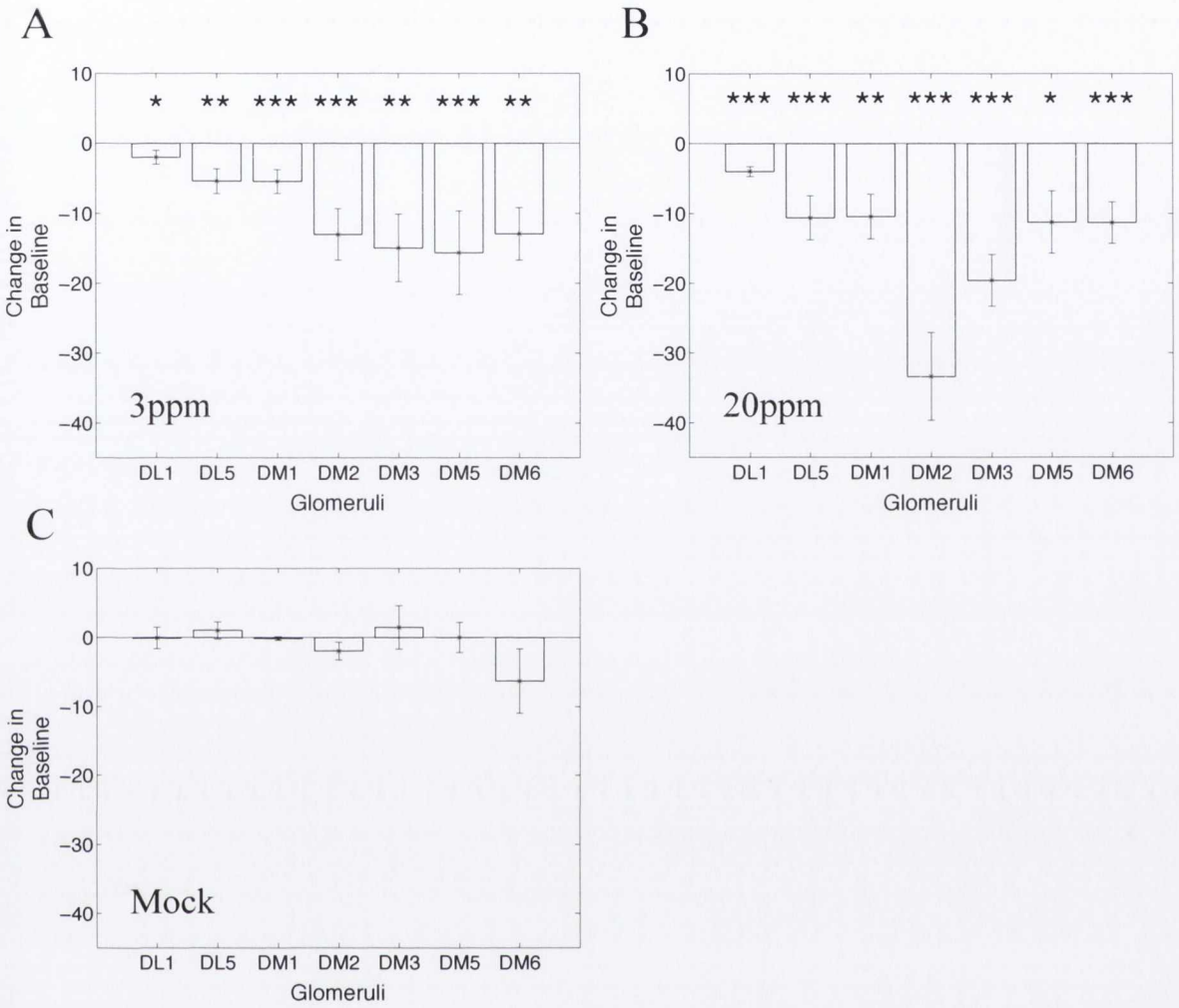


Figure 3.28: Quantified baseline fluorescence changes in OSNs after 15-minute odourant and mock exposure.

Two-photon Ca^{2+}-imaging was performed preceding a naïve and an exposed or 'mock-exposed' 10-second odour presentation to compare GCaMP baseline levels. Depicted are the changes in odour-evoked GCaMP6m baseline fluorescence shown as the paired differences of the GCaMP fluorescence baselines adjacent to the 'exposed'/'mock' and 'naïve' odour pulse (Change in Baseline) **(A)** 15-minute exposure to 3ppm EB had a significant effect on GCaMP baseline fluorescence in OSNs (*Likelihood ratio test, $\chi(7)=43.701$, $p<0.001$, n=13-15/glomerulus* (see Table 5.40)). Significant reductions in baselines were observed in all seven glomeruli (see Table 3.10). **(B)** 15-minute exposure to 20ppm EB had a significant effect on GCaMP baseline fluorescence in OSNs (*Likelihood ratio test, $\chi(7)=85.015$, $p<0.001$, n=11-18/glomerulus* (see Table 5.43)). Significant reductions in baselines were observed in all seven glomeruli (see Table 3.10). **(C)** 15-minute 'mock' exposure had no significant effect on GCaMP baseline fluorescence in OSNs (*Likelihood ratio test, $\chi(7)=5.644$, $p=0.582$, n=6-16/glomerulus* (see Table 5.63)). $*$ $p<0.05$; $**$ $p<0.01$; $***$ $p<0.001$; bars indicate mean $\pm$ SEM.

3.5.2 Local Interneurons

To study whether different types of LNs also show changes in odour-evoked Ca^{2+} influxes, GCaMP6m was expressed under the control of the Gal4 drivers LN1, LN2, and OK371. To facilitate the identification of the glomeruli, the experimental flies additionally carried an Or83b-RFP construct which expresses RFP under the control of the Or83b promotor. For each experiment the correct glomerular layer was determined based on the RFP expression pattern in OSNs and then GCaMP imaging was carried out from the respective LN type. While LN1 and LN2 neurons possess a glomerular structure, the neuronal processes of OK371 neurons were primarily found between glomeruli. This made the identification of the glomerular borders more difficult and also resulted in extremely low GCaMP responses. To study whether odour-evoked Ca^{2+} influxes changed after 15-minute odourant exposure, flies were tested and exposed to an EB concentration of 3ppm according to the standard imaging protocol (see Figure 3.9 and Tables 5.93 - 5.95 for PID measurements). Ca^{2+} dynamics were recorded from the second glomerular layer as the DM5 glomerulus exhibited the largest reduction in Ca^{2+} influxes in both OSNs and PNs (see Figure 3.25 and Figure 3.14).

Naïve EB-evoked GCaMP response traces of LN1 interneurons are shown in Figure 3.29 A (blue traces). LN arborisations in all three glomeruli showed an increase in GCaMP6 fluorescence in response to the EB stimulus. The DM2 glomerulus exhibited the largest increase with 8.346 $\pm$ 1.525 arb. units (n=13) followed by DM5 with 7.495 $\pm$ 1.134 arb. units (n=10) and DM1 with 4.205 $\pm$ 0.8783 arb. units (n=11). Odourant exposure had no significant effect on odour-evoked GCaMP responses in LN1s (*Likelihood ratio test,* $\chi(3)=4.529$, $p=0.210$, Figure 3.29). Although LN1 interneurons innervating the DM2 glomerulus appeared to decrease their odour-evoked GCaMP responses following odourant exposure, this effect was not significant even if tested separately (*t-test,* $p=0.063$, $t=-2.045$, $df=12$, $n=13$).

Naïve EB-evoked GCaMP response detected in LN2 interneurons were larger than those found in LN1s (compare naïve GCaMP traces (blue) in Figure 3.29 A for LN1s and Figure 3.30 A for LN2s). In LN2s, LN arborisations in DM5 showed the largest GCaMP response with 20.846 $\pm$ 3.330 arb. units (n=10) followed by those innervating DM2 13.233 $\pm$ 2.228 arb. units (n =13) and DM1 with 7.861 $\pm$ 1.529 arb. units (n=13). Similarly to LN1s, no significant difference in odour-evoked Ca^{2+} influxes was detected in LN2s after 15-minute EB exposure (*Likelihood ratio test,* $\chi(3)=0.888$, $p=828$, Figure 3.30).

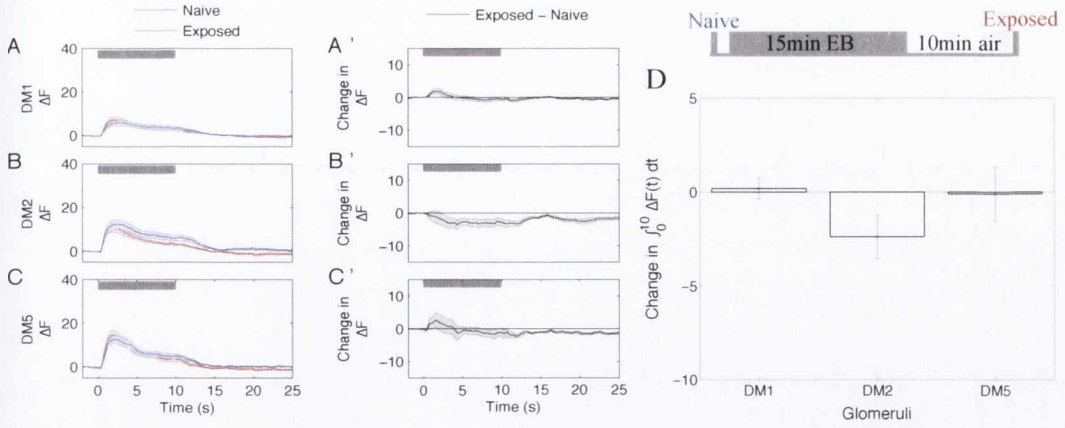


Figure 3.29: Changes in odour-evoked Ca^{2+}-influxes in GABAergic multiglomerular LN1 neurons after 15-minute odourant exposure.
Two-photon Ca^{2+}-imaging was performed in GABAergic LN1 local interneurons during a naïve and an exposed odour presentation to 3ppm EB. Ca^{2+} dynamics were recorded from the DM1, DM2, and DM5 glomerulus. **(A-C)** Mean of EB-evoked increases in GCaMP6m fluorescence to the naïve (blue) and exposed (red) EB presentation shown as changes in fluorescence (ΔF) over time. **(A'-C')** Paired differences of the odour-evoked GCaMP6m increases in A-C) shown as the difference of the changes in fluorescence (Change in ΔF) over time. **(D)** Quantified changes in odour-evoked GCaMP6m fluorescence shown as the area under the curve of the paired differences between the exposed and naïve GCaMP6m responses over a 10 seconds period. EB exposure had no significant effect on odour-evoked GCaMP6 responses in LN1s (*Likelihood ratio test, $\chi(3)=4.529$, $p=0.210$, $n=10$-13/glomerulus* (see Table 5.65)). Graphs and bars represent mean (dark line) ± SEM (shaded region). The grey bars indicate the time window of odour presentation.

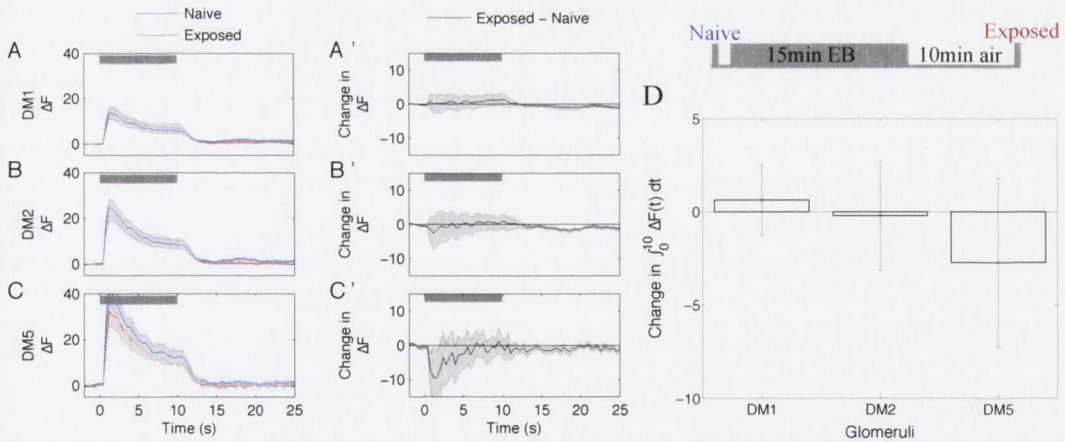


Figure 3.30: Changes in odour-evoked Ca^{2+}-influxes in GABAergic uni- and multiglomerular LN2 neurons after 15-minute odourant exposure.
Two-photon Ca^{2+}-imaging was performed in GABAergic LN2 interneurons during a naïve and an exposed 10-second odour presentation to 3ppm EB. Ca^{2+} dynamics were recorded from the DM1, DM2, and DM5 glomerulus. **(A-C)** Mean of EB-evoked increases in GCaMP6m fluorescence to the naïve (blue) and exposed (red) EB presentation shown as changes in fluorescence (ΔF) over time. **(A'-C')** Paired differences of the odour-evoked GCaMP6m increases in A-C) shown as the difference of the changes in fluorescence (Change in ΔF) over time. **(D)** Quantified changes in odour-evoked GCaMP6m fluorescence shown as the area under the curve of the paired differences between the exposed and naïve GCaMP6m responses over a 10 second period. EB exposure had no significant effect on odour-evoked GCaMP6 responses in LNs (*Likelihood ratio test, $\chi(3)=0.888$, $p=828$, $n=10$-13/glomerulus* (see Table 5.67)). Graphs and bars represent mean (dark line) ± SEM (shaded region). The grey bars indicate the time window of odour presentation.

Naïve EB-evoked GCaMP response in glutamatergic OK371 neurons were substantially smaller than those of GABAergic LNs (naïve GCaMP traces for OK371 are shown in Figure 3.31 A). For these neurons, the largest GCaMP signals were detected in DM5 with 2.204 ± 0.473 arb. units (n=12) followed by DM2 with 1.368 ± 0.1712 arb. units (n=14) and DM1 with 0.807 ± 0.155 arb. units (n=14). In contrast to GABAergic LNs, 15-minute exposure to 3ppm EB had a significant effect on odour-evoked GCaMP6 responses in glutamatergic OK371 LNs (*Likelihood ratio test, $\chi(3)=14.980$, p=0.002*). A reduction of -1.403 ± 0.554 arb. units in odour-evoked GCaMP6 responses was observed in the DM5 glomerulus (*DM5: t-test, p=0.028, t=-2.534, df=11, n=12*) while odour-evoked GCaMP6 fluorescence remained unchanged in the DM1 and DM2 glomerulus (*DM1: t-test, p=0.059, t=-2.066, df=13, n=14, n=13; DM2: t-test, p=0.138, t=-0.158, df=13, n=14*).

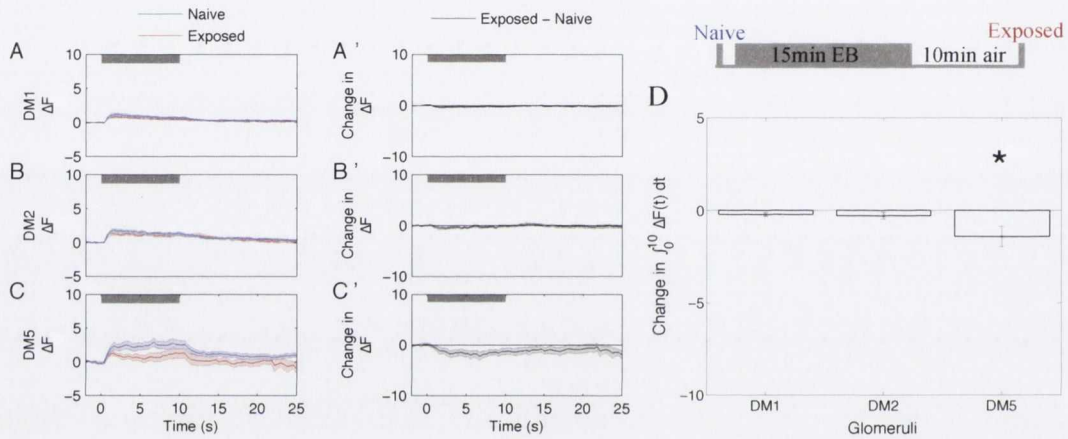


Figure 3.31: Changes in odour-evoked Ca^{2+}-influxes in glutamatergic OK371 neurons after 15-minute odourant exposure.
Two-photon Ca^{2+}-imaging was performed in glutamatergic OK371-labelled local interneurons during a naïve and an exposed 10-second odour presentation to 3ppm EB. Ca^{2+} dynamics were recorded from the DM1, DM2, and DM5. **(A-C)** Mean of EB-evoked increases in GCaMP6m fluorescence to the naïve (blue) and exposed (red) EB presentation shown as changes in fluorescence (ΔF) over time. **(A'-C')** Paired differences of the odour-evoked GCaMP6m increases in A-C) shown as the difference of the changes in fluorescence (Change in ΔF) over time. **(D)** Quantified changes in odour-evoked GCaMP6m fluorescence shown as the area under the curve of the paired differences between the exposed and naïve GCaMP6m responses over a 10 seconds period. EB exposure had a significant effect on odour-evoked GCaMP6 responses in OK371 LNs (*Likelihood ratio test, $\chi(3)=14.980$, p=0.002, n=12-14/glomerulus* (see Table 5.69)). A significant reduction was observed in the DM5 glomerulus (*DM5: t-test, p=0.028, t=-2.534, df=11, n=12*). * $p<0.05$; ** $p<0.01$; *** $p<0.001$; graphs and bars represent mean (dark line) ± SEM (shaded region). The grey bars indicate the time window of odour presentation.

3.5.3 Discussion

The experiments performed in this chapter aimed to investigate changes in odour-evoked neuronal activity in OSNs and LNs induced by continuous 15-minute odourant exposure. As shown in section 3.4, reductions in PN neuronal activity do not appear to result exclusively from $GABA_AR$-mediated inhibition. To study whether other predominant AL neurons show similar changes as PNs and to potentially identify the location where the changes arise, Ca^{2+}-imaging was performed in OSNs and three different populations of LNs.

Naïve EB-Evoked GCaMP Responses in OSNs

At both concentrations investigated, the 10-second EB stimulus elicited a rise in GCaMP levels in presynaptic terminals of all OSN types studied, with the exception of DL5 OSNs which showed a decrease at 20ppm EB. Both, 3ppm and 20ppm odour stimuli evoked largest GCaMP responses in the DM5 and DM6 glomerulus (see Figure 3.24). All other glomeruli apart from DM2 were only weakly activated at 3ppm and showed substantial higher responses at 20ppm (except for DL5). The naïve GCaMP6 responses in OSN terminals are mostly consistent with those reported for PNs in section 3.3 and previously published data (Hallem et al., 2004; Hallem and Carlson, 2006; de Bruyne et al., 2001; Bhandawat et al., 2007)

As for PNs, OSN odour-responsive profiles to a range of odours and concentrations have been widely studied using Ca^{2+} imaging (Wang et al., 2003; Barth et al., 2014; Silbering and Galizia, 2007; Silbering et al., 2008; Schubert et al., 2014). The amplitude of the OSN GCaMP signal was shown to be dependent on odourant concentration (Wang et al., 2003; Silbering et al., 2008). Consistently, in the present study 20ppm EB resulted in significantly higher overall GCaMP responses than 3ppm (see section 3.5.1). None of the Ca^{2+} imaging studies determined the GCaMP responses of the different OSN types to the odourant EB. A direct comparison to the data obtained in this study was therefore not possible. However, EB-evoked GCaMP responses reported here are mostly consistent with OSN spiking as reported by studies using single sensillum recordings (SSRs) (Hallem et al., 2004; Hallem and Carlson, 2006; de Bruyne et al., 2001; Bhandawat et al., 2007, see discussion 3.3.5).

Comparison of Naïve EB-Evoked GCaMP Responses in OSNs and PNs

The naïve EB-evoked GCaMP responses obtained in this study were substantial larger in OSNs than PNs (see Figure 3.13 and 3.24). PN spiking, however, was reported to be on average stronger than that of OSNs (Bhandawat et al., 2007). This discrepancy might be due to different levels of Ca^{2+} influxes in neuronal terminals compared to dendrites or to different levels of GCaMP expression in the two different cell types. In axon terminals, Ca^{2+} influx through voltage-gated Ca^{2+} channels initiates the release of neurotransmitters into the synaptic cleft (Catterall and Few, 2008; Berridge et al., 2000). In dendrites, Ca^{2+} enters through voltage-sensitive and ligand-activated channels as well as through Ca^{2+} release from

intracellular stores and is essential for activity-dependent synaptic plasticity (Sabatini et al., 2001; Zucker, 1999). Besides the different intracellular Ca^{2+} levels which may account for the observed differences, different Gal4 drivers have also been shown to express varying levels of protein (Pfeiffer et al., 2010). Thus, these discrepancies may also result from unequal GCaMP protein expression levels in these neurons making a direct comparison of absolute GCaMP values between different lines difficult.

When GCaMP6 responses of the AL glomeruli were compared independently of their absolute values, commonalities and discrepancies between OSNs and PNs became apparent (see Figure 3.24 for OSNs and Figure 3.13 for PNs). The glomeruli DM5 and DM6 showed the largest naïve EB-evoked GCaMP responses for both OSNs and PNs. However, EB also elicited strong GCaMP responses in PNs projecting to DL1 while OSNs targeting this glomerulus were comparatively weakly activated. Other Ca^{2+} imaging studies, which compared the odour-response profiles of OSNs and PNs directly, found similar but not identical glomerular activation patterns in the two neuronal populations for a given odourant (Wang et al., 2003; Silbering et al., 2008; Root et al., 2007). Potential reasons for the discrepancies are the properties of the OSN/PN synapse and the dense network of local interneurons in the AL which both tune PN responses (Bhandawat et al., 2010; Chou et al., 2010; Carlsson et al., 2010).

The OSN/PN synapse affects the shape of odour-evoked PN responses as well as the total glomerular activation pattern of PNs (Bhandawat et al., 2010; Wilson, 2013). The synapse exhibits a high vesicular release probability and strong short-term depression (Kazama and Wilson, 2008; Wilson, 2011, 2013). These properties make PN responses peak earlier and decay quicker than those of OSNs, thus resulting in more transient PN responses (compare Figure 3.23 A-G and Figure 3.11 A-G). The OSN/PN synapse furthermore transforms the OSN input by a nonlinear function resulting in a broadened PN activation pattern (Bhandawat et al., 2007; Olsen et al., 2010; Wilson, 2013): The nonlinear transformation amplifies small changes in OSN input when presynaptic OSNs fire at a low rate. Small changes in presynaptic input are not amplified, however, when OSNs fire strongly. Thus, while OSN responses tend to cluster in the weak end of the dynamic range of a given OSN, PN responses are distributed more uniformly within their dynamic range. As a result PNs are less selective and show a broader activation pattern than their presynaptic OSNs. Bhandawat et al. (2007) compared neuronal spiking of OSNs and PNs using SSRs and whole-cell recordings. Among other odours, they investigated odour-evoked responses to EB in OSNs and PNs projecting to seven glomeruli. OSNs targeting DM1, DM2, VM2, and VA2 showed strong responses to EB while the other OSN types, namely those projecting to DL1, DM3, and DM4, were only weakly activated. In comparison, PNs exhibited comparatively strong spiking in all these glomeruli (Bhandawat et al., 2007). This result not only demonstrates the broader range of PN activation when compared to OSNs it is also consistent with the observations made in the present study where PNs projecting to DL1 show a stronger EB-evoked GCaMP response than their presynaptic OSNs.

Another factor that most likely contributes to the observed differences in OSN and PN activation is the dense network of LNs which shapes odour responses in the AL. Various neurotransmitters and neuromodulators have been detected including GABA (Chou et al., 2010; Das et al., 2011a), glutamate (Liu and Wilson, 2013), acetylcholine (Huang et al., 2010; Seki et al., 2010; Shang et al., 2007; Olsen et al., 2007), dopamine (Chou et al., 2010) and a range of neuropeptides (Carlsson et al., 2010; Ignell et al., 2009; Nässel and Homberg, 2006). However, only little is known about how transmitter release from these neurons modulates odour responses and under which circumstances they are released. The best known are inhibitory GABAergic LNs which constitute one of the largest classes of LNs (Chou et al., 2010; Das et al., 2011a). GABA release from these neurons has been implicated in providing gain control within the lobe (Olsen and Wilson, 2008b; Root et al., 2008). It has further been suggested that they decorrelate the odour representation within the AL to enable fine discrimination of similar odours (Sachse and Galizia, 2002; Wilson and Laurent, 2005; Barth et al., 2014). Comparatively little is known about the other types of LNs: Glutamatergic LNs seem to inhibit OSNs, PNs, and other LNs (Liu and Wilson, 2013). Acetylcholinergic LNs form gap junctions with PNs and possibly LNs rather than chemical synapses and provide both, depolarisations and hyperpolarisations (Huang et al., 2010; Yaksi and Wilson, 2010). Neuropeptides expressed in LNs include tachikinin related peptide, myoinhibitory peptide, and allatostatin A (Carlsson et al., 2010). However, how these neuropeptides shape neuronal activity in OSNs or PNs is unknown. Extrinsic neuromodulatory neurons which innervate the lobe (Carlsson et al., 2010; Dacks et al., 2009; Roy et al., 2007; Tanaka et al., 2012; Busch et al., 2009; Nässel, 2002) possibly also shape odour-evoked AL responses.

Comparison of Exposure-Induced Changes in EB-Evoked GCaMP Responses in OSNs and PNs

15-minute exposure to EB significantly reduced EB-evoked GCaMP responses in the specific OSN types. While odour-evoked Ca^{2+} influx in OSNs projecting to DM1, DM2, and DM5 were significantly reduced after odourant exposure to 3ppm, all OSN types, apart from those targeting DL5, showed a decreased GCaMP response after exposure to 20ppm EB (see Figure 3.25). Odour-evoked GCaMP responses of OSNs targeting DL5 were significantly increased after 20ppm EB exposure. A summary of the percent changes with respect to the naïve odour-evoked GCaMP responses is shown in table 3.11. 15-minute 'mock' exposure to air only caused small reductions in odour-evoked Ca^{2+}-influxes in OSNs projecting to DM5 (see Figure 3.26). No significant recovery from the reductions in OSN neuronal activity induced by 3ppm or 20ppm EB exposure was observed after 1 hour (Figure 3.27). All OSN types showed reductions in GCaMP fluorescence baseline levels after 3ppm and 20ppm odourant exposure, no baseline shifts were found after 'mock' treatment (Figure 3.28).

The measured reductions in odour-evoked GCaMP responses in OSN terminals are similar to those found in PN dendrites (compare Figure 3.25 for OSNs and Figure 3.14 for PNs, see Table 3.11 for summary). As their cognate OSNs, PNs projecting to the glomeruli DL1,

		DL1	DL5	DM1	DM2	DM3	DM5	DM6
Or83b	**3ppm**	-19% (n.s.)	-174% (n.s.)	-38%	-42%	-42% (n.s.)	-50%	-35% (n.s.)
	20ppm	-36%	+81%	-30%	-31%	-28%	-45%	-34%
GH146	**3ppm**	-34%	+109%	-12% (n.s.)	+9% (n.s.)	-25% (n.s.)	-48%	-29%
	20ppm	-39%	+14% (n.s.)	-42%	+18% (n.s.)	-18% (n.s.)	-66%	-34%

Table 3.11: Summary of exposure-induced changes in glomerular GCaMP responses measured in OSNs or PNs
Percent response change of a given OSN or PN type at the two different concentrations with respect to its naïve EB-evoked GCaMP response as a measure of how much short-term odourant exposure altered naïve odour-evoked GCaMP6 responses. (n.s.) indicates a non-significant change.

DM1, DM3, DM5, and DM6 show similar decrements in their GCaMP responses even if the magnitude of the changes differs and not all changes are statistically significant. The differences in magnitude could arise from modifications of the odour responses through the OSN/PN synapse and the local network of LNs within the lobe, as discussed above. OSNs targeting the DM2 glomerulus show decrements in their odour-evoked GCaMP responses after 15-minute odourant exposure while the PN responses related to this glomerulus tend to increase even if the PN changes are not statistically significant. This observation may suggest that the DM2 glomerulus is innervated by a set of excitatory LNs which enhance PN responses in a way that the changes in OSN neuronal activity are somehow overridden. The DL5 glomerulus which is either not activated or inhibited by a naïve odour stimulus shows an exposure-induced increase in odour-evoked GCaMP responses in OSNs at 20ppm and PNs at 3ppm and 20ppm (although the change of PNs at 20ppm is not statistical significant). The neuronal activity of DL5 OSNs at 3ppm, in contrast, was decreased. This discrepancy can possibly be explained by the very small naïve responses in DL5 and thus may not be meaningful. Another possibility is that odour responses in the DL5 glomerulus are similarly modified by lateral excitation as assumed for the ones in DM2, possibly even in a concentration-dependent manner.

Interestingly, not only the odourant exposure-induced changes in OSNs and PNs were similar they also showed similar characteristics: 'Mock' air exposure did not cause any substantial changes in OSNs or PNs (only small reductions were observed in the DM5 glomerulus), the changes in both, OSNs and PNs, had not returned to their naïve response levels an hour after the odour exposure protocol was performed, and the observed changes were ac-

companied by reductions in GCaMP fluorescence baseline in OSNs and PNs which were not present after 'mock' exposure. All in all, these results suggest that the reductions in neuronal activity occur presynaptically in OSN terminals and are at least partially responsible for the observed parallel changes in odour-evoked responses within PN dendrites.

Potential Causes for Exposure-Induced Changes in EB-evoked GCaMP Responses in OSNs

The similarity of the reported changes in odour-evoked GCaMP responses in OSN terminals and PN dendrites suggests that the changes induced by 15-minute odourant exposure largely arise at the OSN presynapse rather than the PN postsynapse. The presynaptic changes can in principle originate from one or a combination of the following: a) adaptation in odourant transduction, b) adaptation in the axon terminals and c) presynaptic inhibition.

Odourant transduction refers to the process of odour molecule binding to an odour receptor which initiates a second-messenger cascade resulting in neuronal depolarisation of the respective OSN dendrite. Adaptation in the odourant transduction machinery has been reported after a seconds-lasting odour stimulus and is characterized by a slow decay following an initial peak of the OSN spiking response to the adapting stimulus (Nagel and Wilson, 2011). Further characteristics include a delayed response onset and a reduced overall response to subsequent odour stimuli which recover within minutes (Nagel and Wilson, 2011; Störtkuhl et al., 1999). As mutations in either the inositol 1,4,5-trisphosphate receptor (IP_3R) or the transient receptor potential (TRP) channel affect adaptation in *Drosophila* OSNs (Deshpande et al., 2000; Störtkuhl et al., 1999) cytoplasmatic Ca^{2+} is thought to play a role. The second messenger inositol 1,4,5-trisphosphate (IP_3) mediates Ca^{2+} release from intracellular stores through binding to the Ca^{2+} channel IP_3R (Patterson et al., 2004). The trp gene encodes a light activated Ca^{2+} channel (Hardie and Minke, 1992; Peretz et al., 1994). Mutants defective in IP_3R or Trp both show faster recovery from olfactory adaptation (Deshpande et al., 2000; Störtkuhl et al., 1999).

Adaptation in the OSN axon terminals measured by Ca^{2+} imaging using a bioluminescent probe is induced by repeated five seconds-lasting odour stimuli and only recovers after tens of minutes (Murmu et al., 2011). Similar to adaptation in the odourant transduction machinery, this long-lasting form depends on the release of Ca^{2+} from intracellular Ca^{2+} stores (Murmu et al., 2011). Both, genetical and pharmacological approaches show the requirement for the IP_3R and ryanodine receptor (RyRs) for olfactory adaptation induced by repeated odour stimulation (Murmu et al., 2011). RyR is another Ca^{2+} release channel prevalent in intracellular Ca^{2+} stores (Fill and Copello, 2002). Consistently, olfactory adaptation tested behaviourally following a 5 minute odourant exposure is likewise impaired in flies lacking IP_3R or RyR specifically in OSNs (Murmu et al., 2010). Adaptation in the OSN axon terminals is not entirely due to intrinsic mechanisms of the OSN terminals (Murmu et al., 2011). $GABA_AR$ and $GABA_BR$ antagonists impair adaptation as does RNAi targeting to $GABA_BRs$ in OSNs indicating the requirement of presynaptic GABAergic inhibition

(Murmu et al., 2011). In line with this, RNAi mediated $GABA_BR$ knockdown in OSNs impairs behavioural adaptation after 5 minute pre-exposure (Murmu et al., 2011).

The presence of presynaptic inhibition onto OSNs is well known and has been attributed to gain control within the AL (Root et al., 2008; Olsen and Wilson, 2008b). Removing lateral input broadens PN output suggesting that lateral inhibitory input normally suppresses PN responses (Olsen and Wilson, 2008b). As robust lateral inhibition requires active neurotransmitter release from OSN terminals it is assumed to predominantly act presynaptically (Olsen and Wilson, 2008a). It scales with OSN output and involves both, $GABA_AR$ and $GABA_BR$, whereas $GABA_ARs$ mediate the early and $GABA_BRs$ the late phase of inhibition (Hong and Wilson, 2015; Olsen and Wilson, 2008a; Root et al., 2008; Silbering et al., 2008). Since lateral inhibition scales with OSN input and narrows PN output it is thought to mediate presynaptic gain control (Olsen et al., 2010). When only a small subset of OSN types are activated lateral inhibition is weak and the odour response is transmitted to the postsynaptic PN without being lowered. However, when an odour recruits a large number of different OSN types lateral inhibition strongly inhibits OSN transmitter release, thus preventing the postsynaptic PN from saturation and allowing PNs to encode changes in concentration over a broader range of concentrations (Olsen and Wilson, 2008b; Olsen et al., 2010).

Notably, the level of lateral inhibition is largely odour invariant and each glomerulus has a characteristic level of sensitivity to lateral inhibition (Hong and Wilson, 2015; Olsen et al., 2010). Some glomeruli are close to completely insensitive to inhibition, others are nearly completely silenced by inhibition (Hong and Wilson, 2015). GABA sensitivity appears to be intrinsic to a given glomerulus and independent of the LN network (Hong and Wilson, 2015). In line with that, each glomerulus has a unique level of $GABA_BR$ expression (Root et al., 2008). CO_2-sensing OSNs do not express $GABA_BR$ while pheromone-sensing express a high level (Root et al., 2008). The variations of $GABA_BR$ expression in the different glomeruli may thus account for the glomerular-specific sensitivity of lateral inhibition (Root et al., 2008).

Adaptation in the odourant transduction machinery is unlikely to contribute substantially to the changes in odour-evoked OSN responses presented in this study as these adaptations recover almost entirely within minutes after the adapting stimulus is removed (Deshpande et al., 2000; Störtkuhl et al., 1999; Nagel and Wilson, 2011). In the experiments performed here a 10-minute air interval is given after the 15-minute odourant exposure. Changes resulting from adaptation in the transduction machinery are likely to have recovered within this time frame. Adaptation in the axon terminals, however, lasts for tens of minutes (Murmu et al., 2011) and may therefore contribute to the changes in neuronal activity observed here. The reductions in neuronal activity could thus be caused by alterations in Ca^{2+} release from intracellular stores and/or could be mediated by opening of GABA receptors within the OSN membrane. As the protocol performed in this study is different from that in Murmu et al. (2011), who delivered 5 second odour stimuli every 5 minutes, it may induce longer-lasting changes which could explain why no recover was observed after an hour.

Exposure-Induced Changes in LN Responses

In the three different LN types, EB stimulation elicited a rise in GCaMP signals in all three glomeruli studied (see Figure 3.29 A for LN1s, Figure 3.30 A for LN2s and 3.31 A for OK371). However, naïve GCaMP responses varied between LN types and between glomeruli. The magnitude of the GCaMP response was substantially larger in GABAergic LN1s and LN2s than in glutamatergic OK371 LNs. In LN2 and OK371 neurons, odour-evoked Ca^{2+} influxes were largest in the DM5 glomerulus followed by DM2 and DM1. DM2 showed the most pronounced naïve EB response in LN1 neurons. While the GABAergic LN1 and LN2 interneurons did not show a change in odour-evoked GCaMP responses after 15-minute odourant exposure (see see Figure 3.29 B for LN1s and Figure 3.30 B for LN2s) a reduction in odour-evoked Ca^{2+} influxes in OK371 neurons in the DM5 glomerulus was detected (see 3.31 B for OK371).

Odour-evoked Ca^{2+} influxes in LNs have been characterized in detail recently (Hong and Wilson, 2015). GCaMP responses in LNs were reported to be odour-invariant. Private odours - odours that only activate a single OSN type - evoked LN activity in all glomeruli and different glomeruli showed different magnitudes of GCaMP responses which were stereotyped between brains (Hong and Wilson, 2015). In line with this observation, different levels of GCaMP activation in different glomeruli have also been observed in the present study (see Figure 3.29 A for LN1s, Figure 3.30 A for LN2s and Figure 3.31 A for OK371).

LN1 and LN2 neurons have been widely studied in terms of their differences in neuronal activation, morphology, and function (Acebes et al., 2011; Barth et al., 2014; Das et al., 2011b; Larkin et al., 2010; Sachse et al., 2007; Seki et al., 2010; Silbering et al., 2008; Tanaka et al., 2009). Patch-clamp recording revealed burst firing in LN1 neurons whereas a subpopulation of LN2 neurons showed tonic firing (Seki et al., 2010). At a functional level, LN1 neurons have been implemented in olfactory habituation (Das et al., 2011b; Larkin et al., 2010) and discrimination between similar odours (Barth et al., 2014). LN2 neurons, on the other hand, show increased GCaMP responses to CO_2 after four day CO_2 exposure (Sachse et al., 2007) and are believed to contribute to odour-elicited oscillations (Tanaka et al., 2009).

At least two of these studies imply increased transmitter release from LNs after prolonged odourant exposure (Das et al., 2011b; Sachse et al., 2007) suggesting that synaptic plasticity occurs at the LN presynapse. However, in the present study no changes in odour-evoked GCaMP responses were detected after 15-minute odourant exposure. Notably, the fact that Ca^{2+} influx in GABAergic LNs were unchanged does not necessarily mean that synaptic plasticity did not occur in these neurons. In the case of LNs, the most relevant aspect of cellular function is the magnitude of synaptic release as transmitter binding to receptors on the postsynaptic membrane of OSNs and PNs modulates the odour response. While Ca^{2+} influx is correlated with transmitter release (Catterall and Few, 2008; Berridge et al., 2000) the changes in LN Ca^{2+} influxes may have only been small or the changes that affect vesicle release may have occurred downstream of Ca^{2+} release and might thus not be picked up by Ca^{2+} imaging. A fluorescence sensor for vesicle release such as synaptoPhluorin therefore

might be a better choice for detecting small changes in synaptic release of neurotransmitters from these neurons (Miesenböck et al., 1998a; Ng et al., 2002).

Only little is known of glutamatergic LNs, as this population has only been recently described (Das et al., 2011a; Daniels et al., 2008). Glutamatergic LNs are broadly tuned to odours and project their neuronal processes primarily into the spaces between glomeruli suggesting that glutamatergic inhibition may act on a slower time scale compared to GABAergic inhibition as glutamate has to diffuse to the postsynaptic membrane (Liu and Wilson, 2013). Synaptic plasticity has not yet been demonstrated in glutamatergic neurons, however, the results obtained in this study suggest that neuronal activity and/or transmitter release from glutamatergic LNs is reduced after 15-minute odourant exposure. This observation is surprising since a decrease in inhibition should cause larger odour-evoked GCaMP signals. This may indicate that glutamatergic LNs synapse onto other inhibitory LNs and remove inhibition onto them following odourant exposure, thus boosting inhibitory GABAergic input onto OSNs and PNs. In line with this, glutamatergic LNs have been shown to form synaptic connections with other LNs (Liu and Wilson, 2013).

3.6 Measuring Membrane Voltage and Synaptic Vesicle Release

While Ca^{2+} fluorescence sensors are a good indicator of neuronal activity and have substantially contributed to the understanding of neuronal signal processing (Grienberger and Konnerth, 2012), Ca^{2+} imaging is not without its shortcomings (Peterka et al., 2011). Changes in Ca^{2+} concentrations can be significantly slower than changes in membrane voltage, the imaging only captures suprathreshold signals, and Ca^{2+} dynamics are confounded by intracellular Ca^{2+} buffers as well as the diffusion from its source (Peterka et al., 2011). As complimentary approaches, fluorescence indicators that target other aspects of the neuronal machinery such as voltage and presynaptic release have been developed (Barth, 2007; Looger and Griesbeck, 2012; Miyawaki, 2003). The genetically encoded fluorescence indicators ArcLight (Cao et al., 2013), designed to measure voltage, and synaptopHluorin (Miesenböck et al., 1998b), which is an indicator for transmitter release, have both been successfully implemented in flies (Cao et al., 2013; Ng et al., 2002). To ensure that the conclusions made using Ca^{2+} imaging were not confounded by Ca^{2+} kinetics, ArcLight imaging was performed in OSNs and PNs to investigate whether odourant exposure causes reductions in neuronal depolarisation in these cells as predicted. ArcLight and SynaptopHluorin imaging was further conducted in LNs to confirm the absence of changes in neuronal activity in these cells and to address the question of whether transmitter release from LNs is altered following odourant exposure.

The development of voltage indicators capable of reporting electrical activity including subthreshold excitatory and inhibitory events has turned out to be difficult (Peterka et al., 2011). Genetically encoded voltage indicators (GEVIs) long suffered from modest brightness, slow temporal kinetics, and limited signal-to-noise ratio (Peterka et al., 2011). The recently developed GEVI ArcLight, however, shows signals of sufficient amplitude and signal-to-noise ratio to detect single electrical events *in vivo* (Cao et al., 2013). ArcLight is composed of the voltage-sensing domain of the ascidian *Ciona intestinalis* voltage-sensitive phosphatase and super ecliptic pHluorin, a mutant form of the green fluorescent protein from the jellyfish *Aequorea victoria* that has a basic-shifted pH-fluorescence intensity profile (Jin et al., 2012). The ecliptic pHluorin carries a point mutation A227D that results in a large increase in sensitivity, yielding a probe with a several-fold increased signal compared to other GEVIs (Jin et al., 2012).

SynaptopHluorin (synaptobrevin-pHluorin) is a fluorescence probe which is used to monitor exocytosis and endocytosis of synaptic vesicles (Miesenböck et al., 1998b). The pH sensor consists of the synaptic vesicle protein synaptobrevin with a pH-sensitive derivative of GFP at its C terminus (Miesenböck et al., 1998b). It functions by taking advantage of the change in pH that synaptic vesicles undergo upon vesicle fusion with the plasma membrane (Miesenböck et al., 1998b). Normally the lumen of synaptic vesicles has an acidic pH of around 5.5 at which synaptopHluorin fluorescence is low (Kavalali and Jorgensen,

2014). When vesicles fuse with the plasma membrane the pH-sensitive GFP is exposed to the higher extracellular pH resulting in an increased synaptopHluorin fluorescence (Kavalali and Jorgensen, 2014).

The aim of the research performed in this chapter was (a) to check whether voltage changes could be detected in OSNs and PNs following 15-minute odourant exposure and (b) to test whether neuronal activity in LNs and transmitter release from LNs was increased after odourant exposure.

3.6.1 Measuring Membrane Voltage Using ArcLight

Projection Neurons

To investigate whether not only Ca^{2+} influxes but also odour-evoked spiking is reduced after 15-minute odourant exposure to 3ppm EB ArcLight voltage imaging was performed (see Table 5.96 for PID measurements). Although it is possible to detect single action potentials with this sensor (Cao et al., 2013), in the present study it was used as a measure of the degree of depolarisation or hyperpolarisation. Thus, to detect voltage changes in PNs, ArcLight was expressed under the control of the GH146 driver. Voltage changes were recorded from PNs that target the glomeruli DM1, DM2, and DM5. Notably, ArcLight fluorescence emission decreases upon cellular depolarisation (Cao et al., 2013). To facilitate the reading of the figures the graphs presented in this section therefore show $-\Delta F$.

Mean ArcLight traces in response to the 'naïve' and 'exposed' EB stimulus are shown in Figure 3.32 A-C, the paired differences of the naïve and exposed odour presentation are depicted in Figure 3.32 A'-C'. A negative deviation indicates a decrease in odour-evoked depolarisation in the specific PN type. As for GCaMP imaging, naïve odour-evoked ArcLight responses differed between glomeruli. PNs projecting to the DM5 glomerulus showed the largest naïve response with 25.149 $\pm$ 2.365 arb. units (n=26) followed by those targeting DM2 with 11.814 $\pm$ 1.078 arb. units (n=30) and DM1 with 3.331 $\pm$ 0.357 (n=29) (see Figure 3.33 A). 15-minute exposure to 3ppm EB had a significant effect on odour-evoked ArcLight responses in PNs (*Likelihood ratio test,* $\chi(3)=54.837$, $p<0.001$), lowering the response by -0.981 $\pm$ 1.485 arb. units (value determined by a linear mixed-effects model fit by maximum likelihood). Reduction in odour-evoked ArcLight responses were observed in the DM5 and DM1 glomerulus (*DM5: t-test,* $p<0.001$, $t=-6.036$, $df=25$, $n=26$; *DM1: t-test,* $p=<0.001$, $t=-4.143$, $df=28$, $n=29$). Odour-evoked Arclight responses remained unchanged in the DM2 glomerulus (*DM2: t-test,* $p=0.294$, $t=-1.070$, $df=29$, $n=14$, Figure 3.33 B). The percent change with respect to the naïve EB-evoked ArcLight response showed that the largest reduction was detected in PNs projecting to DM5 with -49%, followed by those targeting DM1 with -29% and DM2 with -11%, however the change in DM2 was not statistical significant. No significant difference was found in the overall ArcLight baseline levels recorded preceding the naïve and exposed ArcLight response (*Likelihood ratio test,* $\chi(3)=6.257$, $p=0.100$).

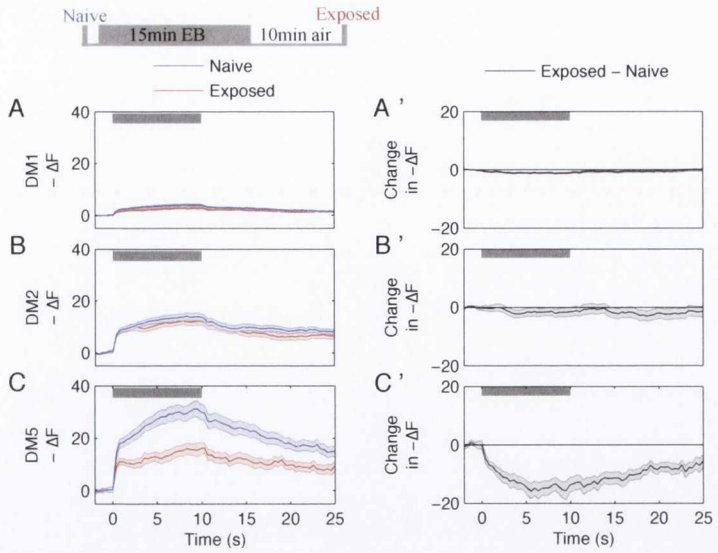


Figure 3.32: Changes in odour-evoked depolarisation in PNs after 15-minute odourant exposure.
Two-photon voltage imaging was performed in GH146-labelled PNs during a naïve and an exposed 10-second odour presentation to 3ppm EB. Voltage dynamics were recorded from PNs innervating the glomeruli DM1, DM2, and DM5. **(A-C)** Mean EB-evoked ArcLight responses to the naïve (blue) and exposed (red) EB presentation shown as changes in fluorescence (-ΔF) over time. **(A'-C')** Paired differences of the odour-evoked ArcLight responses in A-C) shown as the difference of the changes in fluorescence (Change in ΔF) over time. A negative deviation indicates a decrease in odour-evoked depolarisation in PNs after odourant exposure. Graphs represent mean (dark line) ± SEM (shaded region) of ΔF. n=26-30/glomerulus (see Table 5.72). The grey bars indicate the time window of odour presentation.

To check whether the observed changes in ArcLight responses were induced by 15-minute odourant exposure, a 'mock' treatment was performed where flies that expressed the ArcLight sensor in PNs were exposed to air instead of EB (see Table 5.97 for PID measurements of the EB stimuli). Surprisingly, 'mock' treatment had a significant effect on odour-evoked ArcLight responses in PNs (*Likelihood ratio test,* $\chi(3)=12.613$, *p=0.006*), lowering the response by -1.224 ± 1.650 arb. units. A reduction in odour-evoked ArcLight responses was observed in the DM2 and DM1 glomerulus (*DM2: t-test, p=0.009, t=-2.810, df=26, n=27; DM1: t-test, p<0.001, t=-5.254, df=25, n=26*). Odour-evoked Arclight responses remained unchanged in the DM5 glomerulus (*DM5: t-test, p=0.056, t=-2.011, df=23, n=24*, Figure 3.34). Since the ArcLight sensor reduces its fluorescence upon neuronal depolarisation the decrease in ArcLight responses could potentially result from lower baseline ArcLight levels due to fluorophore bleaching. To study whether bleaching of the fluorophore contributes to the decreases in ArcLight responses fluorescence omitted by the sensor was imaged continuously for three minutes and ArcLight baseline fluorescence at the beginning of the recording was compared with that at the end of the recording. No change in ArcLight baseline fluorescence was detected (data not shown). The observed decrease after 'mock' treatment is thus unlikely to result from fluorophore bleaching.

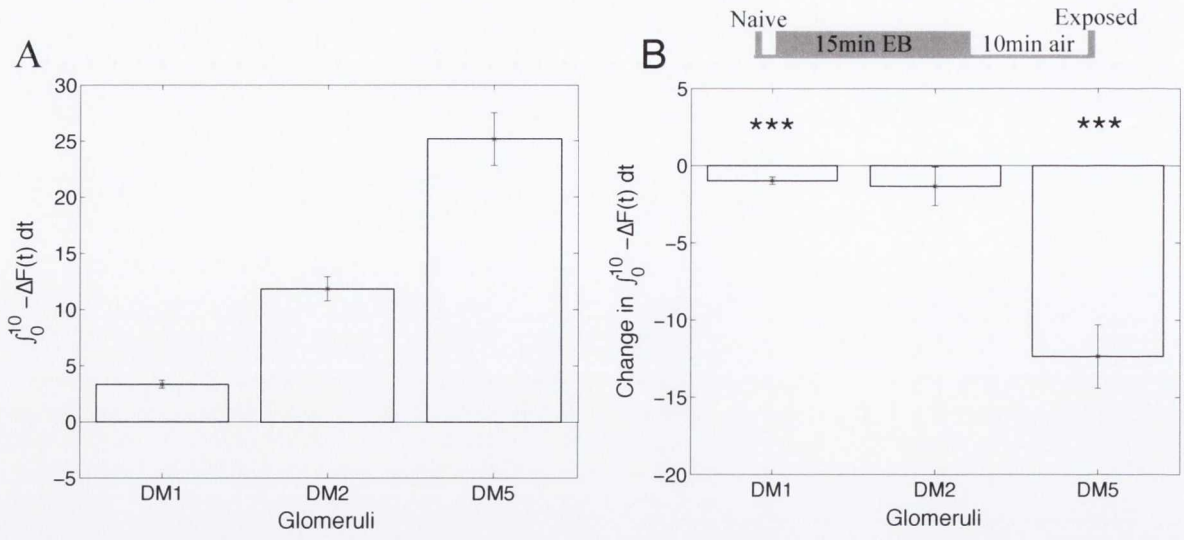


Figure 3.33: Quantified changes in odour-evoked depolarisation in PNs after 15-minute odourant exposure.
Two-photon voltage-imaging was performed in GH146-labelled PNs during a naïve and an exposed 10-second odour presentation to 3ppm EB. Voltage dynamics were recorded from PNs innervating the glomeruli DM1, DM2, and DM5. **(A)** Naïve odour-evoked voltage responses to 3ppm EB shown as the area under the curve of the ArcLight trace over a 10 seconds period. **(B)** Quantified changes in odour-evoked ArcLight responses induced by 15-minute odourant exposure shown as the area under the curve of the paired differences between the exposed and naïve ArcLight response over a 10 seconds period. Odourant exposure had a significant effect on odour-evoked ArcLight responses in PNs (*Likelihood ratio test, $\chi(3)=54.837$, $p<0.001$, n=26-30/glomerulus* (see Table 5.72)). A significant reduction in odour-evoked ArcLight responses was observed in the DM5 and DM1 glomerulus (*DM5: t-test, $p<0.001$, $t=-6.036$, $df=25$, $n=26$; DM1: t-test, $p=<0.001$, $t=-4.143$, $df=28$, $n=29$*). $*$ $p<0.05$; $**$ $p<0.01$; $***$ $p<0.001$; bars represent mean $\pm$ SEM.

Although the decreased ArcLight responses in the DM1 and DM2 glomerulus after 'mock' exposure could not be explained, the changes that occurred after EB exposure appeared to be of a higher magnitude than the ones after 'mock' exposure. It was therefore asked whether there was a significant difference between the response changes after the two different treatments. Importantly, the naïve odour-evoked ArcLight responses did not differ between the two experiments (*Likelihood ratio test, $\chi(3)=4.145$, $p=0.246$*). However, no interaction effect between the treatment (EB or 'mock' exposed) and the odour stimulus ('naïve' or 'mock'/'exposed') could be detected (*Likelihood ratio test, $\chi(1)=1.352$, $p=0.245$*) indicating that the overall changes in ArcLight responses were indistinguishable between the two treatments. If this analysis was restricted to a certain glomerulus, however, an interaction effect was detected for the DM5 glomerulus (*Likelihood ratio test, $\chi(3)=6.160$, $p=0.013$*) but not for the DM1 and DM2 glomeruli (*DM1: Likelihood ratio test, $\chi(3)=0.431$, $p=0.512$; DM2: Likelihood ratio test, $\chi(3)=1.462$, $p=0.227$*) suggesting that the changes observed in DM5 may be due to the odour exposure rather than the experimental procedure.

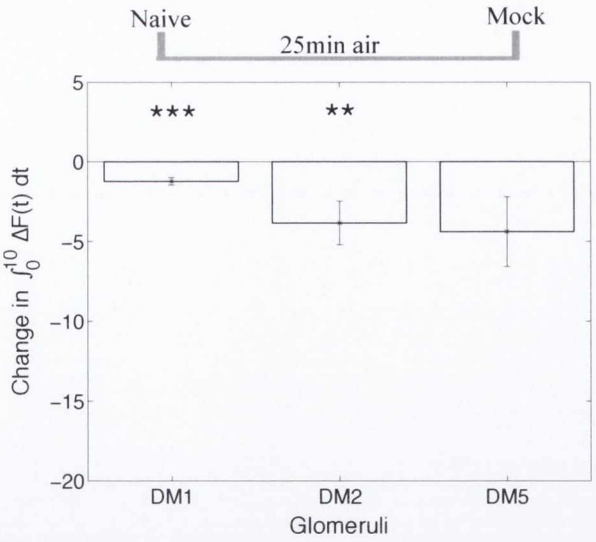


Figure 3.34: Changes in odour-evoked depolarisation in GH146-labelled PNs after 'mock' treatment.
Two-photon voltage-imaging was performed in GH146-labelled PNs during a naïve and a 'mock' air exposed 10-second odour presentation 3ppm EB. Voltage dynamics were recorded from PNs innervating the glomeruli DM1, DM2, and DM5. Quantified changes in odour-evoked ArcLight responses induced by 'mock' treatment are shown as the area under the curve of the paired differences between the 'mock' exposed and naïve ArcLight response over a 10 seconds period. 'Mock' treatment had a significant effect on EB-evoked ArcLight responses in PNs (*Likelihood ratio test, $\chi(3)=12.613$, $p=0.006$, n=24-27/glomerulus* (see Table 5.74)). A significant reduction in odour-evoked ArcLight responses was observed in the DM2 and DM1 glomerulus (*DM2: t-test, $p=0.009$, $t=-2.810$, $df=26$, $n=27$; DM1: t-test, $p<0.001$, $t=-5.254$, $df=25$, $n=26$*). $*$ $p<0.05$; $**$ $p<0.01$; $***$ $p<0.001$; bars represent mean $\pm$ SEM.

Olfactory Sensory Neurons and Local Interneurons

As shown in section 3.5.1, there was a significant reduction in OSN terminal Ca^{2+} responses following 15-minute odourant exposure. To determine whether not only OSN Ca^{2+} influxes but also OSN neuronal activity was reduced after odourant exposure, ArcLight voltage imaging was performed from OSN terminals. To further investigate the role of inhibitory LNs in potentially mediating the exposure-induced changes in OSNs and PNs, ArcLight imaging was further conducted in LNs. Although no changes in Ca^{2+} influx were observed in LNs (see section 3.5.2) there was the possibility that Ca^{2+} imaging failed to detect changes in neuronal activity. ArcLight was therefore expressed in OSNs using the Or83b-Gal4 driver and in GABAergic local interneurons using the LN1-Gal4 and LN2-Gal4 drivers. Voltage dynamics to a naïve and an exposed EB stimulus were recorded from the DM1, DM2, and DM5 glomerulus.

In contrast to voltage imaging in PNs where decreases in ArcLight fluorescence could be reliably detected in almost every fly imaged, the same proved to be substantially more difficult in flies expressing the sensor in OSNs or LNs. In PNs, ArcLight fluorescence was decreased by an average of $-40\Delta F$ in the DM5 glomerulus upon stimulation with 3ppm EB (see Figure 3.32 for mean responses and Figure 3.35 A for the response of a representative fly). In a representative fly, KCL bath application resulted in an ArcLight decrease of around

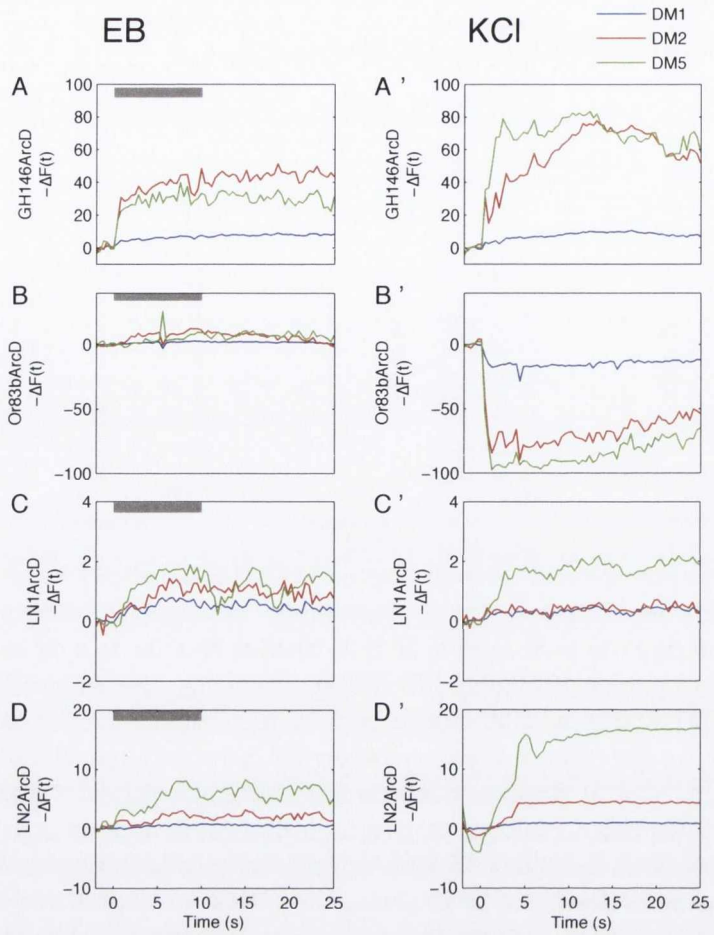


Figure 3.35: ArcLight indicator range in antennal lobe neurons tested by EB odour or KCl bath application in representative neurons

Two-photon voltage-imaging was performed during a 10-second 3ppm EB stimulus (A-D) and during bath application of KCl (A'-D'). The voltage indicator ArcLight was expressed in GH146-labelled PNs (A/A'), Or83b-labelled OSNs (B/B'), as well as LN1- and LN2-labelled LNs (C/C' or D/D' respectively). Voltage dynamics were recorded from PNs innervating the glomeruli DM1 (blue), DM2 (red), and DM5 (green). Depicted are example ArcLight traces of the same fly to the EB stimulus (A-D) and the KCl application (A'-D') shown as changes in fluorescence (-ΔF) over time. A positive deviation indicates depolarisation, a negative one indicates hyperpolarisation of the respective cells. The grey bars signifies the time window of odour presentation.

$-80\Delta F$ in PNs suggesting that the sensor was not saturated by the 3ppm EB stimulus (see Figure 3.35 A'). Flies expressing the ArcLight sensor in OSNs 'responded' less frequently to 3ppm EB and showed substantially less pronounced decreases upon odour stimulation when they did respond (n=13, four of which showed small odour-evoked responses). Example responses of a fly that expressed the ArcLight sensor in OSNs and responded to the odour stimulus are shown in Figure 3.35 B/B'. The largest ArcLight response in this fly of the three glomeruli recorded from was a decrease of around $-10\Delta F$ in the DM2 glomerulus (note that the peak of around $-25\Delta F$ in DM5 is due to movement in the preparation). KCl bath application resulted in an increase of ArcLight fluorescence of around $90\Delta F$ indicating a large hyperpolarising current. This is believed to be due to the activation of inhibitory LNs which provide strong presynaptic inhibition onto the OSN terminals.

In contrast to ArcLight imaging in OSNs, approximately half of the flies that expressed

the voltage sensor in LN1 and LN2 interneurons showed odour-evoked ArcLight responses. However, in the majority of the cases the responses could be barely detected (n=5 for *LN1-Gal4;UAS-ArcLight*, three of which showed very small responses; n=13 for *LN2-Gal4;UAS-ArcLight*, six of which showed mostly small responses). Two example flies that did respond are shown in Figure 3.35 C/C' and D/D'. A fly expressing ArcLight in LN1 showed a decrease of up to $-2\Delta F$ upon EB stimulation. KCl bath application did not seem to result in a larger ArcLight response in this fly (see Figure 3.35 C/C'). Another fly that expressed ArcLight in LN2 neurons showed a decrease in ArcLight fluorescence in DM5 of around $-8\Delta F$ to 3ppm EB and around $-18\Delta F$ to KCl.

All in all, the infrequency of 'responding' flies and in many cases also the amplitude of the ArcLight sensor was deemed too small to enable the quantification of voltage changes induced by short-term exposure in flies expressing the voltage sensor in Or83b OSNs and LN1/LN2 LNs.

3.6.2 Measuring Synaptic Vesicle Release Using SynaptopHluorin

To test whether odourant exposure results in increased transmission from LN1 or LN2 GABAergic interneurons which may result in reduced Ca^{2+} influxes in OSN terminals, the pH sensor synaptoPhluorin was expressed under the control of the LN1-Gal4 or LN2-Gal4 driver. However, no odour-evoked increase in synaptopHluorin fluorescence could be detected in either of the two neuronal types (data not shown, n=5 for *LN1-Gal4;UAS-spH*, n=6 for *LN2-Gal4;UAS-spH*). For potential explanations see the discussion (section 3.6.3).

3.6.3 Discussion

Membrane Voltage Imaging Using ArcLight

The ArcLight indicator has been successfully used for the detection of both action potentials and subthreshold events in a range of neuronal types in *Drosophila* (Cao et al., 2013; Haynes et al., 2015; Klein et al., 2015). Genetically targeted expression of ArcLight in OSNs showed depolarisation and hyperpolarisation in the presynaptic terminals of the OSNs recorded from (Cao et al., 2013). PNs that innervated the same glomeruli as the OSNs all showed depolarisation upon odour presentation (Cao et al., 2013). The ArcLight amplitudes in PNs were roughly twice as large as those in OSNs (Cao et al., 2013).

Cao et al. (2013) reported ArcLight responses of up to -8% $\Delta F/F$ for PNs and up to -4% $\Delta F/F$ for OSNs, both to the odourant 1-butanol. In the present study, ΔF instead of $\Delta F/F$ values were reported due to GCaMP fluorescence baseline changes observed after odourant exposure (see section 2.2.4 for details). A naïve EB-evoked ArcLight peak response of -35ΔF as observed for PNs projecting to the DM5 glomerulus (see Figure 3.32 C blue trace) corresponds to roughly -47% $\Delta F/F$. The example fly shown in Figure 3.35 B which expressed the ArcLight sensor in OSNs exhibited a naïve EB-evoked ArcLight peak response of $-10\Delta F$ in OSNs projecting to the DM2 glomerulus which corresponds to around -12% $\Delta F/F$. These

conversions show that the ArcLight responses obtained in the present study were substantial larger than the ones reported in Cao et al. (2013). As Cao et al. did not specify their concentrations, a potential reason for these discrepancies are different odour concentrations. The EB concentration used here, 3ppm, is well within the receptive range of OSNs (see section 3.2 for details), however one of the EB-sensitive OSNs, Or22a which targets the DM2 glomerulus, begins to respond to EB at a concentration of 2ppb (Andersson et al., 2012). This example illustrates that substantial lower odour concentrations than 3ppm are detected by the *Drosophila* olfactory system. It is thus possible that the odour concentration used by Cao et al. was substantially lower than the one used in the present study, thus accounting for the different magnitudes in the ArcLight signals. Other potential reasons for the discrepancies are that Cao et al. did not record from PNs innervating the DM5 glomerulus, the PNs that showed strongest responses in the present study, and that the two studies used different odours which could result in varying activation levels.

		DM1	DM2	DM5
ArcD	**3ppm**	-29%	-11% (n.s.)	-49%
	mock	-37%	-25%	-18% (n.s.)
GCaMP6m	**3ppm**	-12% (n.s.)	9% (n.s.)	-48%
	20ppm	-42%	18% (n.s.)	-66%
	mock	-21% (n.s.)	+5% (n.s.)	-15% (n.s.)

Table 3.12: Comparison of exposure-induced changes in GCaMP and ArcLight responses in PNs

Percent response change of a given PN type at 3ppm or 20ppm EB with respect to its naïve EB-evoked GCaMP or ArcLight response (n.s.) indicates a non-significant change.

Similar to Ca^{2+} imaging, odour-evoked ArcLight responses changed after 15-minute odourant exposure (see Figure 3.33 B). PNs projecting to the DM1 and DM5 glomerulus showed a significant decrease in odour-evoked depolarisation while PNs innervating DM2 remained unchanged. When comparing the percent changes of odour-evoked ArcLight and GCaMP responses, commonalities were apparent (see Table 3.12). For both indicators, the largest change was observed in PNs targeting the DM5 glomerulus followed by those innervating the DM1 glomerulus, while PNs innervating DM2 remained unchanged for both Ca^{2+} and voltage imaging. However, in contrast to GCaMP imaging, odour-evoked ArcLight fluorescence responses also decreased after 'mock' air exposure (see Figure 3.34). Significant changes were found in the DM1 and DM2 glomerulus. 'Mock' and 3ppm exposure

induced significantly different reductions in ArcLight responses in the DM5 glomerulus, however, the overall ArcLight responses across all glomeruli between the two treatments did not differ (see section 3.6). The possibility of fluorophore bleaching causing the changes observed after 'mock' treatment was ruled out as three minute continuous imaging did not decrease ArcLight baseline fluorescence. Another possible explanation is that the flies were in an 'aroused' state prior to the first odour presentation while they were acclimatized to the experimental setup when the second odour was presented after the 'mock' exposure. However, to allow for acclimatization, each fly was presented to the air stream under the microscope for at least five minutes prior to the first odour presentation, a time period that was deemed sufficient, as no differences in odour-evoked GCaMP responses were observed after 'mock' exposure (see section 3.3.3). Currently we do not have a plausible explanation for the reduced odour-evoked depolarisation in PNs after 'mock' exposure. However, further investigation is required to determine the underlying physiological mechanism.

Flies that expressed the ArcLight sensor in OSNs or the LN1 and LN2 type of local interneurons only infrequently yielded ArcLight responses upon EB stimulation or only showed small odour-evoked responses. Since nearly every fly that expressed the GCaMP sensor in these neuron types 'responded' to EB stimulation, this observation can not be attributed to a faulty preparation but is probably due to the not quite suitable sensitivity range of the ArcLight indicator for voltage imaging from OSNs and local interneurons. Due to restricted access of OSN cell bodies within the antennae, electrophysiological recordings from OSNs are limited to extracellular single sensillum recordings (de Bruyne et al., 2001) which do not allow an investigation of the intrinsic properties of OSNs in comparison to PNs. In contrast, PN and LN odour-evoked response dynamics were recently directly compared by recording odour-evoked synaptic currents from both cell types in whole-cell voltage-clamp mode at a holding potential near rest (60 mV, Nagel et al., 2015). Odour-evoked inward current was found to be more transient in LNs than PNs and the inward currents of PNs were approximately twice as large as those of LNs (Nagel et al., 2015). This differences in LN/PN inward current amplitudes may suggest that the more infrequent and less pronounced ArcLight responses in LNs could be explained by an insufficient sensitivity range of the ArcLight sensor to reliably detect small changes in membrane depolarisation.

Imaging Transmitter Release Using SynaptopHluorin

The pH-sensitive fluorescence indicator synaptoPhluorin has been widely used to measure transmitter release in response to odours or electrical stimulation of the olfactory nerve (Ignell et al., 2009; Ng et al., 2002; Reiff et al., 2005; Root et al., 2008; Shang et al., 2007; Yu et al., 2006). Genetically targeted expression of synaptopHluorin to distinct populations of olfactory neurons such as OSNs, PNs, and inhibitory LNs enabled the characterisation of synaptic transmission within the *Drosophila* antennal lobe (Ng et al., 2002). Notably, these studies performed synaptopHluorin imaging either in an explant preparation resilient to movements and reported a fluorescence increase of up to 5% $\Delta F/F$ (Ignell et al., 2009;

Root et al., 2008) or they availed of a live preparation but added additional Ca^{2+} (3-fold) to detect indicator changes of up to 10% ΔF/F (Ng et al., 2002; Shang et al., 2007).

In the present study, synaptoPhluorin was genetically targeted to the LN1 and LN2 type of local interneurons, a live preparation was used and no additional Ca^{2+} was added. The decision to not add any supplementary Ca^{2+} was made due to the GCaMP fluorescence baseline shifts that were observed after 15-minute odourant exposure (see sections 3.3.4 and 3.5.1). In both OSNs and PNs, odour-evoked reductions in Ca^{2+} influxes were accompanied by reductions in Ca^{2+} baseline levels. Adding extra Ca^{2+} could have potentially changed Ca^{2+} dynamics and thus may have established unnatural conditions, ultimately leading to cell death (Berridge et al., 1998). In the presence of additional Ca^{2+}, the short-term odourant exposure may have induced atypical physiological changes in the responding neurons and their firing patterns. However, without supplementing Ca^{2+} no increases in synaptoPhluorin fluorescence were detected upon odour stimulation in the live preparation. In comparison, Ng et al. (2002) measured a synaptoPhluorin response of up to 5% ΔF/F in LNs in a live preparation when Ca^{2+} was added to the saline. Without the Ca^{2+} supplement these responses would have probably been substantially smaller and most likely not detectable due to the small movements of the live preparation. The kinetics of the synaptoPhluorin sensor were thus deemed insufficient for the purpose of this study.

Notably, synaptopHluorin has not been further developed since it was first published by Miesenböck et al. (1998a). In flies, the sensor displays slower kinetics (Reiff et al., 2005; Ignell et al., 2009) as well as a smaller amplitude in fluorescence change upon odour activation than GCaMP1.3 (Ignell et al., 2009), the first GCaMP indicator available in 2003 (Wang et al., 2003), highlighting obvious drawbacks to other sensors available. The Looger laboratory at Janelia Farm is currently developing a fluorescence indicator for GABA release (*pers. comm.*) which will hopefully have better kinetics than synaptopHluorin and thus may be more suitable for the quantification of GABA release from local interneurons before and after short-term odourant exposure.

3.7 The Effect of Blocking Presynaptic Inhibition

The findings from section 3.5.3 indicate that exposure-induced reductions in odour-evoked Ca^{2+} influxes in OSN terminals are likely to result from adaptation in the axon terminals, presynaptic inhibition or a combination of both. In order to further determine the cause of the decreases it was investigated whether blocking presynaptic inhibition using RNAi-mediated knockdown of *Drosophila* $GABA_A$ or $GABA_B$ receptors in OSNs prevent the change in odour-evoked GCaMP responses in OSN terminals.

There are two major types of GABA receptors in *Drosophila*: ionotropic $GABA_A$ and metabotropic $GABA_B$ receptors ($GABA_A$Rs and $GABA_B$Rs), both of which are expressed in the AL (Aronstein and Ffrench-Constant, 1995; Enell et al., 2007). $GABA_A$Rs are ligand-gated chloride-selective ion channels that open upon binding of GABA and elicit a fast generally inhibitory response via influx of chloride ions (Buckingham et al., 2005; Hosie et al., 1997; Knipple and Soderlund, 2010). $GABA_B$Rs are G-protein-coupled receptors that act on a much slower time scale and often modulate neuronal responses (Mezler et al., 2001). Both, fast and slow GABA-mediated inhibition has been implicated in shaping odour-evoked responses in the *Drosophila* AL (Wilson and Laurent, 2005; Olsen and Wilson, 2008b; Root et al., 2008). $GABA_A$Rs shape odour responses during the early phase of an odour presentation while $GABA_B$Rs mediate odour-evoked inhibition over a longer period (Wilson and Laurent, 2005; Olsen and Wilson, 2008b). Lateral inhibition from inhibitory LNs has been reported to act predominantly presynaptically on OSN terminals and can be blocked by a combination of the $GABA_A$ and $GABA_B$ receptor antagonists picrotoxin and CGP54626 (Olsen and Wilson, 2008b; Root et al., 2008). OSNs are therefore thought to express both receptor types while only the expression of $GABA_B$Rs has been shown explicitly (Root et al., 2008).

The *Drosophila* genome encodes at least three subunits for the ligand-gated $GABA_A$ ion-channel (Buckingham et al., 2005; Hosie et al., 1997; Knipple and Soderlund, 2010): RDL (resistance to dieldrin), LCCH3 (ligand-gated chloride channel homologue 3), and GRD ($GABA_A$ and glycine receptor-like subunit of *Drosophila*) (Ffrench-Constant and Mortlock, 1991; Harvey et al., 1994; Henderson et al., 1993; Hosie et al., 1997; Knipple and Soderlund, 2010). $GABA_A$Rs are pentameric and exist as homomers or heteromers (Hosie et al., 1997). The RDL subunit is widely distributed throughout the *Drosophila* nervous system (Aronstein and Ffrench-Constant, 1995). However, the subunit composition of receptors containing native RDL is poorly understood (Buckingham et al., 2005; Hosie et al., 1997; Knipple and Soderlund, 2010). As RDL homomers display similar pharmacological characteristics as the majority of native $GABA_A$Rs, such as their sensitivity to picrotoxin (Bloomquist et al., 1991), they are believed to be prevalent in the insect nervous system (Buckingham et al., 2005; Hosie et al., 1997). RDL/LCCH3 heteromers form in *vitro* and can be blocked by bicuculline (Zhang et al., 1995) but have not been found in *vivo* (Aronstein et al., 1996). However, it has been suggested that RDL forms heteromultimeric complexes with the inver-

tebrate glutamate-gated chloride channel subunit GluCl (Ludmerer et al., 2002) and other as-yet-unidentified subunits (Buckingham et al., 2005). The ionotropic receptor subunits LCCH3 and GRD form heteromers that function as GABA-gated cation channels (Gisselmann et al., 2004).

$GABA_B$ receptors are seven-transmembrane-domain G-protein-coupled receptors (Mezler et al., 2001). Three subtypes, $GABA_BR1$-3, each encoded by a separate gene have been found so far (Mezler et al., 2001). $GABA_BR1$ and $GABA_BR2$ are expressed in similar regions in the embryonic central nervous system and are only functional as heterodimers (Mezler et al., 2001). They bind GABA and mediate their effects via G-protein activation (Mezler et al., 2001). $GABA_BR3$ has a unique expression pattern and is not activated by GABA on its own or in any combination with the other two receptor types (Mezler et al., 2001).

The aim of the experiments performed in this chapter was to determine whether the odour exposure induced changes in Ca^{2+} influxes in OSNs are due to GABAergic inhibition onto the OSN axon terminals. If this was the case, blocking presynaptic inhibition through targeted expression of transgenic RNAi constructs against the $GABA_AR$ subunit RDL or $GABA_BR$ subtype $GABA_BR2$ would prevent changes in odour-evoked GCaMP responses in OSNs after short-term odourant exposure.

3.7.1 $GABA_A$ and $GABA_B$ Receptors in OSN Terminals

To investigate the effect of RNAi mediated $GABA_B$ receptor knockdown in OSNs onto the exposure-induced changes in Ca^{2+} influxes in OSNs, GCaMP6m and an RNAi construct against the $GABA_B$ receptor subunit $GABA_BR2$ were expressed under the control of the Gal4 driver Or83b. Flies that expressed the Ca^{2+} indicator but not the RNAi construct served as controls. UAS-$GABA_BR2$-RNAi was made by Root et al. (2008) and successfully used to knock down $GABA_BR$ expression when driven by Or83b-Gal4 in adult *Drosophila*.

Naïve EB-evoked GCaMP responses did not differ between the two groups as the genotype had no significant effect on odour-evoked GCaMP6 responses in OSNs (*Likelihood ratio test,* $\chi(3)=2.831$, $p=0.418$, *n=16 per genotype and glomerulus*, see Figure 3.36 A). However, an interaction effect between the genotype and the odour presentation (naïve vs. exposed) was detected (*Likelihood ratio test,* $\chi(1)=15.971$, $p<0.001$, see Figure 3.36 B). *Or83b-Gal4,UAS-GCaMP6m;UAS-GABA$_B$R2-RNAi* flies showed 15.935 ± 3.998 arb. units larger responses after odourant exposure compared to *Or83b-Gal4,UAS-GCaMP6m* flies (value determined by a linear mixed-effects model fit by maximum likelihood) indicating that $GABA_BRs$ are normally involved in lowering OSN Ca^{2+} fluxes. A subsequently performed likelihood ratio test restricted to a single OSN type revealed interaction effects between genotype and odour presentation (naïve vs. exposed) in each of the studied glomeruli (*DM1:* $\chi(1)=9.656$, $p=0.002$; *DM2:* $\chi(1)=11.810$, $p<0.001$; *DM5:* $\chi(1)=4.457$, $p<0.035$). *Or83b-Gal4,UAS-GCaMP6m;UAS-GABA$_B$R2-RNAi* flies showed larger responses in DM1 by 5.985 ± 1.900 arb. units, in DM2 by 23.470 ± 0.001 arb. units and in DM5 by 18.897

± 0.041 arb. units compared to *Or83b-Gal4,UAS-GCaMP6m* flies (see Figure 3.36 B). Notably, while GCaMP responses in all three glomeruli decreased in control flies following odourant exposure, flies that carried the RNAi construct showed increases in odour-evoked GCaMP responses in the DM1 and DM2 glomerulus and a decrease in DM5 (see Figure 3.36 A). The differences between $GABA_BR2$ RNAi expressing flies and controls was likewise reflected in the percentage changes with respect to the naïve EB-evoked GCaMP response in the respective OSN types: Control flies showed similar percentage decreases in all three glomeruli with a reduction of -50% in DM1, of -48% in DM2 and -52% in DM5. RNAi-mediated knockdown of the $GABA_BR$ in OSNs caused increases in DM1 and DM2 of 77% and 70%, respectively, and a smaller percentage decrease in DM5 of -25%.

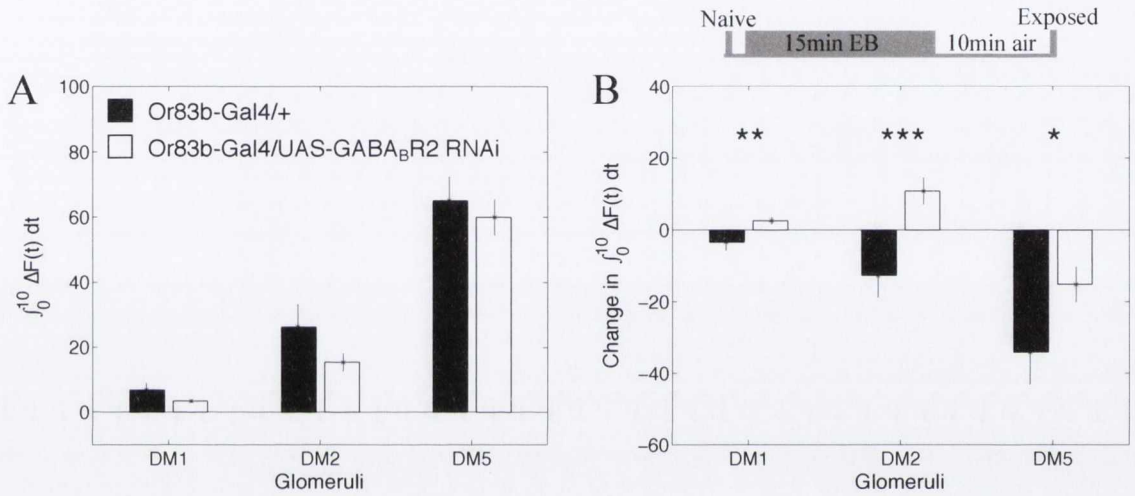


Figure 3.36: $GABA_B$ receptor knockdown in OSNs alters exposure-induced changes in odour-evoked OSN GCaMP responses
Two-photon Ca^{2+}-imaging was performed in Or83b-labelled OSNs during a naïve and an exposed 10-second odour presentation to 3ppm EB. Ca^{2+} dynamics were recorded from OSNs targeting the DM1, DM2, and DM5 glomerulus. Comparisons were made between the experimental group that expressed an RNAi construct against the $GABA_B$ receptor in Or83b neurons (*Or83bGal4,UASGCaMP6m;UAS-GABA$_B$R2-RNAi*, white bars) and controls (*Or83bGal4,UASGCaMP6m*, black bars). (**A**) Naïve odour-evoked Ca^{2+}-influxes in OSNs shown as the area under the curve of the GCaMP trace over a 10 seconds period. The genotype had no significant effect on odour-evoked GCaMP6 responses in OSNs (*Likelihood ratio test, $\chi(3)=2.831$, $p=0.418$, $n=16$ per genotype and glomerulus*). (**B**) Changes in odour-evoked GCaMP6m fluorescence induced by 15-minute odourant exposure shown as the area under the curve of the paired differences between the exposed and naïve GCaMP6m responses over a 10 seconds period. An interaction effect between genotype and odour presentation (naïve vs. exposed) was detected (*Likelihood ratio test, $\chi(1)=15.971$, $p<0.001$, $n=16$ per genotype and glomerulus*). A likelihood ratio test restricted to a single OSN type revealed interaction effects between genotype and odour presentation in each of the three studied glomeruli (*DM1: $\chi(1)=9.656$, $p=0.002$; DM2: $\chi(1)=11.810$, $p<0.001$; DM5: $\chi(1)=4.457$, $p<0.035$*). * $p<0.05$; ** $p<0.01$; *** $p<0.001$; bars indicate mean ± SEM.

Following the finding that $GABA_BRs$ are required for exposure induced changes in OSNs the requirement for $GABA_ARs$ was similarly investigated. Thus, GCaMP6m and an RNAi construct against the $GABA_A$ receptor subunit RDL were expressed under the control of the

Gal4 driver Or83b and the effect of RNAi mediated $GABA_AR$ knockdown on GCaMP responses studied. Flies that expressed the Ca^{2+} indicator but not the RNAi construct again served as controls. The UAS-RDL-RNAi construct was made by Liu et al. (2009) and successfully used to knock down RDL-containing $GABA_AR$ expression in PNs and mushroom body kenyon cells (Das et al., 2011b; Liu et al., 2009).

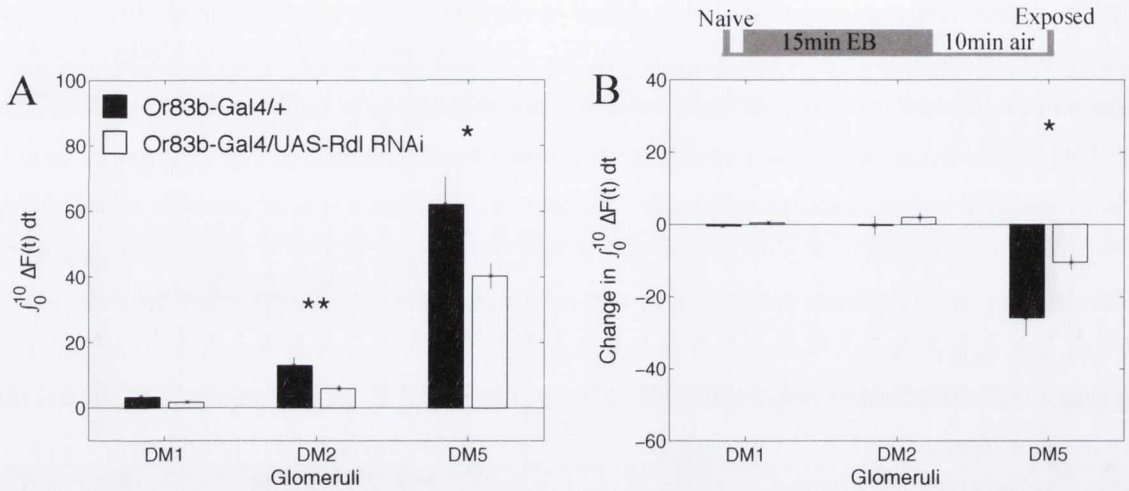


Figure 3.37: $GABA_A$ receptor subunit knockdown in OSNs alters exposure-induced changes in odour-evoked OSN GCaMP responses
Two-photon Ca^{2+}-imaging was performed in Or83b-labelled OSNs during a naïve and an exposed 10-second odour presentation to 3ppm EB. Ca^{2+} dynamics were recorded from OSNs targeting the DM1, DM2, and DM5 glomerulus. Comparisons were made between the experimental group that expressed an RNAi construct against the $GABA_A$ receptor subunit Rdl in Or83b neurons (*Or83bGal4,UASGCaMP6m;UASRdli*, white bars) and controls (*Or83bGal4,UASGCaMP6m*, black bars). (**A**) Naïve odour-evoked Ca^{2+}-influxes in OSNs shown as the area under the curve of the GCaMP trace over a 10 seconds period. The genotype had a significant effect on naïve EB-evoked GCaMP responses in OSNs (*Likelihood ratio test, $\chi(3)=14.607$, $p=0.002$, $n=16$ per genotype and glomerulus*). Subsequent two-sample t-test revealed significant differences between the naïve responses of the two groups in the glomeruli DM2 and DM5 but not DM1 (*DM1: $p=0.076$, $t=1.837$, $df=30$, $n=16$ per group; DM2: $p=0.009$, $t=2.816$, $df=30$, $n=16$ per group; DM5: $p=0.023$, $t=2.398$, $df=30$, $n=16$ per group*). (**B**) Changes in odour-evoked GCaMP6m fluorescence induced by odourant exposure shown as the area under the curve of the paired differences between the exposed and naïve GCaMP6m responses over a 10 seconds period. An interaction effect between the genotype and the odour presentation (naïve vs. exposed) was detected (*Likelihood ratio test, $\chi(1)=3.848$, $p<0.05$, $n=16$ per genotype and glomerulus*). A likelihood ratio test restricted to a single OSN type revealed interaction effects between genotype and odour presentation (naïve vs. exposed) in the DM5 but not DM1 or DM2 glomerulus (*DM1: $\chi(1)=1.348$, $p=0.246$; DM2: $\chi(1)=0.617$, $p=0.432$; DM5: $\chi(1)=5.975$, $p=0.015$*). * $p<0.05$; ** $p<0.01$; *** $p<0.001$; bars indicate mean ± SEM.

In this experiment, the genotype had a significant effect on naïve EB-evoked GCaMP responses in OSNs (*Likelihood ratio test, $\chi(3)=14.607$, $p=0.002$*, see Figure 3.37 A) lowering GCaMP responses by -1.551 ± 6.297 arb. units in *Or83b-Gal4,UAS-GCaMP6m;UAS-RDL-RNAi* flies compared to *Or83b-Gal4,UAS-GCaMP6m* controls. Subsequently performed two-sample t-test revealed significant differences between the naïve responses of the two groups in the glomeruli DM2 and DM5 but not DM1 (*DM1: $p=0.076$, $t=1.837$, $df=30$,*

n=16 per group; DM2: p=0.009, t=2.816, df=30, n=16 per group; DM5: p=0.023, t=2.398, df=30, n=16 per group). An interaction effect between the genotype and the odour presentation (naïve vs. exposed) was further detected (*Likelihood ratio test, $\chi(1)=3.848$, $p<0.05$*, see Figure 3.37 B). *Or83b-Gal4,UAS-GCaMP6m;UAS-RDL-RNAi* flies showed 6.127 ± 3.191 arb. units larger overall responses after odourant exposure compared to *Or83b-Gal4,UAS-GCaMP6m* controls. A subsequently performed likelihood ratio test restricted to a single OSN type revealed interaction effects between genotype and odour presentation (naïve vs. exposed) in the DM5 but not DM1 or DM2 glomerulus (*DM1: $\chi(1)=1.348$, $p=0.246$; DM2: $\chi(1)=0.617$, $p=0.432$; DM5: $\chi(1)=5.975$, $p=0.015$*). *Or83b-Gal4,UAS-GCaMP6m;UAS-RDL-RNAi* flies showed approximately 15.345 ± 6.282 arb. units smaller reductions in DM5 than *Or83b-Gal4,UAS-GCaMP6m* controls (see Figure 3.36 B). The percentage changes with respect to the naïve EB-evoked GCaMP response in the respective OSN types of the two groups were as follows. For control flies small percentage decreases in DM1 and DM2 of -11% and -2% respectively were noted and a more substantial decrease of -42% in the DM5 glomerulus. The experimental group expressing RDL RNAi showed increases of 28% and 32% in DM1 and DM2, respectively, and a decrease of -26% in DM5.

3.7.2 Discussion

The experiments performed in this chapter aimed to investigate whether blockade of presynaptic inhibition using RNAi transgenes against the $GABA_BR$ subtype $GABA_BR2$ or the $GABA_AR$ subunit RDL prevents the changes in Ca^{2+} influxes in OSN terminals induced by 15-minute odourant exposure.

Flies expressing the RNAi construct against $GABA_BR2$ (*Or83b-Gal4,UAS-GCaMP6m;UAS-GABA$_B$R2-RNAi*) showed less pronounced decreases after short-term odourant exposure than control flies without the RNAi transgene (*Or83b-Gal4,UAS-GCaMP6m*) suggesting that $GABA_BRs$ are required for the changes in Ca^{2+} influx observed after odourant exposure. OSNs projecting to all three glomeruli showed significantly lower decreases in activity in $GABA_BR2$-RNAi expressing flies compared to controls. In fact, OSNs targeting DM1 and DM2 exhibited increases in GCaMP responses after odourant exposure. Importantly, no difference in the naïve GCaMP responses between the two genotypes was detected implying that the effects observed were not due to alterations in odour-evoked neuronal activity. Flies expressing an RNAi construct against RDL in OSNs showed a smaller decrease in DM5 GCaMP responses compared to controls. This effect, however, may result from impairments in odour-evoked neuronal activity in RDL-RNAi-expressing flies, as these flies already displayed significantly lower naïve GCaMP responses than controls, and thus cannot be interpreted unambiguously.

Presynaptic Inhibition of Naïve Odour-Evoked GCaMP Responses in OSNs

The $GABA_BR$ has been previously shown to drive presynaptic inhibition in OSNs and to mediate gain control within the olfactory circuit (Root et al., 2008; Olsen and Wilson, 2008b).

Gain control was shown by comparing PN GCaMP responses in the presence and absence of the $GABA_BR$ antagonist CGP54626. Blocking $GABA_BR$ function with CGP54626 resulted in significantly increased PN GCaMP responses at higher odour concentrations but yielded no changes at low concentrations (Root et al., 2008). Similarly, vesicle release from OSN terminals upon electrical stimulation of the olfactory nerve was compared between flies that lack $GABA_BR$ expression in OSNs and controls. Vesicle release measured using the pH-sensitive fluorescence indicator synaptopHluorin was significantly greater in response to high-intensity nerve stimulation in flies bearing the $GABA_BR2$ transgene than control flies. No differences in vesicle release were observed to low-intensity stimuli (Root et al., 2008). In line with this, loose patch clamp recordings in PNs projecting to the VA1lm glomerulus showed that optogenetic activation of the cognate OSN type increased the gain of the PN firing frequency in flies expressing $GABA_BR2$-RNAi in Or83b-labelled OSNs. $GABA_BR$ expression in OSNs thus decreases the gain of PN output (Root et al., 2008).

In the present study, blocking presynaptic inhibition through $GABA_BR$ knockdown in OSNs had no effect on naïve GCaMP responses in OSNs. A potential reason for this discrepancy could be the odour concentration used. Root et al. (2008) show that the effect of $GABA_BR2$-knockdown or $GABA_BR$ antagonist is dependent on the stimulus strength. Synaptic vesicle release, odour-evoked PN Ca^{2+} influxes, and PN spiking in the VA1lm glomerulus were indistinguishable in the presence and absence of $GABA_BR2$-RNAi/$GABA_BR$ antagonist at low-intensity nerve stimulations or low odour concentrations (Root et al., 2008). The odour concentration used in the present study could have therefore been at the lower end of the dynamic range of the given OSN type where $GABA_BR$ blockade had no effect on the GCaMP response. A direct comparison of the odour concentration used in the two studies is not possible as Root et al. (2008) only state concentration as volume dilutions in paraffin oil on a piece of filter paper rather than reporting the odour concentration that is experienced by the fly. It can thus only be speculated that a concentration of 3ppm EB as used in the present study was low enough to not be affected by $GABA_BR$ knockdown.

In the literature, the involvement of $GABA_AR$s in presynaptic inhibition onto OSN terminals appears to be less pronounced compared to $GABA_BR$s (Olsen and Wilson, 2008b; Root et al., 2008). In the experiments performed by Root et al. (2008), the $GABA_AR$ antagonists picrotoxin did not block the reduction in Ca^{2+} influx in OSN terminals elicited by GABA application. Similarly, the $GABA_AR$ antagonist on its own had no effect on presynaptic inhibition in the Olsen and Wilson (2008b) study. However, when additionally added to a bath containing $GABA_BR$ antagonist which blocks the late phase of presynaptic inhibition the residual early phase of inhibition was blocked as well (Olsen and Wilson, 2008b). Thus, $GABA_AR$s appear to only contribute weakly to presynaptic inhibition of OSN neuronal activity.

In contrast to the published literature, RNAi-mediated knockdown of $GABA_AR$s in OSNs had a significant effect on naïve OSN GCaMP responses in the present study (see Figure 3.37). Surprisingly however, naïve odour-evoked GCaMP responses in OSNs target-

ing DM2 and DM5 were reduced in the absence of $GABA_A$Rs while removal of inhibitory input onto these neurons would be expected to increase Ca^{2+} influxes. Notably, flies that express an RNAi construct against the $GABA_B$R subunit likewise showed decreased odour-evoked GCaMP responses, even if these were not statistically significant (see Figure 3.36). Similar observations were made after the application of $GABA_A$ or $GABA_B$ receptor antagonists picrotoxin and CGP54626 and in $GABA_B$R2-RNAi-expressing flies in a previous study (Murmu et al., 2011). As the effect of antagonist application is unspecific and could thus for instance block the respective GABA receptors in the membrane of inhibitory LNs, thus increasing the activity in those neurons and enhancing presynaptic inhibition mediated through the other GABA receptor. RNAi-mediated knockdown of one of the two GABA receptors, on the other hand, is specific to OSNs and thus more difficult to explain. One potential reason is that as GABA receptor expression is prevented from an early developmental stage the effect of lowering odour-evoked neuronal activity in OSNs could be a mechanism to compensate for the lack of GABA receptor expression.

The Effect of Presynaptic Inhibition on Odourant Exposure-Induced Changes in OSNs

Besides its effect on short odour stimuli, GABAergic presynaptic inhibition has also been implicated in longer forms of olfactory adaptation in the OSN terminals (Murmu et al., 2011). Both, $GABA_A$R and $GABA_B$R antagonists prevented reductions in OSN Ca^{2+} influxes after repeated odour presentations (Murmu et al., 2011). RNAi-mediated knockdown of the $GABA_B$R further prevented adaptations in the OSN axon terminals and impaired behavioural adaptation after 5 minute pre-exposure (Murmu et al., 2011).

In line with these findings, blocking presynaptic inhibition through $GABA_B$R2-RNAi also significantly attenuated the reduction in OSN Ca^{2+} influxes following 15-minute odourant exposure (see Figure 3.36). In the case of DM5, the decrements following 15-minute exposure were smaller in flies carrying the RNAi transgene compared to controls. In the DM1 and DM2 glomerulus, odour-evoked GCaMP responses were even increased in the experimental group compared to being decreased in controls. These observations indicate that $GABA_B$R expression is required for exposure-induced decrements in OSN terminal activity. The observation that odour-evoked GCaMP responses in DM5 are not completely abolished in flies expressing $GABA_B$R2-RNAi could be due to insufficient expression of targeted RNAi resulting in an incomplete block of $GABA_B$R2 mRNA. It could otherwise also indicate that presynaptic inhibition required for exposure-induced decrements does not solely rely on $GABA_B$R but also involves other chloride receptor channels such as $GABA_A$ or GluClα receptors. The observation that the DM1 and DM2 glomerulus show increased GCaMP responses following 15-minute exposure in flies expressing $GABA_B$R2-RNAi was surprising and cannot be explained by the removal of inhibitory input on its own. A potential explanation is that the decrements seen in controls are a balance of exposure-induced changes in inhibitory and excitatory local interneuron input onto OSNs, whereas inhibition is predominant. RNAi-mediated knockdown of $GABA_B$Rs, however, prevents the changes in

inhibitory input to have an effect on neuronal activity in OSNs due to the lack of $GABA_BRs$. In that case, the changes in excitatory input may be prevalent resulting in increased neuronal OSN activity upon odour stimulation following 15-minute odourant exposure. Further experiments will be needed to address this hypothesis.

The involvement of $GABA_ARs$ in mediating the decrements observed after 15-minute exposure are less clear. While RNAi-mediated knockdown of the $GABA_AR$ subunit Rdl resulted in significantly smaller reductions in the DM5 glomerulus compared to controls, the naïve odour-evoked GCaMP responses in this and the other two glomeruli also differed between the two groups (see Figure 3.37). As the naïve odour-evoked GCaMP responses are already lower in the experimental animals the smaller reductions following odourant exposure could simply be due to smaller naïve responses. When compared to controls, the naïve odour-evoked GCaMP responses in DM5 were 35% smaller in flies carrying the RNAi transgene. The changes observed after 15-minute odour exposure were, however, 59% lower in the experimental group compared to the control. This quantification, even if crude, suggests that $GABA_AR$ knockdown has an effect on exposure-induced changes independent of its requirement for mediating presynaptic inhibition of odour-evoked OSN responses. All together, both $GABA_A$ and $GABA_B$ receptors thus appear to be required for exposure-induced decrements in odour-evoked OSN activity, whereas the involvement of $GABA_BRs$ seems to be more prevalent.

4. Discussion

The experiments performed in this study aimed a) to investigate whether habituation of the locomotor startle response is driven by the same neuronal circuit motif as the one previously shown for habituation of an olfactory avoidance response, b) to establish an experimental setup for Ca^{2+} imaging, including a stable olfactory delivery system and a short-term exposure protocol, that allows the investigation of physiological changes associated with behavioural olfactory habituation, and c) to study the physiological changes that occur due to 15-minute short-term odourant exposure using Ca^{2+} imaging.

Experiments performed with the odour-evoked locomotor startle response assay (see results chapter 3.1) revealed that olfactory habituation of the locomotor startle response is likely not mediated by the same neuronal circuit mechanism as habituation of an olfactory avoidance response (Das et al., 2011b). Ca^{2+} imaging experiments performed with a newly established protocol and odour delivery system showed that PNs as well as OSNs, that project to distinct glomeruli, exhibit reductions in odour-evoked Ca^{2+} influxes following 15-minute odourant exposure (see results chapters 3.3 and 3.5, respectively). Physiological measurements suggest further that the changes observed are not exclusively mediated through GABAergic inhibition of the PN postsynapse, as suggested by behavioural habituation experiments (Das et al., 2011b), but largely arise from GABA-mediated inhibition of the OSN presynapse (see results chapters 3.4 and 3.7, respectively).

4.1 One Neuronal Circuit Underlying Different Forms of Olfactory Habituation?

Novel odour stimuli elicit a range of behaviours in *Drosophila*, including an olfactory jump reflex, increased walking speed, and avoidance if the odour is aversive. Upon repeated or continuous odourant exposure, the flies habituate to the odourant and the behaviours are attenuated (McKenna et al., 1989; Cho et al., 2004; Das et al., 2011b). Since habituation of these behaviours occurs as the odour stimulus becomes familiar the simplest hypothesis is that all forms of olfactory habituation may occur through the same neuronal circuit mechanism.

Thus, it was aimed to investigate whether one form of olfactory habituation, namely habituation of the locomotor startle response, utilises the same neuronal circuit as habituation of the olfactory avoidance response. Similar to what had been shown to ethanol stimuli (Cho

et al., 2004), repeated exposure to EB resulted in a decreased odour-evoked startle response in wildtype flies whereas flies defective in the adenylate cyclase *rutabaga* showed impairments in this form of habituation (see section 3.1). Habituation of the olfactory avoidance response relies on *rutabaga* expression in GABAergic local interneurons in the antennal lobe (Das et al., 2011b). Two approaches were availed of to check whether habituation of the locomotor startle response likewise requires *rutabaga* in these LNs, firstly RNAi-mediated *rutabaga* knockdown targeted to GABAergic LNs and secondly expression of a functional *rutabaga* construct in GABAergic LNs in a rut^{2080} mutant background, to test for its necessity and sufficiency, respectively. However, *rutabaga* was neither necessary nor sufficient in GABAergic LNs (see Figure 3.4). RNAi-mediated knockdown of the NMDA receptor subunit NR1 in PNs, which is likewise required for habituation of the olfactory avoidance response (Das et al., 2011b), similarly was not necessary for habituation of the locomotor startle response (see Figure 3.4). All together, these results indicate that the two approaches of inducing olfactory habituation may not be mediated through the same neuronal circuit in the *Drosophila* antennal lobe.

This finding is perhaps not surprising. Research in mammals has shown that two forms of olfactory habituation which act over different timescales are controlled through distinct brain areas (Wilson and Linster, 2008; McNamara et al., 2008). While a longer-lasting form resides within the mammalian olfactory bulb, analogous to the insect antennal lobe, a shorter-lasting form is induced in the piriform cortex, the analogous brain structure to the insect mushroom bodies (McNamara et al., 2008; Stevens, 2015). Similar to habituation of the olfactory avoidance response, the longer-lasting form is associated with decreased mitral cell (analogous to PNs) odour-evoked activity and requires NMDA receptors (McNamara et al., 2008; Chaudhury et al., 2010). This form has been hypothesized to result from increased inhibitory input from granule cells (analogous to LN1 interneurons) onto mitral cells leading to a suppression of odour-evoked mitral cell activity (Chaudhury et al., 2010; McNamara et al., 2008). The substantial shorter form of olfactory habituation results from synaptic depression in the mammalian piriform cortex (McNamara et al., 2008). Synaptic depression occurs at the mitral-pyramidal cell in the piriform cortex, is homosynaptic and can be blocked by an agonist of group III metabotropic glutamate receptors (Wilson, 1998b,a; Best and Wilson, 2004).

Interestingly, chemical ablation of the mushroom bodies or their inactivation by tetanus toxin disrupted habituation of the locomotor startle response, suggesting that it might be situated in the mushroom bodies (Cho et al., 2004). Whether it results from homosynaptic depression of the PN-kenyon cell synapse and whether it requires metabotropic glutamate receptors like its potential mammalian counterpart remains to be determined.

Homosynaptic depression of excitatory transmission has long been the primary explanation for the underlying mechanisms of behavioural short-term habituation (Christoffersen, 1997). It has been hypothesized that homosynaptic depression evolved at an early stage in evolution and thus underlies rather simple forms of habituation (Ramaswami, 2014). Habitu-

ation mediated through inhibition on the other hand can have only emerged with the origin of interneurons and thus may mediate more complex forms of habituation (Ramaswami, 2014). If habituation of the locomotor startle response indeed underlies homosynaptic depression, it will be interesting to investigate what the purpose of having two different mechanisms for olfactory habituation may be.

4.2 Physiological Changes Associated with Olfactory Avoidance Habituation

One of the main aims of the presented study was to investigate the neurophysiological changes underlying olfactory short-term habituation. Thus, a Ca^{2+} imaging protocol was established (see section 3.2) that allowed the comparison of odour-evoked Ca^{2+} influxes, as a measure for neuronal activity, before and after a short-term odourant exposure in a range of different neuronal populations. To enable an adequate comparison of the Ca^{2+} responses, an odour delivery system was developed that ensured the delivery of a stable odourant concentration not only for the test pulses but also for the 15-minute exposure (see section 3.2). Following recently performed behavioural experiments, odour-evoked PN responses were suspected to be decreased after short-term odourant exposure (Das et al., 2011b). Ca^{2+} imaging from GH146-labelled PNs using GCaMP6m indeed showed decreased odour-evoked PN responses in three out of the seven PN types recorded from (see section 3.3). PNs projecting to the DL1, DM5, and DM6 glomerulus exhibited reductions at both concentrations studied (see Table 4.1 for a summary).

		DL1	DL5	DM1	DM2	DM3	DM5	DM6
Or83b	**3ppm**	-19% (n.s.)	-174% (n.s.)	-38%	-42%	-42% (n.s.)	-50%	-35% (n.s.)
	20ppm	-36%	+81%	-30%	-31%	-28%	-45%	-34%
GH146	**3ppm**	-34%	+109%	-12% (n.s.)	+9% (n.s.)	-25% (n.s.)	-48%	-29%
	20ppm	-39%	+14% (n.s.)	-42%	+18% (n.s.)	-18% (n.s.)	-66%	-34%

Table 4.1: Summary of exposure-induced changes in OSN and PN activity
Percent response change of a given OSN or PN type at the two different concentrations with respect to its naïve EB-evoked GCaMP response. (n.s.) indicates a non-significant change.

To further test whether these physiological changes could be the neuronal correlate of

the behaviour, it was studied whether the same synaptic proteins were required for the decrements in Ca^{2+} influxes as for the behaviour (see section 3.4). Thus, $GABA_A$ and NMDA receptors were knocked down in PNs as well as synapsin in LNs, both via targeted expression of an RNAi construct against the respective protein. Ca^{2+} imaging was performed from PNs projecting to three glomeruli including DM5 whose odour-evoked PN responses were most substantially reduced after odourant exposure in wildtype flies. Only knockdown of $GABA_A$ receptors in PNs diminished the reductions in the DM5 glomerulus, knockdown of NMDA receptors in PNs or synapsin in LNs did not affect the physiological changes observed (see Figure 3.20 and Figure 3.21).

These findings can be interpreted in at least two different ways. Firstly, RNAi transgene expression against synapsin in LNs and NMDARs in PNs may not have completely knocked down the mRNA of the target proteins and therefore did not block the reductions in odour-evoked neuronal activity induced by odourant exposure despite the proteins being required for the physiological changes. Secondly, the physiological changes detected in this study may not rely on an inhibitory circuit that requires synapsin in LNs and NMDARs in PNs, thus indicating that behavioural olfactory habituation may not underlie the physiological changes described here.

While further experiments are required to clarify whether synapsin and NMDARs were sufficiently knocked down, the notion that the behaviour and the physiology may not be the same can be further supported by the finding that the physiological changes, albeit showing a trend, do not recover within an hour after the habituating protocol (see section 3.3), a time span that is sufficient for behavioural habituation to recover (Das et al., 2011b). Reasons for the discrepancies could be the slightly different induction protocols: The duration of the odourant exposure of the imaging protocol was only 15 minutes compared to 30 minutes for the behaviour, imaged flies were exposed in an odour air stream while for the behavioural tests the flies were exposed in static air and the odour concentration possibly differed between the two protocols (see section 3.2 for a detailed discussion of the differences).

4.3 Peripheral or Central Adaptation?

The adapted protocol for studying the underlying cellular mechanisms of olfactory habituation yielded reduced odour-evoked Ca^{2+} influxes in distinct glomeruli in both, OSN terminals and PN dendrites (see Table 4.1 for a summary). In theory these decreases in sensory neurons may be due to intrinsic changes, generally referred to as sensory adaptations, or to more central mechanisms that could underlie habituation.

Adaptation of the odourant receptor transduction machinery, which is intrinsic to sensory neurons, can contribute substantially to the lowering of odour-evoked neuronal activity (Nagel and Wilson, 2011; Zufall and Leinders-Zufall, 2000). Albeit only investigated in response to relative short odour stimuli, these adaptations recover almost entirely over the course of seconds to minutes (Störtkuhl et al., 1999; Deshpande et al., 2000; Nagel and Wil-

son, 2011; Zufall and Leinders-Zufall, 2000). It was therefore assumed that these adaptations did not substantially contribute to the observed physiological changes as a ten minute air interval was given to ensure that sensory adaptations, which most certainly occurred, recovered before the subsequent odour stimulus was delivered. However, to test this assumption colleague John Lee performed extracellular recordings from the sensillum lymph, so called single sensillum recordings (SSRs), to compare spiking of OSN dendrites housed in a sensillum to the odour stimulus preceding and succeeding odourant exposure (Lee, 2015). SSRs were performed according to the same protocol as the Ca^{2+} imaging and spike rates during the first 500ms of odour-evoked activity of the two odour presentations were compared. Recordings from sensilla that housed OSNs targeting the DM2 and DM5 glomerulus revealed a drop in spiking of -12% and -16%, respectively, following odourant exposure to 3ppm EB. These results show that sensory adaptations in OSNs are not fully recovered after the ten minute air interval following the exposure, however, they also indicate that these adaptations are not sufficient to explain the observed physiological changes. As shown in Table 4.1, decreases in odour-evoked Ca^{2+} influxes in OSN terminals are more pronounced in both OSN types, with decreases of -42% for DM2 and -50% for DM5.

The finding that adaptations in the odourant receptor transduction machinery do not fully explain the physiological changes seen in OSN terminals (and PN dendrites, see Table 4.1), together with the requirement of $GABA_A$ receptors in PNs and $GABA_B$ as well as $GABA_A$ receptors in OSNs (see sections 3.3 and 3.7), points to a central inhibitory mechanisms rather than intrinsic changes in sensory neurons as the underlying mechanisms. A central inhibitory circuit motif would suggest that the physiological changes observed underlie a form of habituation rather than sensory adaptation.

While the synaptic depression model is still the predominant model to explain the underlying mechanisms of habituation it has recently been argued that this model cannot explain all forms of habituation and may just underlie simple forms of habituation (Christoffersen, 1997; Ramaswami, 2014). Classical theories of habituation, like Eugen Sacolovs Stimulus-Model Comparator Theory and Wagner-Konorski Gnostic Unit Theory (outlined in section 1.2.1) are based on an inhibitory motif to suppress the behaviour but have not received much attention due to a lack of experimental support (possibly due to the study of rather simple forms of habituation that are mediated through synaptic depression (Ramaswami, 2014)). Recent advances, however, have identified potentiation of inhibition as the underlying mechanisms for habituation to olfactory and gustatory stimuli in flies (Larkin et al., 2010; Das et al., 2011b; Paranjpe et al., 2012) and habituation to auditory stimuli in mammals (Kato et al., 2015), thus supporting the hypothesis that habituation of more complex percepts may occur through inhibitory circuits (Ramaswami, 2014).

Whether the physiological changes presented here indeed underlie a form of olfactory habituation requires more intense investigation. In particular, it will be necessary to test whether the Ca^{2+} imaging protocol actually induces some kind of behavioural habituation. To do so, it will be required to measure the behaviour directly under the microscope. Due

to the experimental setup where the fly is restricted in a piece of aluminium foil with an open head capsule it is not possible to test for behavioural habituation in one of the common behavioural paradigms. However, recently a technique has been developed that allows the monitoring of both, behaviour and physiology under the microscope (Seelig et al., 2010; Chiappe et al., 2010; Kain et al., 2013). Two-photon Ca^{2+} imaging from neurons in the central brain was performed from head-fixed flies that walked on an air-supported ball. Visual stimuli were presented to the fly and the fly's movements were recorded by tracking the ball's motion. Albeit challenging to setup, a similar technique could potentially be used to measure the physiological changes in OSNs and PNs while at the same time recording the walking speed of the fly. As seen in the established behaviour paradigm, flies' reduce their walking speed upon continuous or repeated odour presentations (see section 3.1).

4.4 Presynaptic vs. Postsynaptic Inhibition

The physiological changes observed in the present study occur at presynaptic terminals, in OSNs, as well as in postsynaptic dendrites, in PNs. Blockade of $GABA_A$ receptors in PNs and $GABA_B$ as well as $GABA_A$ receptors in OSNs diminished or even reversed the changes in odour-evoked Ca^{2+} influxes in these neurons after 15-minute odourant exposure (see sections 3.3 and 3.7, respectively). Thus, GABA receptors are required at the pre- and postsynapse suggesting that pre- and postsynaptic inhibition drive these changes. Presynaptic inhibition in the olfactory system is thought to mediate gain control while postsynaptic inhibition has been suggested to be involved in contrast enhancement and in mediating olfactory habituation (Root et al., 2008; Olsen and Wilson, 2008b; Barth et al., 2014; McGann, 2013; Abraham et al., 2010; Das et al., 2011b).

Presynaptic inhibition onto OSN terminals modulates olfactory responses in the vertebrate and invertebrate nervous system (McGann, 2013; Wang, 2012; Root et al., 2008; Olsen and Wilson, 2008b). It reduces neurotransmitter release from OSNs with the effect of mediating gain control in the olfactory system, thus adjusting the neuronal response to the strength of the odour stimulus: Neuronal responses are lowered in response to high odour concentrations but remain unchanged to low concentrations (McGann, 2013; Wang, 2012; Root et al., 2008; Olsen and Wilson, 2008b). It has been proposed that sensory gain control at OSN terminals preserves synaptic resources during prolonged odourant stimulation, extents the dynamic range of neuronal responses of a certain OSN type, and, as presynaptic inhibition is glomerulus- and thus odourant receptor-specific in vertebrates, 'tunes' different OSN populations to the odourant environment or the behavioural state of the animal (McGann, 2013).

As in the fly antennal lobe, presynaptic inhibition in the mammalian olfactory bulb is mediated via $GABA_B$Rs in the terminals of OSNs (Bonino et al., 1999; Root et al., 2008; Olsen and Wilson, 2008b). The metabotropic receptor triggers a G-protein-mediated second messenger cascade which reduces neurotransmitter release from OSN terminals via down-

regulation of presynaptic Ca^{2+} influx (Chalifoux and Carter, 2011; McGann et al., 2005; Wachowiak et al., 2005; Root et al., 2008). In mammals, presynaptic inhibition occurs through feedback inhibition from uniglomerular GAD65-expressing interneurons that are directly driven by OSNs (GAD65 is an isoform of glutamate decarboxylase and thus indicative for GABA release; Kiyokage et al., 2010; Murphy et al., 2005; Shao et al., 2009; McGann et al., 2005; Pírez and Wachowiak, 2008). In line with this, $GABA_B$-mediated presynaptic inhibition occurs intraglomerular as it only suppresses OSNs of a certain glomerulus and not those that innervate neighbouring glomeruli (McGann et al., 2005). In flies, the local interneuron type that mediates presynaptic inhibition is yet to be identified. A subset of the LN2 class of local interneurons, however, are promising candidates as they arborise within the glomerular rind which coincides with the arborisation of OSN terminals (Okada et al., 2009; Seki et al., 2010; Tanaka et al., 2009, 2012). The arborisation structure of the GABAergic LNs in the *Drosophila* antennal lobe, however, suggests that presynaptic GABAergic inhibition in flies may not be restricted to a single glomerulus. The majority of LNs are multiglomerular or oliglomerular and therefore innervate several glomeruli (Chou et al., 2010; Lai et al., 2008; Okada et al., 2009; Seki et al., 2010; Tanaka et al., 2012). In line with this, intraglomerular inhibition has only been indicated for a few specific OSN types which convey odour information of particular behavioural relevance (Hong and Wilson, 2015).

Besides GABA, dopamine binding to D_2 dopamine receptors in OSN terminals also mediates presynaptic inhibition in the mammalian olfactory bulb (Hsia et al., 1999; Koster et al., 1999). A subpopulation of multiglomerular interneurons that coexpress tyrosine hydroxylase and GAD67, and thus are indicative for releasing dopamine and GABA, are thought to drive dopamine-mediated presynaptic inhibition (Kiyokage et al., 2010). In flies, a few tyrosine hydroxylase-expressing local interneurons have been found (Chou et al., 2010) but whether they are multiglomerular and co-release GABA is unknown. It will be interesting to study whether dopamine likewise has an inhibitory effect on neurotransmitter release from OSNs in the *Drosophila* olfactory system and what the different functions of the two inhibitory neurotransmitters GABA and dopamine are in terms of their modulation of odour-evoked neuronal responses.

Interestingly, mammalian multiglomerular dopamine and GABA co-releasing interneurons undergo long-term plasticity while uniglomerular GABA releasing interneurons appear not to (McGann, 2013). Olfactory deprivation in adult rats results in downregulation of tyrosine hydroxylase and GAD67 expression in multiglomerular interneurons whereas the expression of GAD65 in uniglomerular GABAergic interneurons remains unchanged (Cho et al., 1996; Parrish-Aungst et al., 2011). Although this plasticity occurs over a time span of days rather than minutes, it may still suggest that a homologous interneuron population in the antennal lobe could mediate presynaptic plasticity induced by the 15-minute exposure used in the current study.

In contrast to presynaptic inhibition, postsynaptic inhibition in the *Drosophila* antennal lobe is thought to be mediated through the multiglomerular LN1-type of local interneurons

due to their arborisations in the glomerular core, the location where also PN dendrites reside (Okada et al., 2009; Tanaka et al., 2009, 2012). In mammals, postsynaptic inhibition occurs through GABA-releasing granule cells (Shepherd et al., 2007). Granule cells mediate recurrent and lateral inhibition of mitral cells and are predominantly activated through glutamate-binding onto NMDA receptors (Isaacson and Strowbridge, 1998; Schoppa et al., 1998). Lateral inhibition enhances the contrast between different mitral cells by decorrelation of mitral cell activity evoked by similar stimuli, thus facilitating the discrimination of similar odours (Abraham et al., 2010; Arevian et al., 2008). In line with this, LN1 interneurons in flies have also been implicated in the decorrelation of similar odours (Barth et al., 2014).

Increased postsynaptic inhibition of PN neuronal activity in the fly antennal lobe has further been shown to underlie habituation of an olfactory avoidance response (Das et al., 2011b). While a similar phenomenon has yet to be described in the mammalian olfactory bulb, the mechanisms underlying lateral inhibition are similar to those suggested to suppress PN output in flies during habituation. Lateral inhibition onto mitral cells is gated by postsynaptic firing and the strength of inhibition is dependent on the activity of the postsynaptic mitral cell (Arevian et al., 2008). So far this phenomenon has predominantly been studied with respect to decorrelation of mitral cell activity that is evoked by similar odours (Arevian et al., 2008), however future findings may reveal that a related mechanism is also utilized during olfactory habituation. The strength of recurrent inhibition onto mitral cells which are repeatedly or continuously activated by the same odour could likewise depend on the activity of the respective mitral cell, similar to what has been hypothesized in *Drosophila* (Das et al., 2011b).

4.5 Odour Image or Glomerulus-Specific Inhibition?

To selectively suppress behavioural responses to familiar stimuli, potentiation of inhibition onto active neurons has recently been proposed as a potentially ubiquitous feature of nervous systems (Ramaswami, 2014). The so called 'negative image model' is based on the ability of any pattern of active neurons to project an enhanced inhibitory (or 'negative') image back onto themselves. The inhibitory synaptic weights are suggested to be scaled according to the activity of the active neurons. As the 'negative image' only develops upon repeated or continuous activation of the feedback circuit, salient stimuli evoke only weak 'negative images' and are thus directly transmitted to higher brain centres. Familiar stimuli, on the other hand, encounter strong 'negative images' and their transmission is therefore suppressed yielding in a reduced behavioural output observed during various forms of habituation.

As of yet, this model only constitutes a theoretical frame work, however the findings obtained in the present study largely support this hypothesis. The magnitudes of the changes in odour-evoked Ca^{2+} influxes in distinct neuronal subtypes in OSNs and PNs are largely dependent on naïve odour-evoked responses in the respective neurons. Significant reductions

in odour-evoked responses were mainly observed in those glomeruli that showed strongest activation to the naïve stimulus whereas those only weakly activated did not change (see section 3.3.1 for PNs and section 3.5.1 for OSNs). That these decreases in odour-evoked activity result from potentiation of inhibitory transmission onto these neurons has not explicitly been shown yet but is strongly suggested by the requirement of GABA receptors.

The negative image model assumes that the strength of inhibition is dependent on the activation of the local interneuron network as well as the activation of the certain PN type. PNs that are strongly activated are inhibited more substantially than those that are only weakly activated. However, recent advances have shown that each glomerulus also has a characteristic level of sensitivity to GABAergic inhibition from LNs (Hong and Wilson, 2015; Olsen and Wilson, 2008b; Root et al., 2008). Thus, not only the identity and intensity of an odour stimulus determines the strength of inhibition but also whether the neuronal type it activates is sensitive or insensitive to GABAergic inhibition. Glomeruli that are insensitive to inhibition have been proposed to be encoders of absolute odour concentration while those sensitive to inhibition may encode odour identity as inhibition prevents these glomeruli from saturation and conserves the odour-specific glomerular activation pattern (Hong and Wilson, 2015). The sensitivity to inhibition of a certain glomerulus could further be dependent on how relevant the odour that activates a certain glomerulus is in terms of the fly's odour environment. Being sensitive to inhibition and thus having a large dynamic range may be advantageous for the location of mating partners or food sources (Wang, 2012). Being insensitive to inhibition but sensitive to a weak odour stimulus may, on the other hand, be more important to detect small levels of harmful odours such as CO_2 (Wang, 2012).

While the reduction in odour-evoked OSN and PN responses reported in this study are largely dependent on naïve Ca^{2+} influxes, thus supporting the 'negative image model', differences between the glomeruli are apparent. The glomerulus DM5, for instance, shows an evidently larger percent decrease in odour-evoked activity with respect to its naïve responses than the other glomeruli (see Table 4.1). This may be explained by an increased sensitivity to inhibitory input in the DM5 glomerulus. More interesting, however, is the purpose of this large sensitivity. Little is known about which glomerulus may predominantly encode odour identity, odour concentration or valence, however, the DM5 glomerulus has been linked to mediating aversion (Semmelhack and Wang, 2009). Reducing the activation of the DM5 glomerulus through inhibition could therefore signal a reduced repulsion to the odour stimulus, thus preventing a behavioural action, in line with the reduced behavioural output after olfactory habituation. While reducing the signal propagation of an aversive glomerulus could only account for olfactory habituation to aversive odour stimuli a similar mechanism in a glomerulus mediating appetitive valence could also underlie habituation to appetitive odours. Assuming EB concentrations of 3 and 20ppm indeed elicit behavioural aversion, the DL5 glomerulus may be a potential candidate for mediating appetitive valence. Both OSNs and PNs that project to the DL5 glomerulus are inhibited upon naïve EB presentations (see Figure 3.24 for OSNs and Figure 3.13 for PNs) but mostly show increased odour-evoked

responses following odourant exposure (see Table 4.1). If DL5 mediates appetitive valence, the aversive EB stimulus may initially suppress neuronal activity in the DL5 glomerulus indicating a non-appetitive odour. Following EB exposure, however, EB-evoked responses in DL5 may be suppressed by a smaller degree signalling for a less repulsive odourant. Notably, this interpretation contrasts findings of a previous study which identified DL5 as an aversive glomerulus (Knaden et al., 2012).

The glomeruli DL1, DM1, and DM6 reduce their odour-evoked responses to a similar degree (see Table 4.1) suggesting that these glomeruli have comparable sensitivities to inhibition and may simply encode odour identity. Lowering neuronal activity in these glomeruli may only serve to prevent saturation to preserve the EB-specific glomerular activation pattern that is transmitted to higher brain areas. The DM3 glomerulus, albeit showing trends, does not exhibit significant reductions in odour-evoked neuronal responses following odourant exposure (see Table 4.1) which may indicate that this glomerulus is an encoder for absolute odour concentration. Neuronal activity in this glomeruli may be positively correlated with odour intensity. OSNs and PNs which innervate DM3 exhibit larger neuronal activity in response to 20ppm than 3ppm EB stimulation. However, this holds true for most of the glomeruli studied. The interpretation of the physiological changes associated with the DM2 glomerulus is difficult. Odour-evoked neuronal activity in OSNs targeting DM2 was decreased following odourant exposure while the responses of their respective PNs were increased (see Table 4.1) suggesting that they may be modulated by an excitatory local interneuron network in the AL. How this modulation occurs and to what purpose will have to be addressed by future studies.

4.6 A Modified Neuronal Circuit Model

Ca^{2+} imaging experiments performed in this study revealed that both, OSN terminals and PN dendrites projecting to distinct glomeruli exhibit reductions in odour-evoked Ca^{2+} influxes following short-term odourant exposure (see results chapters 3.3 and 3.5, respectively). Both, OSNs and PNs showed largely coinciding decreases in the DL1, DM1, DM5, and DM6 glomeruli (see Table 4.1). OSNs and PNs projecting to the same glomerulus displayed similar amplitudes in these changes, with the exception of DM2 whose responses are believed to be modulated by the AL interneuron network. The most likely explanation of these observations is that the adaptations predominantly occur in presynaptic OSN terminals whereas the decrements seen in the PN postsynapse are possibly largely due to reduced excitatory input from OSNs (see section 3.5.3 for a more detailed discussion). The presynaptic locus for the changes is further supported by the requirement of $GABA_B$ receptors in OSNs as RNAi-mediated blockade of a $GABA_B$ receptor subunit in OSNs diminished the physiological changes observed (see section 3.7). Future experiments will have to determine whether $GABA_B$ receptors are also required in glomeruli beyond the three studied here. To support the claim that the changes in PNs are predominantly transmitted from the OSN presynapse

it should further be investigated whether $GABA_B$ receptor knockdown in OSNs diminishes the changes seen in PNs in a similar way as in OSNs.

The requirement of $GABA_B$ receptors for the synaptic plasticity observed indicates that the physiological changes are evoked by increased inhibition onto the presynaptic OSN terminals. Indeed, $GABA_B$ receptor-mediated adaptations in the OSN axon terminals that act over a time scale of tens of minutes have been described previously (Murmu et al., 2011). These adaptations require Ca^{2+} release from intracellular Ca^{2+} stores as both, IP3R and RyRs, Ca^{2+} release channels prevalent in intracellular Ca^{2+} stores, are required (Murmu et al., 2011). Whether the physiological changes observed in the present study also rely on Ca^{2+} release from intracellular stores remains to be studied. Alteration in basal Ca^{2+} levels in OSNs following 15-minute odourant exposure were indicated by shifts in GCaMP baseline fluorescence (see Figure 3.28 and discussion 3.3.5). However, baseline Ca^{2+} levels were decreased while Ca^{2+} release from intracellular would be expected to increase the intracellular Ca^{2+} concentration suggesting that changes in baseline Ca^{2+} concentration most likely rely on an independent mechanism. Reductions in baseline Ca^{2+} levels can theoretical result from decreased spontaneous activity or increased clearance of Ca^{2+} from the cytoplasm (see discussion 3.3.5 for details).

The observed presynaptic adaptation possibly mediate gain control to adjust the dynamic range of a given neuron and prevent saturation, as reported previously (Olsen and Wilson, 2008b; Root et al., 2008; Wang, 2012). So far, studies on presynaptic gain control either presented short odour stimuli (Olsen and Wilson, 2008b; Root et al., 2008) or did not differentiate between different glomeruli (Murmu et al., 2011). To our knowledge, this is the first study that reports gain control in distinct glomeruli to 15-minute odour stimulation.

Besides the presynaptically occurring changes in odour-evoked Ca^{2+} influxes, postsynaptically induced changes were implicated by the requirement of $GABA_A$ receptors in PNs projecting to DM5 (see Figure 3.20). As implied by behavioural habituation experiments (Das et al., 2011b), postsynaptic changes in odour-evoked neuronal activity may reduce PN output as salient odour stimuli become familiar with the effect of preventing behavioural output. To elucidate the role of postsynaptic inhibition it will be necessary to investigate whether the physiological decrements observed in other PNs, namely DL1, DM1, and DM6, are also partially mediated by $GABA_A$Rs in PNS. In principle, postsynaptic inhibition could also target a specific set of glomeruli, for instance those that mediate aversion. Candidates are DL1 and DM5 as they have been implicated in negative valence (Knaden et al., 2012; Semmelhack and Wang, 2009; Strutz et al., 2014). Reducing odour-evoked activity in glomeruli mediating aversion could yield in a decreased behavioural aversion. Alternatively, reducing activity in all odour-responsive PNs may be necessary to diminish repulsion.

The purpose of presynaptic inhibition could therefore predominantly be to adjust the dynamic range of a neuron to ensure that the properties of an odour stimuli are transferred to higher brain regions while postsynaptic inhibition could suppress PN output to familiar stimuli. If postsynaptic inhibition indeed suppresses PN output to familiar stimuli low

concentrated odour stimuli should only induce postsynaptic inhibition but not presynaptic inhibition as the dynamic range in that case does not require adjustments. Future research will have to address this hypothesis. If presynaptic and postsynaptic inhibition indeed have different functions they are possibly mediated by two different classes of local interneurons. As mentioned previously, the arborisation patterns of the two interneuron types LN1 and LN2 indicate that a subset of the LN2 class may provide inhibition onto the OSN presynapse while the LN1 class may innervate the PN postsynapse (Tanaka et al., 2009). LN1 and LN2 are thus good candidates for mediating the changes in odour-evoked Ca^{2+} influxes in OSNs and PNs, respectively.

Ca^{2+} imaging performed from LN1 and LN2 interneurons did not reveal any differences in odour-evoked Ca^{2+} responses (see section 3.5.2) suggesting that neuronal activity remains unchanged after 15-minute exposure. However, neuronal spiking does not necessarily have to change for synaptic plasticity to occur in these neurons. To test whether neurotransmitter release from LN1 and LN2 interneurons was increased, synaptopHluorin imaging was performed without detecting any fluorescence increases upon odour presentation. However, there are technical restraints associated with synaptopHluorin that appear to limit its usefulness as a reporter of transmitter release (discussed in 3.6.3). In future, a GABA sensor, currently developed by the Looger lab, will hopefully be available to quantify GABA release from LN1 and LN2 local interneurons. To identify whether output from either of these neuronal types is necessary for pre- or postsynaptic inhibition, transmitter release from these neurons can be blocked in different ways and its impact on the changes in odour-evoked OSN or PN Ca^{2+} influxes can be studied. If the LN2 population indeed mediates the presynaptic changes, blockade of LN2 output will prevent the changes that occur in OSNs similarly to $GABA_B$ receptor knockdown in OSNs. If LN1 neurons, on the other hand, mediate postsynaptic inhibition preventing neurotransmitter release from these neurons will not block the presynaptic changes in OSNs but those observed in PNs similarly to $GABA_A$ receptor knockdown in PNs.

All together, a model is proposed where 15-minute odourant exposure to a medium to high odour concentration results in increased presynaptic and postsynaptic inhibition (see Figure 4.1). Presynaptic inhibition, potentially from a subset of LN2 interneurons, mediates gain control to ensure the transfer of the odour information to higher brain centres without saturation of the neuronal responses. Postsynaptic inhibition, believed to be mediated through LN1 interneurons, is proposed to suppress neuronal responses to familiar odourants, thus preventing behavioural output to non-salient stimuli.

4.7 Concluding Remarks

Inhibition, in the form of feedforward and feedback inhibition, greatly shapes spontaneous and sensory-evoked neuronal excitations throughout cortical areas in the human brain (Isaacson and Scanziani, 2011). The effects of inhibition are numerous. It lowers membrane poten-

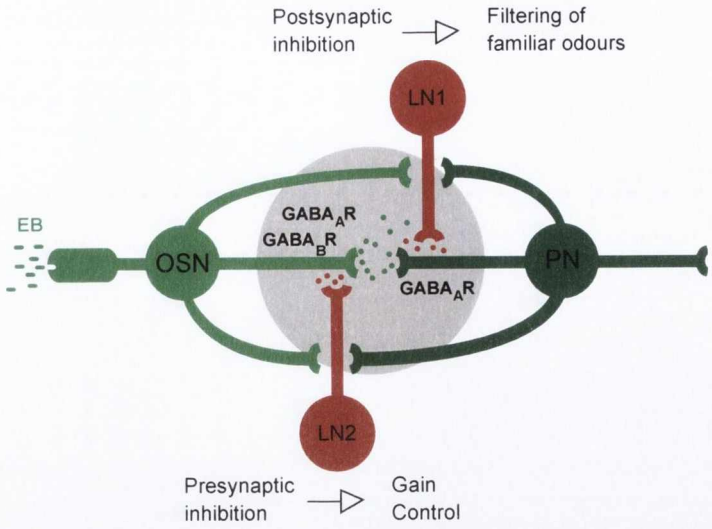


Figure 4.1: Increased pre- and postsynaptic inhibition following odourant exposure
The findings in the present study point to a model where increased GABA-mediated pre- and postsynaptic inhibition decreases odour-evoked neuronal activity in PNs following 15-minute odourant exposure. Presynaptic inhibition is thought to mediate gain control to allow the transmission of odour information to higher brain centres and requires both $GABA_A$ and $GABA_B$ receptors in OSN terminals. Postsynaptic inhibition is thought to suppress neuronal responses to familiar odours, thus filtering the odour information that is transmitted, and requires $GABA_A$ receptors in PNs. Due to their arborisation patterns in the antennal lobes, presynaptic inhibition is thought to be mediated by a subset of LN2 LNs while postsynaptic inhibition is proposed to occur through LN1-type LNs.

tials thus preventing the generation of action potentials or the release of neurotransmitters, it sharpens sensory-evoked neuronal responses and can be tuned to an 'optimal' sensory stimulus (Isaacson and Scanziani, 2011). Recurrent as well as lateral inhibition and its associated synaptic plasticity occurs pre- and postsynaptically (Castillo et al., 2011; Kullmann et al., 2012).

Here, a form of synaptic plasticity is presented that occurs at both presynaptic OSN terminals and postsynaptic PN dendrites in the *Drosophila* antennal lobe, a brain structure analogous to the mammalian olfactory bulb (Stevens, 2015). This neuronal circuit has the advantage that it is substantial simpler than cortical circuits while each neuronal type can be labelled and manipulated separately enabling the study of synaptic changes in great detail. The *Drosophila* AL is, thus, an ideal location to study the effects of short-term synaptic plasticity on neuronal information processing.

5. Appendices

5.1 Appendix I: Fly Crosses

Results Sections	Genotype	Figures
3.1		
CS	$\frac{+}{+};\frac{+}{+};\frac{+}{+}$	3.1, 3.2, 3.3, 3.4
rut^{2080}	$\frac{rut^{2080}}{rut^{2080}};\frac{+}{+};\frac{+}{+}$	3.2
$rut^{2080};UAS-rut^{+}$	$\frac{rut^{2080}}{rut^{2080}};\frac{UAS-rut^{+}}{UAS-rut^{+}};\frac{+}{+}$	3.1, 3.3, 3.4
$Gad1-Gal4>UAS-rutRNAi$	$\frac{+}{+};\frac{Gad1-Gal4}{+};\frac{UAS-rutRNAi}{+}$	3.4
$LN1-Gal4>UAS-rutRNAi$	$\frac{+}{+};\frac{LN1-Gal4}{+};\frac{UAS-rutRNAi}{+}$	3.4
$GH146-Gal4>UAS-dsNR1RNAi$	$\frac{GH146-Gal4}{+};\frac{+}{+};\frac{UAS-dsNR1RNAi}{+}$	3.4
$Gad1-Gal4>rut^{2080};UAS-rut^{+}$	$\frac{rut^{2080}}{rut^{2080}};\frac{Gad1-Gal4}{UAS-rut^{+}};\frac{+}{+}$	3.4
$LN1-Gal4>rut^{2080};UAS-rut^{+}$	$\frac{rut^{2080}}{rut^{2080}};\frac{LN1-Gal4}{UAS-rut^{+}};\frac{+}{+}$	3.4
3.2		
$GH146-QF,UAS-GFP$	$\frac{+}{+};\frac{+}{+};\frac{GH146-QF,UAS-GFP}{GH146-QF,UAS-GFP}$	2.3, 3.6
$GH146-Gal4,UAS-GCaMP3$	$\frac{+}{+};\frac{+}{+};\frac{GH146-Gal4,UAS-GCaMP3}{GH146-Gal4,UAS-GCaMP3}$	3.8
$GH146-Gal4,UAS-GCaMP6m$	$\frac{+}{+};\frac{GH146-Gal4,UAS-GCaMP6m}{GH146-Gal4,UAS-GCaMP6m};\frac{+}{+}$	3.10

3.3		
$GH146-Gal4,UAS-GCaMP6m$	$\frac{+}{+};\frac{GH146-Gal4,UAS-GCaMP6m}{GH146-Gal4,UAS-GCaMP6m};\frac{+}{+}$	3.11, 3.12, 3. 3.14, 3.15, 3. 3.17, 3.18, 3.
3.4		
$GH146-Gal4,UAS-GCaMP6m;$ $UAS-dsNR1RNAi$	$\frac{+}{+};\frac{GH146-Gal4,UAS-GCaMP6m}{GH146-Gal4,UAS-GCaMP6m};\frac{UAS-dsNR1RNAi}{+}$	3.20
$GH146-Gal4,UAS-GCaMP6m;$ $UAS-RDL-RNAi$	$\frac{+}{+};\frac{GH146-Gal4,UAS-GCaMP6m}{GH146-Gal4,UAS-GCaMP6m};\frac{UAS-RDL-RNAi}{+}$	3.20
$GH146-Gal4,UAS-GCaMP6m$	$\frac{+}{+};\frac{GH146-Gal4,UAS-GCaMP6m}{GH146-Gal4,UAS-GCaMP6m};\frac{+}{+}$	3.20
$GH146-LexA,LexAop-GCaMP3/$ $LN1-Gal4;UAS-synRNAi$	$\frac{+}{+};\frac{GH146-LexA,LexAop-GCaMP3}{LN1-Gal4,LexAop-GCaMP3};\frac{UAS-synRNAi}{+}$	3.21
$GH146-LexA,LexAop-GCaMP3/$ $LN1-Gal4$	$\frac{+}{+};\frac{GH146-LexA,LexAop-GCaMP3}{LN1-Gal4,LexAop-GCaMP3};\frac{+}{+}$	3.21
3.5		
$Or83b-Gal4,UAS-GCaMP6m$	$\frac{+}{+};\frac{+}{+};\frac{Or83b-Gal4,UAS-GCaMP6m}{Or83b-Gal4,UAS-GCaMP6m}$	3.23, 3.24, 3. 3.27, 3.26, 3.
$LN1-Gal4;UAS-GCaMP6m$	$\frac{+}{+};\frac{LN1-Gal4}{LN1-Gal4};\frac{UAS-GCaMP6m,Or83b-RFP}{UAS-GCaMP6m,Or83b-RFP}$	3.29
$LN2-Gal4;UAS-GCaMP6m$	$\frac{LN2-Gal4}{LN2-Gal4};\frac{+}{+};\frac{UAS-GCaMP6m,Or83b-RFP}{UAS-GCaMP6m,Or83b-RFP}$	3.30
$OK371-Gal4;UAS-GCaMP6m$	$\frac{+}{+};\frac{OK371-Gal4}{OK371-Gal4};\frac{UAS-GCaMP6m,Or83b-RFP}{UAS-GCaMP6m,Or83b-RFP}$	3.31

3.6		
$GH146-Gal4;UAS-ArcD$	$\frac{+}{+};\frac{GH146-Gal4}{+};\frac{UAS-ArcD}{UAS-ArcD}$	3.32, 3.33, 3.34, 3.35
$Or83b-Gal,UAS-ArcD$	$\frac{+}{+};\frac{+}{+};\frac{Or83b-Gal4,UAS-ArcD}{Or83b-Gal4,UAS-ArcD}$	3.35
$LN1-Gal4;UAS-ArcD$	$\frac{+}{+};\frac{LN1-Gal4}{LN1-Gal4};\frac{UAS-ArcD,Or83b-RFP}{UAS-ArcD,Or83b-RFP}$	3.35
$LN2-Gal4;UAS-ArcD$	$\frac{LN2-Gal4}{LN2-Gal4};\frac{+}{+};\frac{UAS-ArcD,Or83b-RFP}{UAS-ArcD,Or83b-RFP}$	3.35
$LN1-Gal4;UAS-spH$	$\frac{+}{+};\frac{LN1-Gal4}{LN1-Gal4};\frac{UAS-spH,Or83b-RFP}{UAS-spH,Or83b-RFP}$	not shown
$LN2-Gal4;UAS-spH$	$\frac{LN2-Gal4}{LN2-Gal4};\frac{+}{+};\frac{UAS-spH,Or83b-RFP}{UAS-spH,Or83b-RFP}$	not shown
3.7		
$Or83b-Gal4,UAS-GCaMP6m/UAS-GABA_BR2-RNAi$	$\frac{UAS-GBi}{+};\frac{+}{+};\frac{Or83b-Gal4,UAS-GCaMP6m}{UAS-GABA_BR2-RNAi}$	3.36
$Or83b-Gal4,UAS-GCaMP6m/UAS-RDL-RNAi$	$\frac{+}{+};\frac{+}{+};\frac{Or83b-Gal4,UAS-GCaMP6m}{UAS-RDL-RNAi}$	3.37
$Or83b-Gal4,UAS-GCaMP6m$	$\frac{+}{+};\frac{+}{+};\frac{Or83b-Gal4,UAS-GCaMP6m}{+}$	3.36, 3.37

5.2 Appendix II: Statistical Tables

Experiment	Test	Experimental and Null Model
Section 3.3		
GH146 x GCaMP6m		
Comparing 3ppm EB and KCl	Effect of Stimulation	Exp: AUC010 = Stimulation + Glomerulus + Stimulation:Glomerulus Null: AUC010 = Glomerulus
Comparing naïve and exposed/mock (for 3ppm EB, 20ppm EB and mock)	Effect of Run	Exp: AUC010 = Run + Glomerulus + Run:Glomerulus Null: AUC010 = Glomerulus
Comparing baselines (for 3ppm EB, 20ppm EB and mock)	Effect of Run	Exp: Baseline = Run + Glomerulus + Run:Glomerulus Null: Baseline = Glomerulus
Comparing overall responses of 3ppm and 20ppm EB stimulation	Effect of Concentration	Exp: AUC010 = Run + Concentration + Glomerulus + Run:Glomerulus + Concentration*Run + Glomerulus*Concentration Null: AUC010 = Run + Glomerulus + Run:Glomerulus
Comparing exposure-induced changes of 3ppm and 20ppm EB stimulation	Effect of Concentration*Run	Exp: AUC010 = Run + Concentration + Glomerulus + Run:Glomerulus + Concentration*Run + Glomerulus*Concentration Null: AUC010 = Run + Concentration + Glomerulus + Run:Glomerulus + Glomerulus*Concentration
Comparing naïve, exposed and recovery (for 3ppm EB, 20ppm EB and mock)	Effect of Run	Exp: AUC010 = Run + Glomerulus + Run:Glomerulus Null: AUC010 = Glomerulus
Comparing naïve, exposed and recovery of a single glomerulus (for 3ppm EB, 20ppm EB and mock)	Effect of Run	Exp: AUC010 = Run Null: AUC010 = 1
Section 3.4		
GH146,GCaMP6m;RdlRNAi, ***GH146,GCaMP6m;dsNR1RNAi,*** ***GH146,GCaMP3 x LN1;synRNAi*** and ***GH146,GCaMP6m***		
Comparing naïve responses of different genotypes	Effect of Genotype	Exp: AUC010 = Glomerulus + Genotype + Genotype:Glomerulus Null: AUC010 = Glomerulus
Comparing naïve and exposed of different genotypes	Effect of Genotype*Run	Exp: AUC010 = Run + Glomerulus + Genotype + Run:Glomerulus + Genotype:Run + Genotype:Glomerulus Null: AUC010 = Run + Glomerulus + Genotype + Run:Glomerulus + Genotype:Glomerulus
Comparing naïve and exposed of different genotypes and a single glomerulus	Effect of Genotype*Run	Exp: AUC010 = Run + Genotype + Genotype:Run Null: AUC010 = Run + Genotype
Section 3.5		
Or83b x GCaMP6m		
Comparing naïve and exposed (for 3ppm EB, 20ppm EB and mock)	Effect of Run	Exp: AUC010 = Run + Glomerulus + Run:Glomerulus Null: AUC010 = Glomerulus
Comparing baselines (for 3ppm EB, 20ppm EB and mock)	Effect of Run	Exp: Baseline = Run + Glomerulus + Run:Glomerulus Null: Baseline = Glomerulus

Comparing 3ppm and 20ppm EB	Effect of Concentration	Exp: AUC010 = Run + Concentration + Glomerulus + Run:Glomerulus + Concentration*Run + Glomerulus*Concentration Null: AUC010 = Run + Glomerulus + Run:Glomerulus
Comparing 3ppm and 20ppm EB	Effect of Concentration*Run	Exp: AUC010 = Run + Concentration + Glomerulus + Run:Glomerulus + Concentration*Run + Glomerulus*Concentration Null: AUC010 = Run + Concentration + Glomerulus + Run:Glomerulus + Glomerulus*Concentration
Comparing naïve, exposed and recovery (for 3ppm EB and 20ppm EB)	Effect of Run	Exp: AUC010 = Run + Glomerulus + Run:Glomerulus Null: AUC010 = Glomerulus
Comparing naïve, exposed and recovery of a single glomerulus (for 3ppm EB and 20ppm EB)	Effect of Run	Exp: AUC010 = Run Null: AUC010 = 1
LN1 x GCaMP6m, LN2 x GCaMP6m and OK371 x GCaMP6m		
Comparing naïve and exposed	Effect of Run	Exp: AUC010 = Run + Glomerulus + Run:Glomerulus Null: AUC010 = Glomerulus
Section 3.6		
GH146 x ArcD		
Comparing naïve and exposed (for 3ppm EB and mock)	Effect of Run	Exp: AUC010 = Run + Glomerulus + Run:Glomerulus Null: AUC010 = Glomerulus
Comparing baselines (for 3ppm EB and mock)	Effect of Run	Exp: Baseline = Run + Glomerulus + Run:Glomerulus Null: Baseline = Glomerulus
Comparing naïve responses of 3ppm and mock experiments	Effect of Protocol	Exp: AUC010 = Glomerulus + Protocol + Protocol:Glomerulus Null: AUC010 = Glomerulus
Comparing naïve and exposed of 3ppm and mock experiments	Effect of Protocol*Run	Exp: AUC010 = Run + Glomerulus + Protocol + Run:Glomerulus + Protocol:Run + Protocol:Glomerulus Null: AUC010 = Run + Glomerulus + Protocol + Run:Glomerulus + Protocol:Glomerulus
Section 3.7		
Or83b,GCaMP6m;GABA$_B$R2-RNAi, Or83b,GCaMP6m;RDL-RNAi **and** ***Or83b-Gal4,UAS-GCaMP6m***		
Comparing naïve responses of different genotypes	Effect of Genotype	Exp: AUC010 = Glomerulus + Genotype + Genotype:Glomerulus Null: AUC010 = Glomerulus
Comparing naïve and exposed of different genotypes	Effect of Genotype*Run	Exp: AUC010 = Run + Glomerulus + Genotype + Run:Glomerulus + Genotype:Run + Genotype:Glomerulus Null: AUC010 = Run + Glomerulus + Genotype + Run:Glomerulus + Genotype:Glomerulus
Comparing naïve and exposed of different genotypes and a single glomerulus	Effect of Genotype*Run	Exp: AUC010 = Run + Genotype + Genotype:Run Null: AUC010 = Run + Genotype

Table 5.1: Likelihood ratio test models *Figure legend on following page.*

Table 5.1: Likelihood ratio test models
Likelihood ratio test models used to perform *linear mixed effects analyses fit by maximum likelihood.* The column 'Experiment' briefly describes the comparison that was made with the respective *likelihood ratio test*, the column 'Test' depicts the effect that was tested and the column 'Experimental and Null Model' displays the full model with the effect in question (Exp) and the model without the effect in question (Null). Linear mixed effects models were fitted with fixed effects including *stimulation* (EB, KCl), *glomerulus* (DL1, DL5, DM1, DM2, DM3, DM5, DM6), *run* ('naïve','exposed'/'mock','recovery'/'1hr after mock'), *concentration* (3ppm, 20ppm), *genotype* (control, experimental) and protocol (3ppm exposure, mock exposure) and their respective interaction terms (see Table). Random intercept model were fitted with *fly* as the random effect. *AUC010* refers to the area under the curve of the indicator's response during the 10-second odour stimulus. In the case where *run* was a fixed effect, *AUC010* includes data collected from different runs. Otherwise *AUC010* only includes data to the 'naïve' odour presentation. *Baseline* refers to the baseline fluorescence.

A

	Model	df	AIC	BIC	logLik	Test	L.Ratio	p-value
ExpModel	1	16	933.9878	977.4838	-450.9939			
NullModel	2	9	936.0600	960.5265	-459.0300	1 vs 2	16.07221	0.0245

B

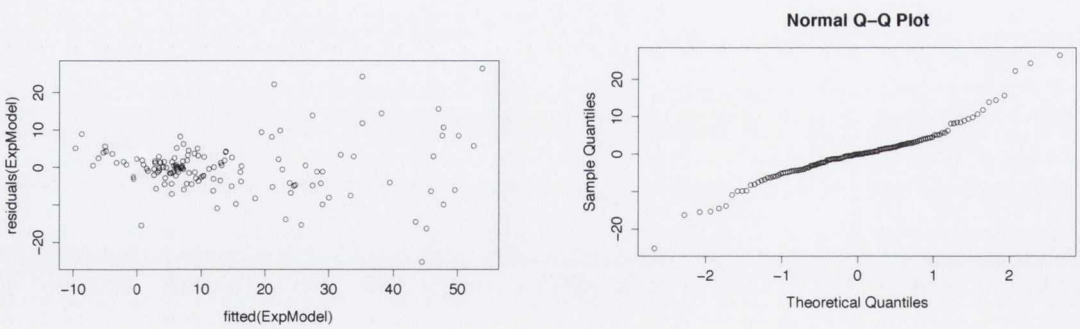


Table 5.2: Linear mixed effects analysis for GH146GCaMP6m 3ppm EB and KCl

	DL1	DL5	DM1	DM2	DM3	DM5	DM6
Number of Glomeruli	7	6	10	10	6	10	7
Number of Flies	7	6	10	10	6	10	7
Mean of Peak Response Change	12.4503	10.1001	0.97969	17.7262	4.2111	30.9976	26.1956
SEM of Peak Response Change	4.7808	3.2216	2.4077	8.3604	2.055	11.1872	6.5934
95% Confidence Interval	[0.75217 24.1484]	[1.8187 18.3816]	[-4.4669 6.4263]	[-1.1862 36.6387]	[-1.0714 9.4936]	[5.6903 56.3048]	[10.0622 42.329]
Anderson-Darling Normality Test (0.05)	n.s.; p=0.1088	n.s.; p=0.12251	n.s.; p=0.52338	p=0.0005	n.s.; p=0.91562	n.s.; p=0.29822	n.s.; p=0.7246
One-Sample Student T-Test (0.05)	p=0.040431; t=2.6042; df=6	p=0.025809; t=3.1351; df=5	n.s.; p=0.69359; t=0.4069; df=9	NaN	n.s.; p=0.09574; t=2.0492; df=5	p=0.021725; t=2.7708; df=9	p=0.0073415; t=3.973; df=6
Wilcoxon Signed Rank Test (0.05)	NaN	NaN	NaN	p=0.0039062; Signed Rank=54	NaN	NaN	NaN

Table 5.3: Paired comparisons for GH146GCaMP6m 3ppm EB and KCl

A

```
          Model df      AIC      BIC    logLik   Test  L.Ratio p-value
ExpModel      1 16 2701.936 2764.290 -1334.968
NullModel     2  9 2777.653 2812.727 -1379.826 1 vs 2 89.71665  <.0001


Linear mixed-effects model fit by maximum likelihood
 Data: reorganisedData
       AIC     BIC    logLik
  2701.936 2764.29 -1334.968

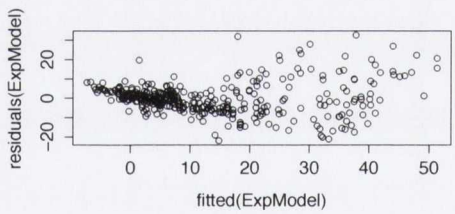
Random effects:
 Formula: ~1 | Fly
        (Intercept) Residual
StdDev:     5.55798 8.660872

Fixed effects: AUC010 ~ Run + Glomerulus + Run:Glomerulus
                            Value Std.Error  DF   t-value p-value
(Intercept)             15.583591  2.238264 305  6.962357  0.0000
RunRun2                 -5.611263  2.793047 305 -2.009011  0.0454
Glomerulusdl5          -18.155537  3.041327 305 -5.969611  0.0000
Glomerulusdm1          -10.281045  2.718093 305 -3.782447  0.0002
Glomerulusdm2           -8.665222  2.731664 305 -3.172140  0.0017
Glomerulusdm3          -13.527242  2.719813 305 -4.973592  0.0000
Glomerulusdm5           24.913422  2.713294 305  9.181985  0.0000
Glomerulusdm6           19.624950  2.710531 305  7.240261  0.0000
RunRun2:Glomerulusdl5    6.968418  4.266450 305  1.633306  0.1034
RunRun2:Glomerulusdm1    4.995835  3.539641 305  1.411396  0.1591
RunRun2:Glomerulusdm2    6.204734  3.539641 305  1.752927  0.0806
RunRun2:Glomerulusdm3    4.981331  3.818991 305  1.304358  0.1931
RunRun2:Glomerulusdm5  -13.480040  3.519944 305 -3.829618  0.0002
RunRun2:Glomerulusdm6   -4.544295  3.781804 305 -1.201621  0.2304

Standardized Within-Group Residuals:
       Min         Q1        Med         Q3        Max
-2.52496641 -0.5624520 -0.04661995  0.42072211  3.76476573

Number of Observations: 364
Number of Groups: 46
```

B



C

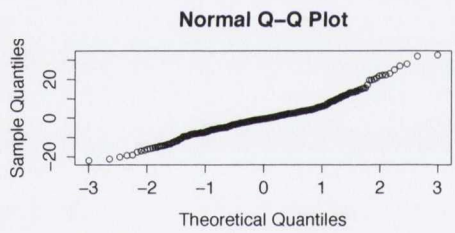
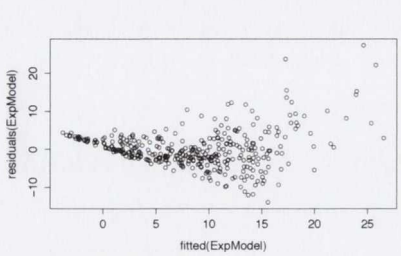


Table 5.4: Linear mixed effects analysis for GH146GCaMP6m 3ppm EB

A

```
          Model df      AIC      BIC    logLik   Test  L.Ratio p-value
ExpModel      1 16 2357.212 2419.566 -1162.606
NullModel     2  9 2404.310 2439.385 -1193.155 1 vs 2 61.09849  <.0001
```

B



C

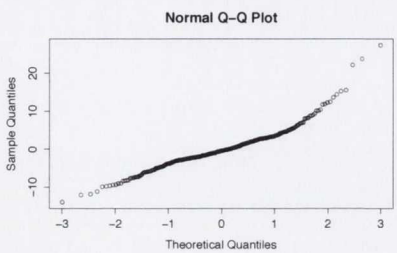


Table 5.5: Linear mixed effects analysis for GH146GCaMP6m 3ppm EB baseline

	DL1	DL5	DM1	DM2	DM3	DM5	DM6
Number of Glomeruli	20	15	33	33	23	34	24
Number of Flies	20	15	29	28	23	29	24
Mean of Naive Response (0-10sec)	16.6846	-1.2498	5.1619	6.6027	2.5554	39.9358	35.3869
SEM of Naive Response	3.3047	0.55701	0.57305	0.9528	1.4185	2.8083	3.2558
Mean of Response Change (0-10sec)	-5.6113	1.3572	-0.61543	0.59347	-0.62992	-19.0913	-10.1556
SEM of Response Change	2.4064	0.53636	0.37303	0.68331	1.0163	2.6177	2.9312
95% Confidence Interval	[-10.648 -0.57452]	[0.20678 2.5075]	[-1.3753 0.14441]	[-0.7984 1.9853]	[-2.7376 1.4778]	[-24.4171 -13.7655]	[-16.2191 -4.092]
Anderson-Darling Normality Test (0.05)	p=0.00093378	n.s.; p=0.081896	n.s.; p=0.54841	n.s.; p=0.46211	p=0.012456	n.s.; p=0.39955	n.s.; p=0.82517
One-Sample Student T-Test (0.05)	NaN	p=0.024016; t=2.5303; df=14	n.s.; p=0.10876; t=-1.6498; df=32	n.s.; p=0.39158; t=0.86852; df=32	NaN	p=2.2771e-08; t=-7.293; df=33	p=0.0021012; t=-3.4647; df=23
Wilcoxon Signed Rank Test (0.05)	p=0.030365; z=-2.1653	NaN	NaN	NaN	n.s.; p=0.95149; z=-0.06083	NaN	NaN
Mean of Baseline Change	-1.8651	-2.3516	-0.76926	-8.116	-6.1548	2.7997	-3.1368
SEM of Baseline Change	0.62408	1.2013	0.22307	1.3489	1.0994	1.433	1.2275
95% Confidence Interval	[-3.1713 -0.55891]	[-4.9282 0.22492]	[-1.2236 -0.31489]	[-10.8637 -5.3683]	[-8.4349 -3.8747]	[-0.1157 5.7151]	[-5.6761 -0.59755]
Anderson-Darling Normality Test (0.05)	n.s.; p=0.77871	p=0.0014842	p=0.0005	n.s.; p=0.16726	n.s.; p=0.25102	n.s.; p=0.49113	n.s.; p=0.73768
One-Sample Student T-Test (0.05)	p=0.0075499; t=-2.9886; df=19	NaN	NaN	p=1.0346e-06; t=-6.0166; df=32	p=1.2545e-05; t=-5.5981; df=22	n.s.; p=0.059247; t=1.9538; df=33	p=0.017683; t=-2.5555; df=23
Wilcoxon Signed Rank Test (0.05)	NaN	n.s.; p=0.072998; Signed Rank=28	p=0.00022451; z=-3.6897	NaN	NaN	NaN	NaN

Table 5.6: Paired comparisons for GH146GCaMP6m 3ppm EB

A

```
          Model df      AIC      BIC    logLik   Test  L.Ratio p-value
ExpModel      1 16 2120.394 2177.730 -1044.197
NullModel     2  9 2199.826 2232.077 -1090.913 1 vs 2 93.43215  <.0001

Linear mixed-effects model fit by maximum likelihood
 Data: reorganisedData
       AIC     BIC    logLik
  2120.394 2177.73 -1044.197

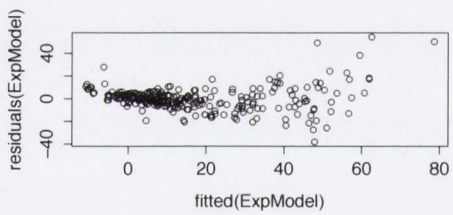
Random effects:
 Formula: ~1 | Fly
        (Intercept) Residual
StdDev:    7.364849  11.1692

Fixed effects: AUC010 ~ Run + Glomerulus + Run:Glomerulus
                          Value Std.Error  DF   t-value p-value
(Intercept)            32.36360  2.936816 219 11.019963  0.0000
RunRun2               -12.25722  3.628795 219 -3.377766  0.0009
Glomerulusdl5         -34.33683  3.773997 219 -9.098267  0.0000
Glomerulusdm1         -26.21449  3.745362 219 -6.999187  0.0000
Glomerulusdm2         -27.12320  3.691435 219 -7.347604  0.0000
Glomerulusdm3         -23.59392  4.019292 219 -5.870168  0.0000
Glomerulusdm5          14.03441  3.745362 219  3.747143  0.0002
Glomerulusdm6          22.97989  3.936345 219  5.837877  0.0000
RunRun2:Glomerulusdl5  12.48720  5.272517 219  2.368356  0.0187
RunRun2:Glomerulusdm1   9.72595  5.070429 219  1.918170  0.0564
RunRun2:Glomerulusdm2  13.22967  5.013901 219  2.638599  0.0089
RunRun2:Glomerulusdm3  10.51003  5.543076 219  1.896065  0.0593
RunRun2:Glomerulusdm5 -18.34153  5.070429 219 -3.617352  0.0004
RunRun2:Glomerulusdm6  -6.86236  5.443193 219 -1.260722  0.2088

Standardized Within-Group Residuals:
       Min         Q1        Med         Q3        Max
-3.40840699 -0.39602329 0.01400248 0.35140633 4.87739468

Number of Observations: 266
Number of Groups: 34
```

B



C

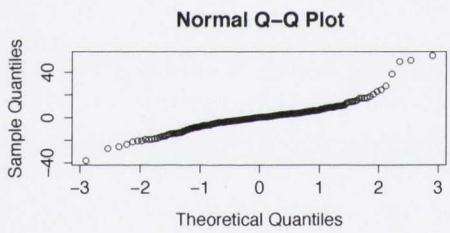
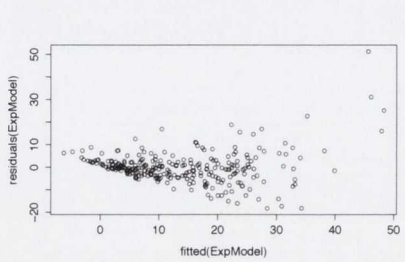


Table 5.7: Linear mixed effects analysis for GH146GCaMP6m 20ppm EB

A

```
          Model df      AIC      BIC    logLik   Test  L.Ratio p-value
ExpModel      1 16 1942.541 1999.877 -955.2706
NullModel     2  9 1973.594 2005.846 -977.7971 1 vs 2 45.05297  <.0001
```

B



C

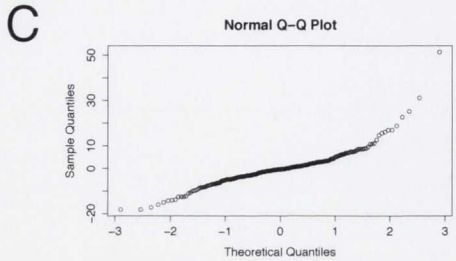


Table 5.8: Linear mixed effects analysis for GH146GCaMP6m 20ppm EB baseline

	DL1	DL5	DM1	DM2	DM3	DM5	DM6
Number of Glomeruli	20	18	21	22	15	21	16
Number of Flies	20	18	21	22	15	21	16
Mean of Naive Response (0-10sec)	31.1538	-1.6295	5.9614	5.3624	9.491	46.2103	55.534
SEM of Naive Response	4.5061	1.6842	0.8262	0.85995	2.114	4.9994	7.1633
Mean of Response Change (0-10sec)	-12.2572	0.22997	-2.5313	0.97245	-1.7472	-30.5987	-19.1196
SEM of Response Change	2.3422	1.4233	0.65849	0.83851	1.1086	3.8134	3.3883
95% Confidence Interval	[-17.1594 -7.355]	[-2.773 3.233]	[-3.9049 -1.1577]	[-0.77133 2.7162]	[-4.1248 0.63046]	[-38.5533 -22.6442]	[-26.3416 -11.8976]
Anderson-Darling Normality Test (0.05)	n.s.; p=0.076024	p=0.0016066	n.s.; p=0.32125	n.s.; p=0.34056	n.s.; p=0.99	n.s.; p=0.23726	n.s.; p=0.99
One-Sample Student T-Test (0.05)	p=4.7343e-05; t=-5.2333; df=19	NaN	p=0.0010128; t=-3.8441; df=20	n.s.; p=0.25917; t=1.1597; df=21	n.s.; p=0.13733; t=-1.5761; df=14	p=1.1127e-07; t=-8.0241; df=20	p=4.6781e-05; t=-5.6428; df=15
Wilcoxon Signed Rank Test (0.05)	NaN	n.s.; p=0.21454; z=1.2412	NaN	NaN	NaN	NaN	NaN
Mean of Baseline Change	-2.806	-3.381	-1.4704	-12.7041	-7.9619	-2.6621	-7.1192
SEM of Baseline Change	0.94242	1.4473	0.50338	1.6954	2.6292	2.6608	1.4222
95% Confidence Interval	[-4.7785 -0.83349]	[-6.4345 -0.32747]	[-2.5204 -0.42033]	[-16.2299 -9.1783]	[-13.6009 -2.3229]	[-8.2124 2.8883]	[-10.1506 -4.0878]
Anderson-Darling Normality Test (0.05)	n.s.; p=0.095998	n.s.; p=0.25965	p=0.029379	n.s.; p=0.15039	p=0.030206	n.s.; p=0.69809	n.s.; p=0.087608
One-Sample Student T-Test (0.05)	p=0.0077385; t=-2.9774; df=19	p=0.031992; t=-2.3361; df=17	NaN	p=2.3128e-07; t=-7.4933; df=21	NaN	n.s.; p=0.32903; t=-1.0005; df=20	p=0.00015664; t=-5.0057; df=15
Wilcoxon Signed Rank Test (0.05)	NaN	NaN	p=0.0057232; z=-2.7632	NaN	p=0.0020142; Signed Rank=9	NaN	NaN

Table 5.9: Paired comparisons for GH146GCaMP6m 20ppm EB

A

```
         Model df      AIC      BIC    logLik   Test  L.Ratio p-value
ExpModel     1 24 4834.575 4941.273 -2393.288
NullModel    2 16 4877.318 4948.449 -2422.659 1 vs 2 58.74247  <.0001


Linear mixed-effects model fit by maximum likelihood
 Data: reorganisedData
      AIC      BIC    logLik
  4834.575 4941.273 -2393.288

Random effects:
 Formula: ~1 | Fly
        (Intercept) Residual
StdDev:    6.377668 9.865366

Fixed effects: AUC010 ~ Run + Concentration + Glomerulus + Run * Glomerulus +      Concentration * Run + Glomerulus * Concentration
                                    Value Std.Error  DF   t-value p-value
(Intercept)                     16.114612  2.323605 530  6.935177  0.0000
RunRun2                         -6.688129  2.388913 530 -2.799653  0.0053
Concentration20ppm              15.698985  2.944055  78  5.332435  0.0000
Glomerulusdl5                  -19.612882  2.977468 530 -6.587102  0.0000
Glomerulusdm1                  -11.310045  2.777680 530 -4.071760  0.0001
Glomerulusdm2                  -10.166803  2.791648 530 -3.641865  0.0003
Glomerulusdm3                  -14.729304  2.728519 530 -5.398278  0.0000
Glomerulusdm5                   25.726297  2.776898 530  9.264401  0.0000
Glomerulusdm6                   19.985375  2.721115 530  7.344552  0.0000
RunRun2:Glomerulusdl5            9.880765  3.340627 530  2.957757  0.0032
RunRun2:Glomerulusdm1            7.074626  2.968206 530  2.383468  0.0175
RunRun2:Glomerulusdm2            9.230082  2.955690 530  3.122818  0.0019
RunRun2:Glomerulusdm3            7.390422  3.221731 530  2.293929  0.0222
RunRun2:Glomerulusdm5          -15.081713  2.957473 530 -5.099526  0.0000
RunRun2:Glomerulusdm6           -5.256146  3.179826 530 -1.652967  0.0989
RunRun2:Concentration20ppm      -4.492225  1.630402 530 -2.755287  0.0061
Concentration20ppm:Glomerulusdl5 -13.403674  3.414328 530 -3.925714  0.0001
Concentration20ppm:Glomerulusdm1 -13.573004  3.364224 530 -4.034513  0.0001
Concentration20ppm:Glomerulusdm2 -14.947837  3.349323 530 -4.462943  0.0000
Concentration20ppm:Glomerulusdm3  -7.282188  3.366030 530 -2.163435  0.0310
Concentration20ppm:Glomerulusdm5 -13.316020  3.365941 530 -3.956106  0.0001
Concentration20ppm:Glomerulusdm6   2.210098  3.326100 530  0.664471  0.5067

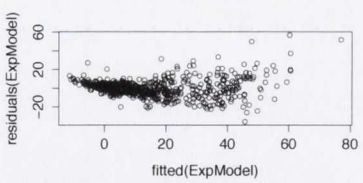
Standardized Within-Group Residuals:
       Min         Q1        Med         Q3        Max
-3.63766108 -0.48128937 -0.02850893  0.40463617 5.75432138

Number of Observations: 630
Number of Groups: 80
```

B

```
         Model df      AIC      BIC    logLik   Test  L.Ratio p-value
ExpModel     1 24 4834.575 4941.273 -2393.288
NullModel    2 23 4840.386 4942.637 -2397.193 1 vs 2 7.810427  0.0052
```

C



D

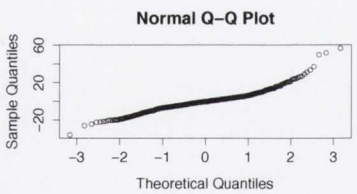


Table 5.10: Linear mixed effects analysis for GH146GCaMP6m comparing 3ppm and 20ppm EB Testing for Concentration (A) and Concentration * Run (B)

A

```
         Model df      AIC      BIC    logLik   Test  L.Ratio p-value
ExpModel     1 16 2120.394 2177.730 -1044.197
NullModel    2  9 2199.826 2232.077 -1090.913 1 vs 2 93.43215  <.0001
```

```
Linear mixed-effects model fit by maximum likelihood
 Data: reorganisedData
       AIC      BIC    logLik
  2579.043 2667.041 -1266.521

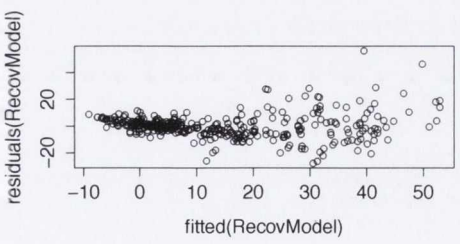
Random effects:
 Formula: ~1 | Fly
        (Intercept) Residual
StdDev:    5.508867 9.511962

Fixed effects: AUC010 ~ Run + Glomerulus + Run:Glomerulus
                              Value Std.Error  DF   t-value p-value
(Intercept)                9.213819  3.257515 292  2.828481  0.0050
RunRun1                    7.923545  4.187695 292  1.892102  0.0595
RunRun3                    8.303045  4.187695 292  1.982724  0.0483
Glomerulusdl5            -11.020636  4.430686 292 -2.487343  0.0134
Glomerulusdm1             -3.510700  3.845540 292 -0.912928  0.3620
Glomerulusdm2              0.306550  3.867655 292  0.079260  0.9369
Glomerulusdm3            -10.144486  4.053312 292 -2.502765  0.0129
Glomerulusdm5             14.300075  3.867655 292  3.697350  0.0003
Glomerulusdm6             18.130369  4.000876 292  4.531600  0.0000
RunRun1:Glomerulusdl5     -9.342169  6.242647 292 -1.496508  0.1356
RunRun3:Glomerulusdl5    -11.262413  6.242647 292 -1.804108  0.0722
RunRun1:Glomerulusdm1     -7.496937  5.128858 292 -1.461717  0.1449
RunRun3:Glomerulusdm1     -9.040685  5.128858 292 -1.762709  0.0790
RunRun1:Glomerulusdm2     -8.579438  5.128858 292 -1.672777  0.0954
RunRun3:Glomerulusdm2    -10.553399  5.128858 292 -2.057651  0.0405
RunRun1:Glomerulusdm3     -8.407289  5.689957 292 -1.477566  0.1406
RunRun3:Glomerulusdm3     -9.891729  5.689957 292 -1.738454  0.0832
RunRun1:Glomerulusdm5     13.268486  5.128858 292  2.587025  0.0102
RunRun3:Glomerulusdm5      0.034882  5.128858 292  0.006801  0.9946
RunRun1:Glomerulusdm6      2.669905  5.596043 292  0.477106  0.6336
RunRun3:Glomerulusdm6     -0.061588  5.596043 292 -0.011006  0.9912

Standardized Within-Group Residuals:
       Min         Q1        Med         Q3        Max
-3.40840699 -0.39602329  0.01400248  0.35140633  4.87739468

Number of Observations: 266
Number of Groups: 34
```

B



C

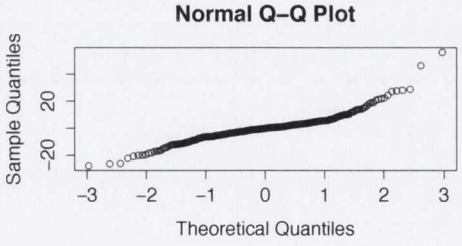
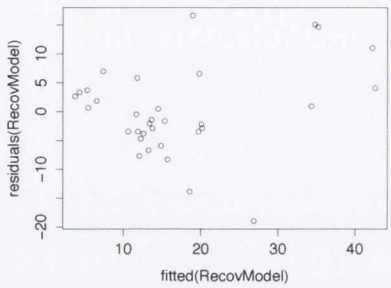


Table 5.11: Linear mixed effects analysis for GH146GCaMP6m 3ppm EB recovery

A

```
           Model df      AIC      BIC    logLik   Test  L.Ratio p-value
RecovModel     1  5 265.7070 273.1895 -127.8535
baseline       2  3 267.1635 271.6530 -130.5817 1 vs 2 5.456497  0.0653
```

B



C

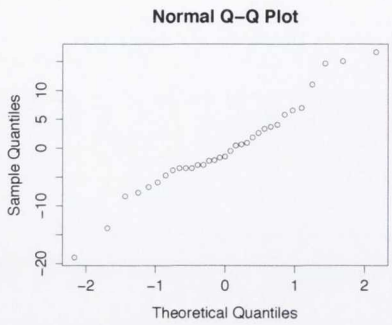


Table 5.12: Linear mixed effects analysis for GH146GCaMP6m 3ppm EB recovery DL1

A

```
           Model df      AIC      BIC    logLik   Test  L.Ratio p-value
RecovModel     1  5 119.3274 125.8066 -54.66372
baseline       2  3 126.1040 129.9915 -60.05199 1 vs 2 10.77654  0.0046
```

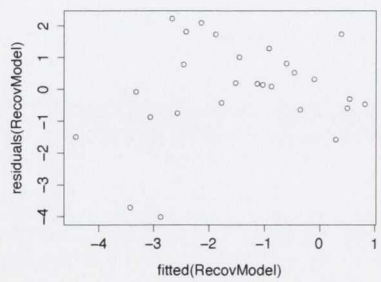
```
        Pairwise comparisons using t tests with pooled SD

data:  reorganisedData$AUC010 and reorganisedData$Run

     Run1   Run2
Run2 0.1451 -
Run3 0.1149 0.0044

P value adjustment method: none
```

B



C

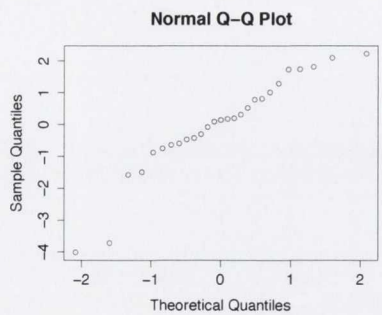


Table 5.13: Linear mixed effects analysis for GH146GCaMP6m 3ppm EB recovery DL5

A

```
          Model df      AIC      BIC    logLik   Test  L.Ratio p-value
RecovModel     1  5 289.3354 300.2836 -139.6677
baseline       2  3 293.0859 299.6549 -143.5430 1 vs 2 7.750579  0.0207
```

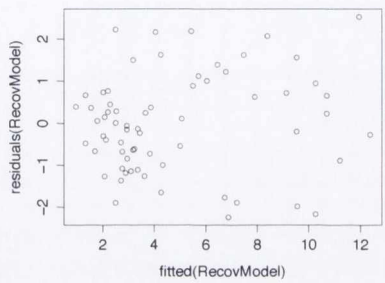
```
        Pairwise comparisons using t tests with pooled SD

data:  reorganisedData$AUC010 and reorganisedData$Run

     Run1 Run2
Run2 0.68 -
Run3 0.27 0.48

P value adjustment method: none
```

B



C

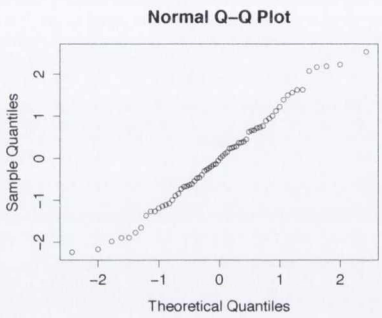
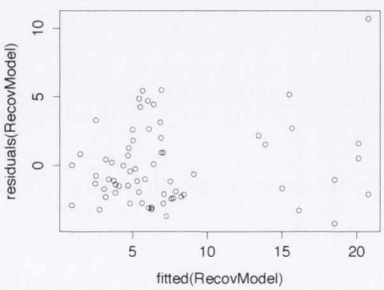


Table 5.14: Linear mixed effects analysis for GH146GCaMP6m 3ppm EB recovery DM1

A

```
          Model df      AIC      BIC    logLik   Test  L.Ratio p-value
RecovModel     1  5 390.5914 401.5396 -190.2957
baseline       2  3 391.9203 398.4893 -192.9601 1 vs 2 5.328935  0.0696
```

B



C

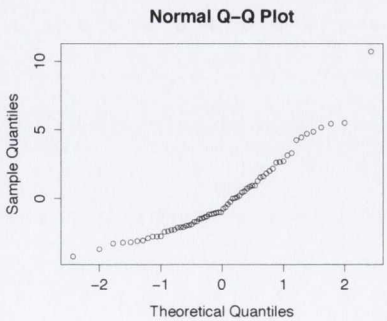
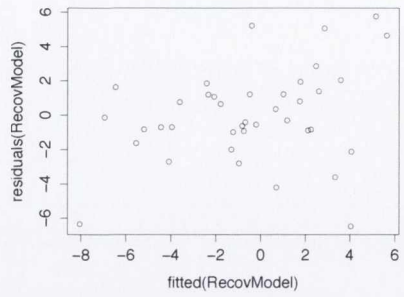


Table 5.15: Linear mixed effects analysis for GH146GCaMP6m 3ppm EB recovery DM2

A

```
           Model df      AIC      BIC    logLik   Test  L.Ratio p-value
RecovModel     1  5 231.5668 239.8846 -110.7834
baseline       2  3 229.2449 234.2356 -111.6225 1 vs 2 1.678102  0.4321
```

B



C

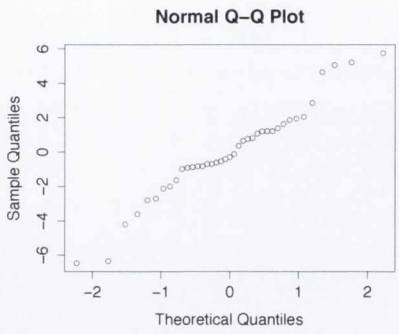


Table 5.16: Linear mixed effects analysis for GH146GCaMP6m 3ppm EB recovery DM3

A

```
           Model df      AIC      BIC    logLik   Test  L.Ratio p-value
RecovModel     1  5 546.7531 557.7013 -268.3765
baseline       2  3 569.4281 575.9971 -281.7141 1 vs 2 26.67508  <.0001
```

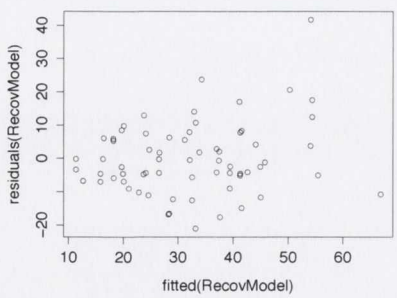
```
        Pairwise comparisons using t tests with pooled SD

data:  reorganisedData$AUC010 and reorganisedData$Run

     Run1    Run2
Run2 4.1e-05 -
Run3 0.0095  0.0876

P value adjustment method: none
```

B



C

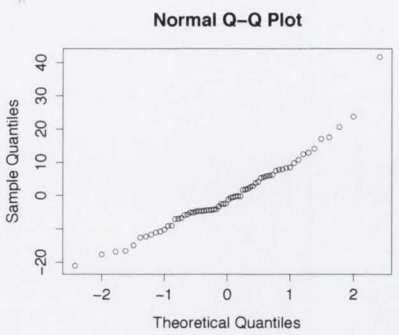
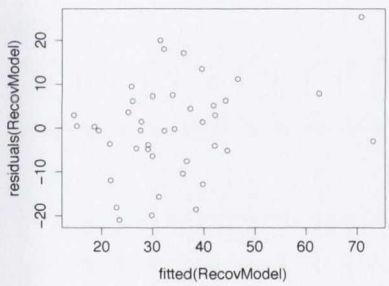


Table 5.17: Linear mixed effects analysis for GH146GCaMP6m 3ppm EB recovery DM5

A

	Model	df	AIC	BIC	logLik	Test	L.Ratio	p-value
RecovModel	1	5	361.3679	370.0563	-175.6840			
baseline	2	3	362.5210	367.7340	-178.2605	1 vs 2	5.153032	0.076

B



C

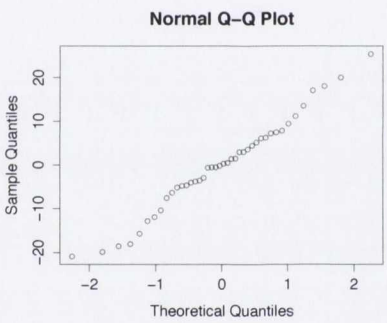


Table 5.18: Linear mixed effects analysis for GH146GCaMP6m 3ppm EB recovery DM6

A

```
          Model df       AIC      BIC    logLik   Test  L.Ratio p-value
RecovModel     1 23  962.3322 1028.637 -458.1661
baseline       2  9 1025.1456 1051.091 -503.5728 1 vs 2 90.81345  <.0001

Linear mixed-effects model fit by maximum likelihood
 Data: reorganisedData
       AIC      BIC    logLik
  962.3322 1028.637 -458.1661

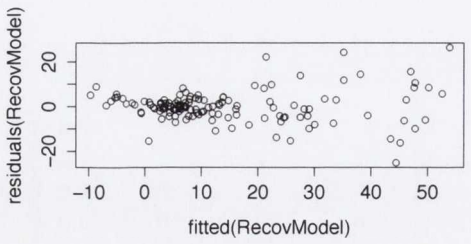
Random effects:
 Formula: ~1 | Fly
        (Intercept) Residual
StdDev:    3.556714 7.351233

Fixed effects: AUC010 ~ Run + Glomerulus + Run:Glomerulus
                            Value Std.Error  DF   t-value p-value
(Intercept)             16.232976  3.296222 100  4.924722  0.0000
RunRun1                 12.767886  4.285008 100  2.979664  0.0036
RunRun3                 -6.260329  4.285008 100 -1.460984  0.1472
Glomerulusdl5          -18.063523  4.473283 100 -4.038091  0.0001
Glomerulusdm1          -11.936915  4.685066 100 -2.547865  0.0124
Glomerulusdm2           -8.395977  4.685066 100 -1.792072  0.0761
Glomerulusdm3           -9.173559  4.507045 100 -2.035382  0.0445
Glomerulusdm5           -1.756327  4.685066 100 -0.374878  0.7085
Glomerulusdm6           17.063951  4.313632 100  3.955820  0.0001
RunRun1:Glomerulusdl5 -16.353019  6.307361 100 -2.592688  0.0109
RunRun3:Glomerulusdl5   7.372287  6.307361 100  1.168839  0.2452
RunRun1:Glomerulusdm1  -9.384947  6.307361 100 -1.487936  0.1399
RunRun3:Glomerulusdm1   6.058785  6.307361 100  0.960590  0.3391
RunRun1:Glomerulusdm2 -11.977682  6.307361 100 -1.899001  0.0604
RunRun3:Glomerulusdm2   7.140762  6.307361 100  1.132131  0.2603
RunRun1:Glomerulusdm3 -12.164269  6.307361 100 -1.928583  0.0566
RunRun3:Glomerulusdm3   3.377695  6.307361 100  0.535516  0.5935
RunRun1:Glomerulusdm5  21.190298  6.307361 100  3.359614  0.0011
RunRun3:Glomerulusdm5  16.453879  6.307361 100  2.608679  0.0105
RunRun1:Glomerulusdm6   1.665743  6.059916 100  0.274879  0.7840
RunRun3:Glomerulusdm6  -4.374729  6.059916 100 -0.721912  0.4720

Standardized Within-Group Residuals:
        Min          Q1         Med          Q3         Max
-3.425216417 -0.501256592 -0.008647327  0.394993937  3.592032698

Number of Observations: 132
Number of Groups: 12
```

B



C

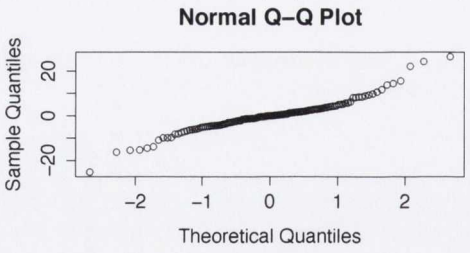


Table 5.19: Linear mixed effects analysis for GH146GCaMP6m 20ppm EB recovery

A

```
           Model df      AIC      BIC    logLik   Test  L.Ratio p-value
RecovModel     1  5 162.0190 167.2416 -76.00949
baseline       2  3 173.0235 176.1570 -83.51173 1 vs 2 15.00449   6e-04
```

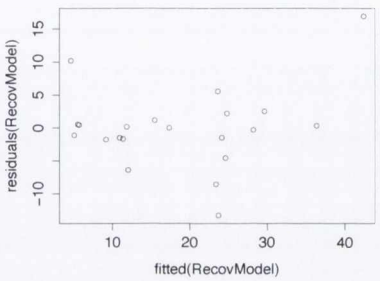
```
        Pairwise comparisons using t tests with pooled SD

data:  reorganisedData$AUC010 and reorganisedData$Run

     Run1   Run2
Run2 0.0474 -
Run3 0.0053 0.3106

P value adjustment method: none
```

B



C

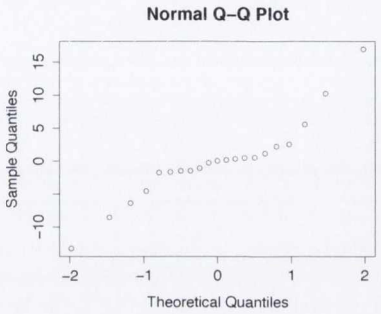


Table 5.20: Linear mixed effects analysis for GH146GCaMP6m 20ppm EB recovery DL1

A

```
           Model df      AIC      BIC    logLik   Test  L.Ratio p-value
RecovModel     1  5 102.7495 107.2014 -46.37477
baseline       2  3 104.7647 107.4358 -49.38233 1 vs 2 6.015126  0.0494
```

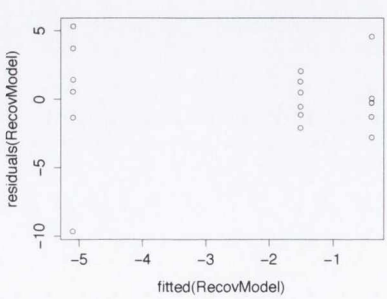
```
        Pairwise comparisons using t tests with pooled SD

data:  reorganisedData$AUC010 and reorganisedData$Run

     Run1  Run2
Run2 0.095 -
Run3 0.034 0.589

P value adjustment method: none
```

B



C

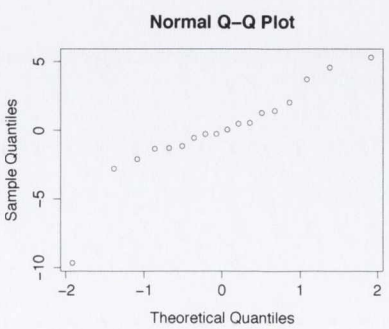


Table 5.21: Linear mixed effects analysis for GH146GCaMP6m 20ppm EB recovery DL5

A

```
          Model df      AIC      BIC    logLik   Test  L.Ratio p-value
RecovModel     1  5 94.80596  99.25782 -42.40298
baseline       2  3 99.06423 101.73534 -46.53211 1 vs 2 8.258265  0.0161

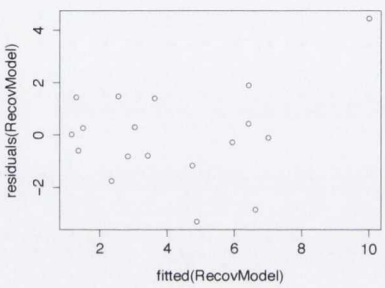

        Pairwise comparisons using t tests with pooled SD

data:  reorganisedData$AUC010 and reorganisedData$Run

     Run1  Run2
Run2 0.082 -
Run3 0.067 0.913

P value adjustment method: none
```

B



C

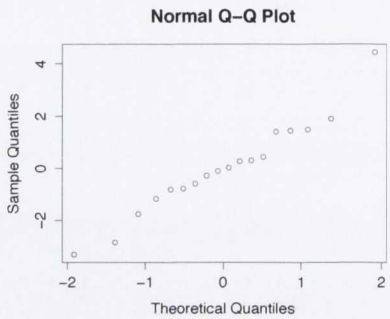
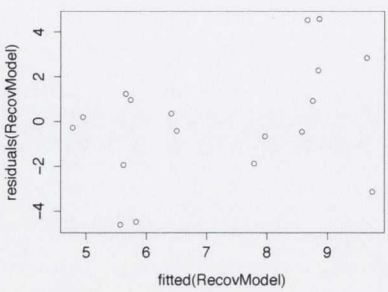


Table 5.22: Linear mixed effects analysis for GH146GCaMP6m 20ppm EB recovery DM1

A

```
          Model df      AIC      BIC    logLik   Test   L.Ratio p-value
RecovModel     1  5 104.5452 108.9971 -47.27260
baseline       2  3 100.8839 103.5551 -47.44197 1 vs 2 0.3387489  0.8442
```

B



C

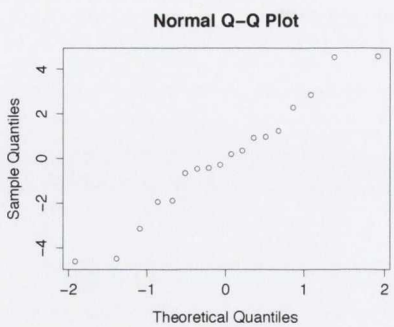
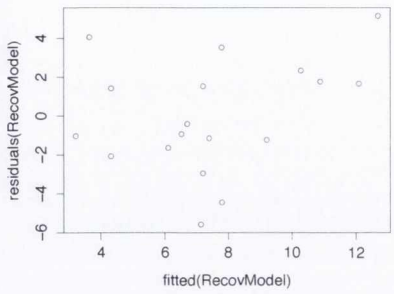


Table 5.23: Linear mixed effects analysis for GH146GCaMP6m 20ppm EB recovery DM2

A

```
           Model df      AIC      BIC    logLik   Test  L.Ratio p-value
RecovModel     1  5 109.6525 114.1044 -49.82626
baseline       2  3 109.1639 111.8350 -51.58196 1 vs 2 3.511394  0.1728
```

B



C

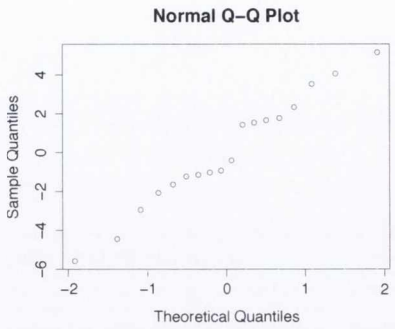


Table 5.24: Linear mixed effects analysis for GH146GCaMP6m 20ppm EB recovery DM3

A

```
           Model df      AIC      BIC    logLik   Test  L.Ratio p-value
RecovModel     1  5 142.4133 146.8652 -66.20666
baseline       2  3 159.3933 162.0644 -76.69664 1 vs 2 20.97997  <.0001

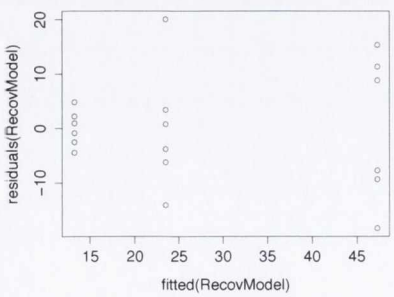

        Pairwise comparisons using t tests with pooled SD

data:  reorganisedData$AUC010 and reorganisedData$Run

     Run1   Run2
Run2 5e-05  -
Run3 0.0014 0.1130

P value adjustment method: none
```

B



C

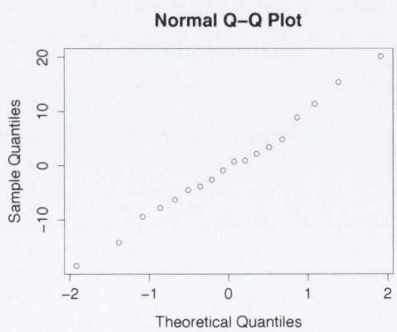


Table 5.25: Linear mixed effects analysis for GH146GCaMP6m 20ppm EB recovery DM5

A

```
          Model df      AIC      BIC    logLik   Test  L.Ratio p-value
RecovModel     1  5 177.3777 182.6003 -83.68885
baseline       2  3 185.0505 188.1841 -89.52526 1 vs 2 11.67283  0.0029
```

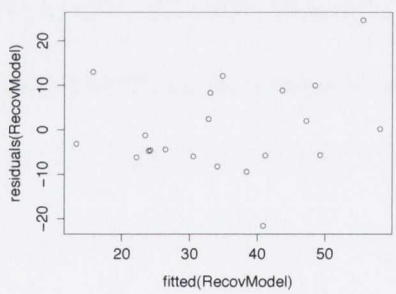
```
        Pairwise comparisons using t tests with pooled SD

data:  reorganisedData$AUC010 and reorganisedData$Run

     Run1   Run2
Run2 0.0870 -
Run3 0.0056 0.1989

P value adjustment method: none
```

B



C

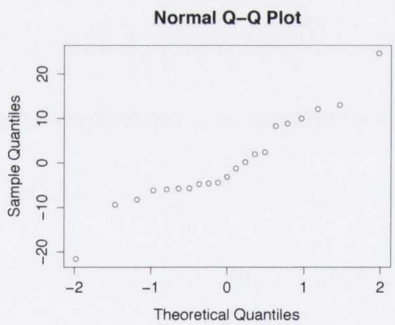
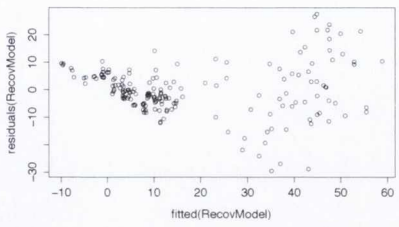


Table 5.26: Linear mixed effects analysis for GH146GCaMP6m 20ppm EB recovery DM6

A

	Model	df	AIC	BIC	logLik	Test	L.Ratio	p-value
RecovModel	1	23	1419.811	1493.629	-686.9053			
baseline	2	9	1401.139	1430.024	-691.5695	1 vs 2	9.328375	0.8095

B



C

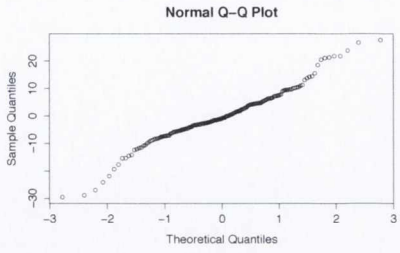
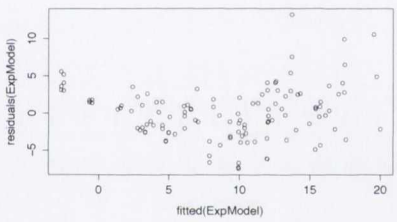


Table 5.27: Linear mixed effects analysis for GH146GCaMP6m mock

A

	Model	df	AIC	BIC	logLik	Test	L.Ratio	p-value
ExpModel	1	16	724.0861	768.9505	-346.0431			
NullModel	2	9	714.7956	740.0318	-348.3978	1 vs 2	4.709472	0.6954

B



C

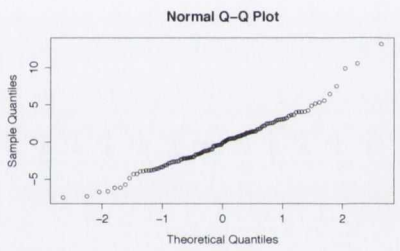
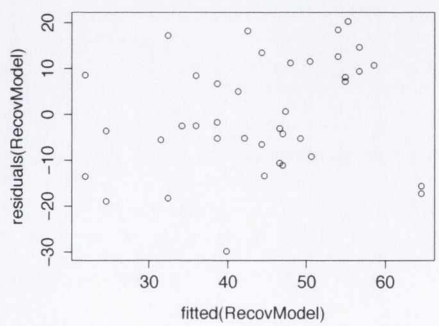


Table 5.28: Linear mixed effects analysis for GH146GCaMP6m mock baseline

A

	Model	df	AIC	BIC	logLik	Test	L.Ratio	p-value
RecovModel	1	5	334.0355	342.3533	-162.0177			
baseline	2	3	334.2151	339.2058	-164.1076	1 vs 2	4.179659	0.1237

B



C

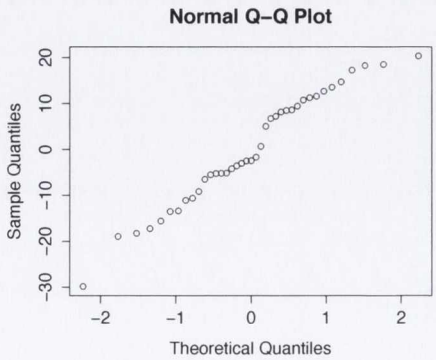
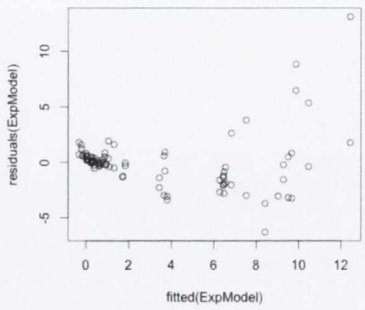


Table 5.29: Linear mixed effects analysis for GH146GCaMP6m mock DM5

A

	Model	df	AIC	BIC	logLik	Test	L.Ratio	p-value
ExpModel	1	8	442.9843	462.6191	-213.4921			
NullModel	2	5	442.2248	454.4965	-216.1124	1 vs 2	5.240505	0.155

B



C

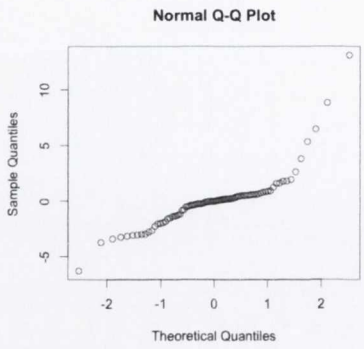
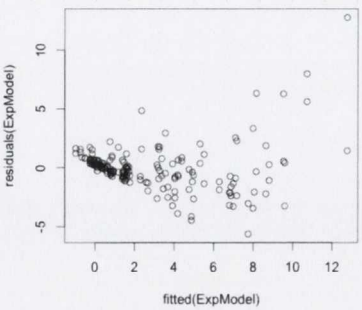


Table 5.30: Linear mixed effects analysis comparing naïve responses of flies expressing Rdl-RNAi in PNs and controls

A

	Model	df	AIC	BIC	logLik	Test	L.Ratio	p-value
ExpModel	1	12	798.5052	836.2751	-387.2526			
NullModel	2	11	798.8441	833.4665	-388.4220	1 vs 2	2.338933	0.1262

B



C

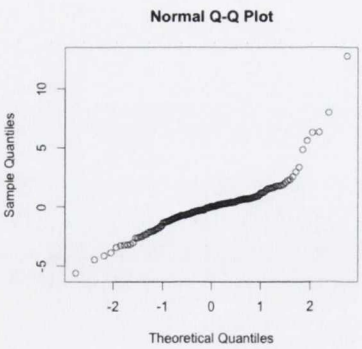
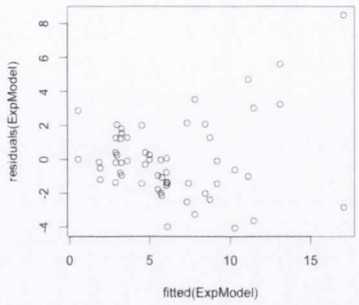


Table 5.31: Linear mixed effects analysis comparing naïve and exposed responses of flies expressing Rdl-RNAi in PNs and controls

A

	Model	df	AIC	BIC	logLik	Test	L.Ratio	p-value
ExpModel	1	6	316.0518	328.4145	-152.0259			
NullModel	2	5	317.9048	328.2071	-153.9524	1 vs 2	3.85303	0.0497

B



C

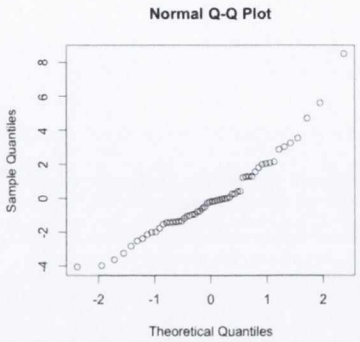
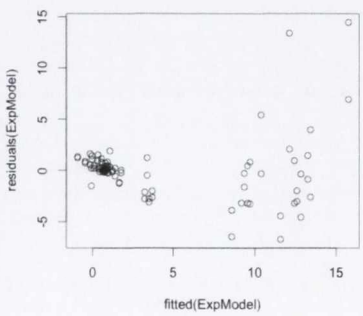


Table 5.32: Linear mixed effects analysis comparing naïve and exposed responses of flies expressing Rdl-RNAi in PNs and controls in DM5

A

	Model	df	AIC	BIC	logLik	Test	L.Ratio	p-value
ExpModel	1	8	447.6358	466.7914	-215.8179			
NullModel	2	5	447.7181	459.6903	-218.8590	1 vs 2	6.082248	0.1077

B



C

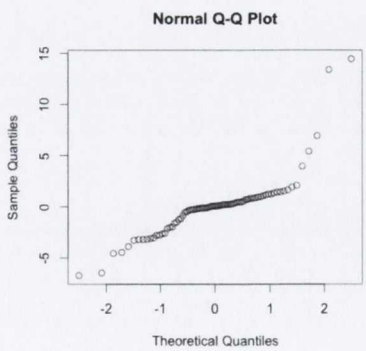
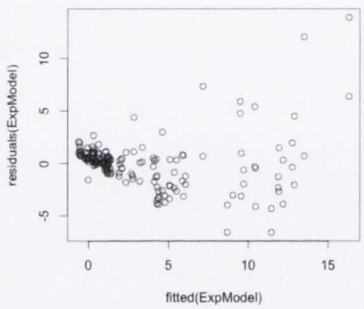


Table 5.33: Linear mixed effects analysis comparing naïve responses of flies expressing NR1-RNAi in PNs and controls

A

	Model	df	AIC	BIC	logLik	Test	L.Ratio	p-value
ExpModel	1	12	816.8523	853.9035	-396.4262			
NullModel	2	11	815.2002	849.1637	-396.6001	1 vs 2	0.3478125	0.5554

B



C

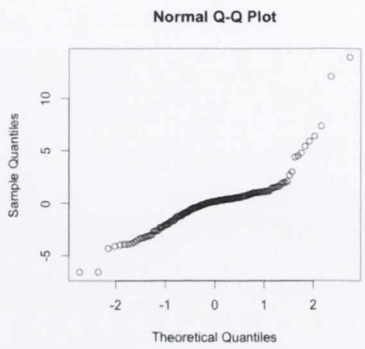
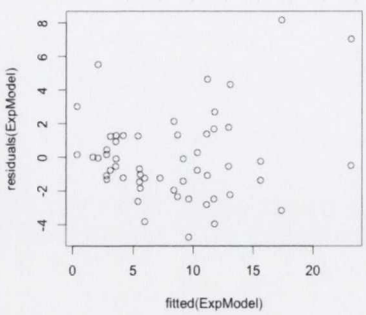


Table 5.34: Linear mixed effects analysis comparing naïve and exposed responses of flies expressing NR1-RNAi in PNs and controls

A

	Model	df	AIC	BIC	logLik	Test	L.Ratio	p-value
ExpModel	1	6	310.6694	322.6033	-149.3347			
NullModel	2	5	310.1896	320.1345	-150.0948	1 vs 2	1.520176	0.2176

B



C

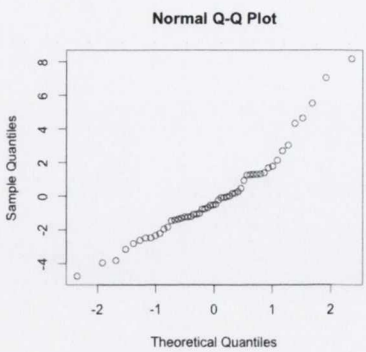
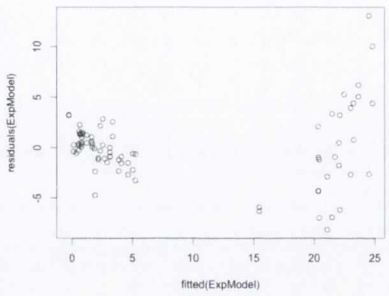


Table 5.35: Linear mixed effects analysis comparing naïve and exposed responses of flies expressing NR1-RNAi in PNs and controls in DM5

A

	Model	df	AIC	BIC	logLik	Test	L.Ratio	p-value
ExpModel	1	8	468.3788	487.4350	-226.1894			
NullModel	2	5	463.2300	475.1401	-226.6150	1 vs 2	0.8512147	0.8372

B



C

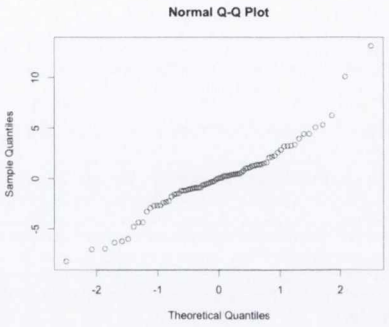
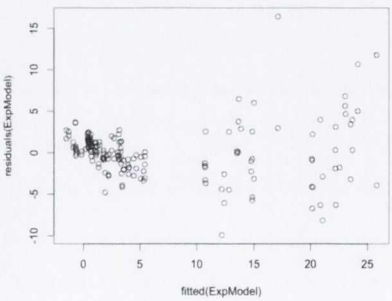


Table 5.36: Linear mixed effects analysis comparing naïve responses of flies expressing Syn-RNAi in LN1s and controls

A

	Model	df	AIC	BIC	logLik	Test	L.Ratio	p-value
ExpModel	1	12	896.5053	933.4074	-436.2526			
NullModel	2	11	894.9695	928.7964	-436.4848	1 vs 2	0.46423	0.4957

B



C

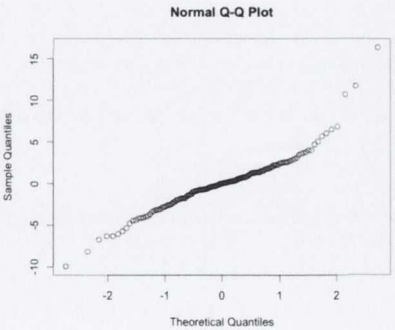


Table 5.37: Linear mixed effects analysis comparing naïve and exposed responses of flies expressing Syn-RNAi in LN1s and controls

A

```
          Model df      AIC      BIC    logLik   Test  L.Ratio p-value
ExpModel      1 16 1537.000 1588.612 -752.5002
NullModel     2  9 1577.166 1606.197 -779.5828 1 vs 2 54.16524  <.0001

Linear mixed-effects model fit by maximum likelihood
 Data: reorganisedData
   AIC      BIC    logLik
  1537 1588.612 -752.5002

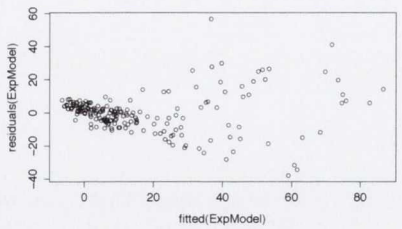
Random effects:
 Formula: ~1 | Fly
        (Intercept) Residual
StdDev:    7.606969 12.65396

Fixed effects: AUC010 ~ Run + Glomerulus + Run:Glomerulus
                            Value Std.Error  DF   t-value p-value
(Intercept)              8.33564  4.176828 147  1.995686  0.0478
RunRun2                 -1.71553  5.161334 147 -0.332380  0.7401
Glomerulusdl5           -8.68048  5.006039 147 -1.734003  0.0850
Glomerulusdm1            0.65849  5.811923 147  0.113301  0.9099
Glomerulusdm2           11.39496  5.811923 147  1.960617  0.0518
Glomerulusdm3           -6.17812  5.181991 147 -1.192229  0.2351
Glomerulusdm5           62.83596  5.811923 147 10.811562  0.0000
Glomerulusdm6           38.18298  5.181991 147  7.368398  0.0000
RunRun2:Glomerulusdl5    1.64756  7.051724 147  0.233640  0.8156
RunRun2:Glomerulusdm1   -1.63522  7.299228 147 -0.224026  0.8230
RunRun2:Glomerulusdm2   -6.54630  7.299228 147 -0.896849  0.3713
RunRun2:Glomerulusdm3    0.71193  7.299228 147  0.097536  0.9224
RunRun2:Glomerulusdm5  -33.40245  7.299228 147 -4.576162  0.0000
RunRun2:Glomerulusdm6  -14.86192  7.299228 147 -2.036095  0.0435

Standardized Within-Group Residuals:
        Min          Q1         Med          Q3         Max
-2.98544967 -0.47146760  0.04393689  0.38473511  4.48061216

Number of Observations: 186
Number of Groups: 26
```

B



C

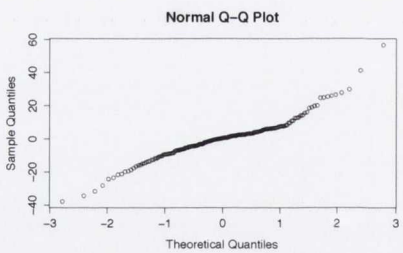
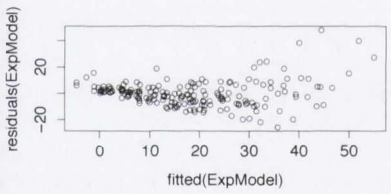


Table 5.38: Linear mixed effects analysis for Or83bGCaMP6m 3ppm EB

A

	Model	df	AIC	BIC	logLik	Test	L.Ratio	p-value
ExpModel	1	16	1479.546	1531.158	-723.7731			
NullModel	2	9	1509.247	1538.279	-745.6237	1 vs 2	43.70102	<.0001

B



C

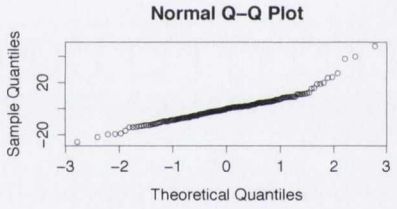


Table 5.39: Linear mixed effects analysis for Or83bGCaMP6m 3ppm EB baseline

	DL1	DL5	DM1	DM2	DM3	DM5	DM6
Number of Glomeruli	13	15	13	13	13	13	13
Number of Flies	13	15	13	13	13	13	13
Mean of Naive Response (0-10sec)	8.8657	0.038744	8.7639	19.5004	2.3877	70.9414	46.7488
SEM of Naive Response	0.80903	0.80808	1.699	4.6209	1.1698	8.5161	6.3429
Mean of Response Change (0-10sec)	-1.7155	-0.067959	-3.3507	-8.2618	-1.0036	-35.118	-16.5774
SEM of Response Change	1.4786	0.4296	1.2341	2.6149	1.1446	7.4888	7.7673
95% Confidence Interval	[-4.937 1.506]	[-0.98936 0.85344]	[-6.0396 -0.66192]	[-13.9593 -2.5644]	[-3.4975 1.4904]	[-51.4348 -18.8012]	[-33.5009 0.34602]
Anderson-Darling Normality Test (0.05)	n.s.; p=0.22279	n.s.; p=0.30774	p=0.0010907	n.s.; p=0.25967	n.s.; p=0.82946	p=0.028512	n.s.; p=0.087944
One-Sample Student T-Test (0.05)	n.s.; p=0.2685; t=-1.1603; df=12	n.s.; p=0.87657; t=-0.15819; df=14	NaN	p=0.0082289; t=-3.1595; df=12	n.s.; p=0.39782; t=-0.87677; df=12	NaN	n.s.; p=0.054142; t=-2.1343; df=12
Wilcoxon Signed Rank Test (0.05)	NaN	NaN	p=0.0080566; Signed Rank=9	NaN	NaN	p=0.00024414; Signed Rank=0	NaN
Mean of Baseline Change	-1.995	-5.3837	-5.4538	-13.0146	-14.9443	-15.6469	-12.9179
SEM of Baseline Change	0.98724	1.7616	1.7096	3.6729	4.8336	5.9822	3.7563
95% Confidence Interval	[-4.1461 0.15597]	[-9.1618 -1.6055]	[-9.1788 -1.7288]	[-21.0173 -5.012]	[-25.4757 -4.4129]	[-28.681 -2.6128]	[-21.1022 -4.7337]
Anderson-Darling Normality Test (0.05)	p=0.0097267	n.s.; p=0.66711	p=0.002801	p=0.0005	n.s.; p=0.44043	p=0.0005	n.s.; p=0.48208
One-Sample Student T-Test (0.05)	NaN	p=0.0085438; t=-3.0562; df=14	NaN	NaN	p=0.0093313; t=-3.0918; df=12	NaN	p=0.0049034; t=-3.439; df=12
Wilcoxon Signed Rank Test (0.05)	p=0.021484; Signed Rank=13	NaN	p=0.00024414; Signed Rank=0	p=0.00024414; Signed Rank=0	NaN	p=0.00024414; Signed Rank=0	NaN

Table 5.40: Paired comparisons for Or83bGCaMP6m 3ppm EB

A

```
         Model df      AIC      BIC    logLik   Test  L.Ratio p-value
ExpModel     1 16 1886.544 1940.987 -927.2719
NullModel    2  9 1954.484 1985.108 -968.2419 1 vs 2 81.93984  <.0001

Linear mixed-effects model fit by maximum likelihood
 Data: reorganisedData
       AIC      BIC    logLik
  1886.544 1940.987 -927.2719

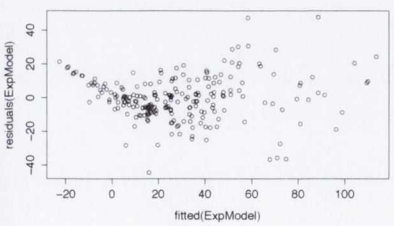
Random effects:
 Formula: ~1 | Fly
        (Intercept) Residual
StdDev:    12.53916 13.87713

Fixed effects: AUC010 ~ Run + Glomerulus + Run:Glomerulus
                          Value Std.Error  DF   t-value p-value
(Intercept)           26.89261  4.245526 180  6.334340  0.0000
RunRun2              -10.68848  4.778848 180 -2.236622  0.0265
Glomerulusdl5        -34.92376  4.856704 180 -7.190836  0.0000
Glomerulusdm1         -7.54562  5.287932 180 -1.426951  0.1553
Glomerulusdm2          7.38960  5.182757 180  1.425806  0.1557
Glomerulusdm3          0.70826  5.226476 180  0.135514  0.8924
Glomerulusdm5         62.68802  5.079836 180 12.340561  0.0000
Glomerulusdm6         29.54875  5.680852 180  5.201464  0.0000
RunRun2:Glomerulusdl5 14.46927  6.856978 180  2.110153  0.0362
RunRun2:Glomerulusdm1  5.51201  6.966308 180  0.791238  0.4298
RunRun2:Glomerulusdm2  0.29621  6.856978 180  0.043198  0.9656
RunRun2:Glomerulusdm3  1.68906  7.224939 180  0.233782  0.8154
RunRun2:Glomerulusdm5 -29.74905  6.758311 180 -4.401847  0.0000
RunRun2:Glomerulusdm6 -8.83974  7.759359 180 -1.139236  0.2561

Standardized Within-Group Residuals:
       Min         Q1        Med         Q3        Max
-3.19269544 -0.49371195 0.01840947 0.59325840 3.45148147

Number of Observations: 222
Number of Groups: 29
```

B



C

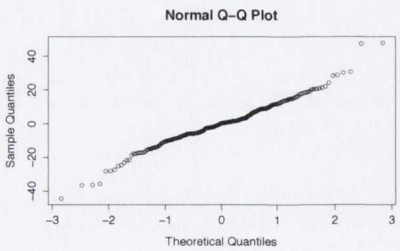
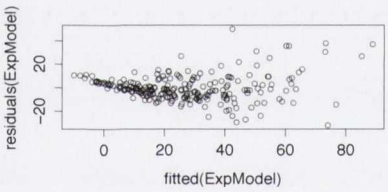


Table 5.41: Linear mixed effects analysis for Or83bGCaMP6m 20ppm EB

A

	Model	df	AIC	BIC	logLik	Test	L.Ratio	p-value
ExpModel	1	16	1839.859	1894.302	-903.9296			
NullModel	2	9	1910.874	1941.498	-946.4370	1 vs 2	85.01493	<.0001

B



C

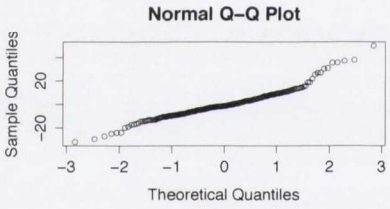


Table 5.42: Linear mixed effects analysis for Or83bGCaMP6m 20ppm EB baseline

	DL1	DL5	DM1	DM2	DM3	DM5	DM6
Number of Glomeruli	18	17	16	17	14	18	11
Number of Flies	18	17	16	17	14	18	11
Mean of Naive Response (0-10sec)	29.5022	-4.6768	17.0232	33.2677	31.976	89.4358	57.1615
SEM of Naive Response	4.1822	2.0838	3.0174	7.1613	5.5689	7.3402	6.5232
Mean of Response Change (0-10sec)	-10.6885	3.7808	-5.1765	-10.3923	-8.9994	-40.4375	-19.5282
SEM of Response Change	1.7159	1.3928	2.1558	4.3887	3.3673	6.0035	7.2063
95% Confidence Interval	[-14.3087 -7.0683]	[0.82826 6.7333]	[-9.7715 -0.58143]	[-19.6959 -1.0886]	[-16.2741 -1.7247]	[-53.1038 -27.7712]	[-35.5849 -3.4716]
Anderson-Darling Normality Test (0.05)	n.s.; p=0.4256	p=0.0005	n.s.; p=0.17535	n.s.; p=0.21464	n.s.; p=0.46463	n.s.; p=0.97024	n.s.; p=0.21626
One-Sample Student T-Test (0.05)	p=9.1613e-06; t=-6.2291; df=17	NaN	p=0.029758; t=-2.4011; df=15	p=0.03082; t=-2.3679; df=16	p=0.019171; t=-2.6725; df=13	p=3.4898e-06; t=-6.7356; df=17	p=0.021938; t=-2.7099; df=10
Wilcoxon Signed Rank Test (0.05)	NaN	p=0.0041839; z=2.864	NaN	NaN	NaN	NaN	NaN
Mean of Baseline Change	-3.9988	-10.6478	-10.4639	-33.4038	-19.6031	-11.2699	-11.3357
SEM of Baseline Change	0.72556	3.172	3.1987	6.306	3.7058	4.4665	2.9465
95% Confidence Interval	[-5.5295 -2.468]	[-17.3722 -3.9235]	[-17.2817 -3.6461]	[-46.7718 -20.0357]	[-27.6089 -11.5973]	[-20.6934 -1.8464]	[-17.901 -4.7704]
Anderson-Darling Normality Test (0.05)	p=0.0095968	p=0.0005	p=0.0038084	n.s.; p=0.076412	p=0.02937	n.s.; p=0.33298	p=0.034723
One-Sample Student T-Test (0.05)	NaN	NaN	NaN	p=7.2239e-05; t=-5.2972; df=16	NaN	p=0.021882; t=-2.5232; df=17	NaN
Wilcoxon Signed Rank Test (0.05)	p=0.00019644; z=-3.7236	p=0.00050263; z=-3.4794	p=0.0016092; z=-3.1542	NaN	p=0.00012207; Signed Rank=0	NaN	p=0.00097656; Signed Rank=0

Table 5.43: Paired comparisons for Or83bGCaMP6m 20ppm EB

A

```
         Model df      AIC      BIC    logLik   Test  L.Ratio p-value
ExpModel     1 24 3415.838 3512.109 -1683.919
NullModel    2 16 3446.127 3510.307 -1707.063 1 vs 2 46.28882  <.0001

Linear mixed-effects model fit by maximum likelihood
 Data: reorganisedData
      AIC      BIC    logLik
  3415.838 3512.109 -1683.919

Random effects:
 Formula: ~1 | Fly
        (Intercept) Residual
StdDev:    10.53312 13.37381

Fixed effects: AUC010 ~ Run + Concentration + Glomerulus + Run * Glomerulus +      Concentration * Run + Glomerulus * Concentration
                                    Value Std.Error  DF   t-value p-value
(Intercept)                      9.73698  4.274922 333  2.277697  0.0234
RunRun2                         -4.87696  3.838114 333 -1.270667  0.2047
Concentration20ppm              16.19995  5.144273  53  3.149123  0.0027
Glomerulusdl5                  -12.18401  4.453396 333 -2.735891  0.0066
Glomerulusdm1                   -1.06640  5.720883 333 -0.186404  0.8522
Glomerulusdm2                    9.74368  5.711273 333  1.706044  0.0889
Glomerulusdm3                   -6.56732  4.623055 333 -1.420559  0.1564
Glomerulusdm5                   62.10079  5.702336 333 10.890412  0.0000
Glomerulusdm6                   36.50318  4.672378 333  7.812549  0.0000
RunRun2:Glomerulusdl5            8.72804  4.902151 333  1.780451  0.0759
RunRun2:Glomerulusdm1            2.46555  5.024078 333  0.490746  0.6239
RunRun2:Glomerulusdm2           -2.59277  4.980154 333 -0.520621  0.6030
RunRun2:Glomerulusdm3            1.55685  5.121511 333  0.303984  0.7613
RunRun2:Glomerulusdm5          -31.28112  4.939019 333 -6.333469  0.0000
RunRun2:Glomerulusdm6          -11.43580  5.297527 333 -2.158706  0.0316
RunRun2:Concentration20ppm      -3.52825  2.741616 333 -1.286924  0.1990
Concentration20ppm:Glomerulusdl5 -19.83245  4.970474 333 -3.990053  0.0001
Concentration20ppm:Glomerulusdm1  -5.30505  6.375860 333 -0.832053  0.4060
Concentration20ppm:Glomerulusdm2  -1.20521  6.325762 333 -0.190523  0.8490
Concentration20ppm:Glomerulusdm3   7.39427  5.276918 333  1.401247  0.1621
Concentration20ppm:Glomerulusdm5   1.09745  6.275996 333  0.174865  0.8613
Concentration20ppm:Glomerulusdm6  -5.73146  5.521950 333 -1.037941  0.3001

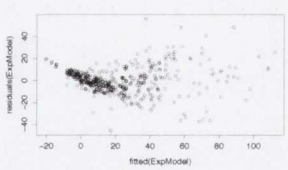

Standardized Within-Group Residuals:
       Min         Q1        Med         Q3        Max
-3.4022186 -0.49882649 -0.02792807  0.46435056  4.17083109

Number of Observations: 408
Number of Groups: 55
```

B

```
         Model df      AIC      BIC    logLik   Test  L.Ratio p-value
ExpModel     1 24 3415.838 3512.109 -1683.919
NulModel     2 23 3415.584 3507.844 -1684.792 1 vs 2 1.746231  0.1864
```

C



D

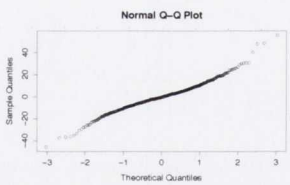


Table 5.44: Linear mixed effects analysis for Or83bGCaMP6m comparing 3ppm and 20ppm Testing for Concentration (A) and Concentration * Run (B)

A

```
          Model df      AIC      BIC    logLik   Test  L.Ratio p-value
RecovModel     1 23 1007.163 1072.398 -480.5818
baseline       2  9 1035.556 1061.083 -508.7783 1 vs 2 56.39303  <.0001

Linear mixed-effects model fit by maximum likelihood
 Data: reorganisedData
       AIC      BIC    logLik
  1007.164 1072.398 -480.5818

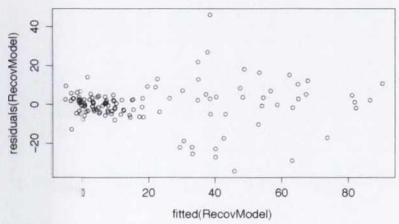
Random effects:
 Formula: ~1 | Fly
        (Intercept) Residual
StdDev:    4.638524 10.39908

Fixed effects: AUC010 ~ Run + Glomerulus + Run:Glomerulus
                            Value Std.Error DF   t-value p-value
(Intercept)              7.33751  5.092283 94  1.440907  0.1529
RunRun1                  2.51586  6.576954 94  0.382526  0.7029
RunRun3                 -2.03906  6.576954 94 -0.310031  0.7572
Glomerulusdl5           -6.30280  6.576954 94 -0.958316  0.3404
Glomerulusdm1            0.38839  7.201575 94  0.053931  0.9571
Glomerulusdm2           11.39498  7.201575 94  1.582289  0.1169
Glomerulusdm3           -8.64364  6.576954 94 -1.314231  0.1920
Glomerulusdm5           47.43032  7.201575 94  6.586104  0.0000
Glomerulusdm6           27.85592  6.576954 94  4.235384  0.0001
RunRun1:Glomerulusdl5 -2.99737  9.301218 94 -0.322255  0.7480
RunRun3:Glomerulusdl5  2.18738  9.301218 94  0.235171  0.8146
RunRun1:Glomerulusdm1  0.35256  9.301218 94  0.037905  0.9698
RunRun3:Glomerulusdm1 -0.69336  9.301218 94 -0.074545  0.9407
RunRun1:Glomerulusdm2  9.72529  9.301218 94  1.045593  0.2984
RunRun3:Glomerulusdm2 -0.96527  9.301218 94 -0.103779  0.9176
RunRun1:Glomerulusdm3 -1.48044  9.301218 94 -0.159167  0.8739
RunRun3:Glomerulusdm3 -0.27361  9.301218 94 -0.029417  0.9766
RunRun1:Glomerulusdm5 25.30586  9.301218 94  2.720704  0.0078
RunRun3:Glomerulusdm5 -3.62844  9.301218 94 -0.390104  0.6973
RunRun1:Glomerulusdm6 27.54959  9.301218 94  2.961934  0.0039
RunRun3:Glomerulusdm6  7.46357  9.301218 94  0.802430  0.4243

Standardized Within-Group Residuals:
       Min         Q1        Med         Q3        Max
-3.28869940 -0.32934037 0.06899592 0.35275525 4.43564298

Number of Observations: 126
Number of Groups: 12
```

B



C

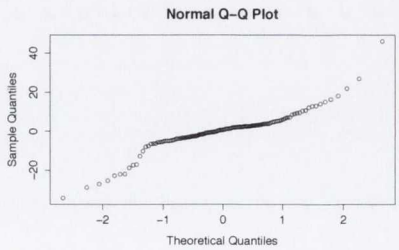


Table 5.45: Linear mixed effects analysis for Or83bGCaMP6m 3ppm EB recovery

A

```
          Model df      AIC      BIC    logLik   Test L.Ratio p-value
RecovModel     1  5 99.65486 104.1067 -44.82743
baseline       2  3 104.84458 107.5157 -49.42229 1 vs 2 9.18972  0.0101
```

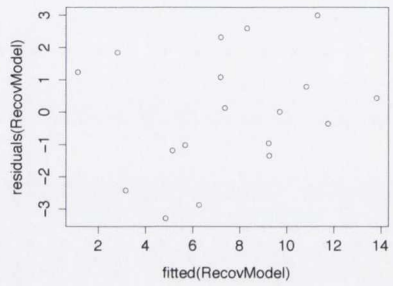
```
        Pairwise comparisons using t tests with pooled SD

data:  reorganisedData$AUC010 and reorganisedData$Run

     Run1  Run2
Run2 0.289 -
Run3 0.065 0.387

P value adjustment method: none
```

B



C

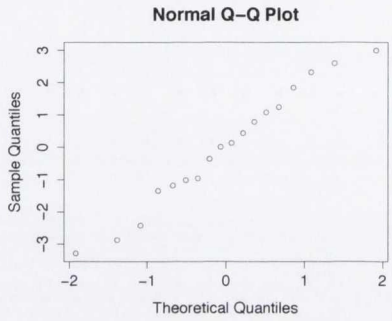
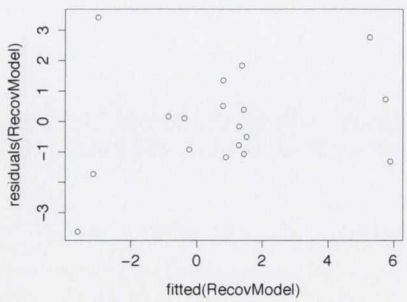


Table 5.46: Linear mixed effects analysis for Or83bGCaMP6m 3ppm EB recovery DL1

A

```
          Model df      AIC      BIC    logLik   Test   L.Ratio p-value
RecovModel     1  5 96.71400 101.16586 -43.35700
baseline       2  3 93.06096  95.73207 -43.53048 1 vs 2 0.3469573  0.8407
```

B



C

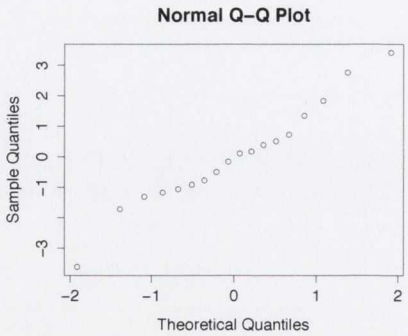


Table 5.47: Linear mixed effects analysis for Or83bGCaMP6m 3ppm EB recovery DL5

A

```
          Model df      AIC      BIC    logLik   Test L.Ratio p-value
RecovModel     1  5 110.7077 115.1595 -50.35384
baseline       2  3 114.8806 117.5517 -54.44028 1 vs 2 8.17288  0.0168
```

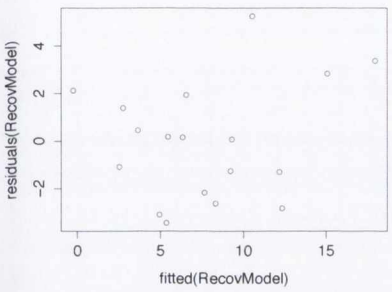
```
        Pairwise comparisons using t tests with pooled SD

data:  reorganisedData$AUC010 and reorganisedData$Run

     Run1 Run2
Run2 0.38 -
Run3 0.10 0.41

P value adjustment method: none
```

B



C

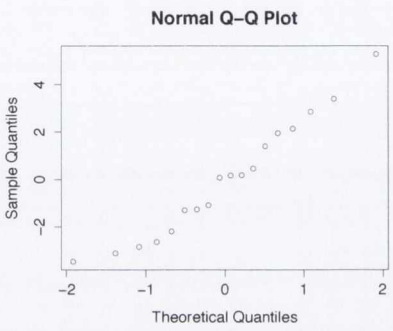


Table 5.48: Linear mixed effects analysis for Or83bGCaMP6m 3ppm EB recovery DM1

A

```
          Model df      AIC      BIC    logLik   Test  L.Ratio p-value
RecovModel     1  5 141.9355 146.3873 -65.96774
baseline       2  3 148.7629 151.4340 -71.38143 1 vs 2 10.82738  0.0045
```

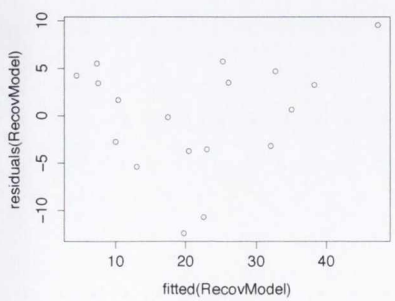
```
        Pairwise comparisons using t tests with pooled SD

data:  reorganisedData$AUC010 and reorganisedData$Run

     Run1  Run2
Run2 0.134 -
Run3 0.067 0.703

P value adjustment method: none
```

B



C

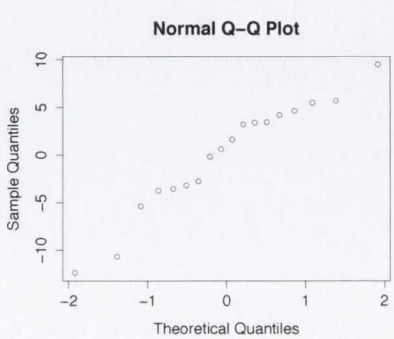
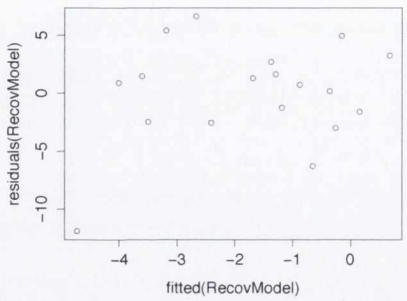


Table 5.49: Linear mixed effects analysis for Or83bGCaMP6m 3ppm EB recovery DM2

A

```
           Model df      AIC      BIC    logLik   Test  L.Ratio p-value
RecovModel     1  5 116.3070 120.7589 -53.15350
baseline       2  3 113.9682 116.6393 -53.98411 1 vs 2 1.661227  0.4358
```

B



C

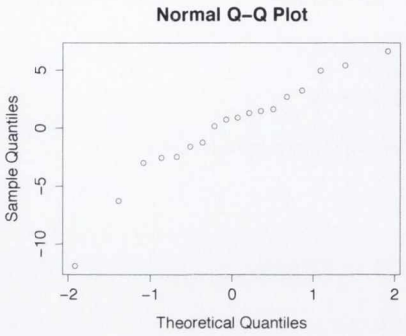


Table 5.50: Linear mixed effects analysis for Or83bGCaMP6m 3ppm EB recovery DM3

A

```
           Model df      AIC      BIC    logLik   Test  L.Ratio p-value
RecovModel     1  5 147.6465 152.0984 -68.82325
baseline       2  3 168.3885 171.0596 -81.19423 1 vs 2 24.74196  <.0001
```

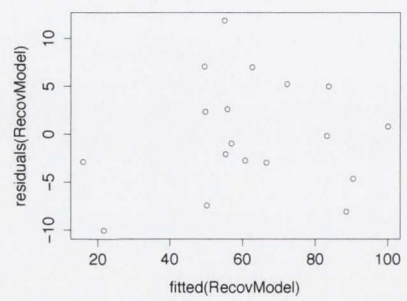
```
        Pairwise comparisons using t tests with pooled SD

data:  reorganisedData$AUC010 and reorganisedData$Run

     Run1  Run2
Run2 0.025 -
Run3 0.009 0.619

P value adjustment method: none
```

B



C

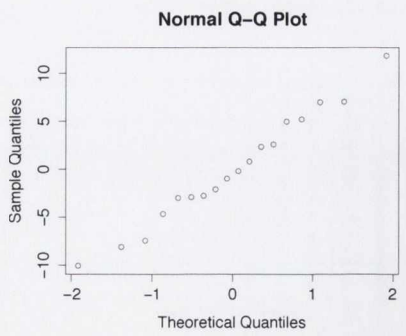


Table 5.51: Linear mixed effects analysis for Or83bGCaMP6m 3ppm EB recovery DM5

A

```
          Model df      AIC      BIC    logLik   Test  L.Ratio p-value
RecovModel     1  5 167.1661 171.6180 -78.58306
baseline       2  3 170.1245 172.7956 -82.06226 1 vs 2 6.958391  0.0308

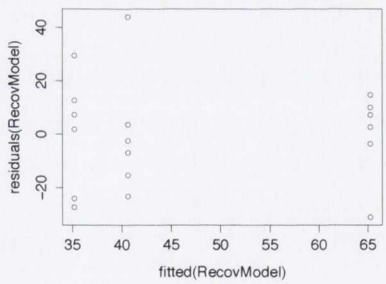

        Pairwise comparisons using t tests with pooled SD

data:  reorganisedData$AUC010 and reorganisedData$Run

     Run1  Run2
Run2 0.025 -
Run3 0.059 0.659

P value adjustment method: none
```

B



C

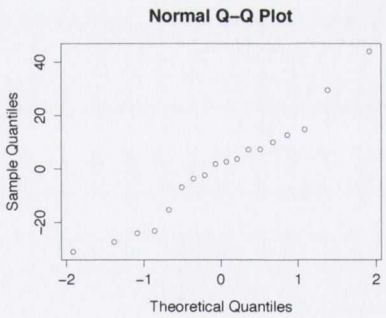


Table 5.52: Linear mixed effects analysis for Or83bGCaMP6m 3ppm EB recovery DM6

A

```
          Model df       AIC      BIC    logLik   Test  L.Ratio p-value
RecovModel     1 23  984.0759 1048.756 -469.0379
baseline       2  9 1031.1773 1056.487 -506.5887 1 vs 2 75.10146  <.0001

Linear mixed-effects model fit by maximum likelihood
 Data: reorganisedData
       AIC      BIC    logLik
  984.0759 1048.756 -469.0379

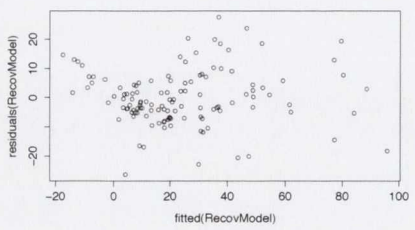
Random effects:
 Formula: ~1 | Fly
        (Intercept) Residual
StdDev:    9.707702 9.822465

Fixed effects: AUC010 ~ Run + Glomerulus + Run:Glomerulus
                            Value Std.Error DF   t-value p-value
(Intercept)              12.71697  5.040349 92  2.523034  0.0134
RunRun1                  10.29367  5.393156 92  1.908655  0.0594
RunRun3                  -1.03329  5.393156 92 -0.191592  0.8485
Glomerulusdl5           -17.87361  5.601887 92 -3.190641  0.0019
Glomerulusdm1             2.21259  6.525452 92  0.339071  0.7353
Glomerulusdm2             7.76345  6.525452 92  1.189719  0.2372
Glomerulusdm3            10.27637  5.977187 92  1.719266  0.0889
Glomerulusdm5            37.94593  6.525452 92  5.815066  0.0000
Glomerulusdm6            27.30051  6.346052 92  4.301967  0.0000
RunRun1:Glomerulusdl5   -15.48698  7.894771 92 -1.961675  0.0528
RunRun3:Glomerulusdl5     2.54836  7.894771 92  0.322791  0.7476
RunRun1:Glomerulusdm1    -8.44123  8.696202 92 -0.970681  0.3343
RunRun3:Glomerulusdm1    -3.40365  8.696202 92 -0.391395  0.6964
RunRun1:Glomerulusdm2    -6.79157  8.696202 92 -0.780982  0.4368
RunRun3:Glomerulusdm2    -2.77835  8.696202 92 -0.319491  0.7501
RunRun1:Glomerulusdm3     0.95799  8.238181 92  0.116287  0.9077
RunRun3:Glomerulusdm3     1.37145  8.238181 92  0.166475  0.8681
RunRun1:Glomerulusdm5    26.46699  8.696202 92  3.043511  0.0030
RunRun3:Glomerulusdm5    -9.37461  8.696202 92 -1.078013  0.2838
RunRun1:Glomerulusdm6    14.80689  8.696202 92  1.702684  0.0920
RunRun3:Glomerulusdm6    -4.59425  8.696202 92 -0.528306  0.5986

Standardized Within-Group Residuals:
       Min         Q1        Med         Q3        Max
-2.6777940 -0.5171713 -0.1389557  0.5368775  2.8010558

Number of Observations: 123
Number of Groups: 11
```

B



C

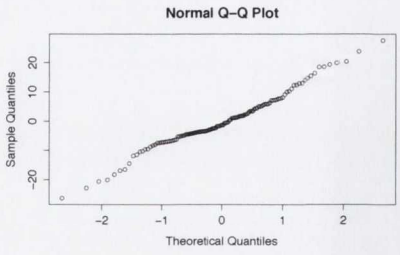


Table 5.53: Linear mixed effects analysis for Or83bGCaMP6m 20ppm EB recovery

A

```
          Model df      AIC      BIC    logLik   Test  L.Ratio p-value
RecovModel     1  5 175.8390 181.7293 -82.91952
baseline       2  3 188.4149 191.9491 -91.20746 1 vs 2 16.57589   3e-04
```

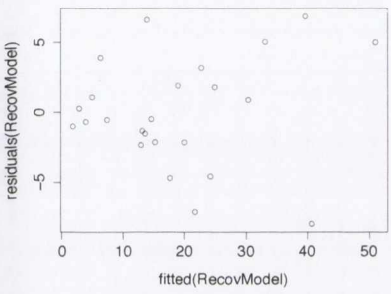
```
        Pairwise comparisons using t tests with pooled SD

data:  reorganisedData$AUC010 and reorganisedData$Run

     Run1 Run2
Run2 0.14 -
Run3 0.11 0.88

P value adjustment method: none
```

B



C

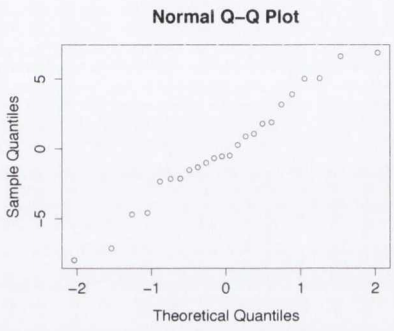


Table 5.54: Linear mixed effects analysis for Or83bGCaMP6m 20ppm EB recovery DL1

A

```
          Model df      AIC      BIC    logLik   Test  L.Ratio p-value
RecovModel     1  5 129.6934 134.9160 -59.84668
baseline       2  3 138.2022 141.3358 -66.10110 1 vs 2 12.50884  0.0019
```

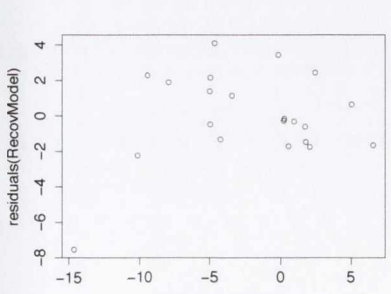
```
        Pairwise comparisons using t tests with pooled SD

data:  reorganisedData$AUC010 and reorganisedData$Run

     Run1  Run2
Run2 0.118 -
Run3 0.048 0.638

P value adjustment method: none
```

B



C

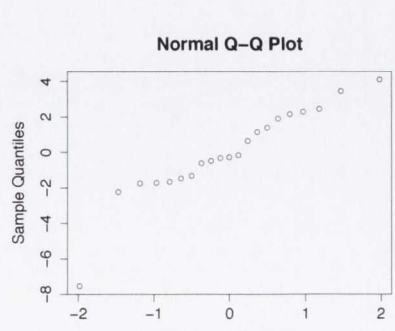
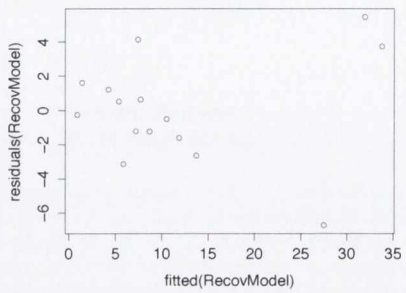


Table 5.55: Linear mixed effects analysis for Or83bGCaMP6m 20ppm EB recovery DL5

A

	Model	df	AIC	BIC	logLik	Test	L.Ratio	p-value
RecovModel	1	5	107.0788	110.6190	-48.53938			
baseline	2	3	108.9546	111.0787	-51.47728	1 vs 2	5.875806	0.053

B



C

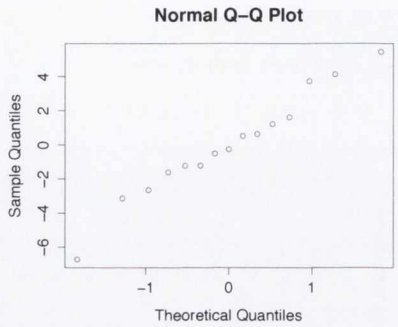
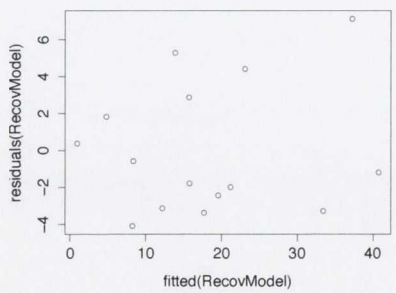


Table 5.56: Linear mixed effects analysis for Or83bGCaMP6m 20ppm EB recovery DM1

A

	Model	df	AIC	BIC	logLik	Test	L.Ratio	p-value
RecovModel	1	5	110.5914	114.1317	-50.29571			
baseline	2	3	112.4078	114.5320	-53.20391	1 vs 2	5.816401	0.0546

B



C

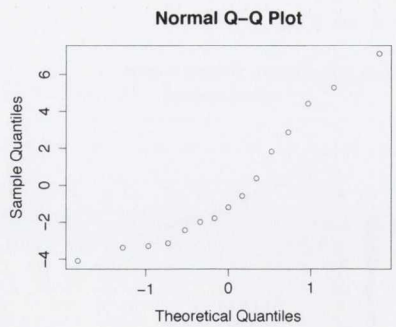


Table 5.57: Linear mixed effects analysis for Or83bGCaMP6m 20ppm EB recovery DM2

A

```
           Model df      AIC      BIC    logLik   Test  L.Ratio p-value
RecovModel     1  5 145.7457 150.1975 -67.87284
baseline       2  3 149.5086 152.1797 -71.75429 1 vs 2 7.762888  0.0206
```

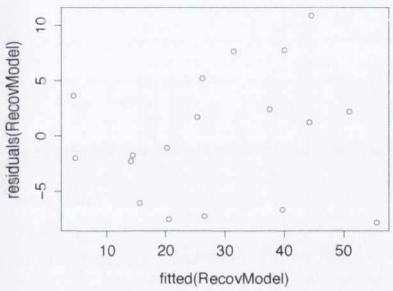
```
        Pairwise comparisons using t tests with pooled SD

data:  reorganisedData$AUC010 and reorganisedData$Run

     Run1 Run2
Run2 0.28 -
Run3 0.29 0.97

P value adjustment method: none
```

B



C

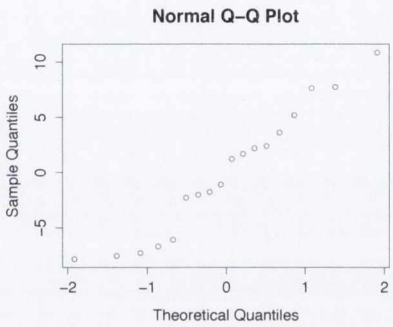


Table 5.58: Linear mixed effects analysis for Or83bGCaMP6m 20ppm EB recovery DM3

A

```
           Model df      AIC      BIC    logLik   Test  L.Ratio p-value
RecovModel     1  5 137.0216 140.5618 -63.51079
baseline       2  3 146.5776 148.7018 -70.28880 1 vs 2 13.55601  0.0011
```

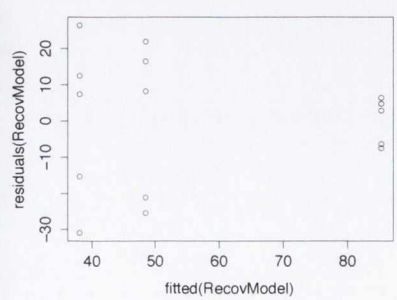
```
        Pairwise comparisons using t tests with pooled SD

data:  reorganisedData$AUC010 and reorganisedData$Run

     Run1   Run2
Run2 0.0090 -
Run3 0.0018 0.3953

P value adjustment method: none
```

B



C

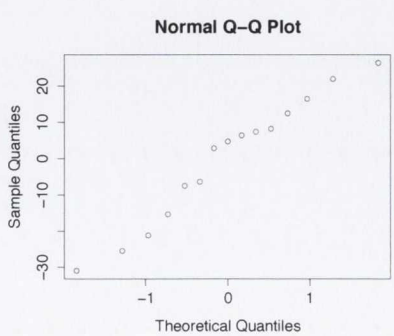


Table 5.59: Linear mixed effects analysis for Or83bGCaMP6m 20ppm EB recovery DM5

A

```
          Model df      AIC      BIC    logLik   Test  L.Ratio p-value
RecovModel     1  5 132.2789 135.8191 -61.13943
baseline       2  3 140.6942 142.8183 -67.34709 1 vs 2 12.41532   0.002

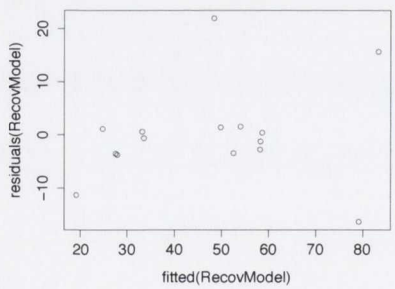

        Pairwise comparisons using t tests with pooled SD

data:  reorganisedData$AUC010 and reorganisedData$Run

     Run1  Run2
Run2 0.066 -
Run3 0.029 0.659

P value adjustment method: none
```

B



C

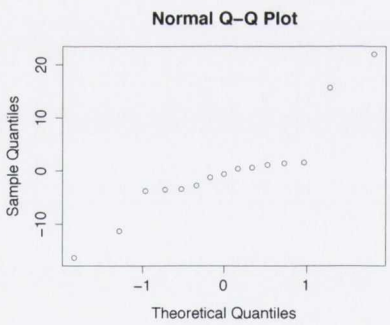
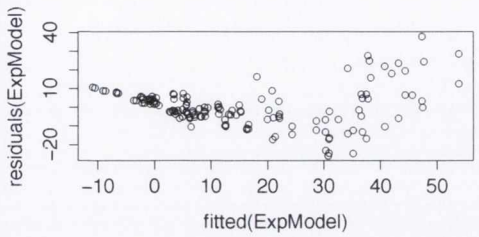


Table 5.60: Linear mixed effects analysis for Or83bGCaMP6m 20ppm EB recovery DM6

A

```
          Model df      AIC      BIC    logLik   Test  L.Ratio p-value
ExpModel      1 16 1151.351 1198.868 -559.6756
NullModel     2  9 1142.625 1169.353 -562.3123 1 vs 2 5.273397  0.6266
```

B



C

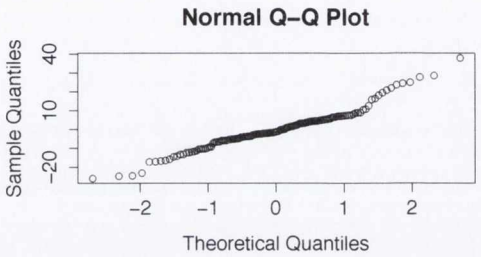
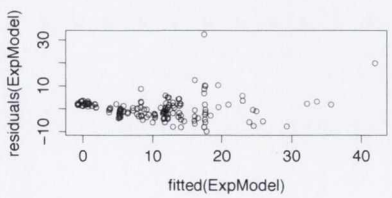


Table 5.61: Linear mixed effects analysis for Or83bGCaMP6m mock

A

```
          Model df      AIC      BIC    logLik   Test  L.Ratio p-value
ExpModel      1 16 955.9758 1003.4928 -461.9879
NullModel     2  9 947.6194  974.3477 -464.8097 1 vs 2 5.643553  0.5819
```

B



C

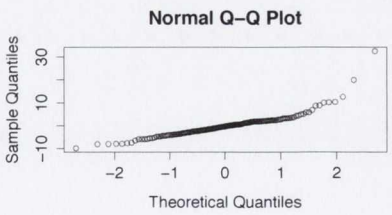


Table 5.62: Linear mixed effects analysis for Or83bGCaMP6m mock baseline

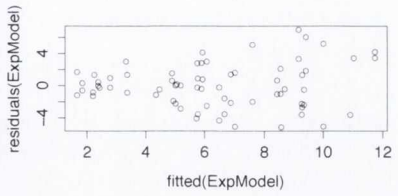
	DL1	DL5	DM1	DM2	DM3	DM5	DM6
Number of Glomeruli	6	6	16	16	6	16	6
Number of Flies	6	6	8	8	6	8	6
Mean of Naive Response (0-10sec)	8.1257	1.2674	3.0631	8.5341	13.9509	40.3142	40.6296
SEM of Naive Response	2.6844	0.62403	0.46242	1.1999	4.732	5.8361	11.4858
Mean of Response Change (0-10sec)	-1.4864	-1.8653	-0.32564	-0.1212	-0.83243	-6.5513	-9.4094
SEM of Response Change	1.1279	1.2534	0.38266	1.1089	3.645	2.1258	7.0831
95% Confidence Interval	[-4.3856 1.4129]	[-5.0874 1.3567]	[-1.1413 0.48998]	[-2.4848 2.2424]	[-10.2021 8.5373]	[-11.0822 -2.0203]	[-27.6172 8.7984]
Anderson-Darling Normality Test (0.05)	n.s.; p=0.13961	n.s.; p=0.42901	n.s.; p=0.31345	n.s.; p=0.059724	n.s.; p=0.3769	n.s.; p=0.71757	n.s.; p=0.89486
One-Sample Student T-Test (0.05)	n.s.; p=0.2447; t=-1.3179; df=5	n.s.; p=0.19687; t=-1.4882; df=5	n.s.; p=0.40815; t=-0.851; df=15	n.s.; p=0.91442; t=-0.10929; df=15	n.s.; p=0.8284; t=-0.22838; df=5	p=0.0075935; t=-3.0819; df=15	n.s.; p=0.24144; t=-1.3284; df=5
Wilcoxon Signed Rank Test (0.05)	NaN	NaN	NaN	NaN	NaN	NaN	NaN
Mean of Baseline Change	-0.095677	1.0178	-0.15531	-1.9643	1.4318	-0.0025244	-6.3257
SEM of Baseline Change	1.5605	1.2517	0.23346	1.2658	3.1582	2.1773	4.6654
95% Confidence Interval	[-4.1072 3.9158]	[-2.1999 4.2354]	[-0.65291 0.34229]	[-4.6624 0.73376]	[-6.6866 9.5502]	[-4.6433 4.6382]	[-18.3184 5.667]
Anderson-Darling Normality Test (0.05)	n.s.; p=0.21382	n.s.; p=0.81443	n.s.; p=0.43839	n.s.; p=0.080918	n.s.; p=0.31155	p=0.0027051	n.s.; p=0.27631
One-Sample Student T-Test (0.05)	n.s.; p=0.95349; t=-0.06131; df=5	n.s.; p=0.45312; t=0.8131; df=5	n.s.; p=0.51599; t=-0.66525; df=15	n.s.; p=0.14155; t=-1.5518; df=15	n.s.; p=0.66928; t=0.45337; df=5	NaN	n.s.; p=0.23316; t=-1.3559; df=5
Wilcoxon Signed Rank Test (0.05)	NaN	NaN	NaN	NaN	NaN	n.s.; p=0.32587; z=0.98247	NaN

Table 5.63: Paired comparisons for Or83bGCaMP6m mock

A

```
          Model df      AIC      BIC    logLik   Test  L.Ratio p-value
ExpModel      1  8 365.3309 383.0869 -174.6654
NullModel     2  5 363.8603 374.9579 -176.9302 1 vs 2 4.529429  0.2097
```

B



C

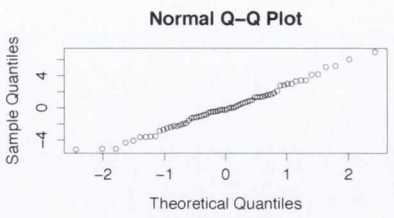


Table 5.64: Linear mixed effects analysis for LN1GCaMP6m 3ppm EB

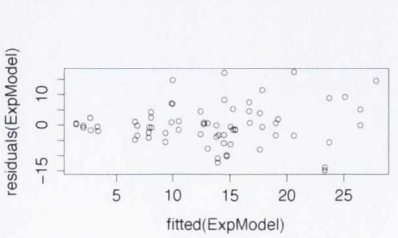
	DM1	DM2	DM5
Number of Glomeruli	11	13	10
Number of Flies	6	7	7
Mean of Naive Response (0-10sec)	4.2048	8.3457	7.4948
SEM of Naive Response	0.87829	1.5245	1.1337
Mean of Response Change (0-10sec)	0.17804	-2.3955	-0.11835
SEM of Response Change	0.55895	1.1715	1.4396
95% Confidence Interval	[-1.0674 1.4235]	[-4.9479 0.15693]	[-3.375 3.1383]
Anderson-Darling Normality Test (0.05)	n.s.; p=0.52477	n.s.; p=0.20652	n.s.; p=0.63923
One-Sample Student T-Test (0.05)	n.s.; p=0.75664; t=0.31852; df=10	n.s.; p=0.063445; t=-2.0449; df=12	n.s.; p=0.93628; t=-0.082205; df=9
Wilcoxon Signed Rank Test (0.05)	NaN	NaN	NaN
Mean of Baseline Change	0.91294	-1.2301	0.0071379
SEM of Baseline Change	0.38464	1.0336	1.3303
95% Confidence Interval	[0.055904 1.77]	[-3.4823 1.022]	[-3.0023 3.0166]
Anderson-Darling Normality Test (0.05)	n.s.; p=0.83506	n.s.; p=0.34711	p=0.0012814
One-Sample Student T-Test (0.05)	p=0.039045; t=2.3735; df=10	n.s.; p=0.25702; t=-1.1901; df=12	NaN
Wilcoxon Signed Rank Test (0.05)	NaN	NaN	n.s.; p=0.23242; Signed Rank=40

Table 5.65: Paired comparisons for LN1GCaMP6m 3ppm EB

A

```
          Model df      AIC      BIC    logLik   Test   L.Ratio p-value
ExpModel      1  8 507.4837 525.6970 -245.7418
NullModel     2  5 502.3713 513.7547 -246.1857 1 vs 2 0.8876674  0.8284
```

B



C

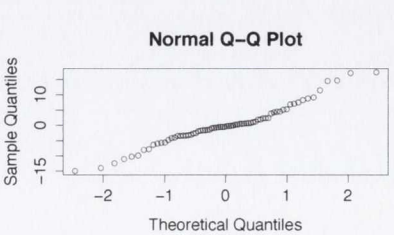


Table 5.66: Linear mixed effects analysis for LN1GCaMP6m 3ppm EB

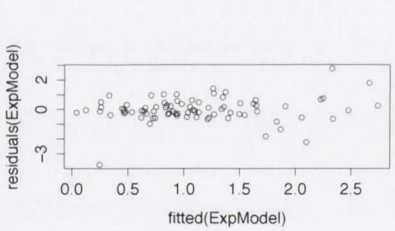
	DM1	DM2	DM5
Number of Glomeruli	13	13	10
Number of Flies	7	7	6
Mean of Naive Response (0-10sec)	7.8608	13.2325	20.8457
SEM of Naive Response	1.5285	2.2278	3.3297
Mean of Response Change (0-10sec)	0.63209	-0.20508	-2.7247
SEM of Response Change	1.8896	2.9357	4.5281
95% Confidence Interval	[-3.485 4.7492]	[-6.6015 6.1913]	[-12.9679 7.5185]
Anderson-Darling Normality Test (0.05)	p=0.0005	p=0.0005	n.s.; p=0.27951
One-Sample Student T-Test (0.05)	NaN	NaN	n.s.; p=0.5622; t=-0.60174; df=9
Wilcoxon Signed Rank Test (0.05)	n.s.; p=0.21631; Signed Rank=27	n.s.; p=0.21631; Signed Rank=27	NaN
Mean of Baseline Change	0.72657	-0.58028	-2.8897
SEM of Baseline Change	0.51683	1.1918	2.3266
95% Confidence Interval	[-0.39949 1.8526]	[-3.1769 2.0164]	[-8.1527 2.3734]
Anderson-Darling Normality Test (0.05)	n.s.; p=0.69206	p=0.012883	n.s.; p=0.9078
One-Sample Student T-Test (0.05)	n.s.; p=0.18513; t=1.4058; df=12	NaN	n.s.; p=0.24561; t=-1.242; df=9
Wilcoxon Signed Rank Test (0.05)	NaN	n.s.; p=0.19092; Signed Rank=26	NaN

Table 5.67: Paired comparisons for LN2GCaMP6m 3ppm EB

A

```
          Model df      AIC      BIC    logLik   Test  L.Ratio p-value
ExpModel      1  8 232.7893 251.8455 -108.3946
NullModel     2  5 241.7695 253.6796 -115.8847 1 vs 2 14.98017  0.0018
```

B



C

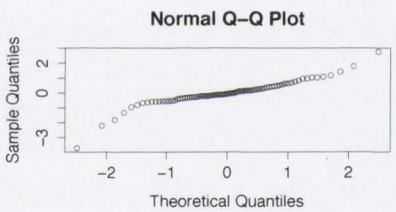


Table 5.68: Linear mixed effects analysis for OK371GCaMP6m 3ppm EB

	DM1	DM2	DM5
Number of Glomeruli	14	14	12
Number of Flies	14	14	12
Mean of Naive Response (0-10sec)	0.80669	1.3679	2.2035
SEM of Naive Response	0.15525	0.17116	0.4729
Mean of Response Change (0-10sec)	-0.21619	-0.28574	-1.4033
SEM of Response Change	0.10462	0.1809	0.55385
95% Confidence Interval	[-0.4422 0.0098329]	[-0.67656 0.10507]	[-2.6223 -0.18424]
Anderson-Darling Normality Test (0.05)	n.s.; p=0.13393	n.s.; p=0.63239	n.s.; p=0.14761
One-Sample Student T-Test (0.05)	n.s.; p=0.059316; t=-2.0664; df=13	n.s.; p=0.13823; t=-1.5795; df=13	p=0.027793; t=-2.5336; df=11
Wilcoxon Signed Rank Test (0.05)	NaN	NaN	NaN
Mean of Baseline Change	0.25869	-0.035555	1.2126
SEM of Baseline Change	0.21055	0.20512	0.6313
95% Confidence Interval	[-0.19618 0.71355]	[-0.47869 0.40758]	[-0.17687 2.6021]
Anderson-Darling Normality Test (0.05)	p=0.015335	n.s.; p=0.26155	n.s.; p=0.45156
One-Sample Student T-Test (0.05)	NaN	n.s.; p=0.86506; t=-0.17334; df=13	n.s.; p=0.081042; t=1.9208; df=11
Wilcoxon Signed Rank Test (0.05)	n.s.; p=0.42627; Signed Rank=66	NaN	NaN

Table 5.69: Paired comparisons for OK371GCaMP6m 3ppm EB

A

```
          Model df      AIC      BIC    logLik   Test  L.Ratio p-value
ExpModel      1  8 1110.761 1135.848 -547.3807
NullModel     2  5 1159.598 1175.277 -574.7989 1 vs 2 54.83654  <.0001

Linear mixed-effects model fit by maximum likelihood
 Data: reorganisedData
       AIC      BIC    logLik
  1110.761 1135.848 -547.3807

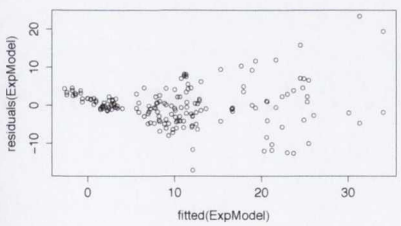
Random effects:
 Formula: ~1 | Fly
        (Intercept) Residual
StdDev:    4.097699 5.552374

Fixed effects: AUC010 ~ Run + Glomerulus + Run:Glomerulus
                            Value Std.Error  DF   t-value p-value
(Intercept)              3.163441  1.505284 150  2.101558  0.0373
RunRun2                 -0.980774  1.484558 150 -0.660650  0.5098
Glomerulusdm2            8.650762  1.473343 150  5.871518  0.0000
Glomerulusdm5           22.004950  1.529822 150 14.383994  0.0000
RunRun2:Glomerulusdm2   -0.357086  2.081913 150 -0.171518  0.8640
RunRun2:Glomerulusdm5  -11.383761  2.159195 150 -5.272224  0.0000
 Correlation:
                       (Intr) RunRn2 Glmrl2 Glmrl5 RR2:G2
RunRun2                -0.493
Glomerulusdm2          -0.498  0.504
Glomerulusdm5          -0.479  0.485  0.489
RunRun2:Glomerulusdm2   0.352 -0.713 -0.707 -0.346
RunRun2:Glomerulusdm5   0.339 -0.688 -0.346 -0.706  0.490

Standardized Within-Group Residuals:
        Min          Q1         Med          Q3         Max
-3.05398225 -0.50298859 -0.03228236  0.41805119  4.22013555

Number of Observations: 170
Number of Groups: 15
```

B



C

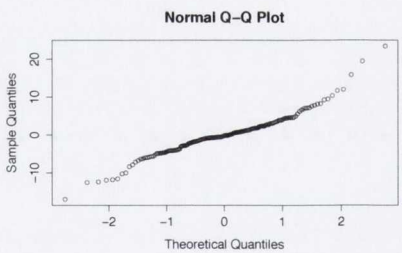
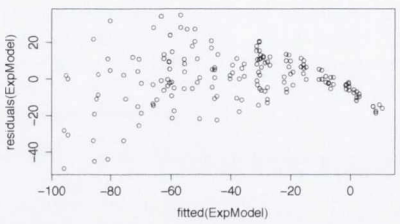


Table 5.70: Linear mixed effects analysis for GH146ArcLight 3ppm EB

A

```
          Model df      AIC      BIC    logLik   Test  L.Ratio p-value
ExpModel      1  8 1450.894 1475.981 -717.4472
NullModel     2  5 1451.151 1466.830 -720.5756 1 vs 2 6.256968  0.0998
```

B



C

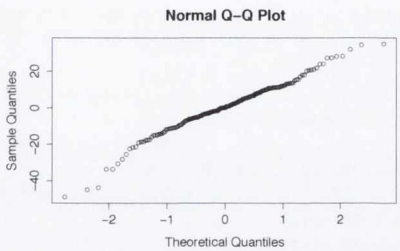


Table 5.71: Linear mixed effects analysis for GH146ArcLight 3ppm EB baseline

	DM1	DM2	DM5
Number of Glomeruli	29	30	26
Number of Flies	15	15	15
Mean of Naive Response (0-10sec)	3.3305	11.8142	25.1486
SEM of Naive Response	0.35745	1.0783	2.3654
Mean of Response Change (0-10sec)	-0.98077	-1.3379	-12.3645
SEM of Response Change	0.23674	1.2507	2.0486
95% Confidence Interval	[-1.4657 -0.49583]	[-3.8959 1.2202]	[-16.5838 -8.1453]
Anderson-Darling Normality Test (0.05)	n.s.; p=0.055778	n.s.; p=0.37605	n.s.; p=0.087319
One-Sample Student T-Test (0.05)	p=0.00028618; t=-4.1428; df=28	n.s.; p=0.2936; t=-1.0697; df=29	p=2.6384e-06; t=-6.0355; df=25
Wilcoxon Signed Rank Test (0.05)	NaN	NaN	NaN
Mean of Baseline Change	0.94077	0.82559	10.3004
SEM of Baseline Change	0.49788	2.2075	3.1818
95% Confidence Interval	[-0.079098 1.9606]	[-3.6893 5.3404]	[3.7473 16.8535]
Anderson-Darling Normality Test (0.05)	n.s.; p=0.1019	n.s.; p=0.33106	n.s.; p=0.69943
One-Sample Student T-Test (0.05)	n.s.; p=0.069215; t=1.8895; df=28	n.s.; p=0.71113; t=0.37399; df=29	p=0.0033912; t=3.2373; df=25
Wilcoxon Signed Rank Test (0.05)	NaN	NaN	NaN

Table 5.72: Paired comparisons for GH146ArcLight 3ppm EB

A

```
          Model df      AIC      BIC    logLik   Test  L.Ratio p-value
ExpModel      1  8 1022.003 1046.299 -503.0016
NullModel     2  5 1028.616 1043.801 -509.3081 1 vs 2 12.61304  0.0056

Linear mixed-effects model fit by maximum likelihood
 Data: reorganisedData
       AIC      BIC    logLik
  1022.003 1046.299 -503.0016

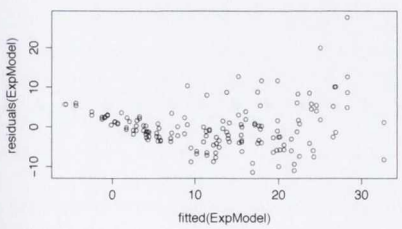
Random effects:
 Formula: ~1 | Fly
        (Intercept) Residual
StdDev:    4.082164  5.83315

Fixed effects: AUC010 ~ Run + Glomerulus + Run:Glomerulus
                            Value Std.Error  DF   t-value p-value
(Intercept)              3.191563  1.615515 135  1.975570  0.0502
RunRun2                 -1.223174  1.650292 135 -0.741186  0.4599
Glomerulusdm2           12.269644  1.636395 135  7.497972  0.0000
Glomerulusdm5           21.232970  1.686842 135 12.587411  0.0000
RunRun2:Glomerulusdm2   -2.613652  2.312155 135 -1.130396  0.2603
RunRun2:Glomerulusdm5   -3.162830  2.381992 135 -1.327809  0.1865
 Correlation:
                        (Intr) RunRn2 Glmrl2 Glmrl5 RR2:G2
RunRun2                 -0.511
Glomerulusdm2           -0.517  0.504
Glomerulusdm5           -0.500  0.489  0.494
RunRun2:Glomerulusdm2    0.365 -0.714 -0.706 -0.349
RunRun2:Glomerulusdm5    0.354 -0.693 -0.349 -0.706  0.494

Standardized Within-Group Residuals:
       Min         Q1        Med         Q3        Max
-1.9454309 -0.5855692 -0.1066038  0.4069743  4.7392187

Number of Observations: 154
Number of Groups: 14
```

B



C

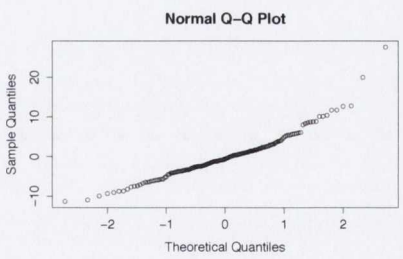


Table 5.73: Linear mixed effects analysis for GH146ArcLight mock

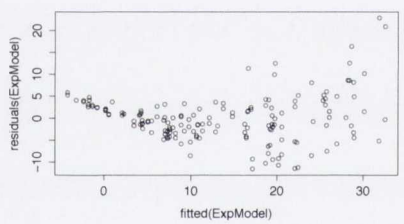
	DM1	DM2	DM5
Number of Glomeruli	26	27	24
Number of Flies	14	14	14
Mean of Naive Response (0-10sec)	3.2794	15.468	24.4326
SEM of Naive Response	0.32483	1.3269	2.2634
Mean of Response Change (0-10sec)	-1.2232	-3.8368	-4.386
SEM of Response Change	0.23279	1.3652	2.1807
95% Confidence Interval	[-1.7026 -0.74373]	[-6.643 -1.0306]	[-8.8972 0.12518]
Anderson-Darling Normality Test (0.05)	n.s.; p=0.65038	n.s.; p=0.3269	n.s.; p=0.35032
One-Sample Student T-Test (0.05)	p=1.9326e-05; t=-5.2543; df=25	p=0.0092767; t=-2.8104; df=26	n.s.; p=0.05616; t=-2.0113; df=23
Wilcoxon Signed Rank Test (0.05)	NaN	NaN	NaN
Mean of Baseline Change	1.4779	3.2997	5.7992
SEM of Baseline Change	0.59337	3.0533	4.5362
95% Confidence Interval	[0.25581 2.6999]	[-2.9765 9.5759]	[-3.5846 15.1831]
Anderson-Darling Normality Test (0.05)	n.s.; p=0.21025	n.s.; p=0.50728	n.s.; p=0.94653
One-Sample Student T-Test (0.05)	p=0.019753; t=2.4906; df=25	n.s.; p=0.28976; t=1.0807; df=26	n.s.; p=0.21385; t=1.2784; df=23
Wilcoxon Signed Rank Test (0.05)	NaN	NaN	NaN

Table 5.74: Paired comparisons for GH146ArcLight mock

A

```
          Model df      AIC      BIC    logLik   Test  L.Ratio p-value
ExpModel      1  8 1087.877 1112.577 -535.9383
NullModel     2  5 1086.022 1101.460 -538.0110 1 vs 2 4.145406  0.2462
```

B



C

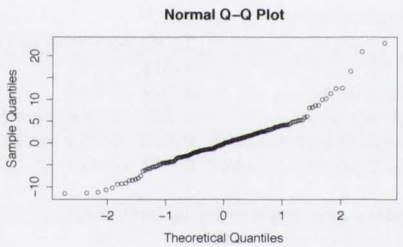
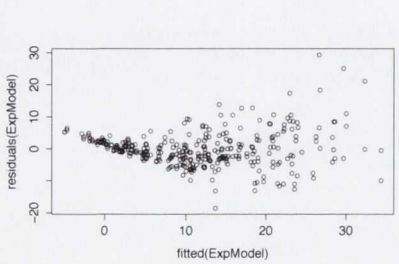


Table 5.75: Linear mixed effects analysis for GH146ArcLight comparing naïve responses of mock and EB

A

```
          Model df      AIC      BIC    logLik   Test  L.Ratio p-value
ExpModel      1 12 2137.129 2182.498 -1056.564
NullModel     2 11 2136.481 2178.069 -1057.240 1 vs 2 1.352101  0.2449
```

B



C

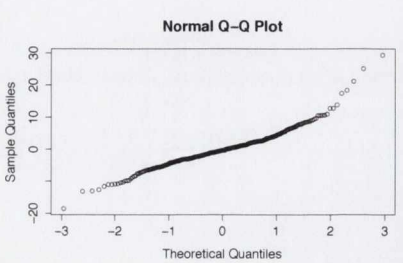
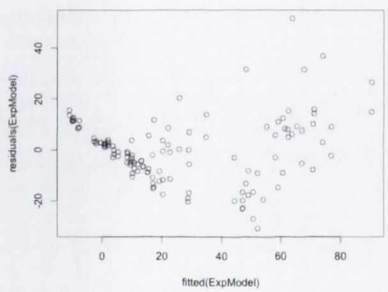


Table 5.76: Linear mixed effects analysis for GH146ArcLight comparing naïve and exposed responses of mock and EB

A

	Model	df	AIC	BIC	logLik	Test	L.Ratio	p-value
ExpModel	1	8	1062.785	1085.347	-523.3925			
NullModel	2	5	1059.616	1073.718	-524.8082	1 vs 2	2.831291	0.4184

B



C

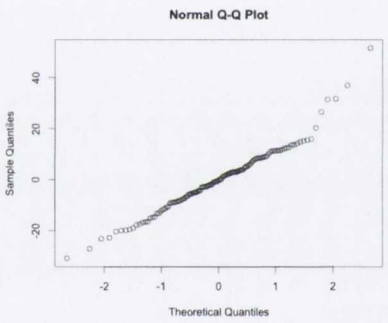


Table 5.77: Linear mixed effects analysis comparing naïve responses of flies expressing GBi-RNAi in OSNs and controls

A

```
          Model df      AIC      BIC    logLik   Test  L.Ratio p-value
ExpModel      1 12 2123.022 2165.183 -1049.511
NullModel     2 11 2136.993 2175.640 -1057.496 1 vs 2 15.97114   1e-04

Linear mixed-effects model fit by maximum likelihood
 Data: reorganisedData
       AIC      BIC    logLik
  2123.022 2165.183 -1049.511

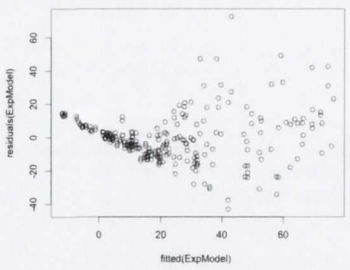
Random effects:
 Formula: ~1 | Fly
        (Intercept) Residual
StdDev:     10.5971 15.34789

Fixed effects: AUC010 ~ Run + Glomerulus + Genotype + Run:Glomerulus + Genotype:Run +      Genotype:Glomerul
us
                                 Value Std.Error  DF   t-value p-value
(Intercept)                    9.47066  4.670809 218  2.027628  0.0438
RunRun2                       -8.81297  3.989170 218 -2.209224  0.0282
Glomerulusdm2                 14.73959  4.225078 218  3.488596  0.0006
Glomerulusdm5                 56.35616  4.516249 218 12.478533  0.0000
GenotypeGABABi                -8.35448  6.058042  20 -1.379072  0.1831
RunRun2:Glomerulusdm2          0.24520  4.723781 218  0.051909  0.9586
RunRun2:Glomerulusdm5        -23.61370  4.979466 218 -4.742216  0.0000
RunRun2:GenotypeGABABi        15.93471  3.998360 218  3.985313  0.0001
Glomerulusdm2:GenotypeGABABi   1.21753  4.743422 218  0.256678  0.7977
Glomerulusdm5:GenotypeGABABi   4.44393  5.057538 218  0.878675  0.3805

Standardized Within-Group Residuals:
       Min         Q1        Med         Q3        Max
-2.79904213 -0.58053354 -0.06445335  0.50145269  4.72799076

Number of Observations: 248
Number of Groups: 22
```

B



C

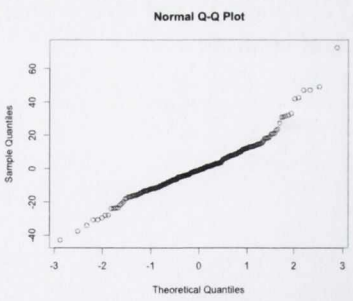


Table 5.78: Linear mixed effects analysis comparing naïve and exposed responses of flies expressing GBi-RNAi in OSNs and controls

A

```
         Model df      AIC      BIC    logLik   Test  L.Ratio p-value
ExpModel     1  6 545.0138 559.8779 -266.5069
NullModel    2  5 552.6701 565.0568 -271.3351 1 vs 2 9.656273  0.0019

Linear mixed-effects model fit by maximum likelihood
 Data: reorganisedData
       AIC      BIC    logLik
  545.0138 559.8779 -266.5069

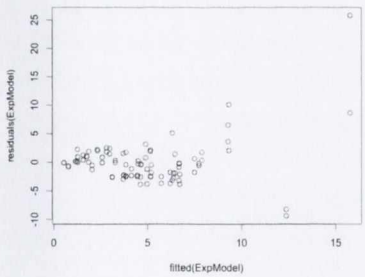
Random effects:
 Formula: ~1 | Fly
        (Intercept) Residual
StdDev:    3.168736 4.334527

Fixed effects: AUC010 ~ Run + Genotype + Genotype:Run
                            Value Std.Error DF   t-value p-value
(Intercept)              6.757036  1.426900 64  4.735467  0.0000
RunRun2                 -3.385723  1.402954 64 -2.413281  0.0187
GenotypeGABABi          -3.379497  1.932031 20 -1.749194  0.0956
RunRun2:GenotypeGABABi   5.984756  1.899609 64  3.150520  0.0025

Standardized Within-Group Residuals:
       Min         Q1        Med         Q3        Max
-2.16766373 -0.52143227 -0.04946163 0.30149815 5.94980220

Number of Observations: 88
Number of Groups: 22
```

B



C

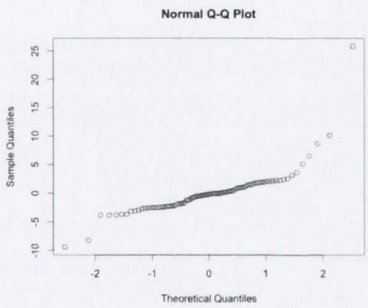


Table 5.79: Linear mixed effects analysis comparing naïve and exposed responses of flies expressing GBi-RNAi in OSNs and controls in DM1

A

```
         Model df      AIC      BIC    logLik   Test  L.Ratio p-value
ExpModel     1  6 769.0935 783.9575 -378.5468
NullModel    2  5 778.9036 791.2903 -384.4518 1 vs 2 11.81006   6e-04

Linear mixed-effects model fit by maximum likelihood
 Data: reorganisedData
       AIC      BIC    logLik
  769.0935 783.9575 -378.5468

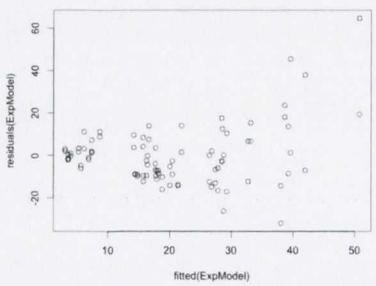
Random effects:
 Formula: ~1 | Fly
        (Intercept) Residual
StdDev:    12.18784 15.24273

Fixed effects: AUC010 ~ Run + Genotype + Genotype:Run
                            Value Std.Error DF   t-value p-value
(Intercept)              26.26554  5.266111 64  4.987654  0.0000
RunRun2                 -12.67835  4.933606 64 -2.569794  0.0125
GenotypeGABABi          -10.90498  7.130348 20 -1.529375  0.1418
RunRun2:GenotypeGABABi  23.47078  6.680134 64  3.513520  0.0008

Standardized Within-Group Residuals:
       Min         Q1        Med         Q3        Max
-2.0839951 -0.5769285 -0.1034366  0.3192533  4.2482795

Number of Observations: 88
Number of Groups: 22
```

B



C

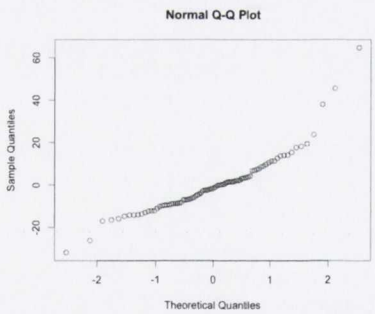


Table 5.80: Linear mixed effects analysis comparing naïve and exposed responses of flies expressing GBi-RNAi in OSNs and controls in DM2

A

```
         Model df      AIC      BIC    logLik   Test  L.Ratio p-value
ExpModel     1  6 666.5898 680.2498 -327.2949
NullModel    2  5 669.0466 680.4299 -329.5233 1 vs 2 4.456778  0.0348

Linear mixed-effects model fit by maximum likelihood
 Data: reorganisedData
       AIC      BIC    logLik
  666.5898 680.2498 -327.2949

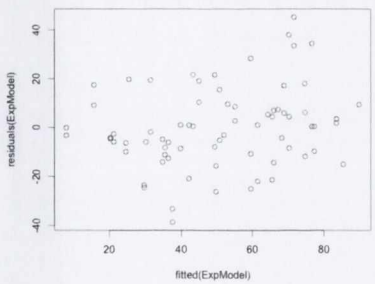
Random effects:
 Formula: ~1 | Fly
        (Intercept) Residual
StdDev:    18.2732 18.46112

Fixed effects: AUC010 ~ Run + Genotype + Genotype:Run
                          Value Std.Error DF   t-value p-value
(Intercept)            64.73555  7.906182 49  8.187966  0.0000
RunRun2               -34.07251  6.716220 49 -5.073168  0.0000
GenotypeGABABi         -1.83716 10.522199 19 -0.174599  0.8632
RunRun2:GenotypeGABABi 18.89721  9.010754 49  2.097184  0.0412

Standardized Within-Group Residuals:
       Min         Q1        Med         Q3        Max
-2.08807756 -0.52781015 -0.05177701  0.47361717  2.45261778

Number of Observations: 72
Number of Groups: 21
```

B



C

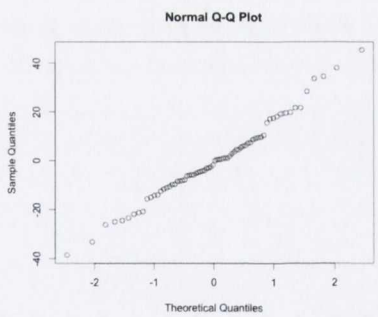


Table 5.81: Linear mixed effects analysis comparing naïve and exposed responses of flies expressing GBi-RNAi in OSNs and controls in DM5

A

```
          Model df      AIC      BIC    logLik   Test  L.Ratio p-value
ExpModel      1  8 791.5978 812.1126 -387.7989
NullModel     2  5 800.2052 813.0269 -395.1026 1 vs 2 14.60736  0.0022

Linear mixed-effects model fit by maximum likelihood
 Data: dataFrame
       AIC      BIC    logLik
  791.5978 812.1126 -387.7989

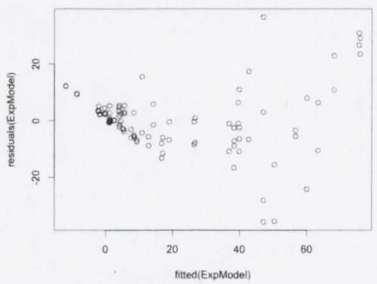
Random effects:
 Formula: ~1 | Fly
        (Intercept) Residual
StdDev:    8.572912 12.26221

Fixed effects: Run1 ~ Glomerulus + Genotype + Genotype:Glomerulus
                                    Value Std.Error DF   t-value p-value
(Intercept)                      3.32328  4.452351 76  0.746410  0.4577
Glomerulusdm2                    9.66890  4.477527 76  2.159428  0.0340
Glomerulusdm5                   58.79704  4.477527 76 13.131588  0.0000
GenotypeOr83bGABAAi             -1.55104  6.296576 14 -0.246330  0.8090
Glomerulusdm2:GenotypeOr83bGABAAi  -5.42326  6.332180 76 -0.856461  0.3944
Glomerulusdm5:GenotypeOr83bGABAAi -20.25474  6.332180 76 -3.198699  0.0020

Standardized Within-Group Residuals:
        Min          Q1         Med          Q3         Max
-2.90611135 -0.48824279 -0.01346536  0.30402282  2.98244267

Number of Observations: 96
Number of Groups: 16
```

B



C

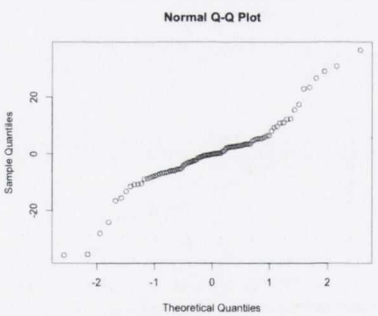


Table 5.82: Linear mixed effects analysis comparing naïve responses of flies expressing Rdl-RNAi in OSNs and controls

A

```
         Model df      AIC      BIC    logLik   Test  L.Ratio p-value
ExpModel     1 12 1513.282 1552.372 -744.641
NullModel    2 11 1515.130 1550.963 -746.565 1 vs 2 3.847946  0.0498

Linear mixed-effects model fit by maximum likelihood
 Data: reorganisedData
       AIC      BIC    logLik
  1513.282 1552.372 -744.641

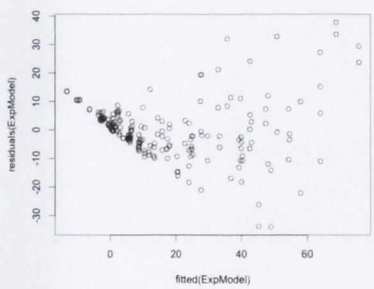
Random effects:
 Formula: ~1 | Fly
        (Intercept) Residual
StdDev:     7.86388 10.76134

Fixed effects: AUC010 ~ Run + Glomerulus + Genotype + Run:Glomerulus + Genotype:Run +      Genotype:Glomerul
us
                                    Value Std.Error  DF   t-value p-value
(Intercept)                      4.63921  3.810223 168  1.217568  0.2251
RunRun2                         -3.00505  3.190735 168 -0.941804  0.3476
Glomerulusdm2                    9.34138  3.384285 168  2.760222  0.0064
Glomerulusdm5                   55.17678  3.384285 168 16.303819  0.0000
GenotypeOr83bGABAAi             -4.18289  5.146882  14 -0.812704  0.4300
RunRun2:Glomerulusdm2            0.79452  3.907836 168  0.203316  0.8391
RunRun2:Glomerulusdm5          -18.24156  3.907836 168 -4.667945  0.0000
RunRun2:GenotypeOr83bGABAAi      6.12729  3.190735 168  1.920338  0.0565
Glomerulusdm2:GenotypeOr83bGABAAi -4.76823  3.907836 168 -1.220170  0.2241
Glomerulusdm5:GenotypeOr83bGABAAi -13.01421  3.907836 168 -3.330286  0.0011

Standardized Within-Group Residuals:
       Min         Q1        Med         Q3        Max
-3.15332110 -0.52260304 -0.03989127  0.38362218  3.51325886

Number of Observations: 192
Number of Groups: 16
```

B



C

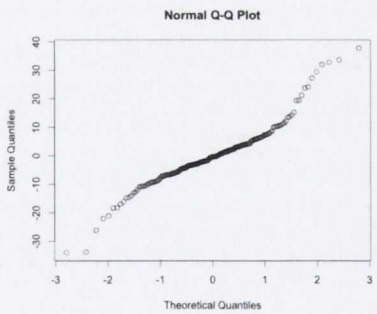
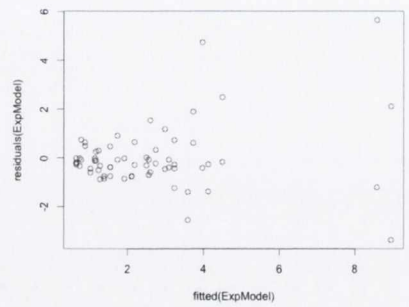


Table 5.83: Linear mixed effects analysis comparing naïve and exposed responses of flies expressing Rdl-RNAi in OSNs and controls

A

```
          Model df      AIC      BIC    logLik   Test  L.Ratio p-value
ExpModel      1  6 277.0411 289.9944 -132.5205
NullModel     2  5 276.3892 287.1837 -133.1946 1 vs 2 1.348156  0.2456
```

B



C

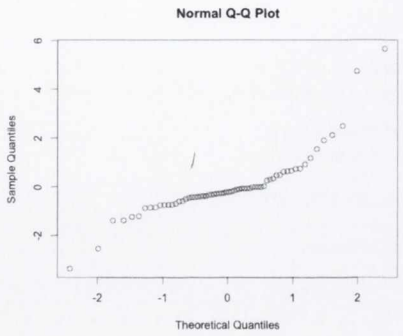
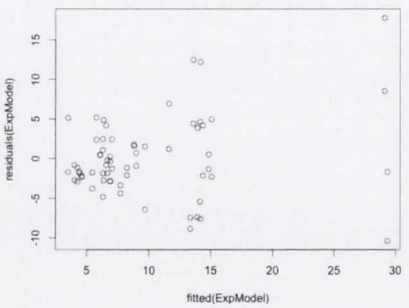


Table 5.84: Linear mixed effects analysis comparing naïve and exposed responses of flies expressing Rdl-RNAi in OSNs and controls in DM1

A

```
          Model df      AIC      BIC    logLik   Test   L.Ratio p-value
ExpModel      1  6 439.7838 452.7371 -213.8919
NullModel     2  5 438.4008 449.1952 -214.2004 1 vs 2 0.6170195  0.4322
```

B



C

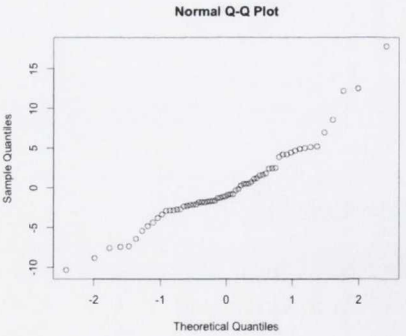


Table 5.85: Linear mixed effects analysis comparing naïve and exposed responses of flies expressing Rdl-RNAi in OSNs and controls in DM2

A

```
         Model df      AIC      BIC    logLik   Test  L.Ratio p-value
ExpModel     1  6 549.0511 562.0044 -268.5255
NullModel    2  5 553.0265 563.8209 -271.5133 1 vs 2 5.975413  0.0145

Linear mixed-effects model fit by maximum likelihood
 Data: reorganisedData
       AIC      BIC    logLik
  549.0511 562.0044 -268.5255

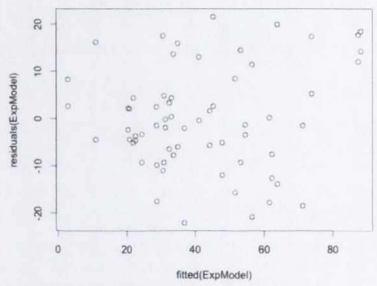
Random effects:
 Formula: ~1 | Fly
        (Intercept) Residual
StdDev:    17.47623 12.16596

Fixed effects: AUC010 ~ Run + Genotype + Genotype:Run
                              Value Std.Error DF   t-value p-value
(Intercept)                62.12032  7.112653 46  8.733776  0.0000
RunRun2                   -25.85528  4.442379 46 -5.820143  0.0000
GenotypeOr83bGABAAi       -21.80577 10.058810 14 -2.167828  0.0479
RunRun2:GenotypeOr83bGABAAi  15.34463  6.282472 46  2.442451  0.0185

Standardized Within-Group Residuals:
       Min         Q1        Med         Q3        Max
-1.7994967 -0.5497393 -0.1123410  0.4941733  1.7631601

Number of Observations: 64
Number of Groups: 16
```

B



C

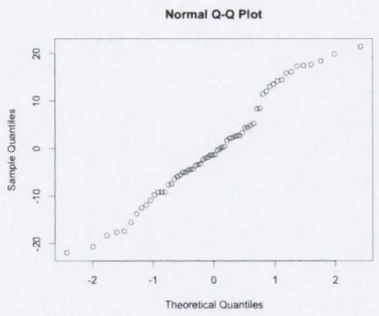


Table 5.86: Linear mixed effects analysis comparing naïve and exposed responses of flies expressing Rdl-RNAi in OSNs and controls in DM5

5.3 Appendix III: PID Measurements

Mean ppm of 1st puff	3.0246
SEM of mean ppm of 1st puff	0.22361
Mean ppm of 2nd puff	3.0339
SEM of mean ppm of 2nd puff	0.22361
Mean of ppm change	0.0093702
SEM of mean of ppm change	0.094961
Anderson-Darling Normality Test (0.05)	p=0.0046738
One-Sample Student T-Test (0.05)	NaN
Wilcoxon Signed Rank Test (0.05)	n.s.; p=0.65814; z=0.44249

Table 5.87: PID measurements for GH146GCaMP6m 3ppm

Mean ppm of 1st puff	16.0921
SEM of mean ppm of 1st puff	0.39278
Mean ppm of 2nd puff	16.5074
SEM of mean ppm of 2nd puff	0.39278
Mean of ppm change	0.4153
SEM of mean of ppm change	0.1626
Anderson-Darling Normality Test (0.05)	p=0.014666
One-Sample Student T-Test (0.05)	NaN
Wilcoxon Signed Rank Test (0.05)	p=0.0035338; z=2.917

Table 5.88: PID measurements for GH146GCaMP6m 20ppm

Mean ppm of 1st puff	7.7979
SEM of mean ppm of 1st puff	0.20397

Table 5.89: PID measurements for GH146GCaMP6m KCl

Mean ppm of 1st puff	1.2115
SEM of mean ppm of 1st puff	0.11073
Mean ppm of 2nd puff	1.4652
SEM of mean ppm of 2nd puff	0.11073
Mean of ppm change	0.25366
SEM of mean of ppm change	0.14143
Anderson-Darling Normality Test (0.05)	n.s.; p=0.68722
One-Sample Student T-Test (0.05)	n.s.; p=0.08551; t=1.7935; df=24
Wilcoxon Signed Rank Test (0.05)	NaN

Table 5.90: PID measurements for Or83bGCaMP6m 3ppm

Mean ppm of 1st puff	14.9996
SEM of mean ppm of 1st puff	0.40442
Mean ppm of 2nd puff	15.3572
SEM of mean ppm of 2nd puff	0.40442
Mean of ppm change	0.35759
SEM of mean of ppm change	0.18485
Anderson-Darling Normality Test (0.05)	n.s.; p=0.46059
One-Sample Student T-Test (0.05)	n.s.; p=0.062866; t=1.9345; df=29
Wilcoxon Signed Rank Test (0.05)	NaN

Table 5.91: PID measurements for Or83bGCaMP6m 20ppm

Mean ppm of 1st puff	6.5853
SEM of mean ppm of 1st puff	0.21473
Mean ppm of 2nd puff	6.6121
SEM of mean ppm of 2nd puff	0.21473
Mean of ppm change	0.026807
SEM of mean of ppm change	0.13434
Anderson-Darling Normality Test (0.05)	p=0.030766
One-Sample Student T-Test (0.05)	NaN
Wilcoxon Signed Rank Test (0.05)	n.s.; p=0.86475; Signed Rank=41.5

Table 5.92: PID measurements for Or83bGCaMP6m mock

Mean ppm of 1st puff	3.7849
SEM of mean ppm of 1st puff	0.16691
Mean ppm of 2nd puff	4.0106
SEM of mean ppm of 2nd puff	0.16691
Mean of ppm change	0.22571
SEM of mean of ppm change	0.078974
Anderson-Darling Normality Test (0.05)	n.s.; p=0.6059
One-Sample Student T-Test (0.05)	p=0.028877; t=2.858; df=6
Wilcoxon Signed Rank Test (0.05)	NaN

Table 5.93: PID measurements for LN1GCaMP6m 3ppm

Mean ppm of 1st puff	2.7974
SEM of mean ppm of 1st puff	0.43566
Mean ppm of 2nd puff	3.7212
SEM of mean ppm of 2nd puff	0.43566
Mean of ppm change	0.92377
SEM of mean of ppm change	0.37546
Anderson-Darling Normality Test (0.05)	p=0.013689
One-Sample Student T-Test (0.05)	NaN
Wilcoxon Signed Rank Test (0.05)	p=0.015625; Signed Rank=28

Table 5.94: PID measurements for LN2GCaMP6m 3ppm

Mean ppm of 1st puff	6.5902
SEM of mean ppm of 1st puff	0.36054
Mean ppm of 2nd puff	6.7898
SEM of mean ppm of 2nd puff	0.36054
Mean of ppm change	0.19962
SEM of mean of ppm change	0.084356
Anderson-Darling Normality Test (0.05)	n.s.; p=0.20996
One-Sample Student T-Test (0.05)	p=0.037391; t=2.3664; df=11
Wilcoxon Signed Rank Test (0.05)	NaN

Table 5.95: PID measurements for OK371GCaMP6m 3ppm

Mean ppm of 1st puff	4.7673
SEM of mean ppm of 1st puff	0.43459
Mean ppm of 2nd puff	5.1057
SEM of mean ppm of 2nd puff	0.43459
Mean of ppm change	0.33838
SEM of mean of ppm change	0.47761
Anderson-Darling Normality Test (0.05)	p=0.024945
One-Sample Student T-Test (0.05)	NaN
Wilcoxon Signed Rank Test (0.05)	n.s.; p=0.59949; Signed Rank=70

Table 5.96: PID measurements for GH146ArcD 3ppm

Mean ppm of 1st puff	3.4822
SEM of mean ppm of 1st puff	0.32014
Mean ppm of 2nd puff	3.8359
SEM of mean ppm of 2nd puff	0.32014
Mean of ppm change	0.35368
SEM of mean of ppm change	0.35348
Anderson-Darling Normality Test (0.05)	n.s.; p=0.56723
One-Sample Student T-Test (0.05)	n.s.; p=0.33531; t=1.0005; df=13
Wilcoxon Signed Rank Test (0.05)	NaN

Table 5.97: PID measurements for GH146ArcD mock

Bibliography

N. M. Abraham, V. Egger, D. R. Shimshek, R. Renden, I. Fukunaga, R. Sprengel, P. H. Seeburg, M. Klugmann, T. W. Margrie, A. T. Schaefer, and T. Kuner. Synaptic inhibition in the olfactory bulb accelerates odor discrimination in mice. *Neuron*, 65(3):399–411, Feb. 2010.

L. Abuin, B. Bargeton, M. H. Ulbrich, E. Y. Isacoff, S. Kellenberger, and R. Benton. Functional architecture of olfactory ionotropic glutamate receptors. *Neuron*, 69(1):44–60, Jan. 2011.

A. Acebes, A. Martín-Peña, V. Chevalier, and A. Ferrus. Synapse loss in olfactory local interneurons modifies perception. *Journal of Neuroscience*, 31(8):2734–2745, Feb. 2011.

B. W. Ache and J. M. Young. Olfaction: diverse species, conserved principles. *Neuron*, 48 (3):417–430, Nov. 2005.

M. D. Adams, S. E. Celniker, R. A. Holt, C. A. Evans, J. D. Gocayne, P. G. Amanatides, S. E. Scherer, P. W. Li, R. A. Hoskins, R. F. Galle, R. A. George, S. E. Lewis, S. Richards, M. Ashburner, S. N. Henderson, G. G. Sutton, J. R. Wortman, M. D. Yandell, Q. Zhang, L. X. Chen, R. C. Brandon, Y.-H. H. Rogers, R. G. Blazej, M. Champe, B. D. Pfeiffer, K. H. Wan, C. Doyle, E. G. Baxter, G. Helt, C. R. Nelson, G. L. Gabor, J. F. Abril, A. Agbayani, H.-J. J. An, C. Andrews-Pfannkoch, D. Baldwin, R. M. Ballew, A. Basu, J. Baxendale, L. Bayraktaroglu, E. M. Beasley, K. Y. Beeson, P. V. Benos, B. P. Berman, D. Bhandari, S. Bolshakov, D. Borkova, M. R. Botchan, J. Bouck, P. Brokstein, P. Brottier, K. C. Burtis, D. A. Busam, H. Butler, E. Cadieu, A. Center, I. Chandra, J. M. Cherry, S. Cawley, C. Dahlke, L. B. Davenport, P. Davies, B. de Pablos, A. Delcher, Z. Deng, A. D. Mays, I. Dew, S. M. Dietz, K. Dodson, L. E. Doup, M. Downes, S. Dugan-Rocha, B. C. Dunkov, P. Dunn, K. J. Durbin, C. C. Evangelista, C. Ferraz, S. Ferriera, W. Fleischmann, C. Fosler, A. E. Gabrielian, N. S. Garg, W. M. Gelbart, K. Glasser, A. Glodek, F. Gong, J. H. Gorrell, Z. Gu, P. Guan, M. Harris, N. L. Harris, D. Harvey, T. J. Heiman, J. R. Hernandez, J. Houck, D. Hostin, K. A. Houston, T. J. Howland, M. H. Wei, C. Ibegwam, M. Jalali, F. Kalush, G. H. Karpen, Z. Ke, J. A. Kennison, K. A. Ketchum, B. E. Kimmel, C. D. Kodira, C. Kraft, S. Kravitz, D. Kulp, Z. Lai, P. Lasko, Y. Lei, A. A. Levitsky, J. Li, Z. Li, Y. Liang, X. Lin, X. Liu, B. Mattei, T. C. McIntosh, M. P. McLeod, D. McPherson, G. Merkulov, N. V. Milshina, C. Mobarry, J. Morris, A. Moshrefi, S. M. Mount, M. Moy, B. Murphy, L. Murphy, D. M. Muzny, D. L. Nelson, D. R. Nelson, K. A. Nelson, K. Nixon, D. R. Nusskern, J. M. Pacleb, M. Palazzolo, G. S. Pittman, S. Pan, J. Pollard, V. Puri, M. G. Reese, K. Reinert, K. Remington, R. D. Saunders, F. Scheeler, H. Shen, B. C. Shue, I. Sidén-Kiamos, M. Simpson, M. P. Skupski, T. Smith, E. Spier, A. C. Spradling, M. Stapleton, R. Strong, E. Sun, R. Svirskas, C. Tector, R. Turner, E. Venter, A. H. Wang, X. Wang, Z. Y. Wang, D. A. Wassarman, G. M. Weinstock, J. Weissenbach,

S. M. Williams, WoodageT, K. C. Worley, D. Wu, S. Yang, Q. A. Yao, J. Ye, R. F. Yeh, J. S. Zaveri, M. Zhan, G. Zhang, Q. Zhao, L. Zheng, X. H. Zheng, F. N. Zhong, W. Zhong, X. Zhou, S. Zhu, X. Zhu, H. O. Smith, R. A. Gibbs, E. W. Myers, G. M. Rubin, and J. C. Venter. The genome sequence of Drosophila melanogaster. *Science*, 287(5461): 2185–2195, Mar. 2000.

M. Ai, S. Min, Y. Grosjean, C. Leblanc, R. Bell, R. Benton, and G. S. B. Suh. Acid sensing by the Drosophila olfactory system. *Nature*, 468(7324):691–695, Dec. 2010.

D.-B. G. Akalal, D. Yu, and R. L. Davis. A late-phase, long-term memory trace forms in the γ neurons of Drosophila mushroom bodies after olfactory classical conditioning. *Journal of Neuroscience*, 30(49):16699–16708, Dec. 2010.

S. J. Akdag, P. G. Nestor, B. F. O'Donnell, M. A. Niznikiewicz, M. E. Shenton, and R. W. McCarley. The startle reflex in schizophrenia: habituation and personality correlates. *Schizophrenia Research*, 64(2-3):165–173, Nov. 2003.

J. Akerboom, T.-W. Chen, T. J. Wardill, L. Tian, J. S. Marvin, S. Mutlu, N. C. Calderón, F. Esposti, B. G. Borghuis, X. R. Sun, A. Gordus, M. B. Orger, R. Portugues, F. Engert, J. J. Macklin, A. Filosa, A. Aggarwal, R. A. Kerr, R. Takagi, S. Kracun, E. Shigetomi, B. S. Khakh, H. Baier, L. Lagnado, S. S.-H. Wang, C. I. Bargmann, B. E. Kimmel, V. Jayaraman, K. Svoboda, D. S. Kim, E. R. Schreiter, and L. L. Looger. Optimization of a GCaMP calcium indicator for neural activity imaging. *Journal of Neuroscience*, 32(40): 13819–13840, Oct. 2012.

M. N. Andersson, F. Schlyter, S. R. Hill, and T. Dekker. What Reaches the Antenna? How to Calibrate Odor Flux and Ligand–Receptor Affinities. *Chemical senses*, 37(5):403–420, June 2012.

A. C. Arevian, V. Kapoor, and N. N. Urban. Activity-dependent gating of lateral inhibition in the mouse olfactory bulb. *Nature Neuroscience*, 11(1):80–87, Jan. 2008.

K. Aronstein and R. Ffrench-Constant. Immunocytochemistry of a novel GABA receptor subunit Rdl in Drosophila melanogaster. *Invertebrate Neuroscience*, 1(1):25–31, June 1995.

K. Aronstein, V. Auld, and R. Ffrench-Constant. Distribution of two GABA receptor-like subunits in the Drosophila CNS. *Invertebrate Neuroscience*, 2(2):115–120, Sept. 1996.

Z. Asztalos, N. Arora, and T. Tully. Olfactory jump reflex habituation in Drosophila and effects of classical conditioning mutations. *Journal of Neurogenetics*, 21(1-2):1–18, Jan. 2007a.

Z. Asztalos, K. Baba, D. Yamamoto, and T. Tully. The fickle mutation of a cytoplasmic tyrosine kinase effects sensitization but not dishabituation in Drosophila melanogaster. *Journal of Neurogenetics*, 21(1-2):59–71, Jan. 2007b.

R. J. Bainton, L. T. Y. Tsai, C. M. Singh, and M. S. Moore. Dopamine modulates acute responses to cocaine, nicotine and ethanol in Drosophila. *Current Biology*, 10(4):187–194, 2000.

B. S. Baker, B. J. Taylor, and J. C. Hall. Are Complex Behaviors Specified by Dedicated Regulatory Genes? Reasoning from Drosophila. *Cell*, 105(1):13–24, Apr. 2001.

A. B. Barron. Anaesthetising Drosophila for behavioural studies. *Journal of insect physiology*, 46(4):439–442, Apr. 2000.

A. L. Barth. Visualizing circuits and systems using transgenic reporters of neural activity. *Current Opinion in Neurobiology*, 17(5):567–571, Oct. 2007.

J. Barth, S. Dipt, U. Pech, M. Hermann, T. Riemensperger, and A. Fiala. Differential associative training enhances olfactory acuity in Drosophila melanogaster. *Journal of Neuroscience*, 34(5):1819–1837, Jan. 2014.

M. F. Bear and R. C. Malenka. Synaptic plasticity: LTP and LTD. *Current Opinion in Neurobiology*, 4(3):389–399, June 1994.

K. M. Beckingham, J. D. Armstrong, M. J. Texada, R. Munjaal, and D. A. Baker. Drosophila melanogaster–the model organism of choice for the complex biology of multi-cellular organisms. *Gravitational and space biology bulletin*, 18(2):17–29, June 2005.

H. J. Bellen, C. Tong, and H. Tsuda. 100 years of Drosophila research and its impact on vertebrate neuroscience: a history lesson for the future. *Nature Reviews Neuroscience*, 11 (7):514–522, July 2010.

R. Benton. On the ORigin of smell: odorant receptors in insects. *Cellular and molecular life sciences*, 63(14):1579–1585, July 2006.

R. Benton, K. S. Vannice, C. Gomez-Diaz, and L. B. Vosshall. Variant ionotropic glutamate receptors as chemosensory receptors in Drosophila. *Cell*, 136(1):149–162, Jan. 2009.

S. Benzer. Behavioural mutants of Drosophila isolated by countercurrent distribution. *Proceedings of the National Academy of Sciences*, 58(3):1112–1119, Sept. 1967.

S. Benzer. Genetic dissection of behavior. *Scientific American*, 229(6):24–37, Dec. 1973.

D. Berdnik, A. P. Fan, C. J. Potter, and L. Luo. MicroRNA processing pathway regulates olfactory neuron morphogenesis. *Current Biology*, 18(22):1754–1759, Nov. 2008.

M. J. Berridge. Neuronal Calcium Signaling. *Neuron*, 21(1):13–26, July 1998.

M. J. Berridge, M. D. Bootman, and P. Lipp. Calcium-a life and death signal. *Nature*, 395 (6703):645–648, Oct. 1998.

M. J. Berridge, P. Lipp, and M. D. Bootman. The versatility and universality of calcium signalling. *Nature reviews. Molecular cell biology*, 1(1):11–21, Oct. 2000.

A. R. Best and D. A. Wilson. Coordinate synaptic mechanisms contributing to olfactory cortical adaptation. *Journal of Neuroscience*, 24(3):652–660, Jan. 2004.

V. Bhandawat, S. R. Olsen, N. W. Gouwens, M. L. Schlief, and R. I. Wilson. Sensory processing in the Drosophila antennal lobe increases reliability and separability of ensemble odor representations. *Nature Neuroscience*, 10(11):1474–1482, Nov. 2007.

V. Bhandawat, J. Reisert, and K.-W. Yau. Signaling by olfactory receptor neurons near threshold. *Proceedings of the National Academy of Sciences*, 107(43):18682–18687, Oct. 2010.

J. R. Bloomquist, R. H. Ffrench Constant, and R. T. Roush. Excitation of central neurons by dieldrin and picrotoxinin in susceptible and resistant Drosophila melanogaster (meigen). *Pesticide Science*, 32(4):463–469, Jan. 1991.

M. Bonino, D. Cantino, and M. Sassoè-Pognetto. Cellular and subcellular localization of γ-aminobutyric acidB receptors in the rat olfactory bulb. *Neuroscience Letters*, 274(3): 195–198, Oct. 1999.

M. D. Bootman, T. J. Collins, C. M. Peppiatt, L. S. Prothero, L. MacKenzie, P. De Smet, M. Travers, S. C. Tovey, J. T. Seo, M. J. Berridge, F. Ciccolini, and P. Lipp. Calcium signalling—an overview. *Seminars in cell & developmental biology*, 12(1):3–10, Feb. 2001a.

M. D. Bootman, P. Lipp, and M. J. Berridge. The organisation and functions of local Ca(2+) signals. *Journal of cell science*, 114(Pt 12):2213–2222, June 2001b.

S. Boynton and T. Tully. latheo, a new gene involved in associative learning and memory in Drosophila melanogaster, identified from P element mutagenesis. *Genetics*, 131:655–672, July 1992.

D. L. Braff, M. A. Geyer, G. A. Light, J. Sprock, W. Perry, K. S. Cadenhead, and N. R. Swerdlow. Impact of prepulse characteristics on the detection of sensorimotor gating deficits in schizophrenia. *Schizophrenia Research*, 49(1-2):171–178, Apr. 2001.

C. R. Bramham and D. G. Wells. Dendritic mRNA: transport, translation and function. *Nature Reviews Neuroscience*, 8(10):776–789, Oct. 2007.

A. H. Brand and N. Perrimon. Targeted gene expression as a means of altering cell fates and generating dominant phenotypes. *Development*, 118(2):401–415, June 1993.

S. D. Buckingham, P. C. Biggin, B. M. Sattelle, L. A. Brown, and D. B. Sattelle. Insect GABA Receptors: Splicing, Editing, and Targeting by Antiparasitics and Insecticides. *Molecular Pharmacology*, 68(4):942–951, Oct. 2005.

N. Buonviso, R. Gervais, M. Chalansonnet, and M. Chaput. Short-lasting exposure to one odour decreases general reactivity in the olfactory bulb of adult rats. *The European journal of neuroscience*, 10(7):2472–2475, July 1998.

S. Busch, M. Selcho, K. Ito, and H. Tanimoto. A map of octopaminergic neurons in the Drosophila brain. *The Journal of comparative neurology*, 513(6):643–667, Apr. 2009.

M. Bykhovskaia. Synapsin regulation of vesicle organization and functional pools. *Seminars in cell & developmental biology*, 22(4):387–392, June 2011.

G. Cao, J. Platisa, V. A. Pieribone, D. Raccuglia, M. Kunst, and M. N. Nitabach. Genetically targeted optical electrophysiology in intact neural circuits. *Cell*, 154(4):904–913, Aug. 2013.

T. J. Carew and E. R. Kandel. Acquisition and retention of long-term habituation in Aplysia: correlation of behavioral and cellular processes. *Science*, 182(4117):1158–1160, Dec. 1973.

T. J. Carew, H. M. Pinsker, and E. R. Kandel. Long-term habituation of a defensive withdrawal reflex in aplysia. *Science*, 175(4020):451–454, Jan. 1972.

M. A. Carlsson, M. Diesner, J. Schachtner, and D. R. Nässel. Multiple neuropeptides in the Drosophila antennal lobe suggest complex modulatory circuits. *The Journal of comparative neurology*, 518(16):3359–3380, Aug. 2010.

S. J. C. Caron, V. Ruta, L. F. Abbott, and R. Axel. Random convergence of olfactory inputs in the Drosophila mushroom body. *Nature*, 497(7447):113–117, May 2013.

V. Castellucci, H. Pinsker, I. Kupfermann, and E. R. Kandel. Neuronal mechanisms of habituation and dishabituation of the gill-withdrawal reflex in Aplysia. *Science*, 167(3926): 1745–1748, Mar. 1970.

V. F. Castellucci and E. R. Kandel. A quantal analysis of the synaptic depression underlying habituation of the gill-withdrawal reflex in Aplysia. *Proceedings of the National Academy of Sciences*, 71(12):5004–5008, Dec. 1974.

P. E. Castillo. Presynaptic LTP and LTD of excitatory and inhibitory synapses. *Cold Spring Harbor Perspectives in Biology*, 4(2):a005728–a005728, Feb. 2012.

P. E. Castillo, C. Q. Chiu, and R. C. Carroll. Long-term plasticity at inhibitory synapses. *Current Opinion in Neurobiology*, 21(2):328–338, Apr. 2011.

W. A. Catterall and A. P. Few. Calcium channel regulation and presynaptic plasticity. *Neuron*, 59(6):882–901, Sept. 2008.

J. R. Chalifoux and A. G. Carter. GABAB receptor modulation of synaptic function. *Current Opinion in Neurobiology*, 21(2):339–344, Apr. 2011.

S. B. C. Chandra and S. Singh. Chemosensory processing in the fruit fly, Drosophila melanogaster: Generalization of a feeding response reveals overlapping odour representations. *Journal of biosciences*, 30(5):679–688, Dec. 2005.

D. Chaudhury, L. Manella, A. Arellanos, O. Escanilla, T. A. Cleland, and C. Linster. Olfactory bulb habituation to odor stimuli. *Behavioral neuroscience*, 124(4):490–499, Aug. 2010.

T.-W. Chen, T. J. Wardill, Y. Sun, S. R. Pulver, S. L. Renninger, A. Baohan, E. R. Schreiter, R. A. Kerr, M. B. Orger, V. Jayaraman, L. L. Looger, K. Svoboda, and D. S. Kim. Ultrasensitive fluorescent proteins for imaging neuronal activity. *Nature*, 499(7458):295–300, July 2013.

M. E. Chiappe, J. D. Seelig, M. B. Reiser, and V. Jayaraman. Walking modulates speed sensitivity in Drosophila motion vision. *Current biology*, 20(16):1470–1475, Aug. 2010.

J. Y. Cho, N. Min, L. Franzen, and H. Baker. Rapid down-regulation of tyrosine hydroxylase expression in the olfactory bulb of naris-occluded adult rats. *The Journal of comparative neurology*, 369(2):264–276, May 1996.

W. Cho, U. Heberlein, and F. W. Wolf. Habituation of an odorant-induced startle response in Drosophila. *Genes, brain, and behavior*, 3(3):127–137, June 2004.

Y.-H. Chou, M. L. Spletter, E. Yaksi, J. C. S. Leong, R. I. Wilson, and L. Luo. Diversity and wiring variability of olfactory local interneurons in the Drosophila antennal lobe. *Nature Neuroscience*, 13(4):439–449, Apr. 2010.

G. R. Christoffersen. Habituation: events in the history of its characterization and linkage to synaptic depression. A new proposed kinetic criterion for its identification. *Progress in Neurobiology*, 53(1):45–66, Sept. 1997.

D. E. Clapham. Calcium signaling. *Cell*, 80(2):259–268, Jan. 1995.

R. E. Clark. The classical origins of Pavlov's conditioning. *Integrative Physiological & behavioral science*, 39(4):279–294, 2004.

P. Clyne, A. Grant, R. O'Connell, and J. R. Carlson. Odorant response of individual sensilla on the Drosophila antenna. *Invertebrate Neuroscience*, 3(2-3):127–135, Sept. 1997.

P. J. Clyne, C. G. Warr, M. R. Freeman, D. Lessing, J. Kim, and J. R. Carlson. A novel family of divergent seven-transmembrane proteins: candidate odorant receptors in Drosophila. *Neuron*, 22(2):327–338, Feb. 1999.

G. L. Collingridge. The induction of N-methyl-D-aspartate receptor-dependent long-term potentiation. *Philosophical transactions of the Royal Society of London.*, 358(1432):635–641, Apr. 2003.

M. Costa-Mattioli, W. S. Sossin, E. Klann, and N. Sonenberg. Translational Control of Long-Lasting Synaptic Plasticity and Memory. *Neuron*, 61(1):10–26, Jan. 2009.

A. Couto, M. Alenius, and B. J. Dickson. Molecular, anatomical, and functional organization of the Drosophila olfactory system. *Current biology*, 15(17):1535–1547, Sept. 2005.

A. M. Dacks, D. S. Green, C. M. Root, A. J. Nighorn, and J. W. Wang. Serotonin modulates olfactory processing in the antennal lobe of Drosophila. *Journal of Neurogenetics*, 23(4): 366–377, Oct. 2009.

R. W. Daniels, M. V. Gelfand, C. A. Collins, and A. DiAntonio. Visualizing glutamatergic cell bodies and synapses in Drosophila larval and adult CNS. *The Journal of comparative neurology*, 508(1):131–152, May 2008.

A. Das, A. Chiang, S. Davla, R. Priya, H. Reichert, K. Vijayraghavan, and V. Rodrigues. Identification and analysis of a glutamatergic local interneuron lineage in the adult Drosophila olfactory system. *Neural systems & circuits*, 1(1):4, Jan. 2011a.

S. Das, M. K. Sadanandappa, A. Dervan, A. Larkin, J. A. Lee, I. P. Sudhakaran, R. Priya, R. Heidari, E. E. Holohan, A. Pimentel, A. Gandhi, K. Ito, S. Sanyal, J. W. Wang, V. Rodrigues, and M. Ramaswami. Plasticity of local GABAergic interneurons drives olfactory habituation. *Proceedings of the National Academy of Sciences*, 108(36):E646–54, Sept. 2011b.

R. L. Davis. Olfactory learning. *Neuron*, 44(1):31–48, Sept. 2004.

R. L. Davis. Olfactory memory formation in Drosophila: from molecular to systems neuroscience. *Annual review of neuroscience*, 28(1):275–302, Mar. 2005.

M. de Bruyne, P. J. Clyne, and J. R. Carlson. Odor coding in a model olfactory organ: the Drosophila maxillary palp. *Journal of Neuroscience*, 19(11):4520–4532, June 1999.

M. de Bruyne, K. Foster, and J. R. Carlson. Odor coding in the Drosophila antenna. *Neuron*, 30(2):537–552, May 2001.

A. del Valle Rodríguez, D. Didiano, and C. Desplan. Power tools for gene expression and clonal analysis in Drosophila. *Nature methods*, 9(1):47–55, Jan. 2012.

M. Deshpande, K. Venkatesh, V. Rodrigues, and G. Hasan. The inositol 1,4,5-trisphosphate receptor is required for maintenance of olfactory adaptation in Drosophila antennae. *Journal of Neurobiology*, 43(3):282–288, June 2000.

J.-M. Devaud, A. Acebes, and A. Ferrús. Odor exposure causes central adaptation and morphological changes in selected olfactory glomeruli in Drosophila. *Journal of Neuroscience*, 21(16):6274–6282, Aug. 2001.

B. J. Dickson. Wired for Sex: The Neurobiology of Drosophila Mating Decisions. *Science*, 322(5903):904–909, Nov. 2008.

A. A. Dobritsa, W. Van Der Goes Van Naters, C. G. Warr, R. A. Steinbrecht, and J. R. Carlson. Integrating the molecular and cellular basis of odor coding in the Drosophila antenna. *Neuron*, 37(5):827–841, Mar. 2003.

J. B. Duffy. GAL4 system in Drosophila: a fly geneticist's Swiss army knife. *Genesis*, 34 (1-2):1–15, Sept. 2002.

H. K. M. Dweck, S. A. M. Ebrahim, S. Kromann, D. Bown, Y. Hillbur, S. Sachse, B. S. Hansson, and M. C. Stensmyr. Olfactory Preference for Egg Laying on Citrus Substrates in Drosophila. *Current Biology*, 23(24):2472–2480, Dec. 2013.

H. K. M. Dweck, S. A. M. Ebrahim, A. Farhan, B. S. Hansson, and M. C. Stensmyr. Olfactory Proxy Detection of Dietary Antioxidants in Drosophila. *Current Biology*, 25(4): 455–466, Feb. 2015a.

H. K. M. Dweck, S. A. M. Ebrahim, M. Thoma, A. A. M. Mohamed, I. W. Keesey, F. Trona, S. Lavista-Llanos, A. Svatoš, S. Sachse, M. Knaden, and B. S. Hansson. Pheromones mediating copulation and attraction in Drosophila. *Proceedings of the National Academy of Sciences*, 112(21):E2829–35, May 2015b.

M. Eddison, A. T. Belay, M. B. Sokolowski, and U. Heberlein. A genetic screen for olfactory habituation mutations in Drosophila: analysis of novel foraging alleles and an underlying neural circuit. *PloS one*, 7(12):e51684, Dec. 2012.

L. Enell, Y. Hamasaka, A. Kolodziejczyk, and D. R. Nässel. gamma-Aminobutyric acid (GABA) signaling components in Drosophila: immunocytochemical localization of GABA(B) receptors in relation to the GABA(A) receptor subunit RDL and a vesicular GABA transporter. *The Journal of comparative neurology*, 505(1):18–31, Nov. 2007.

J. E. Engel and C.-F. Wu. Neurogenetic approaches to habituation and dishabituation in Drosophila. *Neurobiology of Learning and Memory*, 92(2):166–175, Sept. 2009.

J. Esdin, K. Pearce, and D. L. Glanzman. Long-term habituation of the gill-withdrawal reflex in aplysia requires gene transcription, calcineurin and L-type voltage-gated calcium channels. *Frontiers in behavioral neuroscience*, 4:181, Nov. 2010.

Y. Ezzeddine and D. L. Glanzman. Prolonged habituation of the gill-withdrawal reflex in Aplysia depends on protein synthesis, protein phosphatase activity, and postsynaptic glutamate receptors. *Journal of Neuroscience*, 23(29):9585–9594, Oct. 2003.

R. H. Ffrench-Constant and D. P. Mortlock. Molecular cloning and transformation of cyclodiene resistance in Drosophila: an invertebrate gamma-aminobutyric acid subtype A

receptor locus. *Proceedings of the National Academy of Sciences*, 88:7209–7213, Aug. 1991.

A. Fiala and T. Spall. In vivo calcium imaging of brain activity in Drosophila by transgenic cameleon expression. *Science's STKE*, Mar. 2003.

A. Fiala, T. Spall, S. Diegelmann, B. Eisermann, S. Sachse, J.-M. Devaud, E. Buchner, and C. G. Galizia. Genetically expressed cameleon in Drosophila melanogaster is used to visualize olfactory information in projection neurons. *Current biology*, 12(21):1877–1884, Oct. 2002.

M. Fill and J. A. Copello. Ryanodine Receptor Calcium Release Channels. *Physiological Reviews*, 82(4):893–922, Jan. 2002.

J. A. Fischer, E. Giniger, T. Maniatis, and M. Ptashne. GAL4 activates transcription in Drosophila. *Nature*, 332(6167):853–856, Apr. 1988.

M. Fişek and R. I. Wilson. Stereotyped connectivity and computations in higher-order olfactory neurons. *Nature Neuroscience*, 17(2):280–288, Feb. 2014.

E. Fishilevich and L. B. Vosshall. Genetic and functional subdivision of the Drosophila antennal lobe. *Current biology*, 15(17):1548–1553, Sept. 2005.

Q. Gao and A. Chess. Identification of candidate Drosophila olfactory receptors from genomic DNA sequence. *Genomics*, 60(1):31–39, Aug. 1999.

Q. Gao, B. Yuan, and A. Chess. Convergent projections of Drosophila olfactory neurons to specific glomeruli in the antennal lobe. *Nature Neuroscience*, 3(8):780–785, Aug. 2000.

N. Gervasi, P. Tchénio, and T. Preat. PKA dynamics in a Drosophila learning center: coincidence detection by rutabaga adenylyl cyclase and spatial regulation by dunce phosphodiesterase. *Neuron*, 65(4):516–529, Feb. 2010.

K. J. Gingrich and J. H. Byrne. Simulation of synaptic depression, posttetanic potentiation, and presynaptic facilitation of synaptic potentials from sensory neurons mediating gill-withdrawal reflex in Aplysia. *Journal of Neurophysiology*, 53(3):652–669, Mar. 1985.

G. Gisselmann, J. Plonka, H. Pusch, and H. Hatt. Drosophila melanogaster GRD and LCCH3 subunits form heteromultimeric GABA-gated cation channels. *British journal of pharmacology*, 142(3):409–413, June 2004.

D. L. Glanzman. Habituation in Aplysia: the Cheshire cat of neurobiology. *Neurobiology of Learning and Memory*, 92(2):147–154, Sept. 2009.

D. L. Glanzman. Common mechanisms of synaptic plasticity in vertebrates and invertebrates. *Current biology*, 20(1):R31–R36, Jan. 2010.

A. L. Goldman, W. Van Der Goes Van Naters, D. Lessing, C. G. Warr, and J. R. Carlson. Coexpression of two functional odor receptors in one neuron. *Neuron*, 45(5):661–666, Mar. 2005.

T. D. Gover and T. W. Abrams. Insights into a molecular switch that gates sensory neuron synapses during habituation in Aplysia. *Neurobiology of Learning and Memory*, 92(2): 155–165, Sept. 2009.

T. D. Gover, X.-Y. Jiang, and T. W. Abrams. Persistent, exocytosis-independent silencing of release sites underlies homosynaptic depression at sensory synapses in Aplysia. *Journal of Neuroscience*, 22(5):1942–1955, Mar. 2002.

V. Grabe, A. Strutz, A. Baschwitz, B. S. Hansson, and S. Sachse. Digital in vivo 3D atlas of the antennal lobe of Drosophila melanogaster. *The Journal of comparative neurology*, 523(3):530–544, Feb. 2015a.

V. Grabe, A. Strutz, A. Baschwitz, B. S. Hansson, and S. Sachse. Digital in vivo 3D atlas of the antennal lobe of Drosophila melanogaster. *The Journal of comparative neurology*, 2015b.

M. Greenspan. Greenspan: Fly Pushing: The Theory and Practice of Drosophila Genetics, 1989.

C. Grienberger and A. Konnerth. Imaging Calcium in Neurons. *Neuron*, 73(5):862–885, Mar. 2012.

O. Griesbeck. Fluorescent proteins as sensors for cellular functions. *Current Opinion in Neurobiology*, 14(5):636–641, Oct. 2004.

P. M. Groves and R. F. Thompson. Habituation: a dual-process theory. *Psychological review*, 77(5):419–450, Sept. 1970.

J. A. Guiraud, E. Kushnerenko, P. Tomalski, K. Davies, H. Ribeiro, M. H. Johnson, and T. B. Team. Differential habituation to repeated sounds in infants at high risk for autism. *Neuroreport*, 22(16):845, Nov. 2011.

K. G. Hales, C. A. Korey, A. M. Larracuente, and D. M. Roberts. Genetics on the Fly: A Primer on the Drosophila Model System. *Genetics*, 201(3):815–842, Nov. 2015.

E. A. Hallem and J. R. Carlson. Coding of odors by a receptor repertoire. *Cell*, 125(1): 143–160, Apr. 2006.

E. A. Hallem, M. G. Ho, and J. R. Carlson. The molecular basis of odor coding in the Drosophila antenna. *Cell*, 117(7):965–979, June 2004.

P.-L. L. Han, L. R. Levin, R. R. Reed, and R. L. Davis. Preferential expression of the Drosophila rutabaga gene in mushroom bodies, neural centers for learning in insects. *Neuron*, 9(4):619–627, Oct. 1992.

R. C. Hardie and B. Minke. The trp gene is essential for a light-activated Ca2+ channel in Drosophila photoreceptors. *Neuron*, 8(4):643–651, Apr. 1992.

R. J. Harvey, B. Schmitt, I. Hermans-Borgmeyer, E. D. Gundelfinger, H. Betz, and M. G. Darlison. Sequence of a Drosophila ligand-gated ion-channel polypeptide with an unusual amino-terminal extracellular domain. *Journal of neurochemistry*, 62(6):2480–2483, June 1994.

R. D. Hawkins, E. R. Kandel, and C. H. Bailey. Molecular mechanisms of memory storage in Aplysia. *The Biological bulletin*, 210(3):174–191, June 2006.

P. R. Haynes, B. L. Christmann, and L. C. Griffith. A single pair of neurons links sleep to memory consolidation in Drosophila melanogaster. *eLife*, 4:R774, Jan. 2015.

R. Heidelberger, C. Heinemann, E. Neher, and G. Matthews. Calcium dependence of the rate of exocytosis in a synaptic terminal. *Nature*, 371(6497):513–515, Oct. 1994.

G. Heimbeck, V. Bugnon, N. Gendre, A. Keller, and R. F. Stocker. A central neural circuit for experience-independent olfactory and courtship behavior in Drosophila melanogaster. *Proceedings of the National Academy of Sciences*, 98(26):15336–15341, Dec. 2001.

M. Heisenberg. Mushroom body memoir: from maps to models. *Nature Reviews Neuroscience*, 4(4):266–275, Apr. 2003.

M. Heisenberg, A. Borst, S. Wagner, and D. Byers. Drosophila mushroom body mutants are deficient in olfactory learning. *Journal of Neurogenetics*, 2(1):1–30, Feb. 1985.

T. Hendel, M. Mank, B. Schnell, O. Griesbeck, A. Borst, and D. F. Reiff. Fluorescence changes of genetic calcium indicators and OGB-1 correlated with neural activity and calcium in vivo and in vitro. *Journal of Neuroscience*, 28(29):7399–7411, July 2008.

J. E. Henderson, D. M. Soderlund, and D. C. Knipple. Characterization of a putative gamma-aminobutyric acid (GABA) receptor beta subunit gene from Drosophila melanogaster. *Biochemical and biophysical research communications*, 193(2):474–482, June 1993.

J. G. Hildebrand and G. M. Shepherd. Mechanisms of olfactory discrimination: converging evidence for common principles across phyla. *Annual review of neuroscience*, 20:595–631, Mar. 1997.

S. A. Hires, L. Tian, and L. L. Looger. Reporting neural activity with genetically encoded calcium indicators. *Brain cell biology*, 36(1-4):69–86, Aug. 2008.

V. M. Ho, J.-A. Lee, and K. C. Martin. The cell biology of synaptic plasticity. *Science*, 334 (6056):623–628, Nov. 2011.

D. J. Holt, A. P. Weiss, S. L. Rauch, C. I. Wright, M. Zalesak, D. C. Goff, T. Ditman, R. C. Welsh, and S. Heckers. Sustained activation of the hippocampus in response to fearful faces in schizophrenia. *Biological psychiatry*, 57(9):1011–1019, May 2005.

K. S. Honegger, R. A. A. Campbell, and G. C. Turner. Cellular-resolution population imaging reveals robust sparse coding in the Drosophila mushroom body. *Journal of Neuroscience*, 31(33):11772–11785, Aug. 2011.

E. J. Hong and R. I. Wilson. Simultaneous encoding of odors by channels with diverse sensitivity to inhibition. *Neuron*, 85(3):573–589, Feb. 2015.

A. M. Hosie, K. Aronstein, D. B. Sattelle, and R. H. Ffrench-Constant. Molecular biology of insect neuronal GABA receptors. *Trends in neurosciences*, 20(12):578–583, Dec. 1997.

A. Y. Hsia, J.-D. Vincent, and P.-M. Lledo. Dopamine Depresses Synaptic Inputs Into the Olfactory Bulb. *Journal of Neurophysiology*, 82(2):1082–1085, Aug. 1999.

J. Huang, W. Zhang, W. Qiao, A. Hu, and Z. Wang. Functional connectivity and selective odor responses of excitatory local interneurons in Drosophila antennal lobe. *Neuron*, 67 (6):1021–1033, Sept. 2010.

R. Ignell, C. M. Root, R. T. Birse, J. W. Wang, D. R. Nässel, and A. M. E. Winther. Presynaptic peptidergic modulation of olfactory receptor neurons in Drosophila. *Proceedings of the National Academy of Sciences*, 106(31):13070–13075, Aug. 2009.

J. S. Isaacson and M. Scanziani. How inhibition shapes cortical activity. *Neuron*, 72(2): 231–243, Oct. 2011.

J. S. Isaacson and B. W. Strowbridge. Olfactory reciprocal synapses: dendritic signaling in the CNS. *Neuron*, 20(4):749–761, Apr. 1998.

E. A. Jares-Erijman and T. M. Jovin. FRET imaging. *Nature biotechnology*, 21(11):1387–1395, Nov. 2003.

V. Jayaraman and G. Laurent. Evaluating a genetically encoded optical sensor of neural activity using electrophysiology in intact adult fruit flies. *Frontiers in neural circuits*, 1:3, Nov. 2007.

G. S. Jefferis, E. C. Marin, R. F. Stocker, and L. Luo. Target neuron prespecification in the olfactory map of Drosophila. *Nature*, 414(6860):204–208, Nov. 2001.

G. S. X. E. Jefferis, C. J. Potter, A. M. Chan, E. C. Marin, T. Rohlfing, C. R. Maurer, and L. Luo. Comprehensive maps of Drosophila higher olfactory centers: spatially segregated fruit and pheromone representation. *Cell*, 128(6):1187–1203, Mar. 2007.

L. Jin, Z. Han, J. Platisa, J. R. A. Wooltorton, L. B. Cohen, and V. A. Pieribone. Single action potentials and subthreshold electrical events imaged in neurons with a fluorescent protein voltage probe. *Neuron*, 75(5):779–785, Sept. 2012.

M. A. Joiner, C. J. Jones, T. Tully, C.-F. F. Wu, and Z. Asztalos. Effects of mutant Drosophila K+ channel subunits on habituation of the olfactory jump response. *Journal of Neurogenetics*, 21(1-2):45–58, Jan. 2007.

W. D. Jones, P. Cayirlioglu, I. G. Kadow, and L. B. Vosshall. Two chemosensory receptors together mediate carbon dioxide detection in Drosophila. *Nature*, 445(7123):86–90, Jan. 2007.

J. Kain, C. Stokes, Q. Gaudry, X. Song, J. Foley, R. Wilson, and B. de Bivort. Leg-tracking and automated behavioural classification in Drosophila. *Nature communications*, 4:1910, May 2013.

P. Kain, T. S. Chakraborty, S. Sundaram, O. Siddiqi, V. Rodrigues, and G. Hasan. Reduced odor responses from antennal neurons of G(q)alpha, phospholipase Cbeta, and rdgA mutants in Drosophila support a role for a phospholipid intermediate in insect olfactory transduction. *Journal of Neuroscience*, 28(18):4745–4755, Apr. 2008.

E. R. Kandel. The molecular biology of memory storage: a dialogue between genes and synapses. *Science*, 294(5544):1030–1038, Nov. 2001.

E. R. Kandel, J. H. Schwartz, and T. M. Jessell. *Principles of neural science*. The McGraw-Hill Companies, 4th edition, 2000.

J. P. Y. Kao, G. Li, and D. A. Auston. Practical aspects of measuring intracellular calcium signals with fluorescent indicators. *Methods in cell biology*, 99:113–152, 2010.

H. K. Kato, S. N. Gillet, and J. S. Isaacson. Flexible Sensory Representations in Auditory Cortex Driven by Behavioral Relevance. *Neuron*, 88(5):1027–1039, Dec. 2015.

E. T. Kavalali and E. M. Jorgensen. Visualizing presynaptic function. *Nature Neuroscience*, 17(1):10–16, Jan. 2014.

H. Kazama and R. I. Wilson. Homeostatic matching and nonlinear amplification at identified central synapses. *Neuron*, 58(3):401–413, May 2008.

H. Kazama and R. I. Wilson. Origins of correlated activity in an olfactory circuit. *Nature Neuroscience*, 12(9):1136–1144, Sept. 2009.

E. Kiyokage, Y.-Z. Pan, Z. Shao, K. Kobayashi, G. Szabo, Y. Yanagawa, K. Obata, H. Okano, K. Toida, A. C. Puche, and M. T. Shipley. Molecular identity of periglomerular and short axon cells. *Journal of Neuroscience*, 30(3):1185–1196, Jan. 2010.

B. R. Klagges, G. Heimbeck, T. A. Godenschwege, A. Hofbauer, G. O. Pflugfelder, R. Reifegerste, D. Reisch, M. Schaupp, S. Buchner, and E. Buchner. Invertebrate synapsins: a single gene codes for several isoforms in Drosophila. *The Journal of Neuroscience*, 16(10):3154–3165, May 1996.

M. Klein, B. Afonso, A. J. Vonner, L. Hernandez-Nunez, M. Berck, C. J. Tabone, E. A. Kane, V. A. Pieribone, M. N. Nitabach, A. Cardona, M. Zlatic, S. G. Sprecher, M. Gershow, P. A. Garrity, and A. D. T. Samuel. Sensory determinants of behavioral dynamics in Drosophila thermotaxis. *Proceedings of the National Academy of Sciences*, 112(2):E220–9, Jan. 2015.

N. M. Kleinhans, L. C. Johnson, T. Richards, R. Mahurin, J. Greenson, G. Dawson, and E. Aylward. Reduced neural habituation in the amygdala and social impairments in autism spectrum disorders. *The American journal of psychiatry*, 166(4):467–475, Apr. 2009.

M. Knaden and B. S. Hansson. Mapping odor valence in the brain of flies and mice. *Current Opinion in Neurobiology*, 24(1):34–38, Feb. 2014.

M. Knaden, A. Strutz, J. Ahsan, S. Sachse, and B. S. Hansson. Spatial representation of odorant valence in an insect brain. *Cell reports*, 1(4):392–399, Apr. 2012.

D. C. Knipple and D. M. Soderlund. The ligand-gated chloride channel gene family of Drosophila melanogaster. *Pesticide biochemistry and physiology*, 97(2):140–148, June 2010.

N. L. Koster, A. B. Norman, N. M. Richtand, W. T. Nickell, A. C. Puche, S. K. Pixley, and M. T. Shipley. Olfactory receptor neurons express D2 dopamine receptors. *The Journal of comparative neurology*, 411(4):666–673, Sept. 1999.

P. Kuenzer. Verhaltensphysiologische Untersuchungen über das Zucken des Regenwurms. *Zeitschrift für Tierpsychologie*, 15(1):31–49, Jan. 1958.

D. M. Kullmann and K. P. Lamsa. LTP and LTD in cortical GABAergic interneurons: Emerging rules and roles. *Neuropharmacology*, 60(5):712–719, Apr. 2011.

D. M. Kullmann, A. W. Moreau, Y. Bakiri, and E. Nicholson. Plasticity of inhibition. *Neuron*, 75(6):951–962, Sept. 2012.

I. Kupfermann, V. Castellucci, H. Pinsker, and E. Kandel. Neuronal Correlates of Habituation and Dishabituation of the Gill-Withdrawal Reflex in Aplysia. *Science*, 167(3926): 1743–1745, Mar. 1970.

J. Y. Kwon, A. Dahanukar, L. A. Weiss, and J. R. Carlson. The molecular basis of CO2 reception in Drosophila. *Proceedings of the National Academy of Sciences*, 104(9):3574–3578, Feb. 2007.

S.-L. Lai and T. Lee. Genetic mosaic with dual binary transcriptional systems in Drosophila. *Nature Neuroscience*, 9(5):703–709, May 2006.

S.-L. Lai, T. Awasaki, K. Ito, and T. Lee. Clonal analysis of Drosophila antennal lobe neurons: diverse neuronal architectures in the lateral neuroblast lineage. *Development*, 135(17):2883–2893, Sept. 2008.

P. P. Laissue, C. Reiter, P. R. Hiesinger, S. Halter, K. F. Fischbach, and R. F. Stocker. Three-dimensional reconstruction of the antennal lobe in Drosophila melanogaster. *The Journal of comparative neurology*, 405(4):543–552, Mar. 1999.

R. Lamprecht and J. LeDoux. Structural plasticity and memory. *Nature Reviews Neuroscience*, 5(1):45–54, Jan. 2004.

A. Larkin, S. Karak, R. Priya, A. Das, C. Ayyub, K. Ito, V. Rodrigues, and M. Ramaswami. Central synaptic mechanisms underlie short-term olfactory habituation in Drosophila larvae. *Learning & Memory*, 17(12):645–653, Dec. 2010.

M. C. Larsson, A. I. Domingos, W. D. Jones, M. E. Chiappe, H. Amrein, and L. B. Vosshall. Or83b encodes a broadly expressed odorant receptor essential for Drosophila olfaction. *Neuron*, 43(5):703–714, Sept. 2004.

G. Laurent. Olfactory processing: maps, time and codes. *Current Opinion in Neurobiology*, 7(4):547–553, Aug. 1997.

J. A. Lee. Olfactory-avoidance habituation in Drosophila melanogaster. pages 1–239, Aug. 2015.

S. G. Leinwand and S. H. Chalasani. Olfactory networks: from sensation to perception. *Current opinion in genetics & development*, 21(6):806–811, Dec. 2011.

L. R. Levin, P.-L. L. Han, P. M. Hwang, P. G. Feinstein, R. L. Davis, and R. R. Reed. The Drosophila learning and memory gene rutabaga encodes a Ca2+/Calmodulin-responsive adenylyl cyclase. *Cell*, 68(3):479–489, Feb. 1992.

Q. Li and Z. Gong. Cold-sensing regulates Drosophila growth through insulin-producing cells. *Nature communications*, 6:10083, 2015.

L. Liang, Y. Li, C. J. Potter, O. Yizhar, K. Deisseroth, R. W. Tsien, and L. Luo. GABAergic projection neurons route selective olfactory inputs to specific higher-order neurons. *Neuron*, 79(5):917–931, Sept. 2013.

W. W. Liu and R. I. Wilson. Glutamate is an inhibitory neurotransmitter in the Drosophila olfactory system. *Proceedings of the National Academy of Sciences*, 110(25):10294–10299, June 2013.

X. Liu, W. C. Krause, and R. L. Davis. GABAA receptor RDL inhibits Drosophila olfactory associative learning. *Neuron*, 56(6):1090–1102, Dec. 2007.

X. Liu, M. E. Buchanan, K.-A. Han, and R. L. Davis. The GABAA receptor RDL suppresses the conditioned stimulus pathway for olfactory learning. *Journal of Neuroscience*, 29(5): 1573–1579, Feb. 2009.

M. S. Livingstone. Genetic dissection of Drosophila adenylate cyclase. *Proceedings of the National Academy of Sciences*, 82(17):5992–5996, Sept. 1985.

M. S. Livingstone, P. P. Sziber, and W. G. Quinn. Loss of calcium/calmodulin responsiveness in adenylate cyclase of rutabaga, a Drosophila learning mutant. *Cell*, 37:205–215, May 1984.

M. V. Lombardo, B. Chakrabarti, and S. Baron-Cohen. The amygdala in autism: not adapting to faces? *The American journal of psychiatry*, 166(4):395–397, Apr. 2009.

L. L. Looger and O. Griesbeck. Genetically encoded neural activity indicators. *Current Opinion in Neurobiology*, 22(1):18–23, Feb. 2012.

S. W. Ludmerer, V. A. Warren, B. S. Williams, Y. Zheng, D. C. Hunt, M. B. Ayer, M. A. Wallace, A. G. Chaudhary, M. A. Egan, P. T. Meinke, D. C. Dean, M. L. Garcia, D. F. Cully, and M. M. Smith. Ivermectin and nodulisporic acid receptors in Drosophila melanogaster contain both gamma-aminobutyric acid-gated Rdl and glutamate-gated GluCl alpha chloride channel subunits. *Biochemistry*, 41(20):6548–6560, May 2002.

C. Lundin, L. Käll, S. A. Kreher, K. Kapp, E. L. Sonnhammer, J. R. Carlson, G. v. Heijne, and I. Nilsson. Membrane topology of the Drosophila OR83b odorant receptor. *FEBS Letters*, 581(29):5601–5604, Dec. 2007.

S. X. Luo, R. Axel, and L. F. Abbott. Generating sparse and selective third-order responses in the olfactory system of the fly. *Proceedings of the National Academy of Sciences*, 107 (23):10713–10718, June 2010.

A. Mahr and H. Aberle. The expression pattern of the Drosophila vesicular glutamate transporter: a marker protein for motoneurons and glutamatergic centers in the brain. *Gene expression patterns : GEP*, 6(3):299–309, Mar. 2006.

R. C. Malenka and M. F. Bear. LTP and LTD. *Neuron*, 44(1):5–21, Sept. 2004.

R. C. Malenka and R. A. Nicoll. NMDA-receptor-dependent synaptic plasticity: multiple forms and mechanisms. *Trends in neurosciences*, 16(12):521–527, Dec. 1993.

E. C. Marin, G. Jefferis, T. Komiyama, H. Zhu, and L. Luo. Representation of the glomerular olfactory map in the Drosophila brain. *Cell*, 109:243–255, Apr. 2002.

C. Martelli, J. R. Carlson, and T. Emonet. Intensity invariant dynamics and odor-specific latencies in olfactory receptor neuron response. *Journal of Neuroscience*, 33(15):6285–6297, Apr. 2013.

K. C. Martin and R. S. Zukin. RNA trafficking and local protein synthesis in dendrites: an overview. *Journal of Neuroscience*, 26(27):7131–7134, July 2006.

C. J. McBain and M. L. Mayer. N-methyl-D-aspartic acid receptor structure and function. *Physiological Reviews*, 74(3):723–760, July 1994.

C. McCann, E. E. Holohan, S. Das, A. Dervan, A. Larkin, J. A. Lee, V. Rodrigues, R. Parker, and M. Ramaswami. The Ataxin-2 protein is required for microRNA function and synapse-specific long-term olfactory habituation. *Proceedings of the National Academy of Sciences*, 108(36):E655–62, Sept. 2011.

J. P. McGann. Presynaptic inhibition of olfactory sensory neurons: new mechanisms and potential functions. *Chemical senses*, 38(6):459–474, July 2013.

J. P. McGann, N. Pírez, M. A. Gainey, C. Muratore, A. S. Elias, and M. Wachowiak. Odorant representations are modulated by intra- but not interglomerular presynaptic inhibition of olfactory sensory neurons. *Neuron*, 48(6):1039–1053, Dec. 2005.

S. E. McGuire, P. T. Le, A. J. Osborn, K. Matsumoto, and R. L. Davis. Spatiotemporal rescue of memory dysfunction in Drosophila. *Science*, 302(5651):1765–1768, Dec. 2003.

S. E. McGuire, Z. Mao, and R. L. Davis. Spatiotemporal Gene Expression Targeting with the TARGET and Gene-Switch Systems in Drosophila. *Science's STKE*, 2004a.

S. E. McGuire, G. Roman, and R. L. Davis. Gene expression systems in Drosophila: a synthesis of time and space. *Trends in genetics*, 20(8):384–391, Aug. 2004b.

S. E. McGuire, M. Deshazer, and R. L. Davis. Thirty years of olfactory learning and memory research in Drosophila melanogaster. *Progress in Neurobiology*, 76(5):328–347, Aug. 2005.

M. McKenna, P. Monte, S. L. Helfand, C. Woodard, and J. Carlson. A simple chemosensory response in Drosophila and the isolation of acj mutants in which it is affected. *Proceedings of the National Academy of Sciences*, 86(20):8118–8122, Oct. 1989.

A. M. McNamara, P. D. Magidson, C. Linster, D. A. Wilson, and T. A. Cleland. Distinct neural mechanisms mediate olfactory memory formation at different timescales. *Learning & Memory*, 15(3):117–125, Mar. 2008.

U. Meincke, G. A. Light, M. A. Geyer, D. L. Braff, and E. Gouzoulis-Mayfrank. Sensitization and habituation of the acoustic startle reflex in patients with schizophrenia. *Psychiatry research*, 126(1):51–61, Apr. 2004.

M. Mezler, T. Müller, and K. Raming. Cloning and functional expression of GABA(B) receptors from Drosophila. *The European journal of neuroscience*, 13(3):477–486, Feb. 2001.

B. Michels, S. Diegelmann, H. Tanimoto, I. Schwenkert, E. Buchner, and B. Gerber. A role for Synapsin in associative learning: the Drosophila larva as a study case. *Learning & memory*, 12(3):224–231, May 2005.

B. Michels, Y.-C. Chen, T. Saumweber, D. Mishra, H. Tanimoto, B. Schmid, O. Engmann, and B. Gerber. Cellular site and molecular mode of synapsin action in associative learning. *Learning & Memory*, 18(5):332–344, Apr. 2011.

G. Miesenböck, D. A. De Angelis, and J. E. Rothman. Visualizing secretion and synaptic transmission with pH-sensitive green fluorescent proteins. *Nature*, 394(6689):192–195, July 1998a.

G. Miesenböck, D. A. De Angelis, and J. E. Rothman. Visualizing secretion and synaptic transmission with pH-sensitive green fluorescent proteins. *Nature*, 394(6689):192–195, July 1998b.

S. Min, M. Ai, S. A. Shin, and G. S. B. Suh. Dedicated olfactory neurons mediating attraction behavior to ammonia and amines in Drosophila. *Proceedings of the National Academy of Sciences*, 110(14):E1321–9, Apr. 2013.

A. Miyawaki. Fluorescence imaging of physiological activity in complex systems using GFP-based probes. *Current Opinion in Neurobiology*, 13(5):591–596, Oct. 2003.

A. Miyawaki, J. Llopis, R. Heim, J. M. McCaffery, J. A. Adams, M. Ikura, and R. Y. Tsien. Fluorescent indicators for Ca2+ based on green fluorescent proteins and calmodulin. *Nature*, 388(6645):882–887, Aug. 1997.

T. H. Morgan. Sex limited inheritance in Drosophila. *Science*, 32(812):120–122, July 1910.

H. J. Muller. Genetic Variability, Twin Hybrids and Constant Hybrids, in a Case of Balanced Lethal Factors. *Genetics*, 3(5):422–499, Sept. 1918.

M. S. Murmu, J. Stinnakre, and J.-R. Martin. Presynaptic Ca2+ stores contribute to odor-induced responses in Drosophila olfactory receptor neurons. *The Journal of experimental biology*, 213(Pt 24):4163–4173, Dec. 2010.

M. S. Murmu, J. Stinnakre, E. Réal, and J.-R. Martin. Calcium-stores mediate adaptation in axon terminals of olfactory receptor neurons in Drosophila. *BMC neuroscience*, 12(1): 105, Oct. 2011.

G. J. Murphy, D. P. Darcy, and J. S. Isaacson. Intraglomerular inhibition: signaling mechanisms of an olfactory microcircuit. *Nature Neuroscience*, 8(3):354–364, Mar. 2005.

K. I. Nagel and R. I. Wilson. Biophysical mechanisms underlying olfactory receptor neuron dynamics. *Nature Neuroscience*, 14(2):208–216, Feb. 2011.

K. I. Nagel, E. J. Hong, and R. I. Wilson. Synaptic and circuit mechanisms promoting broadband transmission of olfactory stimulus dynamics. *Nature Neuroscience*, 18(1):56–65, Jan. 2015.

T. Nakagawa and L. B. Vosshall. Controversy and consensus: noncanonical signaling mechanisms in the insect olfactory system. *Current Opinion in Neurobiology*, 19(3):284–292, June 2009.

J. Nakai, M. Ohkura, and K. Imoto. A high signal-to-noise Ca(2+) probe composed of a single green fluorescent protein. *Nature biotechnology*, 19(2):137–141, Feb. 2001.

D. R. Nässel. Neuropeptides in the nervous system of Drosophila and other insects: multiple roles as neuromodulators and neurohormones. *Progress in Neurobiology*, 68(1):1–84, Sept. 2002.

D. R. Nässel and U. Homberg. Neuropeptides in interneurons of the insect brain. *Cell and Tissue Research*, 326(1):1–24, Oct. 2006.

E. Neher and T. Sakaba. Multiple Roles of Calcium Ions in the Regulation of Neurotransmitter Release. *Neuron*, 59(6):861–872, Sept. 2008.

E. M. Neuhaus, G. Gisselmann, W. Zhang, R. Dooley, K. Störtkuhl, and H. Hatt. Odorant receptor heterodimerization in the olfactory system of Drosophila melanogaster. *Nature Neuroscience*, 8(1):15–17, Jan. 2005.

M. Ng, R. D. Roorda, S. Q. Lima, B. V. Zemelman, P. Morcillo, and G. Miesenböck. Transmission of olfactory information between three populations of neurons in the antennal lobe of the fly. *Neuron*, 36(3):463–474, Oct. 2002.

T. Niewalda, T. Völler, C. Eschbach, J. Ehmer, W.-C. Chou, M. Timme, A. Fiala, and B. Gerber. A combined perceptual, physico-chemical, and imaging approach to 'odour-distances' suggests a categorizing function of the Drosophila antennal lobe. *PloS one*, 6(9):e24300, Sept. 2011.

M. Oheim, D. J. Michael, M. Geisbauer, D. Madsen, and R. H. Chow. Principles of two-photon excitation fluorescence microscopy and other nonlinear imaging approaches. *Advanced drug delivery reviews*, 58(7):788–808, Sept. 2006.

M. Ohkura, M. Matsuzaki, H. Kasai, K. Imoto, and J. Nakai. Genetically encoded bright Ca2+ probe applicable for dynamic Ca2+ imaging of dendritic spines. *Analytical chemistry*, 77(18):5861–5869, Sept. 2005.

M. Ohkura, T. Sasaki, J. Sadakari, K. Gengyo-Ando, Y. Kagawa-Nagamura, C. Kobayashi, Y. Ikegaya, and J. Nakai. Genetically Encoded Green Fluorescent Ca 2+ Indicators with Improved Detectability for Neuronal Ca 2+ Signals. *PloS one*, 7(12):e51286, Dec. 2012.

M. Oizumi, R. Satoh, H. Kazama, and M. Okada. Functional Differences between Global Pre- and Postsynaptic Inhibition in the Drosophila Olfactory Circuit. *Frontiers in computational neuroscience*, 6:14, Mar. 2012.

R. Okada, T. Awasaki, and K. Ito. Gamma-aminobutyric acid (GABA)-mediated neural connections in the Drosophila antennal lobe. *The Journal of comparative neurology*, 514 (1):74–91, May 2009.

S. R. Olsen and R. I. Wilson. Cracking neural circuits in a tiny brain: new approaches for understanding the neural circuitry of Drosophila. *Trends in neurosciences*, 31(10):512–520, Oct. 2008a.

S. R. Olsen and R. I. Wilson. Lateral presynaptic inhibition mediates gain control in an olfactory circuit. *Nature*, 452(7190):956–960, Apr. 2008b.

S. R. Olsen, V. Bhandawat, and R. I. Wilson. Excitatory interactions between olfactory processing channels in the Drosophila antennal lobe. *Neuron*, 54(1):89–103, Apr. 2007.

S. R. Olsen, V. Bhandawat, and R. I. Wilson. Divisive normalization in olfactory population codes. *Neuron*, 66(2):287–299, Apr. 2010.

P. Paranjpe, V. Rodrigues, K. Vijayraghavan, and M. Ramaswami. Gustatory habituation in Drosophila relies on rutabaga (adenylate cyclase)-dependent plasticity of GABAergic inhibitory neurons. *Learning & Memory*, 19(12):627–635, Nov. 2012.

M. Parnas, A. C. Lin, W. Huetteroth, and G. Miesenböck. Odor discrimination in Drosophila: from neural population codes to behavior. *Neuron*, 79(5):932–944, Sept. 2013.

S. Parrish-Aungst, E. Kiyokage, G. Szabo, Y. Yanagawa, M. T. Shipley, and A. C. Puche. Sensory experience selectively regulates transmitter synthesis enzymes in interglomerular circuits. *Brain Research*, 1382:70–76, Mar. 2011.

R. L. Patterson, D. Boehning, and S. H. Snyder. Inositol 1,4,5-trisphosphate receptors as signal integrators. *Annual review of biochemistry*, 73(1):437–465, July 2004.

G. W. Peckham and E. G. Peckham. Some observations on the mental powers of spiders. *The Journal of Morphology*, 1(2):383–419, 1887.

M. Pellegrino, T. Nakagawa, and L. B. Vosshall. Single sensillum recordings in the insects Drosophila melanogaster and Anopheles gambiae. *Journal of Visualized Experiments*, (36):1–5, Feb. 2010.

D. Pelz, T. Roeske, Z. Syed, M. d. Bruyne, and C. G. Galizia. The molecular receptive range of an olfactory receptor in vivo (Drosophila melanogaster Or22a). *Journal of Neurobiology*, 66(14):1544–1563, Dec. 2006.

A. Peretz, E. Suss-Toby, A. Rom-Glas, A. Arnon, and R. Payne. The light response of Drosophila photoreceptors is accompanied by an increase in cellular calcium: effects of specific mutations. *Neuron*, 12:1257–1267, June 1994.

V. Pérez Koldenkova and T. Nagai. Genetically encoded Ca(2+) indicators: properties and evaluation. *Biochimica et biophysica acta*, 1833(7):1787–1797, July 2013.

J. Perez-Orive, O. Mazor, G. C. Turner, S. Cassenaer, R. I. Wilson, and G. Laurent. Oscillations and sparsening of odor representations in the mushroom body. *Science*, 297(5580): 359–365, July 2002.

D. S. Peterka, H. Takahashi, and R. Yuste. Imaging Voltage in Neurons. *Neuron*, 69(1):9–21, Jan. 2011.

B. D. Pfeiffer, T.-T. B. Ngo, K. L. Hibbard, C. Murphy, A. Jenett, J. W. Truman, and G. M. Rubin. Refinement of tools for targeted gene expression in Drosophila. *Genetics*, 186(2): 735–755, Oct. 2010.

N. Pírez and M. Wachowiak. In vivo modulation of sensory input to the olfactory bulb by tonic and activity-dependent presynaptic inhibition of receptor neurons. *Journal of Neuroscience*, 28(25):6360–6371, June 2008.

C. J. Potter, B. Tasic, E. V. Russler, L. Liang, and L. Luo. The Q system: a repressible binary system for transgene expression, lineage tracing, and mosaic analysis. *Cell*, 141 (3):536–548, Apr. 2010.

M. Ramaswami. Network plasticity in adaptive filtering and behavioral habituation. *Neuron*, 82(6):1216–1229, June 2014.

C. H. Rankin, T. Abrams, R. J. Barry, S. Bhatnagar, D. F. Clayton, J. Colombo, G. Coppola, M. A. Geyer, D. L. Glanzman, S. Marsland, F. K. McSweeney, D. A. Wilson, C.-F. Wu, and R. F. Thompson. Habituation revisited: an updated and revised description of the behavioral characteristics of habituation. *Neurobiology of Learning and Memory*, 92(2): 135–138, Sept. 2009.

D. F. Reiff, A. Ihring, G. Guerrero, E. Y. Isacoff, M. Joesch, J. Nakai, and A. Borst. In vivo performance of genetically encoded indicators of neural activity in flies. *Journal of Neuroscience*, 25(19):4766–4778, May 2005.

T. Riemensperger, T. Völler, P. Stock, E. Buchner, and A. Fiala. Punishment prediction by dopaminergic neurons in Drosophila. *Current biology*, 15(21):1953–1960, Nov. 2005.

T. Riemensperger, U. Pech, S. Dipt, and A. Fiala. Optical calcium imaging in the nervous system of Drosophila melanogaster. *Biochimica et biophysica acta*, 1820(8):1169–1178, Aug. 2012.

V. Rodrigues. Olfactory behavior of Drosophila melanogaster. *Basic life sciences*, 16:361–371, 1980.

V. Rodrigues and O. Siddiqi. Genetic analysis of chemosensory pathway. *Proceedings of the Indian Academy of Sciences*, 87(7):147–160, July 1978.

V. A. Romoser, P. M. Hinkle, and A. Persechini. Detection in living cells of Ca2+-dependent changes in the fluorescence emission of an indicator composed of two green fluorescent protein variants linked by a calmodulin-binding sequence. A new class of fluorescent indicators. *The Journal of biological chemistry*, 272(20):13270–13274, May 1997.

D. Ronderos and D. Smith. Diverse signaling mechanisms mediate volatile odorant detection in Drosophila. *Fly*, 3(4):290–297, Dec. 2009.

C. M. Root, J. L. Semmelhack, A. M. Wong, J. Flores, and J. W. Wang. Propagation of olfactory information in Drosophila. *Proceedings of the National Academy of Sciences*, 104(28):11826–11831, July 2007.

C. M. Root, K. Masuyama, D. S. Green, L. E. Enell, D. R. Nässel, C.-H. Lee, and J. W. Wang. A presynaptic gain control mechanism fine-tunes olfactory behavior. *Neuron*, 59 (2):311–321, July 2008.

B. Roy, A. P. Singh, C. Shetty, V. Chaudhary, A. North, M. Landgraf, K. Vijayraghavan, and V. Rodrigues. Metamorphosis of an identified serotonergic neuron in the Drosophila olfactory system. *Neural development*, 2:20, Oct. 2007.

S. Royer, R. L. Coulson, and M. Klein. Switching off and on of synaptic sites at aplysia sensorimotor synapses. *Journal of Neuroscience*, 20(2):626–638, Jan. 2000.

G. M. Rubin and A. C. Spradling. Genetic transformation of Drosophila with transposable element vectors. *Science*, 218(4570):348–353, Oct. 1982.

E. M. Russell. Changes in the behaviour of Lebistes reticulatus upon a repeated shadow stimulus. *Animal behaviour*, 15(4):574–585, Oct. 1967.

R. Rytz, V. Croset, and R. Benton. Ionotropic receptors (IRs): chemosensory ionotropic glutamate receptors in Drosophila and beyond. *Insect biochemistry and molecular biology*, 43(9):888–897, Sept. 2013.

B. L. Sabatini, M. Maravall, and K. Svoboda. Ca2+ signaling in dendritic spines. *Current Opinion in Neurobiology*, 11(3):349–356, June 2001.

S. Sachse and C. G. Galizia. Role of Inhibition for Temporal and Spatial Odor Representation in Olfactory Output Neurons: A Calcium Imaging Study. *Journal of Neurophysiology*, 87 (2):1106–1117, Feb. 2002.

S. Sachse, E. Rueckert, A. Keller, R. Okada, N. K. Tanaka, K. Ito, and L. B. Vosshall. Activity-dependent plasticity in an olfactory circuit. *Neuron*, 56(5):838–850, Dec. 2007.

M. K. Sadanandappa, B. Blanco Redondo, B. Michels, V. Rodrigues, B. Gerber, K. Vijayraghavan, E. Buchner, and M. Ramaswami. Synapsin function in GABA-ergic interneurons is required for short-term olfactory habituation. *Journal of Neuroscience*, 33 (42):16576–16585, Oct. 2013.

K. Sakamoto, K. Karelina, and K. Obrietan. CREB: a multifaceted regulator of neuronal plasticity and protection. *Journal of neurochemistry*, 116(1):1–9, Jan. 2011.

K. Sato, M. Pellegrino, T. Nakagawa, T. Nakagawa, L. B. Vosshall, and K. Touhara. Insect olfactory receptors are heteromeric ligand-gated ion channels. *Nature*, 452(7190):1002–1006, Apr. 2008.

S. Schmid, D. A. Wilson, and C. H. Rankin. Habituation mechanisms and their importance for cognitive function. *Frontiers in integrative neuroscience*, 8:97, 2014.

C. A. Schneider, W. S. Rasband, and K. W. Eliceiri. NIH Image to ImageJ: 25 years of image analysis. *Nature methods*, 9(7):671–675, July 2012.

N. E. Schoppa, J. M. Kinzie, Y. Sahara, T. P. Segerson, and G. L. Westbrook. Dendrodendritic inhibition in the olfactory bulb is driven by NMDA receptors. *The Journal of Neuroscience*, 18(17):6790–6802, Sept. 1998.

M. Schubert, B. S. Hansson, and S. Sachse. The banana code-natural blend processing in the olfactory circuitry of Drosophila melanogaster. *Frontiers in physiology*, 5:59, Feb. 2014.

J. D. Seelig, M. E. Chiappe, G. K. Lott, A. Dutta, J. E. Osborne, M. B. Reiser, and V. Jayaraman. Two-photon calcium imaging from head-fixed Drosophila during optomotor walking behavior. *Nature methods*, 7(7):535–540, July 2010.

Y. Seki, J. Rybak, D. Wicher, S. Sachse, and B. S. Hansson. Physiological and morphological characterization of local interneurons in the Drosophila antennal lobe. *Journal of Neurophysiology*, 104(2):1007–1019, Aug. 2010.

J. L. Semmelhack and J. W. Wang. Select Drosophila glomeruli mediate innate olfactory attraction and aversion. *Nature*, 459(7244):218–223, May 2009.

S. R. Shanbhag, B. Müller, and R. A. Steinbrecht. Atlas of olfactory organs of Drosophila melanogaster: 1. Types, external organization, innervation and distribution of olfactory sensilla. *international journal of insect morphology embryology*, 28(4):377–397, Oct. 1999.

Y. Shang, A. Claridge-Chang, L. Sjulson, M. Pypaert, and G. Miesenböck. Excitatory local circuits and their implications for olfactory processing in the fly antennal lobe. *Cell*, 128 (3):601–612, Feb. 2007.

Z. Shao, A. C. Puche, E. Kiyokage, G. Szabo, and M. T. Shipley. Two GABAergic Intraglomerular Circuits Differentially Regulate Tonic and Phasic Presynaptic Inhibition of Olfactory Nerve Terminals. *Journal of Neurophysiology*, 101(4):1988–2001, Apr. 2009.

P. Sharma, J. Keane, C. J. O'Kane, and Z. Asztalos. Automated measurement of Drosophila jump reflex habituation and its use for mutant screening. *Journal of neuroscience methods*, 182(1):43–48, Aug. 2009.

G. M. Shepherd, W. R. Chen, D. Willhite, M. Migliore, and C. A. Greer. The olfactory granule cell: from classical enigma to central role in olfactory processing. *Brain Research Reviews*, 55(2):373–382, Oct. 2007.

C. S. Sherrington. Observations on the scratch-reflex in the spinal dog. *The Journal of Physiology*, 34(1-2):1–50, Mar. 1906.

A. F. Silbering and C. G. Galizia. Processing of odor mixtures in the Drosophila antennal lobe reveals both global inhibition and glomerulus-specific interactions. *Journal of Neuroscience*, 27(44):11966–11977, Oct. 2007.

A. F. Silbering, R. Okada, K. Ito, and C. G. Galizia. Olfactory information processing in the Drosophila antennal lobe: anything goes? *Journal of Neuroscience*, 28(49):13075–13087, Dec. 2008.

A. F. Silbering, R. Rytz, Y. Grosjean, L. Abuin, P. Ramdya, G. S. X. E. Jefferis, and R. Benton. Complementary function and integrated wiring of the evolutionarily distinct Drosophila olfactory subsystems. *Journal of Neuroscience*, 31(38):13357–13375, Sept. 2011.

A. J. Silva, J. H. Kogan, P. W. Frankland, and S. Kida. CREB and memory. *Annual review of neuroscience*, 21:127–148, Mar. 1998.

J. H. Simpson. Mapping and manipulating neural circuits in the fly brain. *Advances in genetics*, 65:79–143, 2009.

R. Smart, A. Kiely, M. Beale, E. Vargas, C. Carraher, A. V. Kralicek, D. L. Christie, C. Chen, R. D. Newcomb, and C. G. Warr. Drosophila odorant receptors are novel seven transmembrane domain proteins that can signal independently of heterotrimeric G proteins. *Insect biochemistry and molecular biology*, 38(8):770–780, Aug. 2008.

E. N. Sokolov. Higher nervous functions; the orienting reflex. *Annual review of physiology*, 25(1):545–580, Mar. 1963.

A. C. Spradling and G. M. Rubin. Transposition of cloned P elements into Drosophila germ line chromosomes. *Science*, 218(4570):341–347, Oct. 1982.

J. E. R. Staddon and D. T. Cerutti. Operant conditioning. *Annu Rev Psychol*, 54(1):115–144, Mar. 2003.

M. C. Stensmyr, H. K. M. Dweck, A. Farhan, I. Ibba, A. Strutz, L. Mukunda, J. Linz, V. Grabe, K. Steck, S. Lavista-Llanos, D. Wicher, S. Sachse, M. Knaden, P. G. Becher, Y. Seki, and B. S. Hansson. A conserved dedicated olfactory circuit for detecting harmful microbes in Drosophila. *Cell*, 151(6):1345–1357, Dec. 2012.

C. Stern and E. W. Schaeffer. On Primary Attributes of Alleles in Drosophila Melanogaster. *Proceedings of the National Academy of Sciences*, 29(11):351–361, Dec. 1943.

C. F. Stevens. What the fly's nose tells the fly's brain. *Proceedings of the National Academy of Sciences*, 112(30):9460–9465, July 2015.

R. F. Stocker. The organization of the chemosensory system in Drosophila melanogaster: a rewiew. *Cell and Tissue Research*, 275(1):3–26, Jan. 1994.

R. F. Stocker. Drosophila as a focus in olfactory research: mapping of olfactory sensilla by fine structure, odor specificity, odorant receptor expression, and central connectivity. *Microscopy research and technique*, 55(5):284–296, Dec. 2001.

R. F. Stocker, M. C. Lienhard, and A. Borst. Neuronal architecture of the antennal lobe in Drosophila melanogaster. *Cell and Tissue Research*, 262(1):9–34, Oct. 1990.

R. F. Stocker, G. Heimbeck, N. Gendre, and J. S. de Belle. Neuroblast ablation in Drosophila P[GAL4] lines reveals origins of olfactory interneurons. *Journal of Neurobiology*, 32(5): 443–456, May 1997.

K. F. Störtkuhl, B. T. Hovemann, and J. R. Carlson. Olfactory adaptation depends on the Trp Ca2+ channel in Drosophila. *Journal of Neuroscience*, 19(12):4839–4846, June 1999.

N. J. Strausfeld and J. G. Hildebrand. Olfactory systems: common design, uncommon origins? *Current Opinion in Neurobiology*, 9(5):634–639, Oct. 1999.

A. Strutz, J. Soelter, A. Baschwitz, A. Farhan, V. Grabe, J. Rybak, M. Knaden, M. Schmuker, B. S. Hansson, and S. Sachse. Decoding odor quality and intensity in the Drosophila brain. *eLife*, 3:e04147, Dec. 2014.

C.-Y. Su, K. Menuz, and J. R. Carlson. Olfactory perception: receptors, cells, and circuits. *Cell*, 139(1):45–59, Oct. 2009.

I. P. Sudhakaran, E. E. Holohan, S. Osman, V. Rodrigues, K. Vijayraghavan, and M. Ramaswami. Plasticity of recurrent inhibition in the Drosophila antennal lobe. *Journal of Neuroscience*, 32(21):7225–7231, May 2012.

I. P. Sudhakaran, J. Hillebrand, A. Dervan, S. Das, E. E. Holohan, J. Hülsmeier, M. Sarov, R. Parker, K. Vijayraghavan, and M. Ramaswami. FMRP and Ataxin-2 function together in long-term olfactory habituation and neuronal translational control. *Proceedings of the National Academy of Sciences*, 111(1):E99–E108, Jan. 2014.

G. S. B. Suh, A. M. Wong, A. C. Hergarden, J. W. Wang, A. F. Simon, S. Benzer, R. Axel, and D. J. Anderson. A single population of olfactory sensory neurons mediates an innate avoidance behaviour in Drosophila. *Nature*, 431(7010):854–859, Oct. 2004.

X. R. Sun, A. Badura, D. A. Pacheco, L. A. Lynch, E. R. Schneider, M. P. Taylor, I. B. Hogue, L. W. Enquist, M. Murthy, and S. S.-H. Wang. Fast GCaMPs for improved tracking of neuronal activity. *Nature communications*, 4:2170, July 2013.

Y. N. Tallini, M. Ohkura, B.-R. Choi, G. Ji, K. Imoto, R. Doran, J. Lee, P. Plan, J. Wilson, H.-B. Xin, A. Sanbe, J. Gulick, J. Mathai, J. Robbins, G. Salama, J. Nakai, and M. I. Kotlikoff. Imaging cellular signals in the heart in vivo: Cardiac expression of the high-signal Ca2+ indicator GCaMP2. *Proceedings of the National Academy of Sciences*, 103 (12):4753–4758, Mar. 2006.

N. K. Tanaka, T. Awasaki, T. Shimada, and K. Ito. Integration of chemosensory pathways in the Drosophila second-order olfactory centers. *Current biology*, 14(6):449–457, Mar. 2004.

N. K. Tanaka, K. Ito, and M. Stopfer. Odor-evoked neural oscillations in Drosophila are mediated by widely branching interneurons. *Journal of Neuroscience*, 29(26):8595–8603, July 2009.

N. K. Tanaka, L. Dye, and M. Stopfer. Dual-labeling method for electron microscopy to characterize synaptic connectivity using genetically encoded fluorescent reporters in Drosophila. *Journal of neuroscience methods*, 194(2):312–315, Jan. 2011.

N. K. Tanaka, K. Endo, and K. Ito. Organization of antennal lobe-associated neurons in adult Drosophila melanogaster brain. *The Journal of comparative neurology*, 520(18): 4067–4130, Dec. 2012.

R. F. Thompson. Habituation: a history. *Neurobiology of Learning and Memory*, 92(2): 127–134, Sept. 2009.

R. F. Thompson and W. A. Spencer. Habituation: a model phenomenon for the study of neuronal substrates of behavior. *Psychological review*, 73(1):16–43, Jan. 1966.

L. Tian, S. A. Hires, T. Mao, D. Huber, M. E. Chiappe, S. H. Chalasani, L. Petreanu, J. Akerboom, S. A. McKinney, E. R. Schreiter, C. I. Bargmann, V. Jayaraman, K. Svoboda, and L. L. Looger. Imaging neural activity in worms, flies and mice with improved GCaMP calcium indicators. *Nature methods*, 6(12):875–881, Dec. 2009.

L. Tian, S. A. Hires, and L. L. Looger. Imaging neuronal activity with genetically encoded calcium indicators. *Cold Spring Harbor Protocols*, 2012(6):647–656, June 2012.

S. M. Tomchik and R. L. Davis. Dynamics of learning-related cAMP signaling and stimulus integration in the Drosophila olfactory pathway. *Neuron*, 64(4):510–521, Nov. 2009.

J. Tsien. Linking Hebb's coincidence-detection to memory formation. *Current Opinion in Neurobiology*, 10(2):266–273, Apr. 2000.

T. Tully and S. Koss. *Habituation of the jump reflex to olfactory cues in normal and mutant Drosophila*. Soc Neurosci Abstr, 1992.

G. C. Turner, M. Bazhenov, and G. Laurent. Olfactory representations by Drosophila mushroom body neurons. *Journal of Neurophysiology*, 99(2):734–746, Feb. 2008.

I. Twick, J. A. Lee, and M. Ramaswami. Olfactory habituation in Drosophila-odor encoding and its plasticity in the antennal lobe. *Progress in brain research*, 208:3–38, 2014.

W. Van Der Goes Van Naters and J. R. Carlson. Receptors and neurons for fly odors in Drosophila. *Current biology*, 17(7):606–612, Apr. 2007.

K. J. T. Venken, J. H. Simpson, and H. J. Bellen. Genetic manipulation of genes and cells in the nervous system of the fruit fly. *Neuron*, 72(2):202–230, Oct. 2011.

R. S. Vetter, A. E. Sage, K. A. Justus, R. T. Cardé, and C. G. Galizia. Temporal integrity of an airborne odor stimulus is greatly affected by physical aspects of the odor delivery system. *Chemical senses*, 31(4):359–369, May 2006.

L. B. Vosshall. Into the mind of a fly. *Nature*, 450(7167):193–197, Nov. 2007.

L. B. Vosshall and R. F. Stocker. Molecular architecture of smell and taste in Drosophila. *Annual review of neuroscience*, 30(1):505–533, July 2007.

L. B. Vosshall, H. Amrein, P. S. Morozov, A. Rzhetsky, and R. Axel. A spatial map of olfactory receptor expression in the Drosophila antenna. *Cell*, 96(5):725–736, Mar. 1999.

L. B. Vosshall, A. M. Wong, and R. Axel. An olfactory sensory map in the fly brain. *Cell*, 102(2):147–159, July 2000.

M. Wachowiak, J. P. McGann, P. M. Heyward, Z. Shao, A. C. Puche, and M. T. Shipley. Inhibition of olfactory receptor neuron input to olfactory bulb glomeruli mediated by suppression of presynaptic calcium influx. *Journal of Neurophysiology*, 94(4):2700–2712, Oct. 2005.

S. Waddell and W. G. Quinn. What can we teach Drosophila? What can they teach us? *Trends in genetics*, 17(12):719–726, Dec. 2001.

A. R. Wagner. *Habituation and Memory*. Mechanisms of learning and motivation, 1979.

J. W. Wang. Presynaptic modulation of early olfactory processing in Drosophila. *Developmental neurobiology*, 72(1):87–99, Jan. 2012.

J. W. Wang, A. M. Wong, J. Flores, L. B. Vosshall, and R. Axel. Two-photon calcium imaging reveals an odor-evoked map of activity in the fly brain. *Cell*, 112(2):271–282, Jan. 2003.

K. Wang, J. Gong, Q. Wang, H. Li, Q. Cheng, Y. Liu, S. Zeng, and Z. Wang. Parallel pathways convey olfactory information with opposite polarities in Drosophila. *Proceedings of the National Academy of Sciences*, 111(8):3164–3169, Feb. 2014.

Y. Wang, A. Mamiya, A.-S. Chiang, and Y. Zhong. Imaging of an early memory trace in the Drosophila mushroom body. *Journal of Neuroscience*, 28(17):4368–4376, Apr. 2008.

M. Whitaker. Genetically encoded probes for measurement of intracellular calcium. *Methods in cell biology*, 99:153–182, 2010.

B. H. White and N. C. Peabody. Neurotrapping: cellular screens to identify the neural substrates of behavior in Drosophila. *Frontiers in molecular neuroscience*, 2(20), Nov. 2009.

D. Wicher, R. Schäfer, R. Bauernfeind, M. C. Stensmyr, R. Heller, S. H. Heinemann, and B. S. Hansson. Drosophila odorant receptors are both ligand-gated and cyclic-nucleotide-activated cation channels. *Nature*, 452(7190):1007–1011, Apr. 2008.

D. A. Wilson. Habituation of Odor Responses in the Rat Anterior Piriform Cortex. *Journal of Neurophysiology*, 79(3):1425–1440, Mar. 1998a.

D. A. Wilson. Synaptic Correlates of Odor Habituation in the Rat Anterior Piriform Cortex. *Journal of Neurophysiology*, 80(2):998–1001, Aug. 1998b.

D. A. Wilson and C. Linster. Neurobiology of a simple memory. *Journal of Neurophysiology*, 100(1):2–7, July 2008.

R. I. Wilson. Understanding the functional consequences of synaptic specialization: insight from the Drosophila antennal lobe. *Current Opinion in Neurobiology*, 21(2):254–260, Apr. 2011.

R. I. Wilson. Early olfactory processing in Drosophila: mechanisms and principles. *Annual review of neuroscience*, 36(1):217–241, July 2013.

R. I. Wilson and G. Laurent. Role of GABAergic inhibition in shaping odor-evoked spatiotemporal patterns in the Drosophila antennal lobe. *Journal of Neuroscience*, 25(40): 9069–9079, Oct. 2005.

R. I. Wilson, G. C. Turner, and G. Laurent. Transformation of olfactory representations in the Drosophila antennal lobe. *Science*, 303(5656):366–370, Jan. 2004.

B. Winter. Linear models and linear mixed effects models in R with linguistic applications, May 2014.

F. W. Wolf, A. R. Rodan, L. T.-Y. Tsai, and U. Heberlein. High-resolution analysis of ethanol-induced locomotor stimulation in Drosophila. *Journal of Neuroscience*, 22(24): 11035–11044, Dec. 2002.

F. W. Wolf, M. Eddison, S. Lee, W. Cho, and U. Heberlein. GSK-3/Shaggy regulates olfactory habituation in Drosophila. *Proceedings of the National Academy of Sciences*, 104 (11):4653–4657, Mar. 2007.

A. M. Wong, J. W. Wang, and R. Axel. Spatial representation of the glomerular map in the Drosophila protocerebrum. *Cell*, 109(2):229–241, Apr. 2002.

C.-L. Wu, S. Xia, T.-F. Fu, H. Wang, Y.-H. Chen, D. Leong, A.-S. Chiang, and T. Tully. Specific requirement of NMDA receptors for long-term memory consolidation in Drosophila ellipsoid body. *Nature Neuroscience*, 10(12):1578–1586, Nov. 2007.

L.-G. Wu and P. Saggau. Presynaptic inhibition of elicited neurotransmitter release. *Trends in neurosciences*, 20(5):204–212, May 1997.

S. Xia, T. Miyashita, T.-F. Fu, W.-Y. Lin, C.-L. Wu, L. Pyzocha, I.-R. Lin, M. Saitoe, T. Tully, and A.-S. Chiang. NMDA Receptors Mediate Olfactory Learning and Memory in Drosophila. *Current Biology*, 15(7):603–615, Apr. 2005.

E. Yaksi and R. I. Wilson. Electrical coupling between olfactory glomeruli. *Neuron*, 67(6): 1034–1047, Sept. 2010.

C. A. Yao, R. Ignell, and J. R. Carlson. Chemosensory coding by neurons in the coeloconic sensilla of the Drosophila antenna. *Journal of Neuroscience*, 25(37):8359–8367, Sept. 2005.

J. C. Yin and T. Tully. CREB and the formation of long-term memory. *Current Opinion in Neurobiology*, 6(2):264–268, Apr. 1996.

M. Yoshihara, A. W. Ensminger, and J. T. Littleton. Neurobiology and the Drosophila genome. *Functional & integrative genomics*, 1(4):235–240, Mar. 2001.

D. Yu, A. Ponomarev, and R. L. Davis. Altered representation of the spatial code for odors after olfactory classical conditioning; memory trace formation by synaptic recruitment. *Neuron*, 42(3):437–449, May 2004.

D. Yu, D.-B. G. Akalal, and R. L. Davis. Drosophila α/β Mushroom Body Neurons Form a Branch-Specific, Long-Term Cellular Memory Trace after Spaced Olfactory Conditioning. *Neuron*, 52(5):845–855, Dec. 2006.

T. Zars, M. Fischer, R. Schulz, and M. Heisenberg. Localization of a short-term memory in Drosophila. *Science*, 288(5466):672–675, Apr. 2000a.

T. Zars, R. Wolf, R. Davis, and M. Heisenberg. Tissue-specific expression of a type I adenylyl cyclase rescues the rutabaga mutant memory defect: in search of the engram. *Learning & memory*, 7(1):18–31, Jan. 2000b.

H.-G. Zhang, H.-J. J. Lee, T. Rocheleau, R. H. Ffrench-Constant, and M. B. Jackson. Subunit composition determines picrotoxin and bicuculline sensitivity of Drosophila gamma-aminobutyric acid receptors. *Molecular Pharmacology*, 48(5):835–840, Nov. 1995.

R. S. Zucker. Calcium- and activity-dependent synaptic plasticity. *Current Opinion in Neurobiology*, 9(3):305–313, June 1999.

F. Zufall and T. Leinders-Zufall. The Cellular and Molecular Basis of Odor Adaptation. *Chemical senses*, 25(4):473–481, Aug. 2000.